**Maria Strocchia**

**UNIVERSITÀ DEGLI STUDI DI SALERNO**
**DIPARTIMENTO DI FARMACIA**

DIFARMA

**Dottorato di Ricerca in Scienze Farmaceutiche**

**XIII ciclo NS**
**2012-2015**

# DESIGN AND STRUCTURAL OPTIMIZATION OF NEW MOLECULES AS POTENTIAL ANTIINFLAMMATORY AND/OR ANTICANCER AGENTS

**Design and structural optimization of new molecules as potential antiinflammatory and/or anticancer agents**
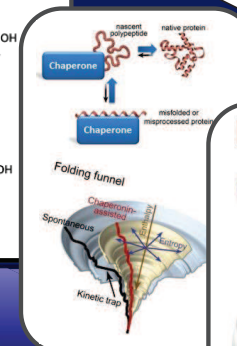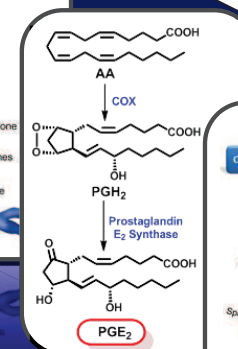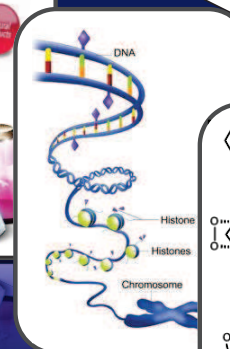
DIFARMA

**Dipartimento di Farmacia**
**Via Giovanni Paolo II, 132**
**84084 Fisciano, Salerno**

*Maria Strocchia*

UNIVERSITÀ DEGLI STUDI DI SALERNO

DIFARMA

**UNIVERSITÀ DEGLI STUDI DI SALERNO**
**Dipartimento di Farmacia**

Dottorato di ricerca
in Scienze Farmaceutiche
Ciclo XIII NS &mdash; Anno di discussione 2015

Coordinatore: Chiar.mo Prof. *Gianluca Sbardella*

# *Design and structural optimization of new molecules as potential antiinflammatory and/or anticancer agents*

settore scientifico disciplinare di afferenza: CHIM/06

| | |
|---|---|
| **Dottorando** | **Tutore** |
| **Dott.** *Maria Strocchia* | **Chiar.ma Prof.** *Ines Bruno* |

*To my Parents and my Brother*

**Preface**

My PhD three years course in Pharmaceutical Sciences at the Department of Pharmacy of Salerno University was started in 2012 under the supervision of Prof. Ines Bruno.

My research project was mainly focused on the design and synthesis of small molecules as new modulators of emerging targets involved in inflammatory and cancer processes. Specifically, my research activity was addressed to the investigation of three major targets:

- the epigenetic family of readers, Bromodomain (BRD) containing proteins;
- the membrane enzyme, microsomal Prostaglandin $E_2$ synthase-1 (mPGES-1);
- the molecular chaperone, Heat shock protein 90 (Hsp90).

The entire work was carried out under the direct supervision of Prof. Ines Bruno and Dr. Stefania Terracciano.

Computational guided design of compounds was performed in collaboration with Prof. Giuseppe Bifulco's research group.

Biological screenings were performed in collaboration with Dr. Panagis Filippakopoulos of the Structural Genomics Consortium (Oxford) in the case of BRDs, with Prof. Oliver Werz of Friedrich Schiller University (Germany) in the case of mPGES-1, and with Prof. Antonietta Leone and Fabrizio Dal Piaz of Salerno University in the case of Hsp90.

Furthermore, to improve my knowledge on mPGES-1, in 2013 I joined Prof. Hans Hebert's research group at the Department of Biosciences and Nutrition of Karolinska Institutet (Sweden), where I spent seven months. During that period, my research was carried out under the supervision of Dr. Caroline Jegerschöld and was addressed to the heterologous expression and two-dimensional crystallization of human mPGES-1.

**List of publications related to the scientific activity performed during the three years PhD course in Pharmaceutical Sciences**

**Papers:**

➢ Lauro G., **Strocchia M.**, Terracciano S., Bruno I., Fischer K., Pergola C., Werz O., Riccio R., Bifulco G. "Exploration of the dihydropyrimidine scaffold for the development of new potential anti-inflammatory agents blocking prostaglandin $E_2$ synthase-1 enzyme (mPGES-1)". *Eur J Med Chem* **2014**, *80,* 407-415.

➢ Terracciano S., Lauro G., **Strocchia M.**, Fischer K., Werz O., Riccio R., Bruno I., Bifulco G. "Structural insights for the optimization of dihydropyrimidin-2(1H)-one based mPGES-1 inhibitors". *ACS Med Chem Lett* **2015**, *6*, 187–191.

➢ **Strocchia M.,**‡ Terracciano S.,‡ Chini M. G., Vassallo A., Vaccaro M. C., Dal Piaz F., Leone A., Riccio R., Bruno I., Bifulco G. "Targeting the Hsp90 C-terminal domain by the chemically accessible dihydropyrimidinone scaffold". *Chem Commun* **2015**, *Article in press*, DOI: 10.1039/C4CC10074C.

➢ Picaud S.,‡ **Strocchia M.,**‡ Terracciano S., Lauro G., Mendez J., Daniels D.L., Riccio R., Bifulco G., Bruno I., Filippakopoulos P. "The 9*H*-purine scaffold reveals induced-fit pocket plasticity of the BRD9 bromodomain". *J Med Chem*. Accepted.

‡ These authors contributed equally to this work.

**Conference proceedings:**

➢ Terracciano S., **Strocchia M.**, Chini M. G., Bruno I., Dal Piaz F., Bifulco G., Riccio R. "Structure-based approach for the discovery of potent inhibitors of the Hsp90 molecular chaperone bearing the triazole scaffold". XXXIV National Meeting of Italian Chemical Society, Organic Chemistry Division, Pavia (Italy), September 10-14, 2012.

➢ **Strocchia M.**, Terracciano S., Riccio R., Bruno I., Jegerschöld C. "Human microsomal prostaglandin $E_2$ synthase-1 (mPGES-1) overexpression in LEMO21(DE3) E. Coli strain". Giornate di Facoltà di Farmacia e Medicina, Salerno (Italy), May 22-23, 2014.

➢ Terracciano S., **Strocchia M.**, Chini M. G., Vassallo A., Vaccaro M. C., Dal Piaz F., Leone A., Riccio R., Bifulco G., Bruno I. "3,4-dihydropyrimidin-2(1H)-one as a useful scaffold for Hsp90 C-terminal inhibition". XXV National Meeting of Italian Chemical Society, Rende (Italy), September 7-12, 2014.

➢ **Strocchia M.**, Terracciano S., Lauro G., Werz O., Riccio R., Bruno I., Bifulco G. "Identification of dihydropyrimidine derivatives as new mPGES-1 inhibitors". XXV National Meeting of Italian Chemical Society, Rende (Italy), September 7-12, 2014.

➢ **Strocchia M.**, Terracciano S., Lauro G., Werz O., Riccio R., Bruno I., Bifulco G. "New 3,4-dihydropyrimidin-2(1H)-one derivatives as efficient modulators of microsomal prostaglandin $E_2$ synthase-1". Ischia Advanced School of Organic Chemistry, Ischia (Italy), September 21-25, 2014.

# Table of Contents

**Abstract**

Inflammation and cancer are two complex pathological processes, involving a variety of molecular actors. The deeply connection and crosstalk between cancer and inflammation is well-known and the modulation of these processes is one of the main goals of modern medicinal chemistry. The identification of new molecular entities able to interfere with biological targets placed at the crossroads of these two pathways is strongly needed, both for the development of new promising drug candidates and as chemical probes useful to further investigate less understood biological aspects. Three main targets, involved at different levels in inflammation and cancer, have been thoroughly investigated: bromodomain (BRD) containing proteins, microsomal Prostaglandin $E_2$ Synthase-1 (mPGES-1) and Heat-shock protein 90 (Hsp90). The results obtained can be summarized in the three main sections, reported below according to the target of interest:

**a) Discovery of new modulators of human bromodomains by structure-based and computer-aided combined approaches.** BRDs are evolutionary conserved modules which act as readers of the histone code, by recognizing acetyl-lysine (Kac) residues on histone tails. The contribution of BRD containing proteins has recently emerged in a number of diseases, especially in cancer processes. With the aim of identifying a new Kac mimetic chemotype, a structure-guided approach was undertaken starting from small fragment-like 9*H*-purine scaffolds. One of the initial identified fragments (**2a**), that was shown to be a BRD binder, was systematically modified employing organic synthesis approaches in order to gather a structure activity relationships profile to be exploited in the next structural optimization process. These studies allowed to disclose potent nanomolar ligands for BRD9 (compounds **7d** and **11**), showing only residual micromolar affinity towards BRD4. Binding of **7d** and **11** to BRD9 was investigated by crystallography and flexible docking

experiments and resulted in an unprecedented rearrangement of residues forming the Kac cavity, affecting plasticity of the protein in an induced-fit pocket. Finally, the compounds did not exhibit any cytotoxic effect in HEK293T cells and displaced the BRD9 bromodomain from chromatin in bioluminescence proximity assays without remarkably affecting the BRD4/histone complex.

**b) Identification and structural optimization of DHPM-based mPGES-1 inhibitors.** mPGES-1 is a homotrimeric membrane protein involved in the arachidonic acid cascade, which acts as downstream synthase in the cyclooxygenase (COX) pathway by catalyzing the biosynthesis of Prostaglandin (PG) $E_2$ from the $PGH_2$ precursor. Inhibition of mPGES-1 can represent a valid therapeutic approach to interfere with inflammation-induced $PGE_2$ formation without affecting the constitutively formed prostanoids. In order to find a new molecular platform for mPGES-1 modulation, a structure-based design approach was carried out on a focused collection of 3,4-dyhidropyrimidin-2(1H)-one (DHPM)-based molecules, docked in the first high resolution X-ray crystal structure of the enzyme in its active form (PDB code: 4AL0). The key interactions with the receptor counterpart were introduced as a qualitative filter for the selection of the most promising compounds to be synthesized. Biological results were consistent with the computational suggestions and disclosed two molecules (**48** and **49**) showing a promising *in vitro* mPGES-1 inhibitory activity. The most recently crystallized structure of mPGES-1 with the inhibitor LVJ (PDB code: 4BPM) was used to optimise compound **48** ($IC_{50} = 4.16 \pm 0.47$ μM) to give compound **53**, a 10-fold more potent mPGES-1 inhibitor ($IC_{50} = 0.41 \pm 0.02$ μM).

In order to deeply investigate this complex enzyme, a heterologous expression of human $His_6$-tagged mPGES-1 and two-dimensional crystallographic studies were also carried out.

**c) The DHPM core as new chemotype for Hsp90 C-terminal modulation.** Hsp90 is a molecular chaperone highly involved in the development, survival and proliferation of cancer cells. Traditional inhibitors of Hsp90 target its N-terminal domain. Nevertheless, this type of modulation produces scheduling and toxicity issues connected to the induction of the deleterious heat shock response. Although less explored, C-terminal inhibition of Hsp90 represents a very promising approach for developing new potential anti-cancer drugs as it is devoid of the negative effects triggered by the heat shock response. In an attempt to identify non-natural inspired modulators of Hsp90 C-terminus, a collection of DHPM derivatives was synthesized. The rationale for targeting Hsp90 C-terminal domain by DHPMs derives from the structural analogy between the DHPM core and uridine triphosphate (UTP), a nucleotide shown to selectively interact with the chaperone C-terminal site, but not with its N-terminus. Biological evaluation revealed that the privileged DHPM core can be considered as a new template for the modulation of Hsp90 chaperoning function, through the binding to its C-terminal region. In particular, compound **54** was identified as a novel promising antiproliferative agent against Hsp90 C-terminus.

# INTRODUCTION

# -CHAPTER 1-

**1.1 The role of organic chemistry in drug discovery**

The drug discovery process requires interdisciplinary approaches involving a multitude of scientific areas, e.g., biology, medicinal and synthetic organic chemistry, statistics, pharmacology, medicine, toxicology, structural biology, chembioinformatics, computational chemistry, genomics and proteomics.[1] These disciplines work synergistically along the hard and complex journey toward the identification of a new drug.[2] Indeed, the drug discovery and development process is one of the most challenging human endeavors, as the optimal balance between efficacy and safety of a drug must be ensured.[3, 4] Moreover, the development of a new drug is a long, difficult, expansive and highly risky process, as the market access environment is very restrictive. Research and development for most of the available medicines has required 12–24 years for a single new medicine, from the beginning of the project to the launch of the drug.[5]

The process of drug discovery starts with the identification of a molecular target, whose modulation is expected to have positive therapeutic effect.[6, 7] The selection of an appropriate target is a relevant issue: ideally, the biological target should be fully validated and its modulation should provide an unambiguous therapeutic response, with no susceptibility to the induction of resistance mechanisms.[8] Appropriate assays, designed for the selected biological target are then needed to identify putative modulators.[9] At this stage, the drug discovery process is focused on small organic molecules, as they are the main class of marketed drugs.[10] Organic synthetic chemistry acts as the main player at this step, as its role is to identify and structurally optimize new active compounds both in potency and in their pharmacokinetic profile.[11, 12] Actually, organic synthesis should be able to provide a more or less complex compound with high selectivity and efficiency.[13] Many are the aims that organic chemistry is expected to achieve in the drug discovery process. Such examples include: to develop novel structural motifs with

improved pharmacological properties, to identify new synthetic methods and strategies, to expand applications of organic synthesis into the field of biology, to apply the information derived from structural biology studies on the selected target in order to synthesize molecules that can appropriately fit the receptor, to chemically modify an emerged lead structure in order to draw a structure–activity relationships (SARs) profile useful for its rapid optimization.[14-18] Today, synthetic organic chemistry can rely on a wide range of tools for overcoming the several hurdles in the drug discovery process. These new tools include advances in synthetic, analytical and purification methods such as transition-metal-catalysed carbon–carbon couplings,[19] multicomponent and domino reactions,[20] microwave-assisted and flow chemistry,[21, 22] high-field NMR[23] and preparative high-performance liquid chromatography (HPLC),[24] as well as computer-assisted approaches,[25] combinatorial chemistry[26] and high-throughput screening (HTS).[27]

An active compound, referred as a "hit" in the drug discovery process, may arise in many ways. It may be found in large or more focused compounds libraries, which have demonstrated prior reliability in drug discovery programs. If inhibitors or ligands of a given target are known, potential new binders may be selected on the basis of structural similarities through a "ligand-based design" approach.[28] Alternatively, when the crystal structure of the target has been elucidated, structural complementarity to the binding site can be evaluated through "structure-based design" approaches.[29] In this case, virtual screening studies can be also carried out, in order to select promising compounds belonging to a commercially available database.[30] The resulting hits generally have modest activity, typically at micromolar concentrations, while the marketed drugs are commonly active at low nanomolar range.[31] Development of the hit to a potent compound is the process of "lead" optimization.[32] At this step, organic synthetic chemistry plays again a crucial role, as much synthetic effort is required to generate a large collection of

structurally related derivatives.[33] In the course of this process, other problems related to drug pharmacokinetic profile must be taken into due account.[34]

Indeed, organic and medicinal chemistry should also work synergistically to overcome pharmacokinetic liabilities of test compounds. To this end, the prediction of "drug-like" properties has to be accomplished.[32] Highly lipophilic compounds with high molecular weight are generally more potent *in vitro*, but they tend to be usually not drug-like because of their poor pharmacokinetics and oral bioavailability. As a predictor of drug-likeness, Lipinski *et al.*[35] formulated the "rule of five" which consists of four important properties, each related to the number 5 (molecular mass <500 Da; calculated LogP <5; hydrogen-bond donors <5; and hydrogen-bond acceptors <10). However, this rule tries to predict oral bioavailability in a very basic manner, but drug discovery implies a very careful determination of the ADMET (absorption, distribution, metabolism, elimination, and toxicology) parameters of a drug, which implies more than Lipinski's "rule of five".[36] An example is represented by antibiotics, cytostatic and many other drugs which suffer from the so-called "molecular obesity",[31] as they have higher molecular mass than the border of 500 Da, but possess elevated efficiency and bioavailability. Actually, the aim of lead optimization phase is to maintain favourable properties in lead compound, while improving any deficiencies in its structure. This represents a very complex issue and indeed, all the information gathered about the molecule at this stage will allow for the optimization of a target candidate profile which, together with toxicological and other control assays, will lay the basis first for preclinical candidate selection and finally for entering clinical trials.[37-39]

In the present PhD project, thanks to combined approaches of organic synthesis, computational chemistry and structural studies, new chemical entities with antiinflammatory or antitumor effects have been successfully identified.

**1.2 The crosstalk between cancer and inflammation**

It is beyond the scope of this thesis to discuss the complex mechanisms of cancer and inflammation, but the close relationship between these two pathological processes deserves some considerations. Although the involved pathways and the correlations between them have not been fully understood yet, the crosstalk between cancer cells and inflammatory mediators has been known for a long time.[40]

The first example of inflammatory processes related to cancer development in tissues was reported in the nineteenth century by the German physician Rudolf Virchow, who described leukocyte infiltrates within tumours.[41] These leukocyte infiltrates were at first related to the immune surveillance and antitumor immune response, but it is now understood that they can act both as tumour-suppressors and as tumour-promoters.[42-45]

Cancers are composed of multiple cell types such as fibroblasts and epithelial cells, innate and adaptive immune cells, blood and lymphatic cells, as well as specialized cell types unique to each tissue.[46, 47] Inflammation is a key component of the cancer microenvironment, also in tumours which are not related to an obvious inflammatory cause. Relevant aspects of cancer-related inflammation include the infiltration of white blood cells (mainly tumour-associated macrophages), the presence of inflammatory mediators (cytokines and chemokines) and the occurrence of tissue remodelling and angiogenesis.[48]

Both the intrinsic and the extrinsic inflammatory pathways have been related to cancer.[44, 49, 50] The intrinsic one is activated by genetic events, mainly activation of oncogenes, resulting in the transformation of cells which trigger the expression of inflammation-related programs contributing to produce an inflammatory environment.[51, 52] In the extrinsic pathway, chronic inflammatory conditions or infections increase the risk of developing cancer (e.g, prostatitis for prostate cancer, papillomavirus for cervical carcinoma).[53-55] The two pathways converge in the activation of transcription factors, mainly

NF-κB and STAT3 which have emerged as key mediators in cancer development and progression.[56, 57]

In this context, it is not surprising that the traditional six hallmarks of cancer (self-sufficiency in proliferative signals, insensitivity to anti-growth signals, tissue evasion and metastasis, limitless replicative potential, sustained angiogenesis, resistance to cell death)[58] have been joined by four additional emerging hallmarks (avoidance of immune destruction, induction of tumour-promoting inflammation, genome instability and mutation, and deregulation of cellular metabolism)[59] which are all directly or indirectly related to the inflammatory process (**Figure 1.1**).
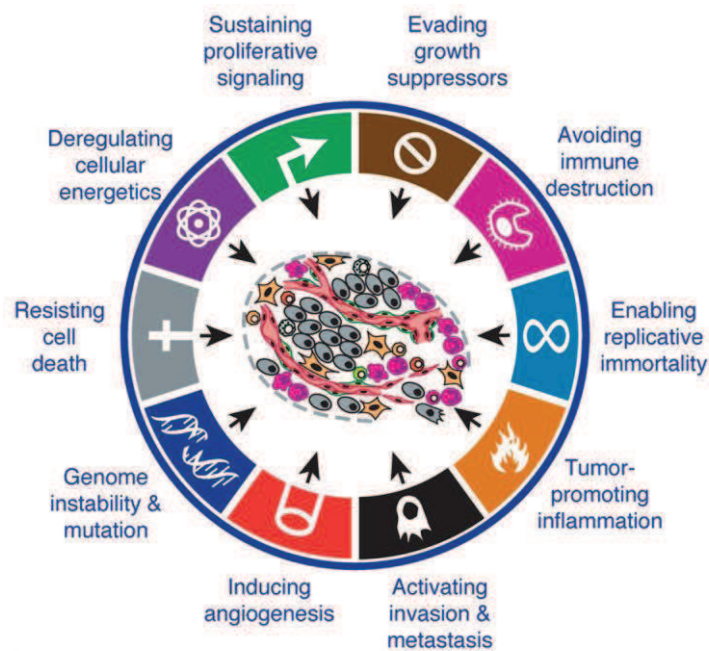


**Figure 1.1** *The ten hallmarks of cancer (adapted from ref. 59).*

Both premalignant and malignant tissues have been found in an inflammatory state driven by cells of the immune system which ultimately disclose the tumour-promoting effect of the inflammatory response (**Figure 1.2**). Furthermore, inflammatory mediators contribute to genomic instability and to the occurrence of mutations associated with tumours, as many of them act as direct mutagens or as deregulators of DNA repair mechanisms and cell

cycle checkpoints, resulting in the acquired ability of cancer cells to proliferate, invade and escape from host defence, in particular from T and B lymphocytes, macrophages, and natural killer cells.[60-63]
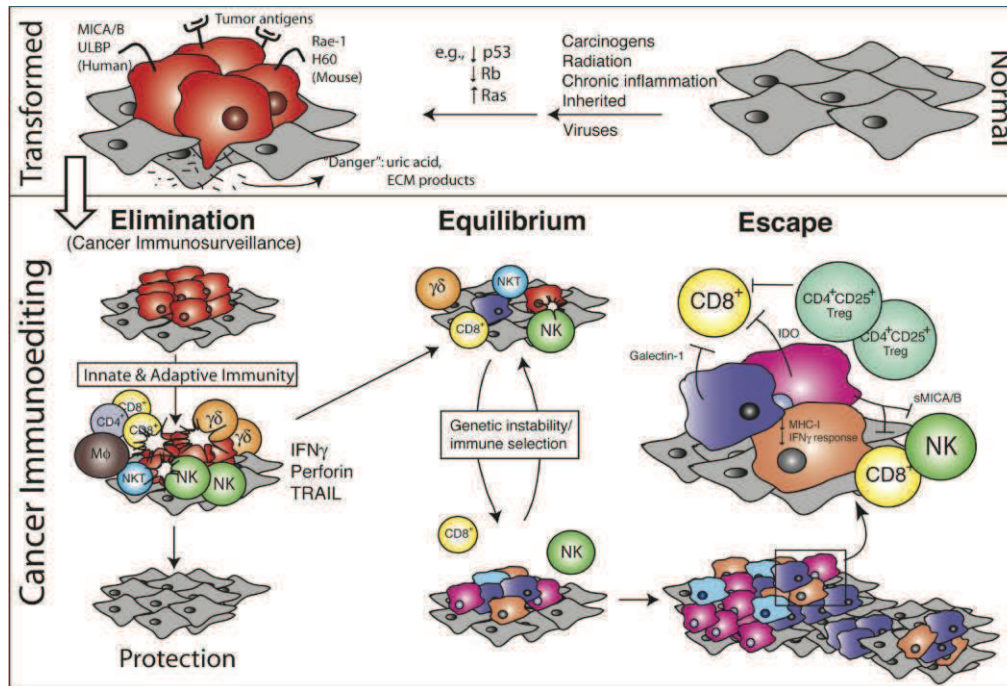


**Figure 1.2** *Role of inflammation in cancer development.*[63]

Whereas chronic innate immune inflammation in premalignant cells might promote cancer development, adaptive immune response to the tumour might result in abolition of the malignancy, a mechanism known as cancer immunosurveillance (**Figure 1.2**).[64, 65] Adaptive immune cells can directly modulate cancer by inhibiting tumour growth through T-cell activity and cytokine-mediated lysis of malignant cells.[66]

These considerations highlight the dual opposite function of inflammatory reactions, which can result both in antitumour and in tumour-promoting effects.[67, 68] Anyway, many evidences have been gathered supporting the improved therapeutic efficacy that can be achieved by blocking the two signalling networks and their pathways.[69-73] In this respect, targeting inflammatory and neoplastic pathways can be accomplished at different levels

through, the modulation of specific proteins involved in key steps of these processes.

In the context of my PhD, three biological targets involved both in inflammation and cancer have been investigated: Bromdomain (BRD) containing proteins, microsomal Prostaglandin $E_2$ synthase-1 (mPGES-1) and the chaperone Heat Shock Protein 90 (Hsp90). Although each of them is known for its major implication in inflammation (in the case of mPGES-1) or in tumour (in the case of BRDs and Hsp90), several evidences suggest their involvement in both processes, standing for an additional evidence of the crosstalk between cancer and inflammation.

## 1.3 Epigenetic readers of acetylated lysines: bromdomains

The array of post-translational modifications (PTMs) introduced on histone tails gives rise to the so-called "histone code",[74] a cellular language generated by proteins which introduce (writers) or remove (erasers) PTMs.[75-77] Furthermore, this complex code involves also some evolutionarily conserved domains, found in structurally heterogeneous proteins, which act as readers of PTMs by recognizing covalent marks on histones.[78-81]

The combination of PTMs (acetylation, methylation, phosphorylation, ribosylation, biotinylation, citruillination, crotonylation and SUMOylation[82-84] modulates chromatin plasticity and its functionality.[85-89] For instance, ε-N-acetylation of lysine residues (Kac) is associated with neutralization of the positive charge of histone tails, resulting in an open chromatin structure (euchromatin) and transcriptional activation.[90-94] Although lysine acetylation has been connected for a long time only to the histone code, this widespread PTM occurs throughout the entire proteome,[95-99] and alterations in its levels have been associated to a large number of diseases, especially cancer.[98, 100-103] In the context of epigenetics, the acetyl group is deposited on lysine residues by histone acetyl-transferases (HATs),[104] removed by histone deacetylases

(HDACs)[105] and recognized by conserved protein modules such as bromodomains,[106] as well as the more recently discovered YEATS domains.[107]

There are 61 bromodomains (BRDs) that have been identified in 46 different proteins in the human genome,[108] which mainly act as transcriptional co-regulators and chromatin modifying enzymes, e.g., HATs and HAT associated proteins (PCAF, GCN5, BRD9),[109-112] helicases (SMARCA),[113] ATP-dependent chromatin-remodelling complexes (BAZ1B),[114] SET domain containing methyl-transferases (MLL and ASH1L),[115, 116] transcriptional co-activators (TAF1, TRIM/TIF1),[117, 118] nuclear scaffolding proteins (polybromo PB1)[119] and transcriptional regulators (BET family).[120, 121] All BRDs share an architecturally conserved tertiary structure with an "atypical left-handed four-helix bundle" (αZ, αA, αB, αC) linked by two main loop regions (ZA and BC loops) (**Figure 1.3A**), a structural motif identified in the early 90s in the Drosophila melanogaster *brahma* gene.[122] Despite the conserved BRD fold, the overall sequence similarity of the BRD family members is not high, as considerable variations have been found especially in ZA and BC loops.[123] Nevertheless, the amino acids engaged in Kac recognition are among the most conserved in the hydrophobic Kac binding pocket and correspond to highly conserved asparagine and tyrosine residues (in BRD4(1): Asn140 and Tyr97).[108] A peculiar feature of this module is also the presence of a network of water molecules, which form hydrogen bonds with carbonyl groups of the protein backbone at the base of the domain and are relatively conserved in most BRDs (**Figure 1.3B**).[124-127] A large scale structure-based analysis of the human BRD family, using 34 high resolution crystal structures and 4 NMR models, as well as secondary structure prediction algorithms, grouped the 61 BRD modules into 8 distinct sub-families (**Figure 1.3C**).[108] The BET subfamily of BRDs (group II) has attracted particular attention, as its members (BRD2, BRD3, BRD4 and BRDT) play a central role in cell cycle progression, cellular proliferation and apoptosis.[128]
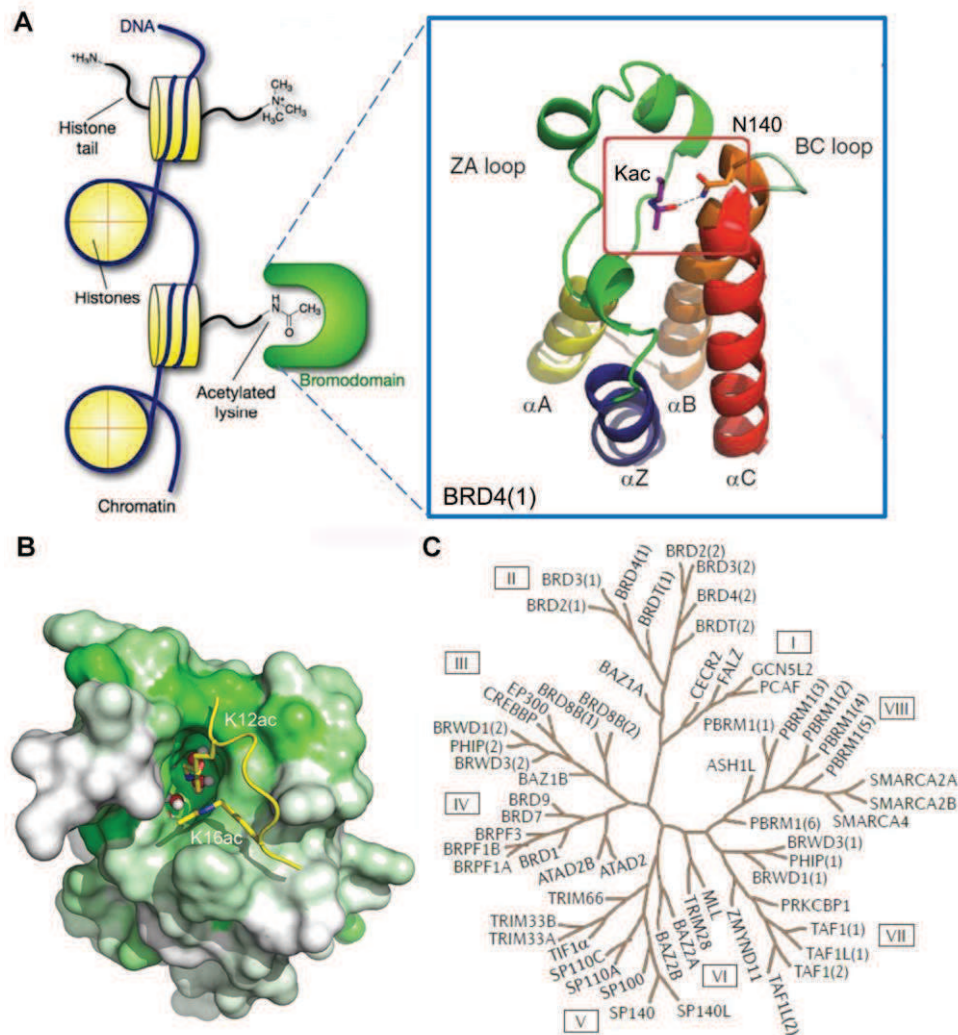
**Figure 1.3** *Structure and classification of the bromodomain family.(**A**) The atypical left-handed four-helix bundle structural motif in BRD4(1). Highlighted is the interaction with the conserved asparagine residue. (**B**) Molecular surface of the bromodomain of BRD4(1) showing conservation of Kac binding site. Green represents more conserved regions, and white less conserved ones, as obtained from a multiple sequence alignment of all human BRDs. Conserved water molecules at the bottom of the Kac binding pockets are shown as ball-and-stick models.(**C**) Phylogenetic tree of human BRDs.*

BETs contain two N-terminal BRD modules that interact with acetylated histones,[120] transcription factors[129, 130] or other acetylated transcriptional regulators,[131, 132] an extra terminal (ET) recruitment domain[133] and a C-terminal motif responsible for the recruitment of the positive transcription elongation factor B (P-TEFb),[121] in the case of BRD4 and BRDT.[134] BET

BRDs have been successfully targeted by small molecule inhibitors, such as the triazolothienodiazepine (+)-JQ1[134] (**Figure 1.4A**) and the triazolobenzodiazepine IBET762[135] (**Figure 1.4A**) which were identified employing phenotypic screening [136] and have consolidated the emerging role of BRDs as viable therapeutic targets.[137, 138] The discovery of these two compounds prompted in the last years a number of medicinal chemistry efforts, which resulted in a growing number of novel and structural diverse Kac mimetics targeting bromodomains, exhibiting excellent potency and selectivity, especially against the BETs (**Figure 1.4A**).[139] More recently, a number of kinase inhibitors have also been identified as interacting with the Kac binding pocket of some bromodomains (**Figure 1.4B**).[140, 141] Potent and selective molecules against non-BET proteins have also emerged, mainly targeting the bromodomain of CREBBP.[142, 143] Finally, it was also possible to modulate more challenging BRDs such as BRPF1,[144] ATAD2[145, 146] and BAZ2B[147] (**Figure 1.4C**), even though they had emerged as difficult to target from a druggability analysis carried out on all BRDs.[148] In this context, fragment-based programs proved to be very reliable approaches to identify fragments interacting with these less druggable BRDs.[145-147, 149-154]

Potent and selective small molecules that inhibit the Kac−BRD interaction have been employed as chemical probes in elucidating the biology of several families of bromodomain-containing proteins, by shedding more light also on their role in pathological conditions. For instance, BET inhibition suppresses tumour growth in diverse mouse models of cancer, e.g., NUT midline carcinoma, acute myeloid and mixed lineage leukemia, multiple myeloma, glioblastoma, melanoma, Burkitt's lymphoma, neuroblastoma and prostate cancer, leading to a number of clinical trials seeking to modulate BET function in diverse tumour settings.[138]
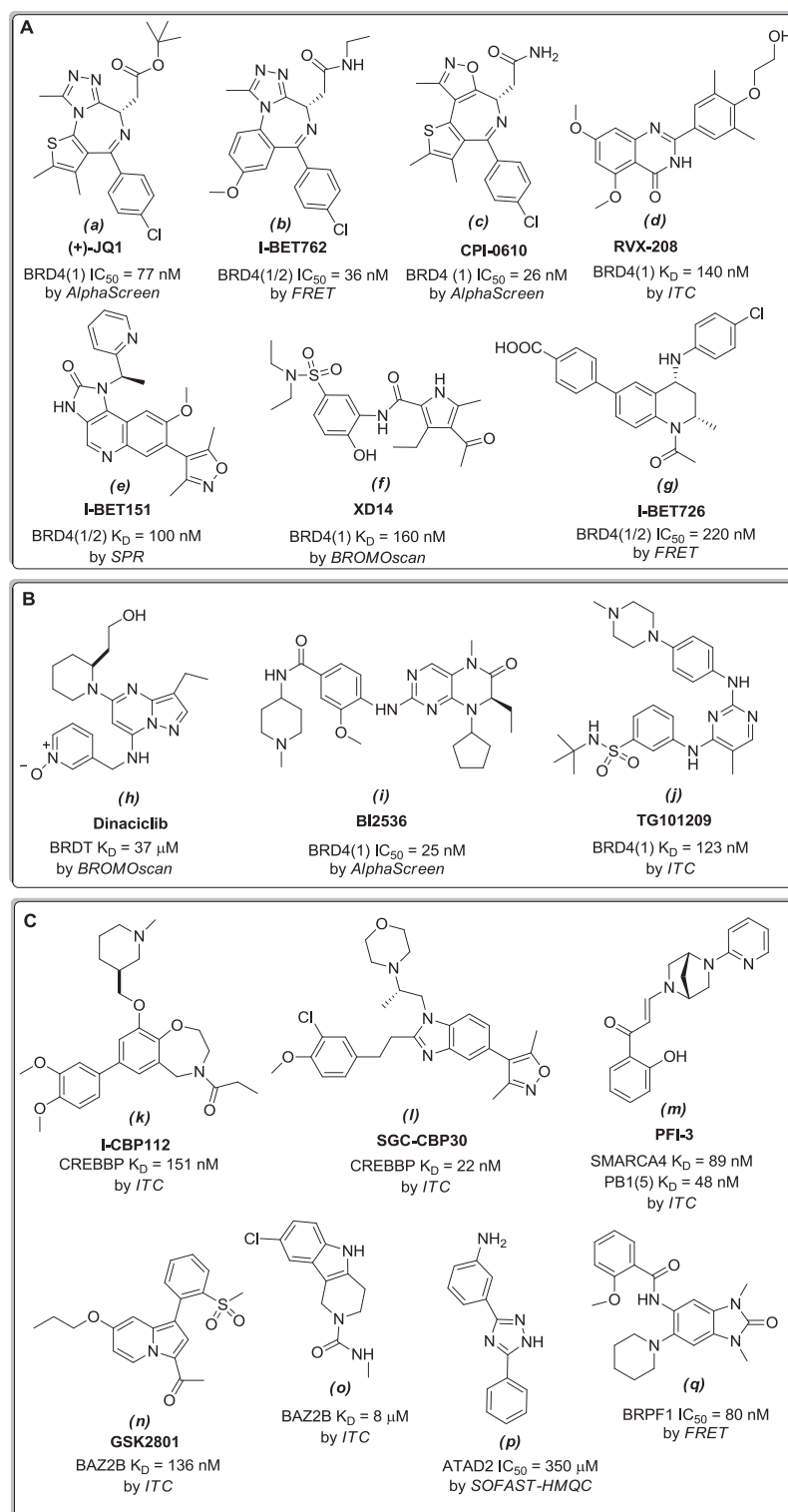
**Figure 1.4** *Bromodomain Inhibitors. (A) Representative BET inhibitors.*[134, 135, 155-159] *(B) Some dual kinase-BRD inhibitors.*[140] *(C) Non-BET inhibitors.*[142, 144, 146, 147, 160, 161]

The first study to demonstrate the efficacy of a bromodomain inhibitor in a preclinical cancer model was carried out by Filippakopoulos *et al.*[134] with the aim of evaluating the effect of (+)-JQ1 on mice bearing a NUT midline carcinoma (NMC) xenograft, a rare but aggressive form of cancer determined by the BRD4-NUT oncoprotein.[162] Treatment with (+)-JQ1 induced a reduction of tumour volume and promoted survival with minimal toxicity against normal tissues.[134] This outcome paved the way for some BET inhibitors to enter clinical trials in a range of malignancies, including NUT midline carcinoma (ClinicalTrials.gov identifiers: NCT01587703, NCT01987362), progressive lymphoma (ClinicalTrials.gov identifier: NCT01949883), solid tumours (ClinicalTrials.gov identifier: NCT02259114), glioblastoma (ClinicalTrials.gov identifier: NCT02296476), acute leukemia and other hematological malignancies (ClinicalTrials.gov identifiers: NCT01943851, NCT01713582).

The role of BETs in cancer is more than obvious, but these transcriptional factors have a relevant function also in inflammatory conditions, as emerged especially in the case of BRD4.[163-169] The pan-BET inhibitor I-BET762 was shown to suppress inflammation by strongly attenuating the expression of LPS-induced pro-inflammatory genes during late macrophage activation.[135] BET proteins have also emerged as an essential connection between chromatin signalling and IL-17-producing T helper cells differentiation and activation, which suggests their potential therapeutic role in autoimmune conditions.[170] A very recent study has demonstrated the ability of (+)-JQ1 to interfere with the interaction between BRD4 and the transcription factor NF-κB.[171] As described in the previous paragraph, NF-κB is the central mediator involved in the crosstalk between cancer and inflammation: its master function in modulating the immune response is regulated by the acetylation of Lys130 on its RelA subunit, which triggers transcriptional activation of NF-κB target genes and contributes to maintain its persistently active form in tumors.[172, 173] This event

can be suppressed through depletion or inhibition of BRD4, as this BET member has been shown to bind to acetylated Lys310 of RelA and to regulate the transcriptional activity of NF-κB. As a consequence of Brd4 deletion or inhibition upon treatment with (+)-JQ1, NF-κB activation mediated by TNF-α is suppressed, as well as the expression of NF-κB-dependent target genes.[171] Another BRD4 inhibitor, I-BET151, also exhibited anti-inflammatory properties, as it was shown to selectively regulate IL-6 production.[174] In a chronic model of inflammation involving IL-6 (autoimmune encephalomyelitis used as a model of multiple sclerosis), treatment with I-BET151 resulted in a significant delay in the onset of clinical symptoms.[174]

Finally, BET bromodomains are involved also in heart failure,[175, 176] adipogenesis[177] and in viral transcription of HIV, herpesviruses, Merkel cell polyomavirus and murine leukaemia virus, suggesting potential therapeutic applications of BRD inhibitors also in these fields.[178-184]

## 1.4 Microsomal prostaglandin $E_2$ synthase-1 (mPGES-1)

Prostaglandin $E_2$ synthases (mPGES-1, mPGES-2 and cPGES) are downstream enzymes that specifically catalyze the biosynthesis of the crucial inflammatory mediator $PGE_2$ from $PGH_2$.[185]

$PGE_2$ and all other eicosanoids are biologically active mediators, produced from the oxidation of long-chain 20 carbon atoms polyunsaturated fatty acids and obtained, either *via* the cyclooxygenases (COX-1 and COX-2) pathway, or *via* the lipoxygenase (LO) one.[186-191] The COXs pathway generates prostanoids, which include prostaglandins (PGs), prostacyclin and thromboxane (TXA), while the LO pathway results in the biosynthesis of leukotrienes (LTs).[187] These inflammatory mediators are synthetized by most mammalian cells and tissues and their effect is mediated by the interaction with individual receptors, mainly G-protein coupled receptors (GPCR).[192, 193] The biosynthesis of eicosanoids is initiated by release of arachidonic acid

(AA) from cell membrane by phospholipase $A_2$ (PLA$_2$), in response to any inflammatory stimulus inducing an increase of intracellular $Ca^{2+}$ levels.[194, 195] In the case of prostanoids (**Figure 1.5A**), AA is converted to PGH$_2$ by COX-1/2, in a process that requires two successive steps: firstly, AA is oxidized to generate endoperoxide PGG$_2$ in the cyclooxygenase site of the COXs, and this AA-derived mediator is then reduced at the peroxidase site of COXs into PGH$_2$.[196] PGH$_2$ is very unstable[197] and is rapidly converted to PGD$_2$, PGE$_2$, PGF$_{2\alpha}$, PGI$_2$ (prostacyclin) and TXA$_2$ (thromboxane), depending on the expression of specific terminal enzymes of the biosynthetic pathway.[198, 199]

Among the three PGE$_2$ synthases, cPGES and mPGES-2 are constitutively expressed, whereas mPGES-1 is an inducible isoform[200, 201] specifically coupled with COX-2.[202, 203] Low but constitutive expression of mPGES-1 is ubiquitous, but its level is up-regulated in response to various inflammatory stimuli and mediators, for example, cytokines (LPS, IL-1β and TNF-α).[204-207] Identification of mPGES-1 was reported in 1999 by Jackobsson *et al.*,[208] who recognized it as a member of the Membrane-Associated Proteins in Eicosanoid and Glutathione Metabolism (MAPEG) family,[209] which includes five additional proteins (MGST1, MGST2, MGST3, FLAP, LTC4S).[210, 211]

The first high resolution X-ray crystal structure of mPGES-1 in the active conformation was described by Sjögren *et al.*[212] in 2013, who revealed that the protein is a membrane homotrimer with three active sites partially occupied by the cofactor (glutathione, GSH). The asymmetric monomer is characterized by four-helix, and each active site is oriented toward the cytoplasmic part of the protein, in particular between N-terminal parts of helix II and IV of a monomer and the C-terminal part of helix I and the cytoplasmic domain of the adjacent monomer (**Figure 1.5B**). This protein folding generates a pronounced deep active site occupied by GSH, and in the outer part, an extended groove between helix I of a monomer and helix IV of the adjacent monomer is observable (**Figure 1.5C**). Sjögren *et al.*[212] also proposed a mechanism for

PGH$_2$ isomerization to PGE$_2$ mediated by the GSH cofactor (**Figure 1.5A**). According to this suggested mechanism, Ser127 activates the thiol function of GSH to form a thiolate anion that exerts a nucleophilic attack on the endoperoxide oxygen atom of PGH$_2$, producing an unstable intermediate. Subsequently, Asp49 mediates the abstraction of the proton at C-9 followed by the cleavage of S-O bond, which results in the regeneration of GSH and in the formation of PGE$_2$.
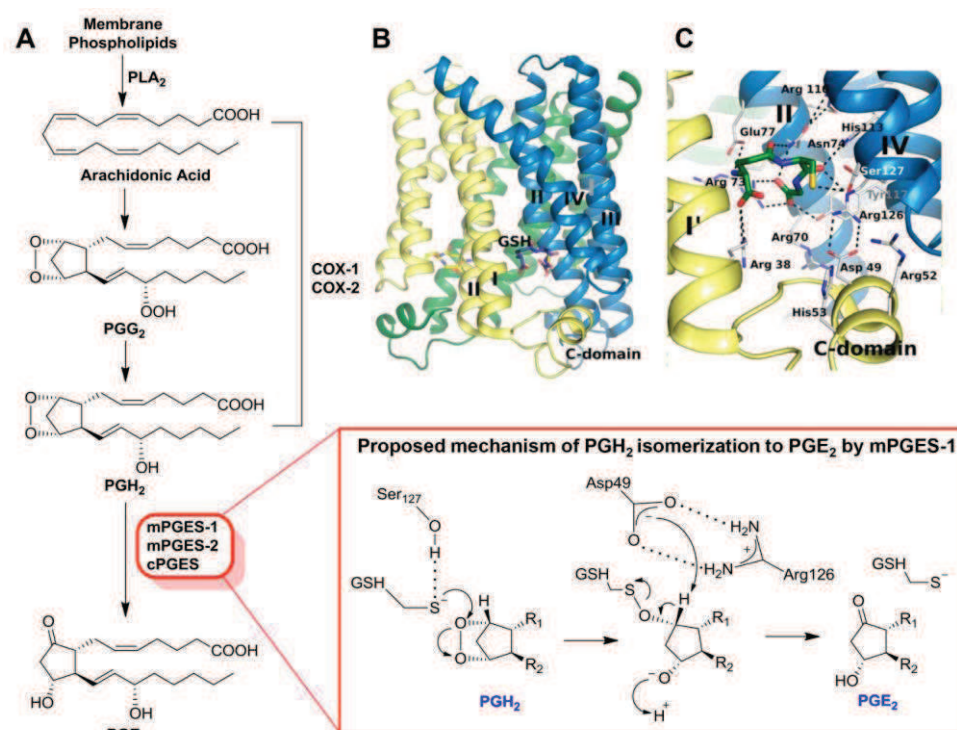


**Figure 1.5** *Biosynthetic pathway of PGE$_2$ and structure of mPGES-1. (A) PGE$_2$ biosynthesis and proposed mechanism of PGH$_2$ isomerisation by mPGES-1, as reported by Sjörgen et al.[212] (B) Overall structure of mPGES-1. (C) Interaction of mPGES-1 with the cofactor (GSH).*

**A**

IC$_{50}$ (cell-free) = 0.007 μM
no inhibitory activity in HWB assay

**B**

IC$_{50}$ (cell-free) = 0.001 μM
IC$_{50}$ (HWB) = 1.3 μM

**C**

IC$_{50}$ (cell-free) = 0.001 μM
IC$_{50}$ (HWB) = 1.6 μM

**D**

IC$_{50}$ (cell-free) = 0.2 μM
IC$_{50}$ (HWB) = ND

**E**

IC$_{50}$ (cell-free) = 0.002 μM
IC$_{50}$ (HWB) = 2.1 μM

**F**

IC$_{50}$ (cell-free) = 0.016 μM
IC$_{50}$ (HWB) = 5 μM

**G**

IC$_{50}$ (cell-free) = 0.031 μM
IC$_{50}$ (HWB) = ND

**H**

IC$_{50}$ (cell-free) = 2.1 μM
IC$_{50}$ (HWB) = ND

**I**

IC$_{50}$ (cell-free) = 0.68 μM
IC$_{50}$ (HWB) = ND

**J**

IC$_{50}$ (cell-free) = 0.016 μM
IC$_{50}$ (HWB) = 5 μM

**K**

IC$_{50}$ (cell-free) = 0.009 μM
IC$_{50}$ (HWB) = 0.7 μM

**L**

IC$_{50}$ (cell-free) = 0.003 μM
IC$_{50}$ (HWB) = 0.1 μM

**Figure 1.6** *Some optimised scaffolds for mPGES-1 inhibition: (A) indole;[213] (B) phenanthrene imidazole;[214, 215] (C) biaryl imidazole;[216] (D) pirinixic acid;[217-219] (E) trisubstituted urea;[220] (F) oxicam;[221] (G) imidazoquinoline;[222] (H) arylpyrrolizine;[223] (I) 1,2,3-triazole;[224, 225] (J) 1,2,4-triazine;[226] (K) 1,2,4-triazole;[226] (L) benzoxazole.[227] HWB: human whole blood, ND: not determined.*

Traditional treatment of inflammation is based on the use of NSAIDs, which inhibit PGs production by blocking both COX-1 and COX-2. However, their incapability to discriminate between the two COXs is responsible for their gastric side effects,[228-230] mainly due to the massive inhibition of $PGE_2$ synthesis, which is known to have a protective effect on the gastrointestinal mucosa. In order to circumvent this undesired effect, selective inhibitors of the inducible COX-2 (COXibs) were developed.[231] However, they were shown to be associated with increased cardiovascular risk in patients after long-term treatments due to unbalanced levels of $PGI_2$ and $TXA_2$.[232-234]

In the light of the side effects connected to NSAIDs and COXibs, the development of inhibitory strategies, which specifically target the downstream PGs synthases, is the current goal of research in the modulation of AA inflammatory cascade. In particular, inhibitors of mPGES-1 are expected to manifest reduced adverse effects, by better maintaining the gastric mucosa integrity compared to traditional NSAIDs and by avoiding increased incidence of cardiovascular side effects related to COXibs. Modulation of mPGES-1 may not be associated with the perturbations in $PGI_2$ and $TXA_2$ metabolism, as indicated by Cheng *at al.*,[235] who reported that mPGES-1 deletion does not result in hypertension or predisposition to thrombosis in normolipidemic mice, differently from deletion, disruption or inhibition of COX-2.

Inhibition of mPGES-1 offers a wide range of opportunities for therapeutic application. The potential use of mPGES-1 inhibitors is not limited to inflammatory condition, since mPGES-1 plays a crucial role in various phatological conditions such as pain,[236, 237] fever,[238] rheumatoid arthritis,[239, 240] cardiovascular diseases,[241] cancer.[242-245] The impact of mPGES-1 in tumours is particularly relevant, as it results overexpressed in a number of neoplasias, including gastrointestinal cancers (esophageal, gastric, colorectal, liver and pancreatic cancer),[246-251] brain cancers (glioma and medulloblastoma),[252, 253] breast cancer,[254] thyroid cancer[255] and several cancers derived from epithelium

(head and neck, penis, lungs, larynx, cervix, endometrium and ovary).[256-261] Elevated levels of mPGES-1 correlate with a worse prognosis in late stages of colorectal cancer,[262] suggesting that this synthase may play a key role in cancer progression. Moreover, mPGES-1-derived $PGE_2$, in cooperation with vascular endothelial cell growth factor (VEGF), seems to play a critical role in the development of inflammatory granulation and angiogenesis.[263] Indeed, mPGES-1 deficiency has been well documented to be associated with reduced induction of VEGF in the granulation tissue.[237]

Despite the numerous potential applications in therapy and even though many companies and academic groups have worked to develop mPGES-1 inhibitors (**Figure 1.6**),[264] since the discovery of this MAPEG member in 1999, no clinical trials have been reported yet. This can be ascribed to the poor in cell potency of many identified inhibitors, even though they showed very high and selective inhibitory potency on the recombinant human enzyme (**Figure 1.6**).[265] An additional problem is sequence dissimilarity of mPGES-1 isoforms in the diverse species, as first described by Merck scientists.[215] For example, potent inhibitors against the human enzyme may partially or completely lose potency against the rat isoform, mainly due to the variation between human and rat mPGES-1 in three individual amino acids located in transmembrane helix IV, which play a crucial role as gatekeepers for the active site of mPGES-1, regulating the access of an inhibitor in the enzyme. In the human enzyme, these residues are rather small (Thr131, Leu135 and Ala-138) but in the rat isoform they are bulkier or aromatic (Val131, Phe135 and Phe138), and thereby prevent the access to inhibitors for steric hindrance reasons.[266] Similar bulky/aromatic residues are found also in mouse ortholog, but not in the guinea pig enzyme, suggesting the use of this specie as an animal model in pre-clinical studies.[215]

Although better results in terms of cellular activity have been obtained for some of the optimised templates (**Figure 1.6**) and, despite in few cases *in vivo*

studies displayed promising effects,[219, 227] none of these compounds has entered clinical trials yet. Despite the challenging problems connected with the exploration of the biological target, selective inhibition of mPGES-1 might represent a promising approach for the design of effective anti-inflammatory drugs lacking the severe side effects related to the classic use of NSAIDs. However, whether mPGES-1 inhibitors are less afflicted with side effects and can achieve the same therapeutic efficiency of COX inhibition remains to be thoroughly investigated.[267] In this context, the development of new selective mPGES-1 inhibitors is highly desirable in order to fully clarify this issue.

## 1.5 Heat shock protein 90 (Hsp90)

The key role of the molecular chaperone family of proteins is to prevent protein aggregation, to assist the maturation and folding of proteins and to generally maintain protein homeostasis (proteostasis).[268-272] According to a general definition, a molecular chaperone is any protein that interacts, stabilizes and assists a client protein in the acquisition of its functional conformation. Heat shock proteins (HSPs) are highly conserved chaperones, classified according to their molecular weights (small HSPs (<40 kDa), Hsp40, Hsp60, Hsp70, Hsp90, and Hsp100) which can be localized in cytosol, mitochondria or in endoplasmic reticulum.[273] Among them, Hsp90 is of particular interest as it is extremely conserved from bacteria to eukaryotes and is one of the most abundant proteins in the cell, thus confirming its key role in maintaining protein homeostasis.[272, 274, 275] Hsp90 represents 1–2% of total cytosolic proteins in non-stressed eukaryotic cells, and its level can increase up to 4–6% in stressful conditions.[276-278] Its expression is up-regulated as a consequence to external and cellular stress including infections, heat, drugs, fever, oxidative stress, inflammation, hormonal stimulation, and cancer.[279-281] The two major Hsp90 isoforms are found in the cytoplasm and correspond to the inducible Hsp90α and the constitutive Hsp90β.[282] In addition, two non-

cytosolic forms are known, namely the Hsp75/tumor necrosis factor receptor associated protein 1 (Trap1) and the endoplasmic reticulum resident Hsp90 isoform, 94 -kDa gluclose-regulated protein (Grp94). The former resides in the mitochondrial matrix and is involved in oxidative cell death and in maintaining mitochondrial integrity,[283] the latter assists the folding of both secreted and membrane proteins and plays an eminent role in embryonic development, immune response, $Ca^{2+}$ balance, and cell adhesion.[284] Hsp90 client proteins belong to different families and do not share any apparent functional or structural similarities.[285, 286] A common feature may be their intrinsic instability and the conformational changes required in order to achieve their functional state. To date, more than 300 proteins are known whose maturation is regulated by Hsp90.[287]

Hsp90 offers important therapeutic opportunities. Its inhibition by cytotoxic agents induces the degradation of client proteins which are subsequently addressed to ubiquitinylation-mediated proteasomal degradation (**Figure 1.7**).[288-290] Compounds that exhibit such effect have excellent therapeutic potential as anticancer drugs, as multiple signalling pathways involved in pathologies can be modulated.[291, 292] On the other hand, non-toxic compounds inducing the expression of chaperone levels showed to reduce the accumulation of aggregated proteins, suggesting promising application against neuronal disorders (**Figure 1.7**).[293-296]

Hsp90 is overexpressed in many human cancers and plays a relevant role in the progression of malignancy, as its level in cancer cells can be increased up to 10-fold than in normal cells.[297-300] Malignant cells are dependent on its chaperoning function, mainly due to the adverse microenvironment (hypoxia, low pH and poor nutritional status)[300] which results in an altered state of cellular proteins, consequently requiring a higher production of Hsp90 for repairing degraded proteins[280, 301]. Hsp90 prevents aggregation and misfolding

of overexpressed and mutated client oncoproteins, e.g., ErbB2, Akt, p53, Bcr-Abl, Her-2, Cdk4, Cdk6, Raf-1, v-Src, MET, telomerase and survivin.[302-304]
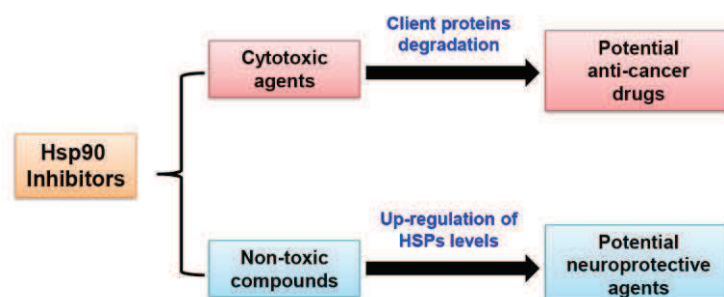


**Figure 1.7** *Therapeutic opportunities for Hsp90 inhibitors*

Hsp90 represents an exciting therapeutic target for the treatment of cancer and its inhibition allows for a combinatorial attack on transformed cells through the disruption of various signalling pathways.[305, 306] Indeed, disruption of the Hsp90 protein folding machinery directly affects all hallmarks of cancer, by preventing maturation of proteins directly associated with each hallmark (**Figure 1.8A**).[291, 307, 308] No other cellular protein has been ascribed to affect all cancer hallmarks, thus making Hsp90 one of the most promising targets for anti-tumour therapy at this time.[309]

In addition, Hsp90 is an investigated target also for neurodegenerative diseases, derived from cell death in the central nervous system such as Alzheimer's, Huntington's, and Parkinson's disease.[310] The reason for neuronal cell death in these pathologies can be ascribed to a variety of factors, but an important general aspect is the accumulation of misfolded proteins responsible for cytotoxicity. The rationale behind targeting Hsp90 in neurological disorders is based on the principle that non-cytotoxic small molecule inhibitors of this chaperone can up-regulate the expression of heat shock proteins through the induction of the heat shock response mechanism, which ultimately leads to solubilisation of protein aggregates and refolding of misfolded proteins.[311]

Particularly relevant is also the emerging role of Hsp90 in innate immunity, evidencing the deep connection between cellular stress and inflammation.[312] The common player is again the transcription factor NF-κB, as Hsp90 is required for IκB kinase (IKK) biogenesis, homeostasis and activation.[313-315] Inhibition of NF-κB pathway is observed upon treatment with the Hsp90 N-terminal inhibitor geldanamycin, suggesting the potential to prevent cancer development during chronic inflammation.[316, 317] Moreover, the inhibitor SNX-7081 blocked nuclear translocation of NF-κB and strongly inhibited cytokines production in animal models of rheumatoid arthritis,[318] modulation of Hsp90 function by radicicol attenuated intestinal inflammation,[319] while 17-DMAG reduced inflammation in macrophages by suppressing Akt and NF-κB pathways[320] and also attenuated inflammatory responses in atherosclerosis.[321] The relationship between inflammation and chaperones is revealed also by Hsp90 involvement in endotoxin-induced uveitis,[322] inflammatory myopathies,[323] inflammatory bowel disease,[324, 325] gastric inflammation and ulcer healing,[326, 327]colitis,[328] liver injury,[329] autoimmune encephalomyelitis,[330] and inflammatory microenvironment associated with cancer prostate.[331]

Structurally, Hsp90 functions as a dimer, with each monomer consisting of an N-terminal ATP-binding domain, a middle domain, and a C-terminal dimerisation domain (**Figure 1.8B**).[332] The N-terminal site triggers the conformational change of the protein through ATP hydrolysis, supplying the required energy for the chaperoning function;[333] the middle domain regulates client protein interactions and interacts with the γ-phosphate of ATP;[334] the C-terminal contains a second nucleotide binding region,[335-337] which does not exhibit ATPase activity, and is involved in the control of Hsp90 conformational rearrangement and in the binding of co-chaperones through a conserved pentapeptide sequence (MEEVD).[338] In addition, a dimerisation motif, implicated in the functional switch between the open and closed protein conformation, is present at the C-terminus.[339]
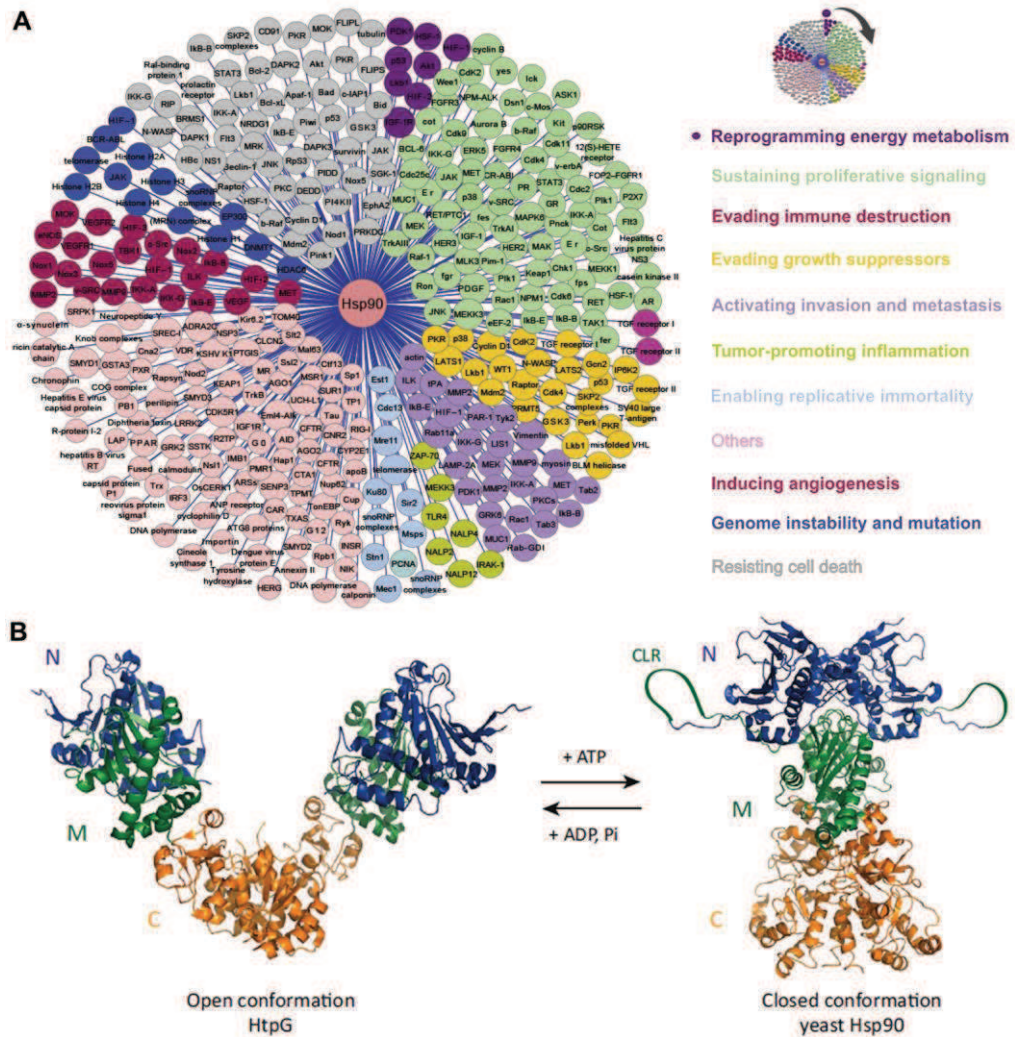
**Figure 1.8** *Hsp90 client proteins and structure of the Hsp90 dimer. (A) Involvement of Hsp90 client proteins in cancer hallmarks. (B) Hsp90 switch between open and closed conformation upon ATP binding.*

In the absence of ATP, Hsp90 adopts an open conformation.[340] Upon nucleotide binding, the N-terminal domain closes over the bound nucleotide and the two N-terminal domains of the dimer subsequently associate.[341] A flexible loop of the middle domain interacts with the ATP-binding pocket of the N-terminal domain resulting in a twisted, closed conformation of Hsp90 and in ATP hydrolysis.[342] In the final step of its chaperoning cycle, Hsp90 switches back to the open conformation and the hydrolyzed nucleotide is

released (**Figure 1.8B**). In this process, Hsp90 interacts with a number of co-chaperones which also mediate the maturation of client proteins.[343, 344]

Hsp90 contains several small molecule binding sites. The N-terminal ATP region has been the most extensively investigated, while less is known about the binding sites in the C-terminal and middle domains. The most common Hsp90 inhibitors bind competitively to the N-terminal domain and they include both natural products such as geldanamycin (GDA) and radicicol (RDC), and synthetic compounds such as GDA and RDC derivatives, purine-based molecules, benzamide- and resorcinol-containing inhibitors.[345, 346]

A number of clinical trials have been initiated from 1999 in order to evaluate the potential use of Hsp90 N-terminal inhibitors in cancer.[347, 348] Although some N-terminal inhibitors are still under clinical investigation,[349-352] many trials have failed due to toxicity issues and to the occurrence of resistance against these agents,[353-355] mainly associated with the induction of the deleterious heat shock response.[356, 357] A strategy to circumvent this problem may be to target the less-explored Hsp90 C-terminal domain, as its modulation does not trigger the undesired heat shock response.[358, 359] Potential Hsp90 C-terminal inhibitors, in fact, may maintain the anti-proliferative activity, without being associated with the side effects reported for N-terminal modulators and representing thus promising candidates for drug development.[360, 361] However, only poor structural information on Hsp90 C-terminus are currently available representing a strong limitation for rational design of selective inhibitors. While the binding mode of Hsp90 N-terminal inhibitors has been well characterized by X-ray crystallography, there is no reported co-crystal structure of its C-terminal domain with any inhibitor.

The natural coumarin antibiotic novobiocin was identified as the first Hsp90 C-terminal inhibitor,[362] followed by its analogues chlorobiocin and coumermycin A1 (**Table 1**). Novobiocin's binding site is located at the C-terminal region of the chaperone containing amino acids 538-728.[362, 363]

Mechanistically, the binding of novobiocin to Hsp90 induces a conformational change of the protein that is dissimilar from that induced by N-terminal inhibitors.[336, 364] For instance, novobiocin was shown to protect Hsp90α from cleavage with proteolytic enzymes in correspondence of two main sites at the C-terminus (Arg400 and Lys615/Arg620) and of a minor site at middle domain;[364, 365] moreover, it prevents binding of TPR-containing co-chaperones to the C-terminal MEEVD motif.[366] Given the weak interaction of novobiocin with Hsp90 C-terminus ($IC_{50}$ = 700 μM in SKBr-3 breast cancer cells),[362, 363] a number of structural analogues (novologues) have been synthesized and have exhibited a significant improved potency (**Table 1**).[367-370] Other inhibitors of the Hsp90 C-terminal domain include epigallocatechin gallate (EGCG),[371, 372] cisplatin,[373] taxol[374] and sansalvamide A derivatives[375-377] (**Table 1**).

Further strategies to circumvent the liabilities of N-terminal inhibitors may be the development of isoform-selective inhibitors[378-380] or modulators that work by alternative mechanisms, for example, co-chaperone disruptors.[381-383] Even though more challenging, the modulation of Hsp90 through the inhibition of its C-terminal domain, together with the other alternative strategies, may allow to develop new potential effective anticancer drug candidates, that are expected to be free from side effects connected with the use of traditional N-terminal binders.

**Table 1** *Known Hsp90 C-terminal inhibitors and their optimised analogues.*

| Lead compound | Optimised derivatives | Ref. |
|---|---|---|
|  **Taxol** | – | 361, 374 |
|  **Cisplatin** | – | 361, 373 |
|  **(-)-Epigallocatechin-3-gallate** $IC_{50}$ (MCF-7) = 74.4 $\mu$M $IC_{50}$ (SKBr3) = 100.16 $\mu$M |  $IC_{50}$ (MCF-7) = 13.10 $\mu$M $IC_{50}$ (SKBr3) = 15.42 $\mu$M  $IC_{50}$ (MCF-7) = 3.99 $\mu$M $IC_{50}$ (SKBr3) = 21.45 $\mu$M | 371, 372, 384 |
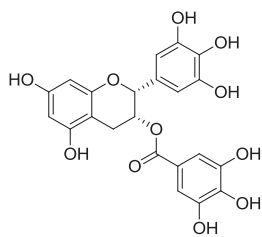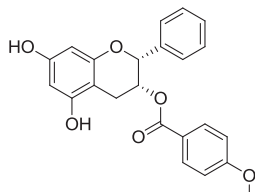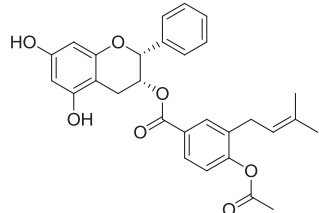
IC$_{50}$ (SKBr3) = 0.5 μM



IC$_{50}$ (SKBr3) = 0.8 μM
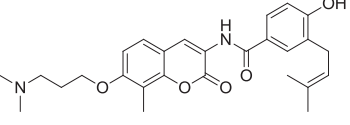


IC$_{50}$ (SKBr3) = 0.4 μM
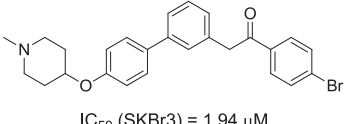


IC$_{50}$ (SKBr3) = 1.94 μM
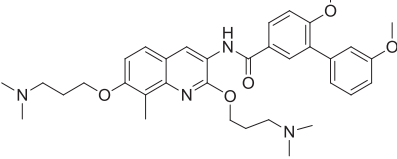


IC$_{50}$ (SKBr3) = 0.34 μM
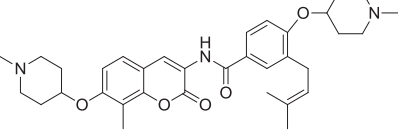


IC$_{50}$ (SKBr3) = 0.21 μM
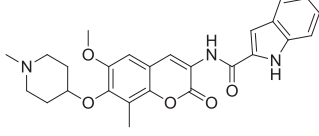


IC$_{50}$ (SKBr3) = 0.11 μM
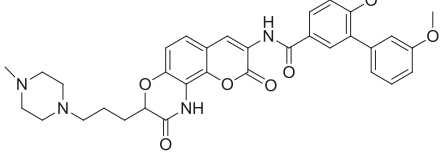


IC$_{50}$ (SKBr3) = 0.2 μM

363,
367-
370,
385-
389



**Novobiocin**
IC$_{50}$ (SKBr3) = 700 μM



**Chlorobiocin**
IC$_{50}$ (SKBr3) = 60 μM



**Coumermycin A1**

IC$_{50}$ (SKBr3) = 70 μM

**Sansalvamide A**
(Hsp90 allosteric modulator)

IC$_{50}$ (mean against the NCI
cell line panel) = 27.4 $\mu$M

IC$_{50}$ (HCT-116) = 7.4 $\mu$M

IC$_{50}$ (HCT-116) = 5.0 $\mu$M

IC$_{50}$ (HCT-116) = 2.9 $\mu$M

375-
377,
390,
391

## 1.6 Workflow of the research project

The main goal of the present PhD research project has been the design, synthesis and biological evaluation of new inhibitors able to interfere with the activity of three relevant biological targets, involved both in cancer-related and inflammatory processes.

The general method employed in this study can be described through these main steps:

1. design of potential inhibitors of the target protein through fragment-based design, structure-based design, ligand-based design;

2. chemical synthesis of compounds selected by computational analysis or driven by structure-based approach;

3. biological evaluation and individuation of possible hits or lead compounds;

4. rationalisation of ligand/protein interaction by crystallographic or computational methods;

5. structural optimization of the identified lead compound in order to improve its biological profile.

Concerning step 1, fragment-based, structure-based and ligand-based approaches were used for the identification of a scaffold able to interfere with the target of interest. In more details, the 9*H*-purine and the 3,4-dihydropyrimidin-2(1H)-one (DHPM) cores have been disclosed to appropriately fit with the receptor counterparts. These chemical templates are considered "privileged scaffolds" in medicinal chemistry being endowed with relevant biological activities and, when appropriately decorated, they can selectively modulate diverse receptors, channels or enzymes responsible for a wide range of pharmacological effects.[392, 393]

With respect to step 2, suitable synthetic procedures have been employed and optimized in order to successfully obtain the desired compounds. For the synthesis of 6-aryl-9*H*-purine derivatives, a suitable strategy to overcome the necessity of a N9-protecting group[394] in the Suzuki-Miyaura cross-coupling has been exploited. Indeed, the use of microwave irradiation and an appropriate aqueous solvent systems allowed to perform the Suzuki coupling by using boronic acids directly on the 6-halo-9*H*-purine precursors, at high yields and in short reaction times (**Scheme 1.1**).[395] Concerning the synthesis of N9-alkylated purines, it is generally accomplished through the Mitsunobu reaction with alcohols[396] or by strong basic conditions (NaH, $K_2CO_3$) with a variety of alkyl and benzyl halides.[397] However, these reactions require long times (4–48 h), low temperatures for the Mitsunobu conditions or high temperatures for the basic conditions, and an inert atmosphere (**Scheme 1.2**).[398] In our case, an alternative approach was employed, by using

tetrabutylammonium fluoride (TBAF) and alkyl halides at room temperature, a mild and efficient procedure that enabled to easily and rapidly accomplish the synthesis of N9-alkylpurines (**Scheme 1.2**).[399]

**Scheme 1.1** *Synthesis of 6-aryl-9H-purines by the Suzuki–Miyaura cross-coupling.*
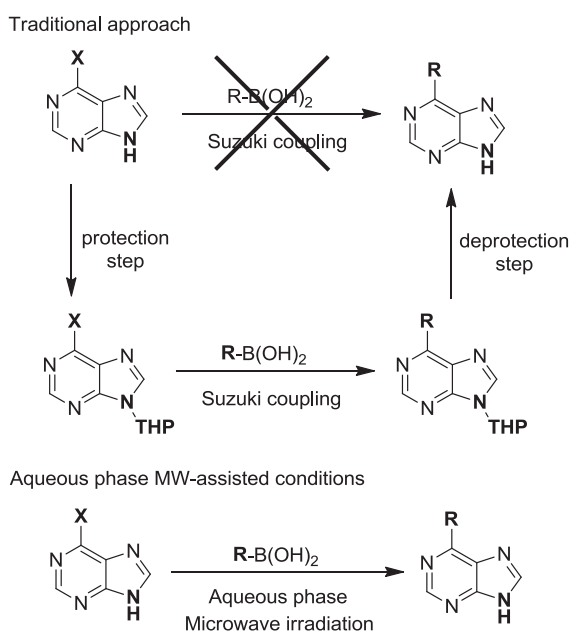


**Scheme 1.2** *Preparation of 9-alkylpurines.*
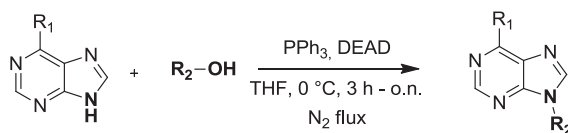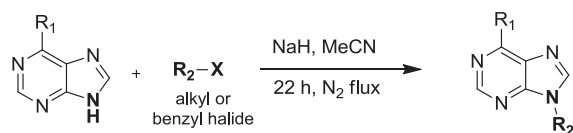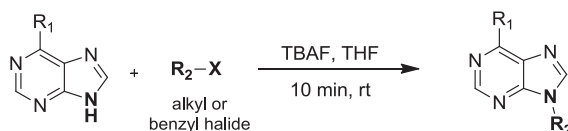
Regarding the DHPM core, it can be efficiently obtained by the well-known Biginelli reaction, a one-pot acid-catalyzed condensation of three components (urea, benzaldehyde and ethyl acetoacetate) that was first reported by the Italian chemist Pietro Biginelli in 1893 (**Scheme 1.3**). In the last decades, several procedures have been reported, replacing the traditional use of strong Brønsted acids[400-402] with different Lewis acids such as $FeCl_3$,[403] $LaCl_3$,[404] $Cu(OTf)_2$,[405] $SnCl_2$,[406] $InCl_3$,[407] $Yb(OTf)_3$,[408] TMSCl.[409] The use of phase-transfer catalyst,[410] ionic liquids,[411, 412] solvent-free conditions,[413] polymer supported catalyst,[414] solid-phase approaches,[415] asymmetric synthesis[416] have also been described. In addition, several high-speed microwave-assisted methods for the generation of diverse DHPM collections were developed in order to enhance product yield and reduce reaction time.[417-421] In our case, DHPMs have been obtained through a protocol of the Biginelli reaction promoted by chlorotrimethylsilane (TMSCl)[422] and microwave-irradiation.

**Scheme 1.3** *The Biginelli multicomponent reaction between benzaldehyde, urea and ethyl acetoacetate, as reported by Pietro Biginelli.*
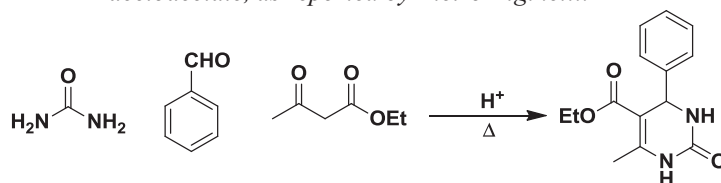


Concerning step 3, biological evaluation of the synthesized compounds has been accomplished using suitable assays for each of the three investigated targets, e.g., thermal shift and isothermal titration calorimetry (ITC) assays in the case of BRDs, a cell-free assay using the microsomal fraction of interleukin-1β-stimulated human A549 cells to evaluate the effect of compounds on mPGES-1 activity, and finally Surface Plasmon Resonance (SPR), cytotoxicity and western blot assays in the case of Hsp90.

Regarding step 4, the rationalization of ligand/protein interaction has been performed using the support of X-ray crystallography and docking studies.

Lastly, the structure optimization step has required structure-based approaches that allowed to perform focused chemical modifications on the emerged lead molecule in order to improve its biological profile.

# RESULTS AND DISCUSSION

# -CHAPTER 2-

Induced-fit pocket plasticity of the BRD9 bromodomain

upon binding to 9*H*-purine inhibitors.

## 2.1 Background

A number of medicinal chemistry studies have been addressed to target bromodomains, in particular BET proteins, with the aim of identifying novel scaffolds as mimetics of acetylated lysine (Kac), the natural substrate of these conserved protein modules. Phenotypic screening, fragment-based and molecular docking approaches were shown to be successful tools for the discovery of Kac-mimetics, as they enabled to find a number of new chemotypes, including 3,4-dimethylisoxazoles,[423, 424] 3-methyl-3,4-dihydroquinazolinones,[425] indolizinethanones, N-phenylacetamides and N-acety-2-methyl-tetrahydroquinolines,[149] triazolopyrimidines, methylquinoline and chloropyridones,[426] thiazolidinones,[152] 4-acylpyrroles[158] and triazolophtalazines[427] (**Figure 2.1**).
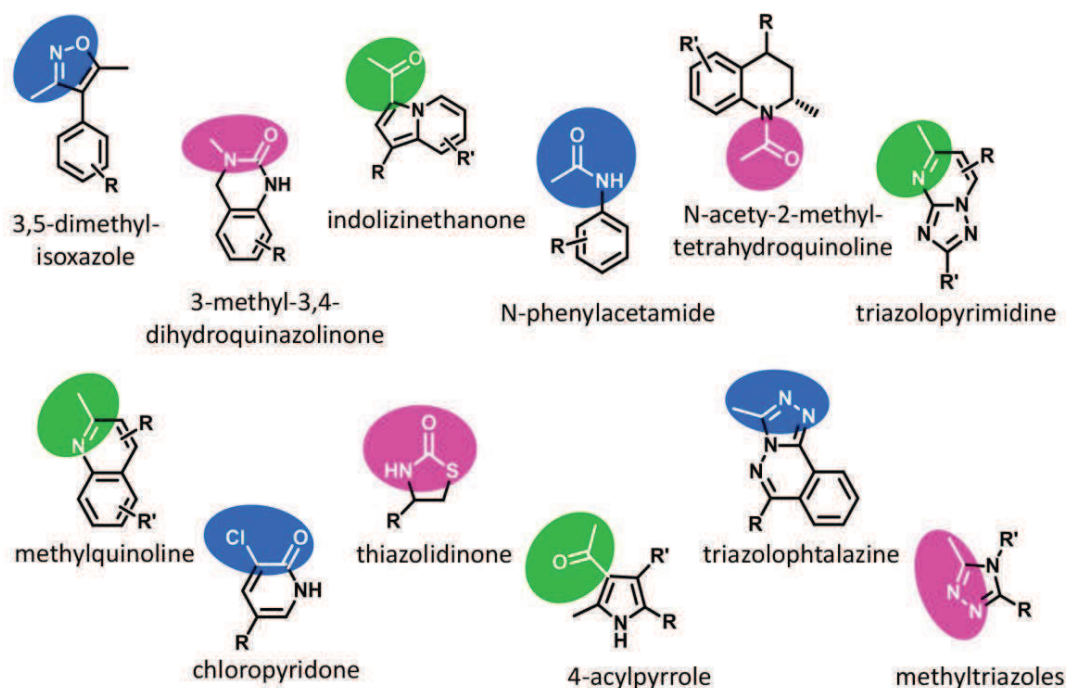


**Figure 2.1** *Acetyl lysine (Kac) mimetic templates reported to bind to bromodomain proteins. The Kac mimetic portion of each substructure is highlighted in colored circles.*

Kac-mimetic fragments allowed to develop potent and selective BET inhibitors,[151, 154] suggesting that it is possible to identify new BRD modulators

*via* initial fragment screening. In addition, fragment based approaches also allowed the discovery of new scaffolds able to modulate BRDs outside the BET family, such as CREBBP/p300,[142] ATAD2,[145, 146] BAZ2B[147] and BRPF1.[144]

Recent results disclosed some kinase inhibitors as interesting compounds endowed with high affinity and selective binding to the BET BRDs.[140] Crystal structures with BRD4(1) revealed an acetyl-lysine mimetic binding of kinase inhibitors, without any significant distortion when compared to kinase complexes, indicating the possibility to develop dual inhibitors targeting both BRD and kinases at the same time. Interestingly, the cyclin-dependent kinase inhibitor dinaciclib was also identified as a binder of BRD4[428] suggesting thus that other inhibitors classes might be good starting points for the discovery of new BRDs inhibitors.

In light of the successful fragment-based approaches and their reliability for the discovery of BRDs inhibitors, the purine scaffold was chosen to evaluate its putative Kac mimetic character. Purine is a privileged chemical core, as it is one of the most abundant N-based heterocycle in nature,[429] and it is present in a number of currently approved drugs used for the treatment of cancer (6-mercaptopurine, 6-thioguanine), viral infections such as AIDS and Herpes (Carbovir, Abacavir, Acyclovir, Ganciclovir), hairy cell leukemia (Cladribine), and organ rejection (Azathioprine).[430]

Moreover, purine based compounds have emerged as reliable chemical-biology tools since they modulate a variety of biological targets involved in number of diseases. Some examples include their activity as microtubules (Myoseverin), 90-heat shock protein (PU3), sulfotransferase (NG38), adenosine receptor (KW-6002), and cyclin-dependent kinase (olomoucine, roscovitine) inhibitors.[393, 431]

## 2.2 9*H*-purines: new modulators of human bromodomains

In order to evaluate the binding of purine fragments to human BRDs, molecular docking experiments were initially performed employing the previously determined crystal structure of the complex of BRD4(1) with a 5-methyl-triazolopyrimidine ligand (PDB ID: 4MEN).[426] To this end, binding of purine fragments **1**, **2a** and **2b** (**Figure 2.2**) was investigated, seeking to determine acetyl-lysine competitive binding modes, within the BRD cavity, with promising predicted binding affinities, ideally establishing favorable interactions with residues implicated in acetyl-lysine peptide recognition. In order to verify a possible conformational change of the receptor's binding site cavity upon ligand binding, the Induced Fit docking protocol[432, 433] was employed (as implemented in the Schrödinger software package).
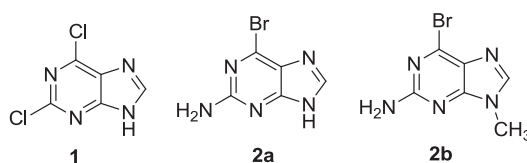


**Figure 2.2** *Purine fragments tested on human BRDs.*

Molecular modeling disclosed a good accommodation of the investigated purine fragments within the Kac binding site of BRD4(1), mainly packing between the ZA-loop hydrophobic residues (Val87, Leu92, Leu94) and Ile146 from helix C, in a groove that is capped, on one end by Tyr97, and Tyr139 and Trp81, on the other end (**Figure 2.3**). Different poses of compound **1** were observed within the BRD4(1) cavity, with the two chloro- functions pointing to the top of the pocket (**Figure 2.3A**) or adopting a Kac mimetic pose with one chlorine inserting deep into the pocket (**Figure 2.3B**). Compound **2a** was also found in two different states, either orienting its primary amine function away from the conserved asparagine (Asn140 – **Figure 2.3C**), or directly engaging this residue and orienting its 6-Br substituent towards the ZA-loop

(**Figure 2.3D/E**). In all cases, the ligand poses resulted in promising predicted binding affinity values (-9.13 kcal/mol for **1**, -9.95 kcal/mol for **2a**, and -9.13 kcal/mol for **2b**). In the case of compound **2a**, computational outcomes disclosed poses in which the halogen at position 6 resulted well exposed, suggesting thus the possibility to further optimise this fragment (**Figure 2.3D/E**). Contrariwise, the presence of the 2-Cl substituent or the methyl substituent at N9 (compounds **1** and **2b** respectively) resulted in steric clashes that would not allow for subsequent modifications. Given the multiple docking conformations observed, the purine scaffold was systematically investigated, employing synthetic chemistry and structure activity relationships, in order to better understand the binding mode of the this template to BRDs.

Fragments **1** (2,6-dichloro-9*H*-purine) and **2a** (2-amino-6-bromo-9*H*-purine) were purchased from commercial source, while compound **2b** was synthesized employing a TBAF-assisted N-9 methylation on the purine ring of **2a** (**Scheme 2.1**). A thermal shift assay ($\Delta T_m$ assay) was employed to confirm binding of these fragments to human bromodomains, in collaboration with dr. Panagis Filippakopoulos of the Structural Genomics Consortium (Oxford). This assay was previously used successfully with fragments and various bromodomains.[134, 156, 423, 434] It is usually performed using 100 μM of compounds in the case of fragments but, with **1**, **2a** and **2b**, binding was already detectable at 10 μM. In particular these purine fragments exhibited affinity for BET BRDs, especially BRD4(1), while the optimized CDK inhibitor olomoucine (**Figure 2.4A**) did not bind to any proteins in the panel (**Figure 2.4B**). This result encouraged a further investigation of these compounds, that were thus tested also against five other BRDs in order to cover most of the human BRD phylogenetic tree (**Figure 2.4C**). Interestingly, despite their structural diversity, the BRDs of CREBBP, PB1(5) and BRD9 exhibited weak binding.
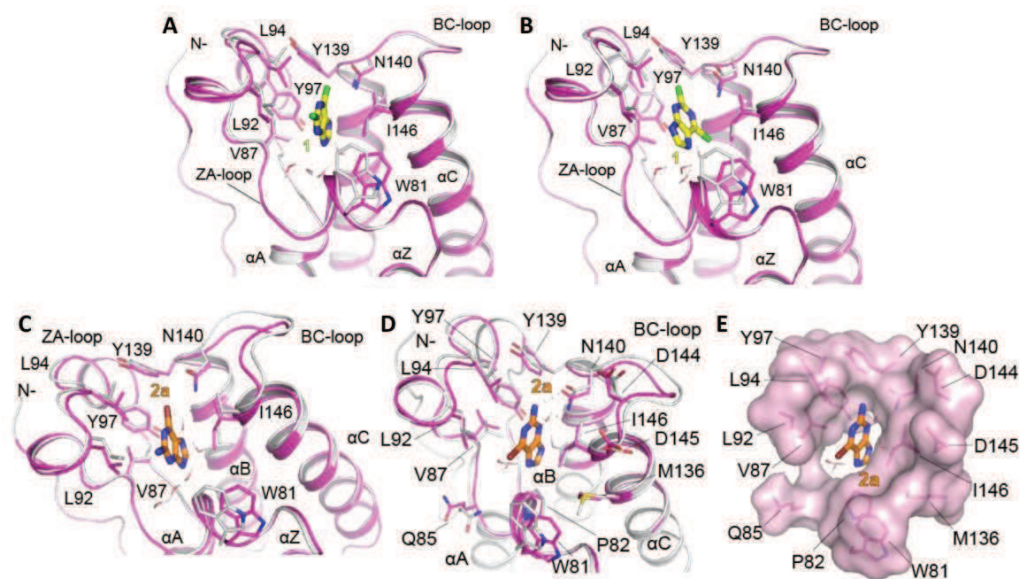
**Figure 2.3** *Induced-fit docking of fragments 1 and 2a in BRD4(1). (A) Docking pose of 1 (yellow sticks) into the bromodomain of BRD4(1). (B) Alternative binding of compound 1 in BRD4(1) with the 6-Chloro substituent adopting a Kac-mimetic pose. (C) Docking of fragment 2a (orange sticks) in BRD4(1). (D) Alternative docking of 2a into BRD4(1). The ligand adopts a Kac-mimetic pose, with the amine group directly engaging the conserved asparagine (N140). (E) Surface representation of BRD4(1) with compound 2a.*

A relevant outcome was obtained for fragment **2a** which showed affinity for BRD9. In fact, until now only few compounds were shown to bind to this domain such as some triazolo-phthalazines,[427] which exhibited cross-reactivity towards BET BRDs and CREBBP. BRD9 is a component of the SWI/SNF complex[435] and has been associated with a number of different cancer types, including non-small cell lung cancer,[436] cervical[437] as well as hepatocellular carcinoma.[438] Moreover, its BRD reader module has been frequently found mutated in lung squamous cell carcinoma, prostate adenocarcinoma as well as uterine corpus endometrial carcinoma.[439-441]

Hence, binding of **2a** onto BRD9 was investigated by induced fit docking, using the crystallized apo structure of the protein (PDB ID 3HME).[108] As in the case of BRD4(1), two main binding poses were obtained for this compound, with the most energetically favored one (predicted binding affinity = -9.06 kcal/mol) exhibiting an extended hydrogen bond network with the

conserved Asn100 and π-π interactions with the ZA-loop Tyr57 and Tyr106 from helix C, while the 6-Br substituent was oriented towards Phe47 of the ZA-loop, suggesting that modifications on this position would not be tolerated without affecting the ligand orientation in the acetyl-lysine cavity (**Figure 2.5A)**.



**Figure 2.4** *(A) Structures of fragments **1, 2a, 2b** and of the kinase inhibitor olomoucine. (B) Fragments were tested in a thermal shift assay against bromodomains of the BET subfamily as well as representative members from other families. (C) Phylogenetic tree of the human bromodomain family. Domains tested for fragments binding are annotated in bold typeface and are highlighted with a red star, covering most subfamilies of human BRDs.*

Nevertheless, an alternative binding pose was also disclosed (predicted binding affinity = -8.62 kcal/mol), in which the ligand maintained the hydrogen-bond to Asn100, and inserted its primary amine towards the conserved asparagine, establishing also a π- π interaction with Tyr106 from helix C, while orienting the modifiable 6-Br substituent towards the top of the BRD cavity (**Figure 2.5B**), offering a promising vector for subsequent modifications. On the basis of these initial findings, a number of 2-amino-9*H*-purine analogues were synthesized (**Figure 2.6**) and tested against human BRDs, primarily of the BET subfamily (sub-family II), but also against representative BRDs from other structural sub-families (family I: PCAF;

family III: CREBBP; family IV: BRD9; family V: BAZ2B; family VIII: PB1(5) – see **Figure 2.5C**) in order to probe structurally diverse proteins against this chemical template.
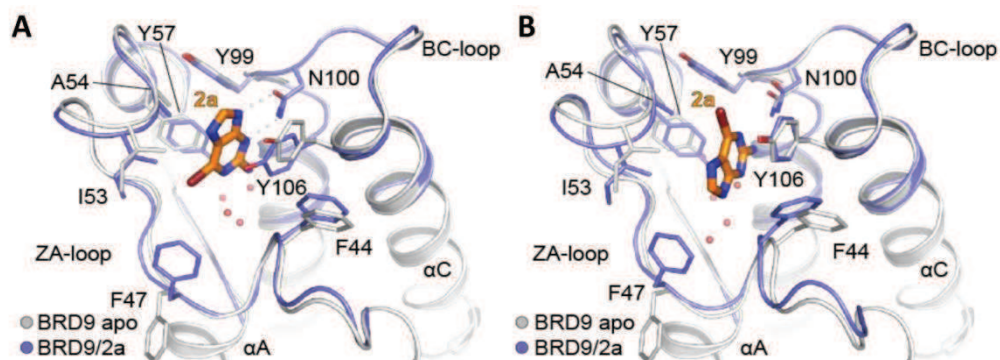


**Figure 2.5** *(A) Docking of compound **2a** (orange sticks) into the bromodomain of BRD9 (PDB ID: 3HME). The ligand adopts a Kac-mimetic pose as in the case of BRD4(1), directly engaging the protein at the conserved asparagine (Asn100) via N3 and N9 while sterically packing between the ZA-loop Ile53/Ala54 and F47/F44 at the front of the BRD cavity. (**B**) Alternative docking mode of **2a** in BRD9 inserting the primary function towards the conserved asparagine (Asn100) while retaining the steric packing within the ZA-loop residues.*

An aqueous-phase Suzuki-Miyaura cross-coupling reaction was employed to synthesize the 2-amino-6-aryl-9*H*-purine derivatives, yielding highly C-6 decorated 9*H*-purines, in a one step procedure, and a subsequent TBAF-assisted N-9 alkylation was performed to access N-9 substituted analogues (**Scheme 2.1).** The coupling step was accomplished under microwave irradiation with $Pd(OAc)_2$ and triphenylphosphine-3,3',3''-trisulfonic acid trisodium salt as the catalytic system, with $Cs_2CO_3$ as base, in a water-acetonitrile reaction solvent. This approach allowed the synthesis of 2-amino-6-aryl-9*H*-purines with very short reaction times (5-15 min), at high yields and purity (**Scheme 2.1**).
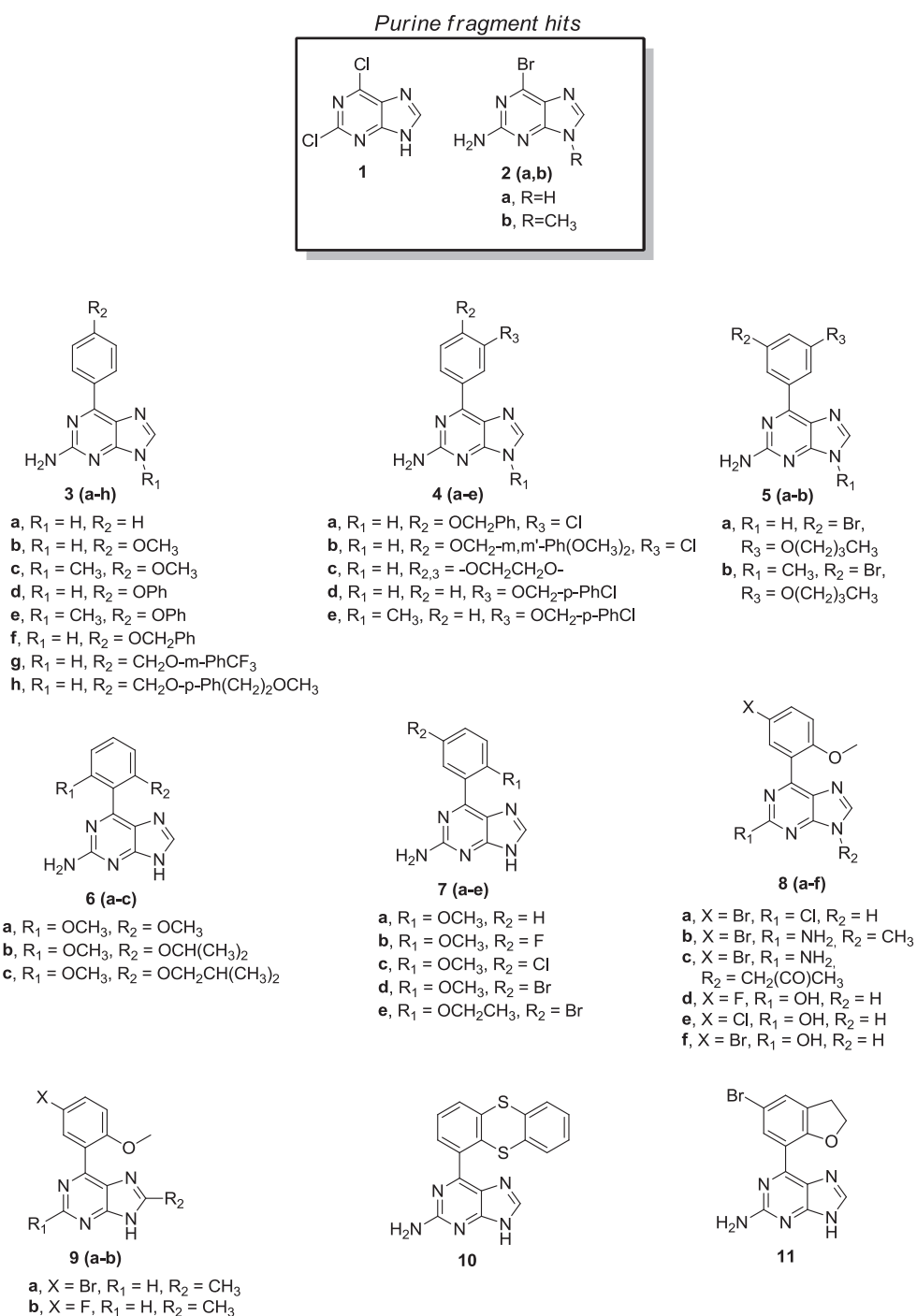
**Figure 2.6** *Chemical structures of compounds **1-11**.*

**Scheme 2.1** *General procedures for the synthesis of purine derivatives.*
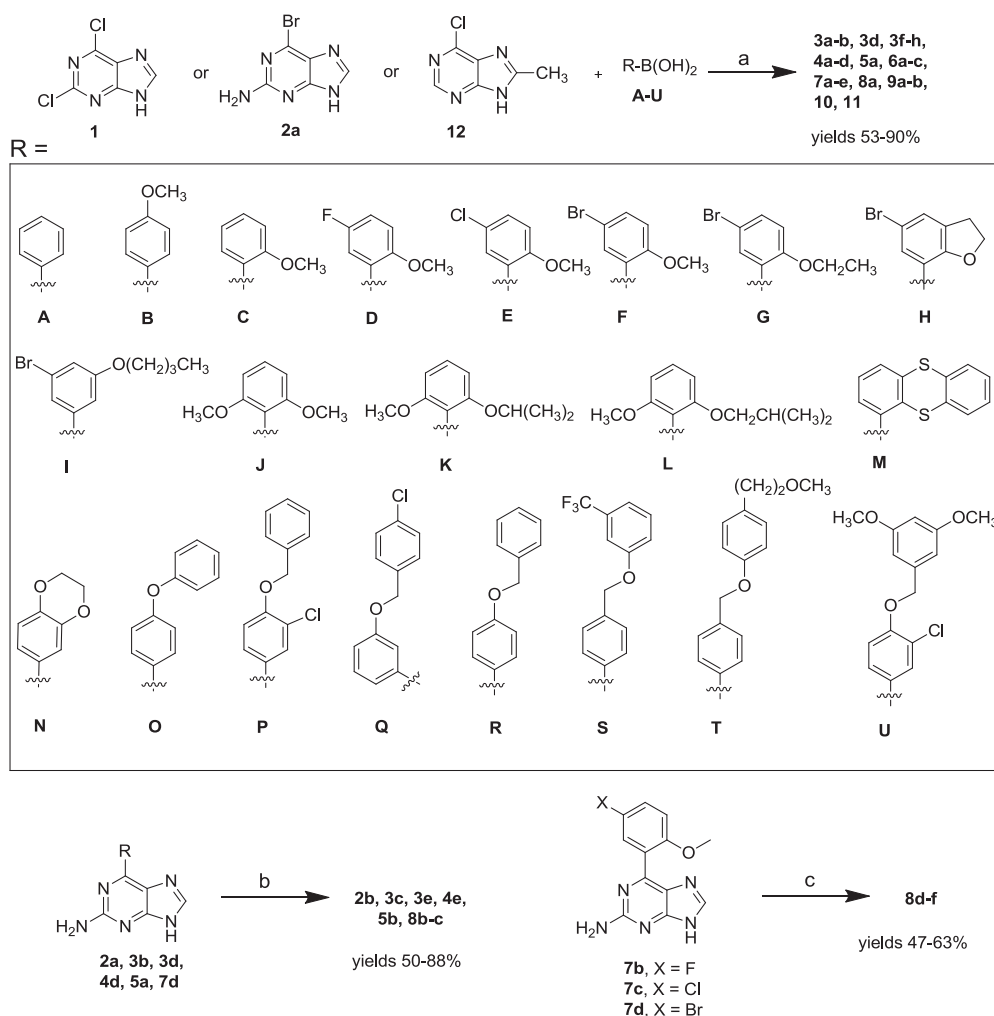


Reagents and conditions: (a) $Pd(OAc)_2/P(C_6H_4SO_3Na)_3$, $Cs_2CO_3$, $MeCN/H_2O$ (1:2), MW, 150 °C, 5-15 min; (b) $CH_3I$ or $CH_3COCH_2Cl$, TBAF, THF, rt, 10 min; (c) 50 % $H_2SO_4$, $NaNO_2$, -10 °C, 2 h, then 50 °C, 1 h.

First, an unsubstituted phenyl ring was introduced at position 6 of the core purine scaffold, leading to compound **3a** which was shown to stabilize BRD2(1), BRD4(1) and PCAF in thermal shift assays (**Figure 2.7A/B**). Binding to BRD4(1) was validated by isothermal titration calorimetry and a dissociation constant of 11.99 μM was measured (**Figure 2.7C** and **Table 2.1**). The lack of affinity of **3a** towards BRD9 in the $\Delta T_m$ assay was reputed an anomalous outcome, since the initial fragment hit, compound **2a**, had

exhibited a thermal shift of 1.6 ˚C towards that domain. **3a** was therefore tested also by isothermal titration calorimetry against BRD9 and a dissociation constant of 8.5 μM was measured (**Figure 2.7D**, **Table 2.2**) suggesting that the thermal shift assay may not be very robust in the case of BRD9 when applied to weak ligands.
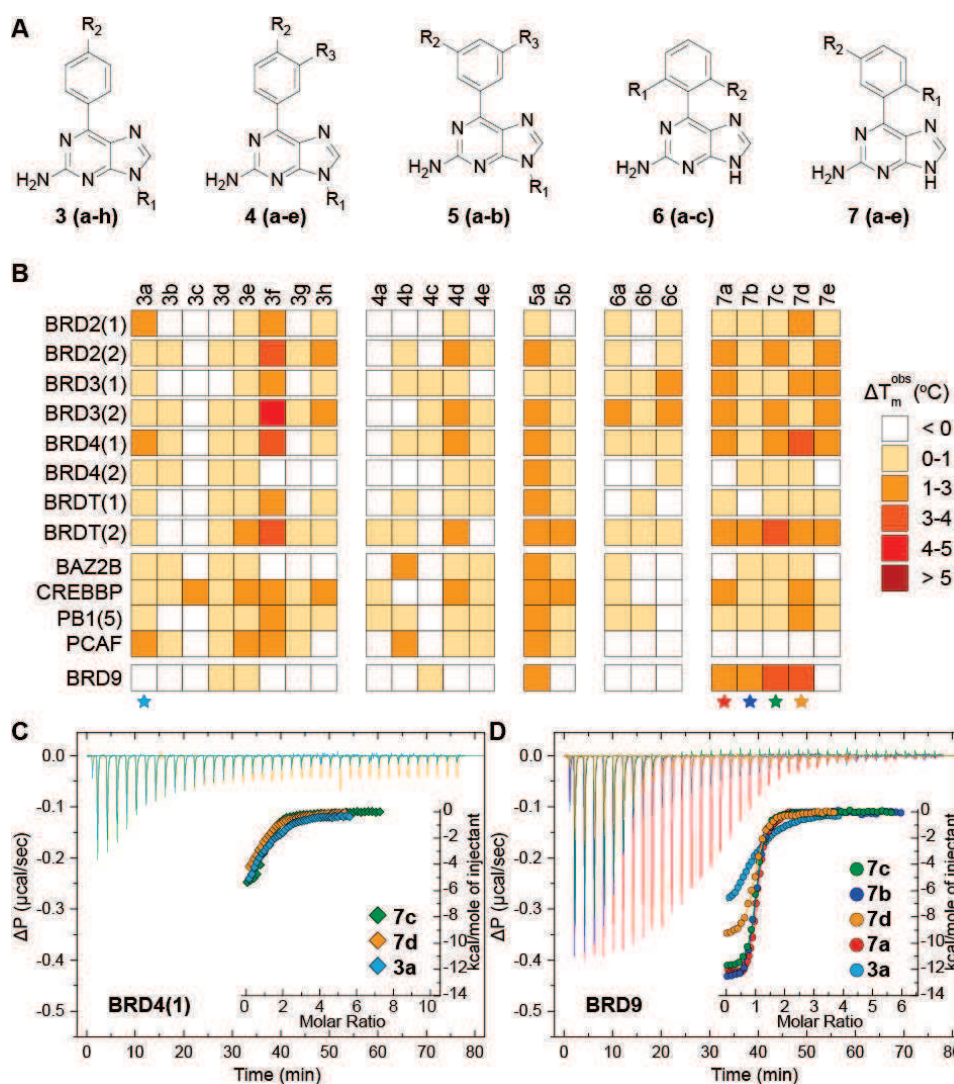


**Figure 2.7** *Decoration patterns explored in the first group of purine compounds and biological screening for binding to human bromodomains. (A) Substitution patterns explored. (B) Thermal shift assay against human bromodomains. Compounds highlighted with a colored star were further validated by isothermal titration calorimetry. (C) Isothermal titration calorimetry validation of key compounds binding to BRD4(1) showing raw injection heats for titrations of protein into compound. (D) Compounds bearing ortho,meta'- substitutions gain potency towards BRD9 as demonstrated by ITC experiments.*

**Table 2.1** *Isothermal Titration Calorimetry of human BRD4(1) with 9H-purines. Titrations were carried out in 50 mM HEPES pH 7.4 (at 25 ℃), 150 mM NaCl and 15 ℃ while stirring at 295 rpm. In both cases the protein was titrated into the ligand solution (reverse titration). Titrations were performed in triplicate. Ligand efficiencies (LE) have been calculated, where ΔG values were available (LE = ΔG/N, where N= number of non-hydrogen atoms (kcal/mol)).*

| Ligand | [P] (μM) | [L] (μM) | $K_D$ (nM) | $\Delta H^{obs}$ (kcal/mol) | N | TΔS (kcal/mol) | ΔG (kcal/mol) | LE |
|---|---|---|---|---|---|---|---|---|
| 2a | 680 | 15 | No binding/weak | | | | | |
| 3a | 402 | 16 | 11990 ± 743 | -9.45 ± 0.55 | 1.03 ± 0.049 | -2.97 | -6.48 | 0.41 |
| 7c | 485 | 14 | 2037 ± 118 | -6.21 ± 0.09 | 1.05 ± 0.012 | 1.29 | -7.50 | 0.39 |
| 7d | 307 | 12 | 4651 ± 197 | -6.09 ± 0.14 | 0.99 ± 0.018 | 0.94 | -7.03 | 0.37 |
| 11 | 382 | 30 | 1370 ± 29 | -6.39 ± 0.02 | 1.09 ± 0.002 | 1.34 | -7.73 | 0.39 |

**Table 2.2** *Isothermal Titration Calorimetry of human BRD9 with 9H-purines. Titrations were carried out in 50 mM HEPES pH 7.4 (at 25 ℃), 150 mM NaCl and 15 ℃ while stirring at 295 rpm. In both cases the protein was titrated into the ligand solution (reverse titration). Titrations were performed in triplicate. Ligand efficiencies (LE) have also been calculated where ΔG values were available (LE = ΔG/N, where N= number of non-hydrogen atoms (kcal/mol)).*

| Ligand | [P] (μM) | [L] (μM) | $K_D$ (nM) | $\Delta H^{obs}$ (kcal/mol) | N | TΔS (kcal/mol) | ΔG (kcal/mol) | LE |
|---|---|---|---|---|---|---|---|---|
| 2a | 740 | 30 | No binding/weak | | | | | |
| 2b | 385 | 30 | No binding/weak | | | | | |
| 3a | 477 | 26 | 8475 ± 237 | -9.11 ± 0.12 | 0.99 ± 0.010 | -2.42 | -6.69 | 0.42 |
| 5b | 392 | 30 | No binding/weak | | | | | |
| 7a | 385 | 34 | 641 ± 33 | -12.71 ± 0.07 | 1.06 ± 0.004 | -4.55 | -8.16 | 0.45 |
| 7b | 385 | 13.5 | 351 ± 18 | -13.04 ± 0.07 | 0.97 ± 0.004 | -4.52 | -8.52 | 0.45 |
| 7c | 378 | 14 | 297 ± 10 | -12.05 ± 0.04 | 0.98 ± 0.003 | -3.46 | -8.59 | 0.45 |
| 7d | 235 | 10 | 397 ± 19 | -9.63 ± 0.06 | 0.97 ± 0.005 | -1.18 | -8.45 | 0.44 |
| 8a | 381 | 18 | 7874 ± 258 | -8.30 ± 0.15 | 1.06 ± 0.014 | -1.57 | -6.73 | 0.35 |
| 8b | 392 | 30 | No binding/weak | | | | | |
| 8e | 451 | 32 | 7576 ± 365 | -5.35 ± 0.09 | 1.05 ± 0.013 | 1.40 | -6.75 | 0.36 |
| 9a | 378 | 20 | No binding/weak | | | | | |
| 11 | 381 | 30 | 278 ± 15 | -10.28 ± 0.04 | 1.03 ± 0.003 | -1.63 | -8.65 | 0.43 |

Although the first bromodomain of BRD4 has been constantly shown to bind to weak compounds employing the thermal melt assay, it has been noted that other BRDs do not always display high temperature shifts despite they bind to several compounds very potently.[161] Different patterns of functions were introduced on the 6-phenyl substituted 9*H*-purine scaffold in order to investigate the effect of diverse substitutions, including para-substitutions (compounds **3b-h)**, meta-,para-substitutions (compounds **4a-e**), meta-,meta'-

substitutions (compounds **5a-b**), ortho-, ortho'-substitutions (compounds **6a-c**) and ortho-meta'-substitutions (compounds **7a-e**) (**Figure 2.6** and **2.7A**). Binding of these analogues was evaluated towards the 13 BRDs previously mentioned, employing the same thermal shift assay. Interestingly, compounds that carried a N9-methyl group (**3c**, **3e**, **4e**, **5b**) displayed very weak or no binding towards most BRDs while showing small thermal shifts (1.0 – 1.3 ˚C) for the bromodomain of CREBBP. Para-substitutions of the 6-phenyl-9*H*-purines (**3b-3h**) exhibited very weak effect across all BRDs, however, compound **3f** showed binding towards all BRDs without any hints of selectivity towards BRD9. Meta-substitution (compounds **4a-4e**) resulted in lower stabilisation of BRDs with no affinity for BRD9. Interestingly, meta-,meta'- substitution (compound **5a**) resulted in binding to most BRDs, albeit weak, with $\Delta T_m$ values between 1.1 and 1.8 ˚C. As expected, no binding was detected in the case of the N9-methyl analogue (compound **5b**). Affinity was not improved with ortho-, ortho'- substitutions of the 6-phenyl 9*H*-purine scaffold (compounds **6a-6c**) (**Figure 2.7B**). Since methyl substitution at N9 could not be tolerated in BRD4(1) or BRD9 binding, it can be deduced, at this stage, that the five member ring points towards the bottom of the acetyl-lysine binding cavity, as predicted in docking models (**Figure 2.3D/E** and **2.5B**), with the 6-substituted position towards the front of the pocket in order to accommodate the larger phenyl-substituted functions.

Combinations in ortho-meta'- substituted compounds were further tested by first maintaining a methoxy functionality at the ortho position while changing the steric hindrance at the meta'- position (compounds **7a-7d**). 2-methoxyphenyl substitution (compound **7a**) resulted in thermal shifts between 1.4 and 2.5 ˚C for BET BRDs, while significantly stabilizing BRD9 compared to all previous tested compounds (2.9 ˚C) (**Figure 2.7B**). This interaction was confirmed by ITC with a measured dissociation constant of 641 nM against BRD9 (**Figure 2.7D**, **Table 2.2**). This result prompted to test halide analogues

at the meta'- position (compounds **7b**-**7d**) maintaining the ortho-methoxy group. All of them exhibited improved thermal shifts against BRD9, while BET affinity was variable. Observed $\Delta T_m$ values followed the order H < F < Cl > Br, highlighting the importance of steric bulk and charge at the meta'- position, with compound **7c** showing a $\Delta T_m$ of 3.8 ˚C against BRD9 (**Figure 2.7B**). Binding was confirmed by ITC with measured dissociation constants of 351, 297 and 397 nM against BRD9 for compounds **7b**, **7c** and **7d**, respectively (**Figure 2.7D**, **Table 2.2**). Interestingly, although BRD4(1) exhibited $\Delta T_m$ values of 1.1 and 3.2˚C for compounds **7c** and **7d**, it was found to bind more weakly to these scaffolds by ITC, and measured dissociation constants were 2.04 and 4.7 µM respectively (**Figure 2.7C**, **Table 2.1**). Affinity for BRD9 was lost with compound **7e** which carried a bromine function at the meta'- position and an ethoxy- substituent at the ortho-position, suggesting that a bulkier group at the ortho position was not tolerated.

To verify whether the primary amine function at position 2 of the 9*H*-purine scaffold was necessary for binding to bromodomains, it was replaced by a chlorine group in compound **8a** (**Figure 2.6** and **2.8A**), resulting in loss of affinity towards all BRDs in the panel (**Figure 2.8B**). In the case of BRD9 this finding was validated by isothermal titration calorimetry measurement which resulted in a $K_D$ of 7.8 µM (**Figure 2.8C**). As with compounds from previous series, the N9-methyl analogue **8b** (**Figure 2.8A**) manifested no affinity for bromodomains as measured both by thermal melt (**Figure 2.8B**) and ITC assays in the case of BRD9 (**Figure 2.8C**), while larger substituents (compound **8c**) were not tolerated. Introduction of a hydroxy substituent at position 2, while retaining a 6-(5-*halide*-2-methoxyphenyl) moiety (compounds **8d**-**8f**), had variable effects on the 9*H*-purine affinity towards BRDs. Furthermore, fluoro- (**8d**) and bromo- (**8f**) substituted compounds lost affinity across the panel, while the chloro-substituted compound (**8e**) bound to most bromodomains in the $\Delta T_m$ assay, albeit weaker than its primary amine

analogue **7c** (**Figure 2.8A/B**), suggesting that the interactions initiated by the hydroxyl group and the conserved asparagine (Asn100 in BRD9; Asn140 in BRD4(1)) are not favored over the primary amine.
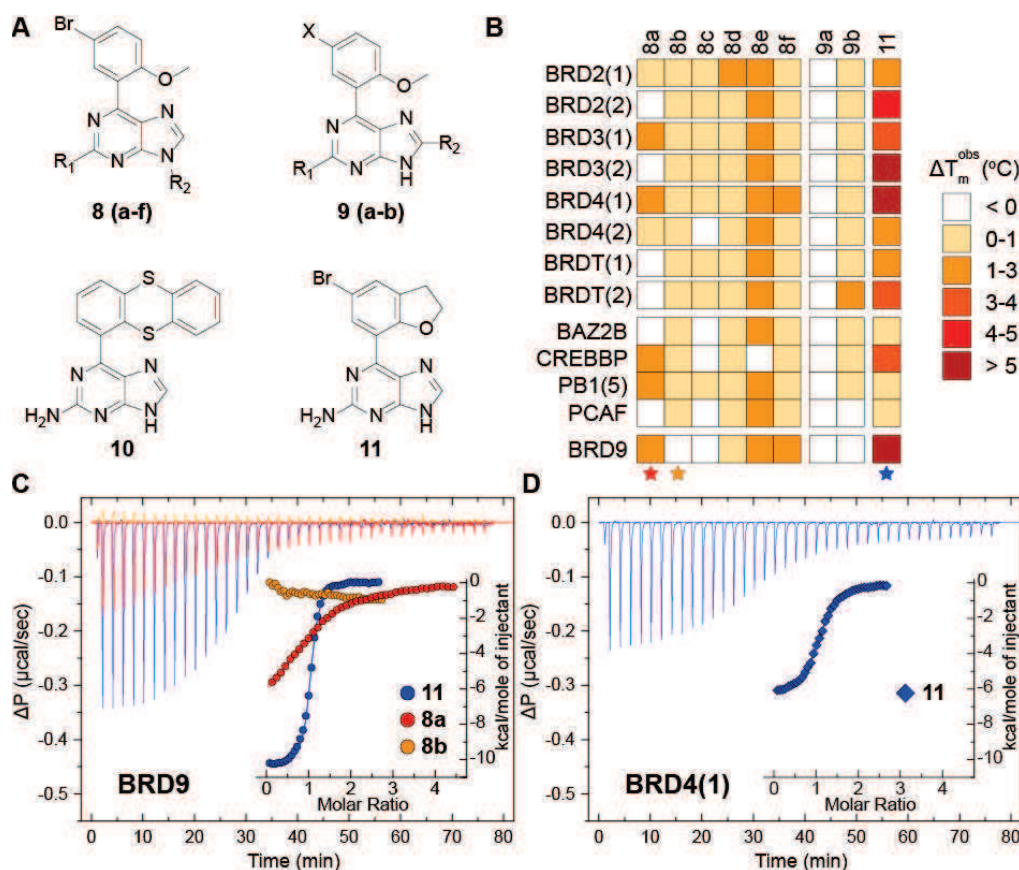


**Figure 2.8** *BRD pocket SAR. (A) Compounds designed to probe the acetyl-lysine mimetic character of the purine scaffold. (B) Thermal shift assay against human bromodomains. Compound 10 was heavily colored and interfered with the assay. Compounds highlighted with a colored star were further validated by ITC. (C) Substitution of the primary amine group to a hydroxyl (compound 8a) impairs binding towards BRD9 as demonstrated by ITC experiments while cyclisation of the aromatic substituent results in enhanced potency (compound 11). (D) Isothermal titration calorimetry validation of compound 11 binding to BRD4(1).*

In an attempt to direct the purine core deeper inside the bromodomain cavity, a methyl group was introduced at position 8 of the 9*H*-purine core (compounds **9a** and **9b**). The poor solubility of compound **9a** did not allow for any measurements, but compound **9b** exhibited weak binding to all bromodomains in the panel with the exception of BRDT(2), suggesting that

this compound did not carry a suitable decoration pattern to improve affinity toward BRD9. An attempt to insert a fluorine atom at position 8, through a C-8 electrophilic fluorination on the bis(tetrahydropyran-2-yl)-protected derivative of **2a**, following a reported metalation-fluorination reaction with N-fluorobenzenesulfonimide,[442] was also unsuccessful, as the formation of the corresponding 8-phenylsulfonyl product instead of the 8-fluoro derivative was observed, similar to the reported results by Roy *et al.*,[443] even under heterogeneous conditions (**Scheme 2.2**).

**Scheme 2.2** *C-8 electrophilic fluorination reaction on the bis(THP)-derivative of* **2a***.*
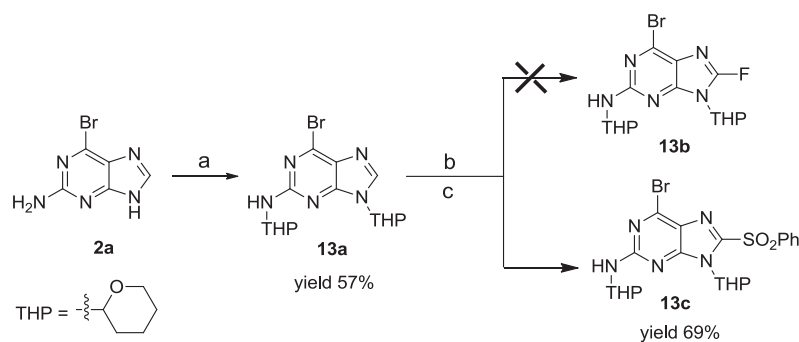


Reagents and conditions: (a) 3,4-dihydro-2H-pyran, HCl cat., anhydrous DMF, 60 °C, 6 h; (b) LDA 2.0 M solution in heptane/THF/EtPh, anhydrous THF, −78 °C, 2 h; (c) N-fluorobenzenesulfonimide (NFSI), −78 °C, 1.5 h, then 0 °C, 30 min.

Next, the size of the 6-(5-*halide*-2-methoxyphenyl) substituent was increased, leading to compounds **10** and **11**. Unfortunately the bright yellow color and low solubility of compound **10** did not allow for further evaluation. The analogue of **7d** obtained by cyclising the 2-methoxyphenyl ring into a 2,3-dihydrobenzofuran-7-yl (compound **11**) exhibited a remarkable increase in affinity for BRD9 (6.5 ˚C). Isothermal titration calorimetry yielded a dissociation constant of 278 nM for BRD9 (**Figure 2.8C**) while BRD4(1) binding resulted in a much weaker affinity (1.4 µM) (**Figure 2.8D**).

## 2.3 Induced fit binding of 9*H*-purines to the bromodomain of BRD9

Our fragment and structure based design allowed to identify the 2-amino-9*H*-purine as a new chemotype able to mimic Kac residue. Iterative optimization of the purine fragment precursor **2a** allowed to find that some of its 6-aryl derivatives exhibited nanomolar affinity towards BRD9, with lower activity towards BRD4. In particular, two excellent inhibitors were discovered, namely compounds **7d** and **11**, which exhibited nanomolar and micromolar affinity toward BRD9 and BRD4, respectively, from ITC experiments. In order to investigate the interaction of **7d** and **11** with both BR9 and BRD4(1), crystallography and docking studies were carried out. Crystal structures of **7d**/BRD9 and **7d**/BRD4(1) were determined. In both cases, the ligand was found to occupy Kac pocket (**Figure 2.9A** and **2.10A**) and was clearly defined in the electron density map (**Figure 2.9B** and **2.10B**).
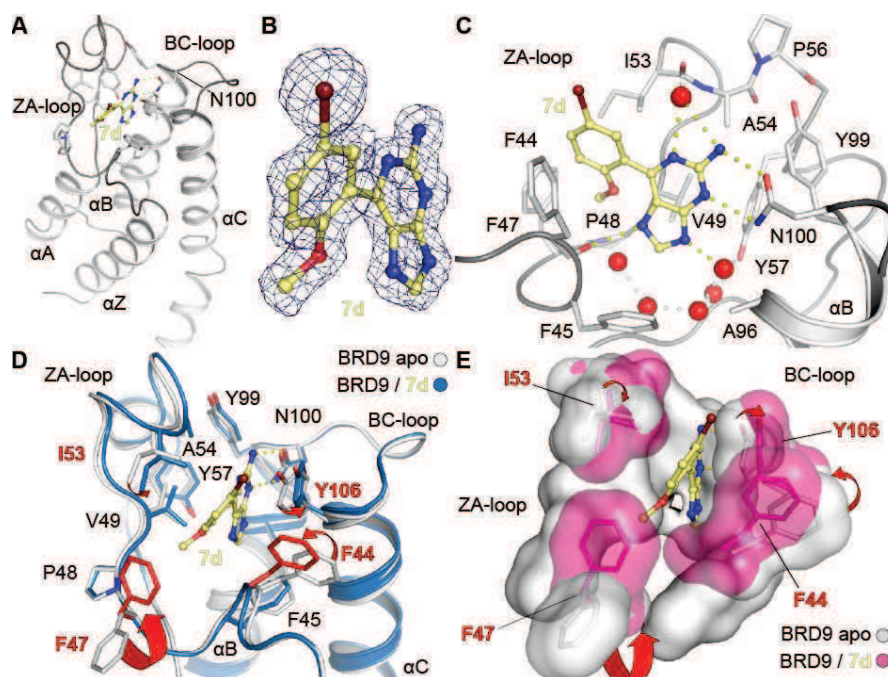


**Figure 2.9** *Induced fit binding of 9H-purines to BRD9. (**A**) Overall fold of BRD9/**7d** crystal structure. (**B**) 2FcFo map of **7d** in complex with BRD9 contoured at 2σ. (**C**) **7d** occupies the Kac binding cavity of the bromodomain module initiating direct interactions with the conserved asparagine (N100). (**D**) Binding of **7d** to BRD9 results in a distinct re-arrangement of the BRD fold. (**E**) Surface view of the side-chain re-arrangement in BRD9 pocket, highlighting the induced pocket upon binding of **7d**.*

The primary amine function and nitrogen atom at position 3 of **7d** established a direct interaction with the conserved asparagine in both structures (Asn140 in BRD4(1); Asn100 in BRD9) as well as a number of hydrogen bonds to the protein backbone and to the network of conserved water molecules in the pocket (**Figure 2.9C** and **2.10C**). Moreover, compound **7d** engaged hydrogen bonds to a water molecule which, in turn, linked the ligand to the ZA-loop and to the carbonyl of Ile53 (in the case of BRD9) or Asn93 (in the case of BRD4(1)). A comparable binding mode was observed for **7d** and (+)-JQ1, a well-known BRD4(1) modulator, with the purine ring superimposing well with the methyl-triazole of (+)-JQ1 (**Figure 2.10D**).
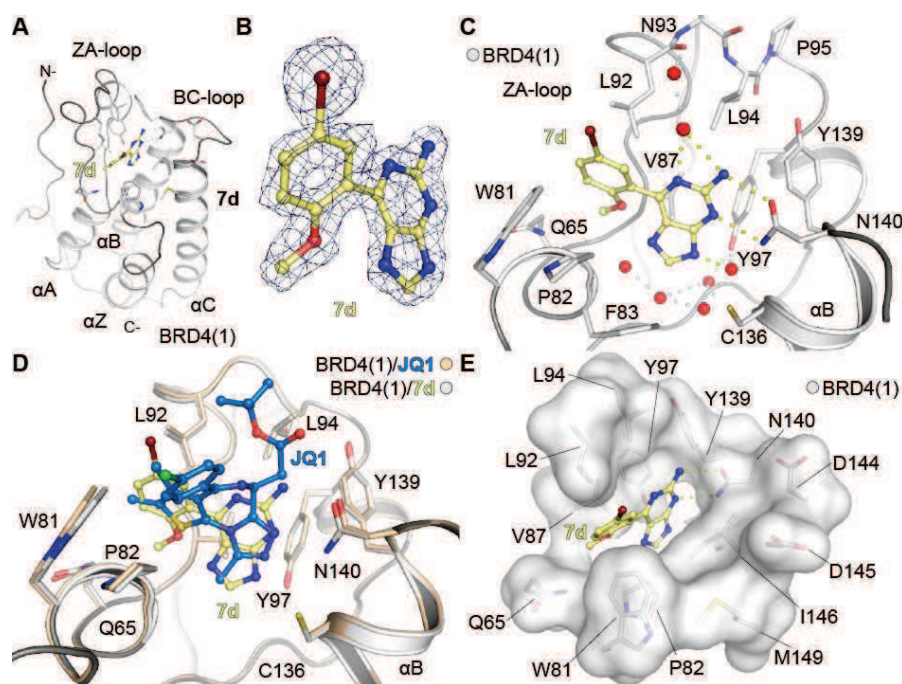


**Figure 2.10** *Binding of compound **7d** to BRD4(1) (**A**) Overall fold of BRD4(1)/**7d** crystal structure. (**B**) 2FcFo map of **7d** in complex with BRD4(1) contoured at 2σ. (**C**) Similar to the BRD9 complex, **7d** occupies the acetyl lysine binding cavity of the BRD4(1) bromodomain module initiating direct interactions with the conserved asparagine (N140). (**D**) The mode of **7d** binding to BRD4(1) is similar to that of JQ1 (PDB ID: 3MXF) with the five member ring of the purine core mimicking the methyl-tiazolo function of JQ1. (**E**) Surface representation of the binding cavity of BRD4(1) in complex with **7d**.*

In accordance with the induced fit computational models described for fragment **2a** in BRD9, superimposition of the BRD9/**7d** complex to the apo

structure of BRD9 (PDB ID: 3HME)[108] revealed rotations of the side-chains of Phe47 and Phe44, while the top of the ZA loop collapsed towards the ligand (**Figure 2.9D/E**). These marked re-arrangements within the BRD9 cavity had never been previously observed and are consistent with an induced fit binding of **7d** to BRD9 pocket. Interestingly, the structural re-arrangements observed were unique to BRD9: the structure of compound **7d** in complex BRD4(1) did not reveal any re-arrangements of Kac binding cavity, as the inhibitor packed between Trp81 and Leu92 of the ZA-loop (**Figure 2.10D/E**).
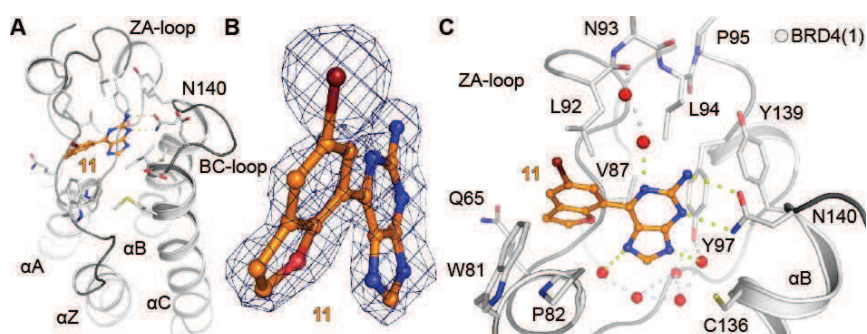


**Figure 2.11** *Complex of compound 11/BRD4(1). (A) Overview of the complex of compound 11 with BRD4(1). (B) FcFo map of compound 11 in complex with BRD4(1) contoured at 2σ. (C) Detail of compound 11 biding to BRD4(1) demonstrating the acetyl-lysine mimetic binding mode, initiating interactions with the conserved asparagine (N140).*

In the case of compound **11**, it readily crystallized with BRD4(1) and was found to occupy the acetyl-lysine binding cavity (**Figure 2.11A**) in a well defined electron density map (**Figure 2.11B**). The ligand directly engaged the conserved asparagine (Asn140) and established a network of interactions with conserved water molecules, while packing between the ZA-channel tryptophan (Trp81) and the ZA-loop leucine (Leu92) (**Figure 2.11C**). However, any attempts to obtain a crystal structue of **11** in BRD9 was unsuccessful, as no diffracting quality crystals, suitable for structure determination, were generated. Computational methods were therefore employed to account for its binding to BRD9. Rigid docking into the BRD9/**7d** complex structure resulted in a conformation similar to that observed with compound **7d**, with the ligand engaging the conserved asparagine *via* its primary amine function and the 6-

aryl-substituted ring packing betweent he ZA-loop Ile53 and Phe44 (**Figure 2.12A**). Afterwards, induced-fit docking was carried out using the complex of BRD9/**7d**, yielding a pose whereby the 2-amine function inverted and inserted in the BRD pocket, without any changes in the surrounding side chains of Phe44, Phe47, Ile 53 and Tyr106 (**Figure 2.12B**).
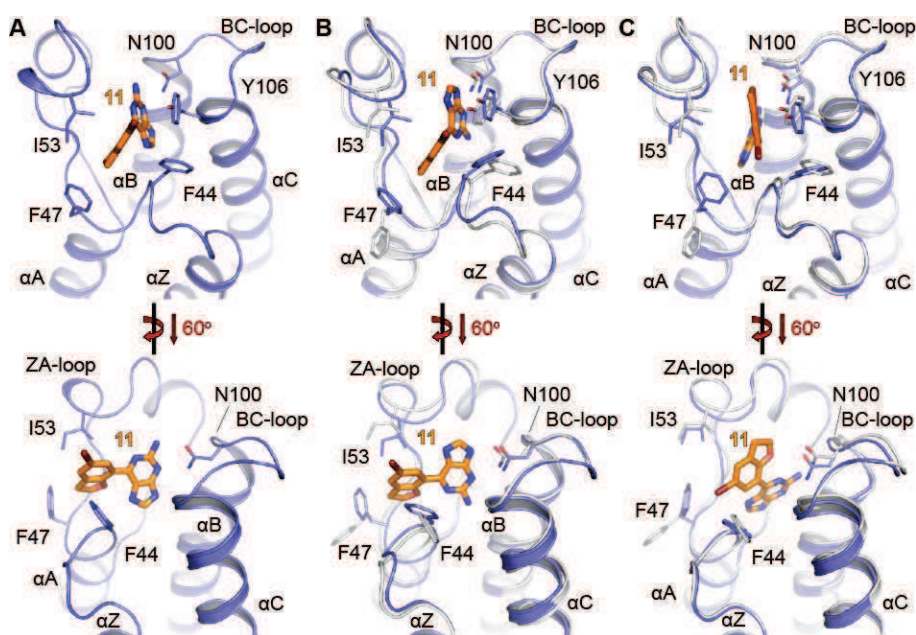


**Figure 2.12** *Docking of compound **11** to BRD9. (A) Rigid docking of compound **11** into the complex structure of BRD9/**7d** results in a minimal energy pose that resembles the **7d**/BRD9 complex. (B) Induced fit of compound **11** into the cavity of the BRD9/**7d** complex results in an orientation of the ligand that inverts its primary amine function, without affecting the side-chains of the residues within the binding site of BRD9. (C) Induced fit docking of compound **11** into the apo site of BRD9 (PDB ID 3HME) results in a re-arrangement of the binding site residues in a similar mode to that observed in the case of compound **7d**, however the ligand rotates its 6-aryl substituent by 180 degrees. The bottom panel shows a clockwise 60 degree rotation of the structures, highlighting the tilt of the ligand poses with respect to each other.*

Intrigued by this finding, another induced fit docking experiment was performed in the BRD9 apo structure, allowing the flexibility of key residues upon compound binding. A similar set of side-chain re-arrangements within the BRD9 acetyl lysine cavity was displayed, including a rotation of Phe47, resulting in capping of the binding groove, as well as a repositioning of Phe44 from helix C and Ile53 from the ZA-loop (**Figure 2.12C**). These results

revealed that compound **11** can also affect plasticity of BRD9 Kac binding cavity, as obtained for **7d** through crystallographic experiments.

In the case of the BRD family of proteins, an induced fit binding was previously observed only for CREBBP upon binding to a dihydroquinoxalinone-based inhibitor. The ligand was shown to insert under an arginine residue of the CREBBP BRD, resulting in re-structuring of the Kac binding site of this bromodomain.[143] Intriguingly, in our case the structural re-arrangement of BRD9 binding site was more extensive, with several side-chains rotating and shifting to accommodate the small purine ligands.

## 2.4 In cell validation of 9*H*-purines

In order to verify that the developed 2-amine-9*H*-purine scaffolds are active in a cellular environment and can perturb the interaction of BRD9 with acetylated histones, cellular assays were carryed out in collaboration with Jacqui Mendez and Danette Daniels of Promega Corporation (U.S.A.). BRD9 is a component of the large SWI/SNF complex[435] and its bromodomain was shown to bind to acetylated histone H3 peptides.[108] To assess whether 9*H*-purines were able to competitively displace the bromodomain of BRD9 from chromatin, a bioluminescence resonance energy transfer (BRET) system was set-up, combining NanoLuc Luciferase fusions of the BRD9 bromodomain (**Figure 2.13A**) or full length BRD4 and Halo-tagged Histone H3.3 as BRET pairs. This assay is an excellent tool to quantify protein-ligand interactions in a cellular system[444] and has recently been used to determine cellular $IC_{50}$ values for the inhibition of the histone/bromodomain interaction in the case of BRPF1, using a 1,3-dimethyl benzimidazolone scaffold.[144] As a first step, incorporation of Halo-tagged histone H3.3 into chromatin was confirmed by fluorescence microscopy (**Figure 2.13B**).
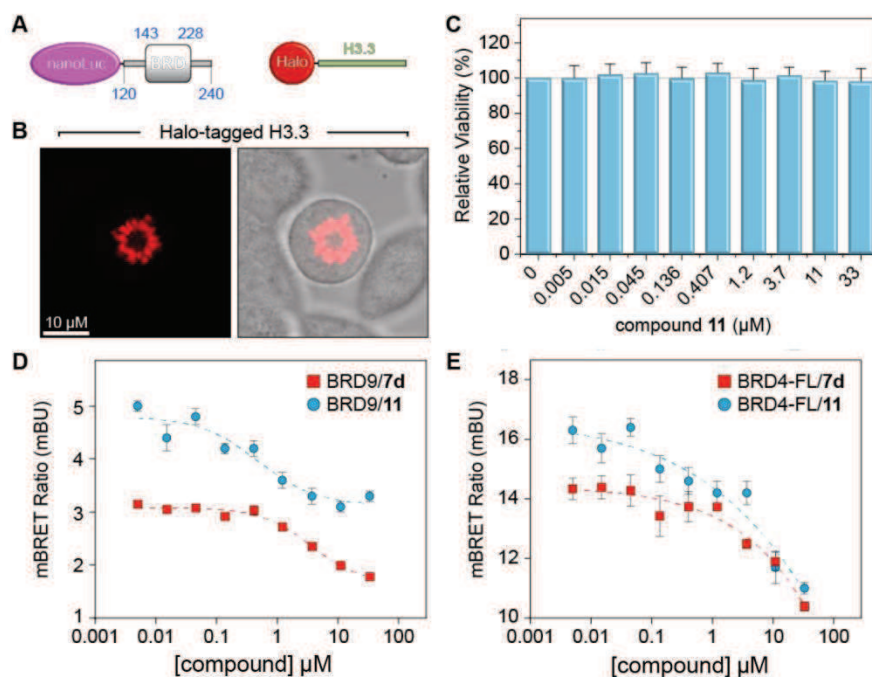
**Figure 2.13** *In cell validation of compounds **7d** and **11**. (A) NanoLuc fusion construct of the bromodomain of BRD9 (UniProt: Q9H8M2, residues 120-240) used to probe binding to Halo-tagged histone H3.3 in a BRET assay. (B) Confocal images of halo-tagged histone H3.3 transfected into HEK293 cells demonstrating incorporation into the nucleus. (C) Cytotoxicity assay demonstrating that compound **11** is not toxic to HEK293 cells in the concentration range used for the BRET assay. (D) Titration of compounds **7d** and **11** into HEK293 cells transfected with nanoLuc-fused full length BRD9 and halo-tagged histone H3.3. (E) Titration of compounds **7d** and **11** into HEK293 cells transfected with nanoLuc-fused full length BRD4 (UniProt: O60885) and halo-tagged histone H3.3.*

Afterwards, dose response experiments were carried out, showing that the NanoLuc-BRD9 bromodomain was readily displaced from chromatin upon treatment with compounds **7d** and **11** with cellular $IC_{50}$ values of $3.5 \pm 0.11$ μM and $477 \pm 194$ nM, respectively (**Figure 2.13D**). In contrast, full-length BRD4 was not completely displaced in this assay up to concentrations of 33 μM for both compounds (**Figure 2.13D**), suggesting that the compounds retained the *in vitro* selectivity towards BRD9 in this cellular system. Toxicity of compound **11** was evaluated towards HEK293 cells, using cell viability in the presence of the compound in the concentration regime of BRET experiments as a readout and no cytotoxic effect was observed (**Figure

**2.13C**), suggesting that this compound can be used in cellular systems to target BRD9/Kac interactions without affecting BRD4/Kac interactions or causing any cytotoxic responses.

In summary, 9*H*-purine scaffold has emerged as a simple template suitable to generate initial tools for the bromodomain of BRD9, which have not attracted attention until now. Fragment based design, structural activity relationships and iterative optimization allowed to identify compounds **7d** and **11** which bound to BRD9 with nanomolar affinity and only weak residual micromolar affinity for BRD4. These compounds were able to competitively displace the BRD9 bromodomain from histone H3.3 in cellular environment. Finally, high-resolution X-ray crystal structure of compound **7d** in complex with BRD9 revealed exstensively structural re-arrangements of the Kac binding cavity of BRD9 upon **7d** binding, resulting in an unprecedented cavity shape. Docking studies suggested that compound **11** was also able to induce the same type of structural re-arrangements.

# -CHAPTER 3-

Dihydropyrimidin-2(1H)-one: a new template for the modulation of microsomal Prostaglandin E$_2$ Synthase-1 (mPGES-1).

**3.1 Targeting mPGES-1: rationale from high-resolution X-ray crystal structures**

Structural information on the key functional groups, including a defined pharmacophore, have been the major issue for the development of new mPGES-1 inhibitors through rational design approaches.

In our previous works,[224, 225] in which some triazole-based mPGES-1 inhibitors have been described, it was used the MGST-1 structure solved by Hebert *et al.*[445] in 2006 for computational-guided design, due to the lack of a mPGES-1 crystal structure in its active conformation. At that time, the only available mPGES-1 crystal structure had been elucidated by electron crystallography, but in that case, the protein was in its inactive closed state[446] and was not suitable to be used for the classical receptor-based approach in drug discovery. Therefore, the structure of MGST-1, a homotrimer also belonging to the MAPEG family and showing the 38% of homology sequence with mPGES-1,[447] represented an appropriate alternative for our purposes.

The first detailed information about the three dimensional structure of this glutathione-dependent membrane protein in the active form were only recently provided by means of X-ray crystallography by Sjögren *et al.*[212] in 2013. The solved structure revealed that the mPGES-1 homotrimer has three active site cavities within the membrane-spanning region at each monomer interface. The asymmetric monomer is formed by a four-helix bundle, each active site is between the N-terminal parts of helix II and IV of a monomer and the C-terminal part of helix I and the cytoplasmic domain of the adjacent monomer, toward the cytoplasmic part of the protein (**Figure 3.1**). The cofactor (GSH) adopts a U-shape due to the strong interactions between its two terminal carboxylic functions and a positively charged region in the deeper part of the binding site. In 2014, a second X-ray crystal structure of human mPGES-1 in lipidic mesophase was reported in a structural biology study in complex with the inhibitor LVJ (2-[[2,6-bis(chloranyl)-3-[(2,2dimethylpropanoylamino)-

methyl]phenyl]amino]-1-methyl-6-(2-methyl-2-oxidanyl-propoxy)-N-[2,2,2-tris-(fluoranyl)ethyl]-benzimidazole-5-carboxamide).[448] This structure provided more information on the structural elements required for the interaction with the enzyme, as it is the first reported ligand/mPGES-1 co-crystal structure.
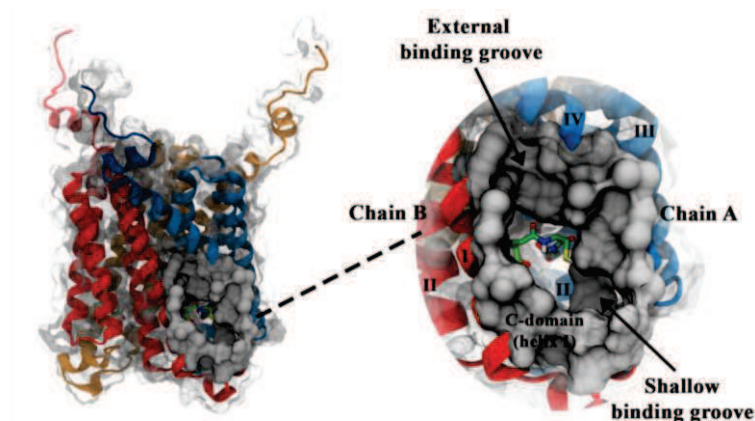


**Figure 3.1** *Microsomal prostaglandin synthase-1 (mPGES-1) structure (PDB code: 4BPM) (secondary structure: chain A blue, chain B red, chain C orange). Glutathione as cofactor is depicted in licorice mode; molecular surface focused to the binding site colored in gray.*

## 3.2 DHPMs designed from MGST-1 structure

At the beginning of my PhD, in 2012, a high-resolution crystal structure of mPGES-1 in active conformation was not yet available. Therefore, for the rational design of new mPGES-1 inhibitors, it was initially used the structure of MGST-1,[445] another member of the MAPEG family sharing 38% of homology with our target protein.[447] The dihydropyrimidin-2(1)H-one (DHPM) core was chosen as template for biological investigation, as it represents a privileged structure, being endowed with several relevant pharmacological effects, including calcium channel modulation for the treatment of cardiovascular diseases, $\alpha_{1a}$–adrenergic receptor antagonism, useful for benign prostatic hyperplasia, and mitotic kinesin inhibition with potential anticancer application.[392] In addition to its interesting biological

profile, the DHPM core has received considerable attention in drug-discovery processes due to its synthetical accessibility through the easy, cheap and rapid Biginelli one-pot multicomponent reaction.[449] Consequently, molecular docking calculations were carried out in order to select the most promising compounds, among a large collection of designed synthetically accessible DHPMs. It was subsequently accomplished the synthesis of the selected compounds which showed the highest binding affinity with MGST-1 active site (**Scheme 3.1**).

The first group of molecules (**14a-e**) was synthesized by a microwave-assisted protocol of the Biginelli reaction promoted by chlorotrimethylsilane (TMSCl), a procedure that allowed very short reaction times and good yields also in the case of N-susbstituted urea derivatives and thioureas which are notably known to give very complex reaction mixtures and poor amount of the desired DHPM (**Scheme 3.1**).[418, 422] The synthesis of the second group (**14f-l**) was accomplished in a two-step procedure: firstly, the dihydropyrimidine-2-thione precursors **14m-q** were produced through the same protocol of the multicomponent reaction, and subsequently, final desired compounds were obtained through a Liebeskind–Srogl cross-coupling.[450] Liebeskind-Srogl reaction is a carbon-carbon cross-coupling, involving the Pd(0)-catalyzed, Cu(I)-mediated reaction of a variety of different thioorganic compounds with boronic acids under neutral conditions.[451-456] This desulfitative carbon-carbon coupling requires stoichiometric amounts of a Cu(I) carboxylate, such as Cu(I)-thiophene-2-carboxylate (CuTC)[457] as metal cofactor. In the context of scaffold decoration of heterocycles, the Liebeskind-Srogl cross-coupling reaction can also be applied to cyclic thioureas,[458] such as the dihydropyrimidine-2-thiones from the Biginelli condensation. Hence, this procedure was employed to synthesize compounds **14f-l**, using Pd(PPh$_3$)$_4$ as a catalyst, CuTC as Cu(I) source and THF as solvent system, under microwave irradiation at 100 °C (**Scheme 3.1**).

**Scheme 3.1** *Structures of selected DHPMs 14a-l and synthetic strategies.*
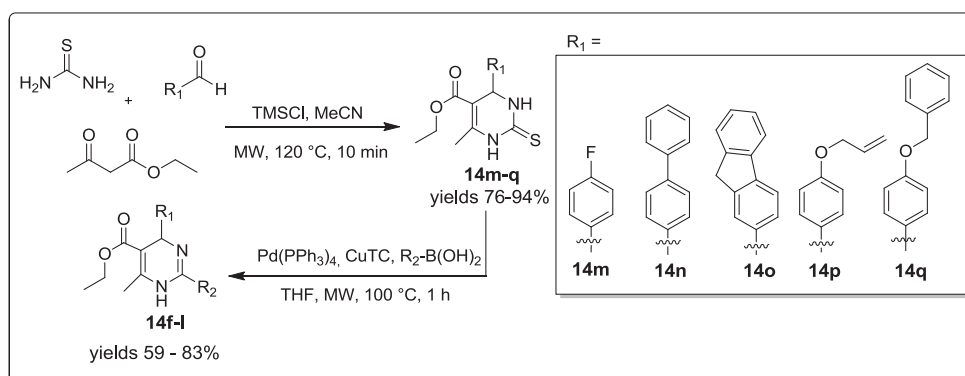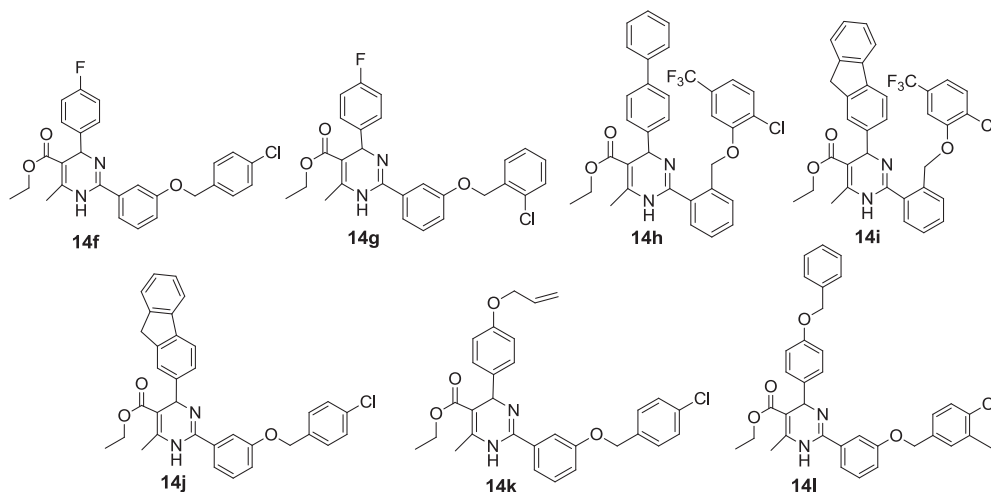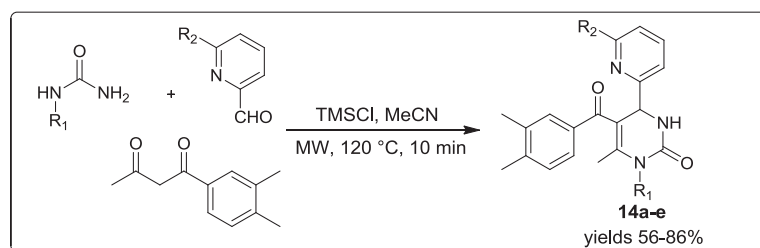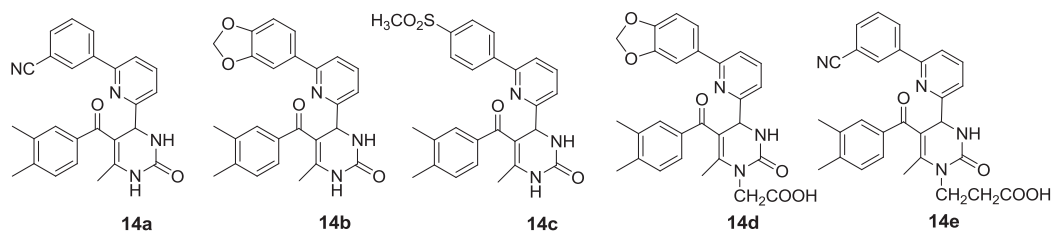
Interference of the synthesized compounds on mPGES-1 activity was investigated in a cell-free assay using the microsomal fraction of interleukin-1β-stimulated human A549 cells,[225] in collaboration with professor Oliver Werz of Friedrich Schiller University (Germany). The tested DHPMs manifested no effect or only a moderate inhibitory activity against mPGES-1. In particular, mPGES-1 remaining activity, after treatment with 10 μM of **14a-l**, was not affected in all the cases, except for compounds **14e-g** which showed to inhibit the enzyme of about 30-35% (**Figure 3.2**). Nevertheless, since the maximal inhibition value was lower than 40%, an $IC_{50}$ value could not be obtained . These data were not in accordance with modeling predictions, thus suggesting that the structure of MGST-1, successfully used in the case of rational design of triazole-based mPGES-1 inhibitors, was probably unsuitable in the case of the DHPM core. However, potent DHPM-based mPGES-1 inhibitors have been successfully identified utilizing the high-resolution X-ray crystal structures of the protein, as illustrated in the next sections.
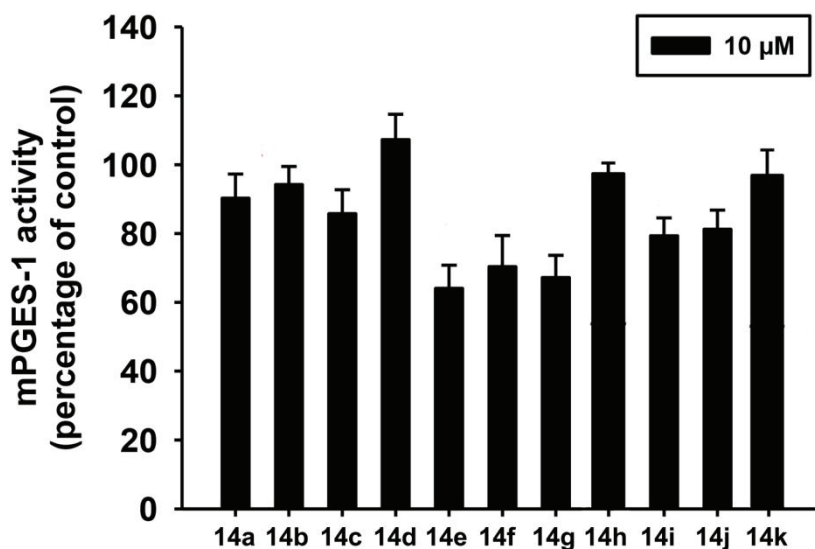


**Figure 3.2** *Effect of compounds **14a-k** on the activity of mPGES-1. Experiments were performed in triplicate.*

**3.3 Investigation of DHPM-based compounds as mPGES-1 modulators: rationale from X-ray crystal structure**

On the basis of the additional structural information derived from the high-resolution X-ray crystal structure of mPGES-1 elucidated in 2013,[212] a new structure-based drug design was undertaken, focused on the DHPM core for mPGES-1 modulation. As a first step, a focused *in silico* virtual screening was performed on a small set of synthetically accessible compounds, by molecular docking (**15-50**, **Table 3.1**). A qualitative computational filter was introduced, based on the respect of some key interactions with the receptor counterpart, in order to identify a set of compounds for the subsequent step of chemical synthesis and biological evaluation. Molecular docking calculations were performed using the first crystallized structure of mPGES-1 (PDB code: 4AL0) by Sjögren *et al.*,[212] who also proposed a mechanism for $PGE_2$ isomerisation through a dynamic process in which $PGH_2$ reaches the binding site to interact with GSH and other key residues. Accordingly, it can be supposed that a potential mPGES-1 inhibitor can act either as a false substrate ($PGH_2$) or as a cofactor analogue (GSH), or at last it can behave in both ways.[459] In the latter case, the inhibitor can displace not only the substrate but also the cofactor in the enzyme pocket. In order to simulate the partial or total displacement of GSH, molecular docking calculations were performed removing the cofactor from the active site. New putative dihydropirymidin-2(1H)-one-featured inhibitors were designed taking into account the synthetic accessibility of the selected molecules. Hence, a first computational study was focused on a small set of compounds (**Table 3.1**) derived from the combination of the following chemical synthons:

1.  urea, thiourea or N-methyl urea;

2.  ethyl 3-oxobutanoate or ethyl 4-(4-methoxyphenyl)-2,4-dioxobutanoate as 1,3-dicarbonyl compound;

3.  seven different aldehydes with increasing steric hindrance.

**Table 3.1** *3,4-dihydropyrimidin-2-one derivatives **15-50***.
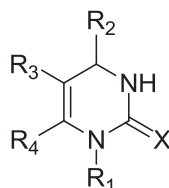


| Entry | $R_1$ | $R_2$ | $R_3$ | $R_4$ | X |
|-------|-------|-------|-------|-------|---|
| 15 | H | phenyl | $CO_2C_2H_5$ | $CH_3$ | O |
| 16 | $CH_3$ | phenyl | $CO_2C_2H_5$ | $CH_3$ | O |
| 17 | H | phenyl | $CO_2C_2H_5$ | $CH_3$ | S |
| 18 | H | phenyl | 4-(methoxybenzoyl) | $CO_2C_2H_5$ | O |
| 19 | $CH_3$ | phenyl | 4-(methoxybenzoyl) | $CO_2C_2H_5$ | O |
| 20 | H | phenyl | 4-(methoxybenzoyl) | $CO_2C_2H_5$ | S |
| 21 | H | 3-formylphenyl | $CO_2C_2H_5$ | $CH_3$ | O |
| 22 | $CH_3$ | 3-formylphenyl | $CO_2C_2H_5$ | $CH_3$ | O |
| 23 | H | 3-formylphenyl | $CO_2C_2H_5$ | $CH_3$ | S |
| 24 | H | 3-formylphenyl | 4-(methoxybenzoyl) | $CO_2C_2H_5$ | O |
| 25 | $CH_3$ | 3-formylphenyl | 4-(methoxybenzoyl) | $CO_2C_2H_5$ | O |
| 26 | H | 3-formylphenyl | 4-(methoxybenzoyl) | $CO_2C_2H_5$ | S |
| 27 | H | 3-ethoxybenzoyl | $CO_2C_2H_5$ | $CH_3$ | O |
| 28 | $CH_3$ | 3-ethoxybenzoyl | $CO_2C_2H_5$ | $CH_3$ | O |
| 29 | H | 3-ethoxybenzoyl | $CO_2C_2H_5$ | $CH_3$ | S |
| 30 | H | 3-ethoxybenzoyl | 4-(methoxybenzoyl) | $CO_2C_2H_5$ | O |
| 31 | $CH_3$ | 3-ethoxybenzoyl | 4-(methoxybenzoyl) | $CO_2C_2H_5$ | O |
| 32 | H | 3-ethoxybenzoyl | 4-(methoxybenzoyl) | $CO_2C_2H_5$ | S |
| 33 | H | (4-cyanophenyl)pyridin-2-yl | $CO_2C_2H_5$ | $CH_3$ | O |
| 34 | $CH_3$ | (4-cyanophenyl)pyridin-2-yl | $CO_2C_2H_5$ | $CH_3$ | O |
| 35 | H | (4-cyanophenyl)pyridin-2-yl | $CO_2C_2H_5$ | $CH_3$ | S |
| 36 | H | (4-cyanophenyl)pyridin-2-yl | 4-(methoxybenzoyl) | $CO_2C_2H_5$ | O |
| 37 | $CH_3$ | (4-cyanophenyl)pyridin-2-yl | 4-(methoxybenzoyl) | $CO_2C_2H_5$ | O |
| 38 | H | (4-cyanophenyl)pyridin-2-yl | 4-(methoxybenzoyl) | $CO_2C_2H_5$ | S |
| 39 | H | 6,8-dibromo-4-oxo-4H-chromen-3-yl | $CO_2C_2H_5$ | $CH_3$ | O |
| 40 | $CH_3$ | 6,8-dibromo-4-oxo-4H-chromen-3-yl | $CO_2C_2H_5$ | $CH_3$ | O |
| 41 | H | 6,8-dibromo-4-oxo-4H-chromen-3-yl | $CO_2C_2H_5$ | $CH_3$ | S |
| 42 | H | 6,8-dibromo-4-oxo-4H-chromen-3-yl | 4-(methoxybenzoyl) | $CO_2C_2H_5$ | O |
| 43 | $CH_3$ | 6,8-dibromo-4-oxo-4H-chromen-3-yl | 4-(methoxybenzoyl) | $CO_2C_2H_5$ | O |
| 44 | H | 6,8-dibromo-4-oxo-4H-chromen-3-yl | 4-(methoxybenzoyl) | $CO_2C_2H_5$ | S |
| 45 | H | 5-(3-(trifluoromethyl)phenyl)furan-2-yl | $CO_2C_2H_5$ | $CH_3$ | O |
| 46 | $CH_3$ | 5-(3-(trifluoromethyl)phenyl)furan-2-yl | $CO_2C_2H_5$ | $CH_3$ | O |
| 47 | H | 5-(3-(trifluoromethyl)phenyl)furan-2-yl | $CO_2C_2H_5$ | $CH_3$ | S |
| 48 | H | 5-(3-(trifluoromethyl)phenyl)furan-2-yl | 4(methoxybenzoyl) | $CO_2C_2H_5$ | O |
| 49 | $CH_3$ | 5-(3-(trifluoromethyl)phenyl)furan-2-yl | 4(methoxybenzoyl) | $CO_2C_2H_5$ | O |
| 50 | H | 5-(3-(trifluoromethyl)phenyl)furan-2-yl | 4(methoxybenzoyl) | $CO_2C_2H_5$ | S |

The combination of the most simple aldehydic building block (benzaldehyde) with the two dicarbonyl compounds and the three urea derivatives yielded a first group of structurally diverse molecules (**15-19**) to submit to docking calculations in order to verify the presence of some key interactions with the receptor counterpart, namely:

- π-π with Tyr130(A), indicative of a good accommodation within the GSH binding site;
- a polar interaction with Ser127(A), a key residue involved in PGH$_2$ recognition;
- polar interactions with Thr131(A), Gln134(A), and van der Waals interactions with Tyr28(B) and Ile32(B), belonging to the external binding groove.

None of these 6 compounds was able to properly occupy the external groove, establishing at the same time the π- π with Tyr130(A). In particular, compounds **15-17**, featuring aliphatic substituents at position 5 and 6, were not able to interact with both the sites, showing only a partial placement in the GSH binding site. However, it was found a pose of **18** in which the 4-phenyl group was partially accommodated in the external groove, while the 5-(4-methoxybenzoyl) moiety was properly oriented to establish a π-π with Tyr130(A) (**Figure 3.3**). A similar binding mode was found for N1-methyl derivative **19** and for the thio-analog **20**. Since the remaining part of the external groove was only partially occupied by the meta-position of the 4-phenyl group, the substitutions in this direction were gradually expanded. Preserving all the other substituents, a new set of compounds featuring a new 4-(3-formyl-phenyl) moiety was evaluated (**21-26**). The data obtained showed that, even though a better accommodation of 5-(4-methoxybenzoyl) was reached, the external groove was still not fully occupied. Furthermore, the poses obtained showed that compounds **21-23**, featuring aliphatic substituents at C5 and C6, were not at all compatible with this binding mode. For these

reasons, it was progressively increased the steric hindrance at the C4 position of the dihydropyrimidine scaffold, with the introduction of 3-ethoxybenzyl (**27-32**), (4-cyanophenyl)pyridine-2yl (**33-38**), 6,8 dibromo-4-oxo-4H-chromen-3-yl) (**39-44**), and 5-(3-(trifluoromethyl)phenyl)furan-2-yl) (**45-50**) substituents, respectively. The introduction of heteroaromatic rings is due to the aim of increasing the possible polar interactions with the hydrophilic residues in the external groove. As expected, docking poses, satisfying the contemporary π-π interaction with Tyr130(A), were found only in compounds featuring 5-(3-methoxybenzoyl) and 6-ethylcarboxylate groups. In more detail, docking calculations showed for the 4-(3-ethoxybenzyl) derivatives a binding mode comparable to that found for the previously considered 4-(3-formylphenyl) derivatives. Furthermore, together with the π-π interaction between the 4-methoxybenzoyl in C5 and Tyr130 (A), only a partial accommodation of the larger 4-cyanophenyl (pyridine-2yl) and 6,8-dibromo-4-oxo-4H-chromen-3-yl) substituents in the external groove was detected. Regarding compounds **48-50**, docking analysis showed that the orientation of the 4-(5-(3-(trifluoromethyl)phenyl)furan-2-yl) allows better interactions with the binding groove counterpart (**Figure 3.4**).
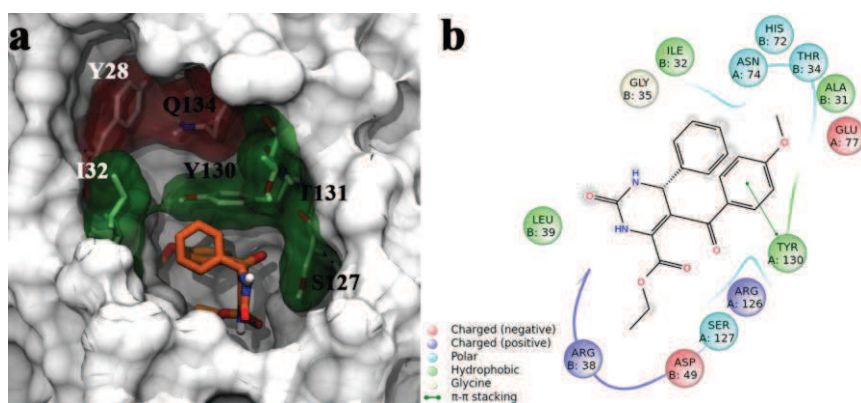


**Figure 3.3** (*a*) *3D model of **18** in docking with mPGES-1 (PDB code: 4AL0); residues in the active site represented in licorice (black captions for residues in chain A and white captions for those in chain B) and related molecular surfaces depicted in transparent green (for residues able to interact with **18**) and transparent red (for residues not able to interact with **18**). (b) 2D panel representing interactions between **18** and residues in mPGES-1 binding site.*

In order to corroborate computational outcomes, compounds **24**, **30**, **36**, **42**, **48** were initially synthesized (**Scheme 3.2**) and submitted to biological screening. In particular, in this first group of molecules, only the substituent at position 4 was varied, while in all compounds the ethyl 4-(4-methoxyphenyl)-2,4-dioxobutanoate was employed as 1,3-dycarbonil synthon, as it was significantly favored over the alkyl analogue in docking simulations. Moreover, in consideration that a similar behavior was observed for urea, thiourea and N-methylurea derivatives in docking calculations, only urea was employed at this stage as Biginelli ureidic synthon.

With the optimized general conditions reported in **Scheme 3.2**, the synthesis of these compounds was performed through a TMSCl-mediated microwave-assisted Biginelli reaction, as described above.
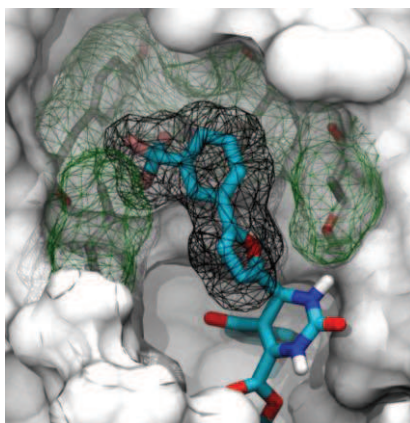


**Figure 3.4** *Shape complementarity between 6-(5-(3-(trifluoromethyl)phenyl)furan-2-yl) substituent and external binding groove of mPGES-1 (PDB code: 4AL0).*

Interference of the test compounds with mPGES-1 activity was investigated in a cell-free assay, using the microsomal fraction of interleukin-1β-stimulated human A549 cells. Inhibition of mPGES-1 by the test compounds was perfectly in line with computational predictions. In fact, among the tested compounds, an interesting $IC_{50}$ value of $4.16 \pm 0.47$ μM was detected for compound **48** (**Table 3.2**), confirming our previsions regarding the appropriate accommodation of a putative inhibitor in the mPGES-1 binding site.

**Scheme 3.2** *Synthetic protocol and chemical structures of synthesized DHPM derivatives.*
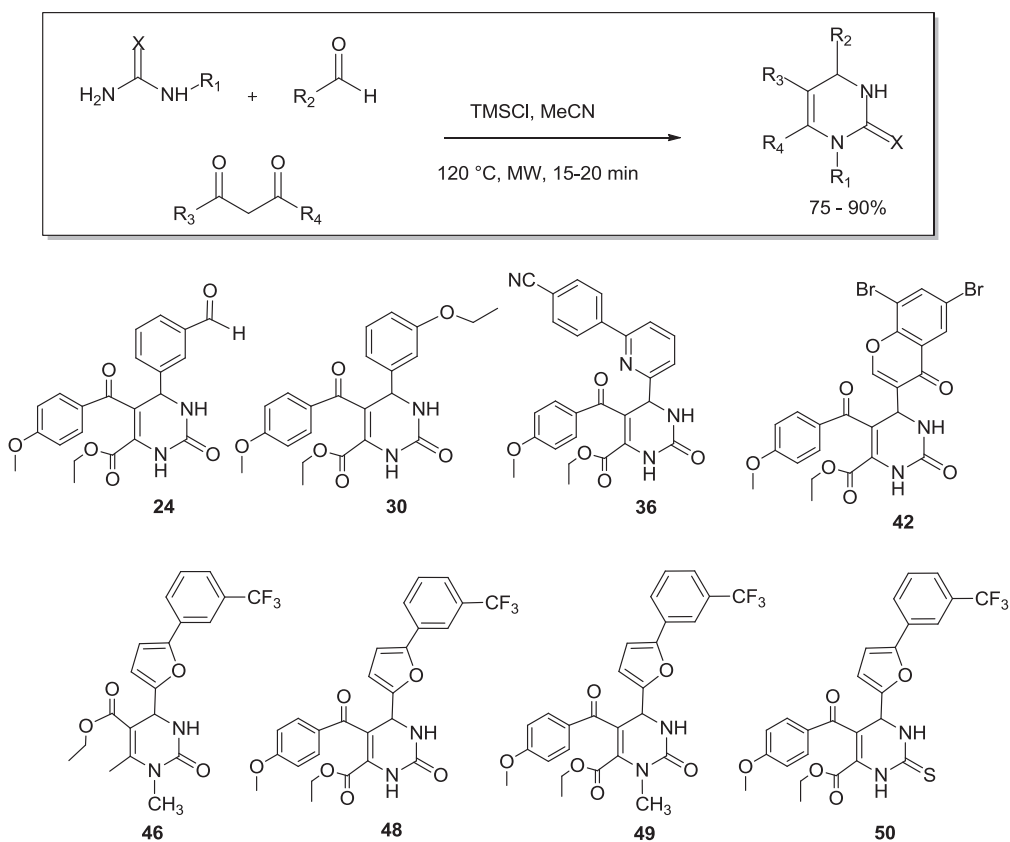




**Table 3.2** *mPGES-1 inhibition by tested DHPM compounds. Experiments were performed in triplicate.*

| Entry | $IC_{50} \pm SEM$ (µM) |
|-------|------------------------|
| 24    | > 30                   |
| 30    | > 30                   |
| 36    | > 30                   |
| 42    | > 30                   |
| 46    | > 30                   |
| 48    | $4.16 \pm 0.47$        |
| 49    | $7.56 \pm 0.94$        |
| 50    | > 30                   |

Moreover, maintaining the crucial 4-, 5- and 6- substituents on the dihydropyrimidine core, two **48**-related compounds were synthesized and tested for their biological activity, namely the N1-methyl derivative **49** and the thio-analog **50** (**Scheme 3.2**). The results obtained showed an efficient inhibitory activity for **49** ($IC_{50} = 7.56 \pm 0.94$ μM), but a weak and incomplete suppression of mPGES-1 activity for **50** (37% inhibition at 10 μM, $IC_{50} > 30$ μM) (**Table 3.2**). Since the docking model of **50** confirms the respect of the key interactions found for **48** and **49**, the differences in biological activities could be most likely ascribed to the influence of the chemical properties of sulfur *versus* oxygen (such as dimensions, electronegativity), not properly weighted by the scoring functions of the docking software. To further confirm that the presence of both 4-methoxybenzoyl group at C5, and 5-(3-(trifluoromethyl)phenyl)furan-2-yl) group at C4 is necessary for the activity, compound **46** was synthesized as negative control.

As expected, compound **46**, lacking the aromatic substituent at C5 was found to be inactive. In **figure 3.5** the docking model related to the active compound **48** is depicted. The 5-(3-methoxybenzoyl) group establishes a π-π interaction with Tyr130(A), while the bulky 4-(5-(3-(trifluoromethyl)phenyl)furan-2-yl) substituent occupies the external binding groove, interacting with Thr31(B), Ile32(B), Gln134(A), and Leu135(A); more specifically, trifluoromethyl terminal group contributes to these interactions, making contacts with Tyr28(B). The 6-ethylcarboxylate function interacts with a shallow groove directed toward the cytoplasmic side of the protein, while the urea containing portions of the molecules establish polar contacts with Ser127(A). Similar binding modes have been observed for the derivatives **49** and **50**, while **46** lacked these fundamental interactions.

These outcomes have thus allowed to disclose the DHPM scaffold as an emerging molecular platform useful for the development of mPGES-1 inhibitors. Compound **47** and **48** have emerged as new inhibitors of this

complex membrane protein and have highlighted the structure-based design utilized as a reliable approach in the rational discovery of new mPGES-1 modulators.
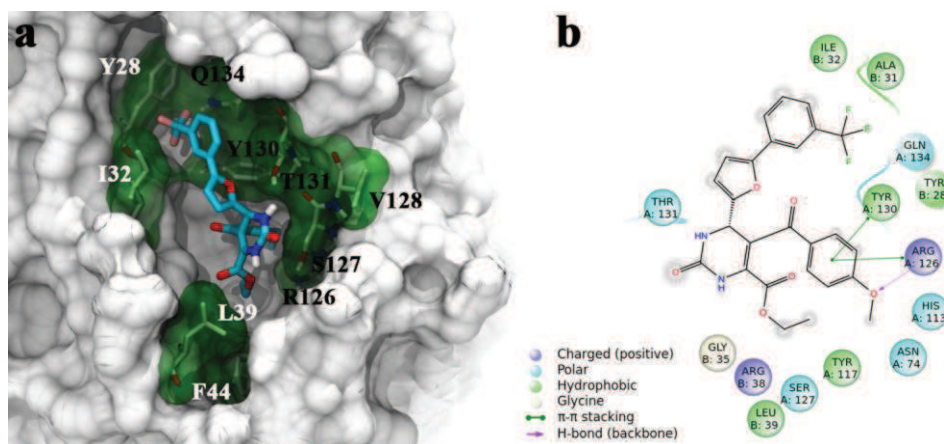


**Figure 3.5** *(a) 3D model of **48** docked in mPGES-1 active site (PDB code: 4AL0); residues in the active site represented in licorice (captions for residues in chain A and white captions for those in chain B) and related molecular surfaces depicted in transparent green. (**b**) 2D panel representing interactions between **48** and residues in mPGES-1 binding site.*

## 3.4 Structural optimization of compound 48, the promising DHPM-based mPGES-1 inhibitor

The second crystallized structure of mPGES-1 in complex with the inhibitor LVJ (PDB code: 4BPM)[16] offered new structural information for the optimization of the identified lead compound **48** (IC$_{50}$ = 4.16 ± 0.47 μM), which contains the privileged DHPM chemical core. Since this was the first reported co-crystal ligand-protein structure, the binding mode of LVJ was carefully analyzed in order to get useful information and to clarify the molecular basis for the interaction of a mPGES-1 inhibitor with the receptor counterpart. Firstly, LVJ acts as a substrate competitive inhibitor, but is unable to displace the cofactor GSH. Its 3D model (**Figure 3.6**) shows the presence of an extended set of polar and hydrophobic interactions of GSH with the key residues responsible for the catalytic activity of the investigated protein (A:ARG126, A:SER127, A:THR131).
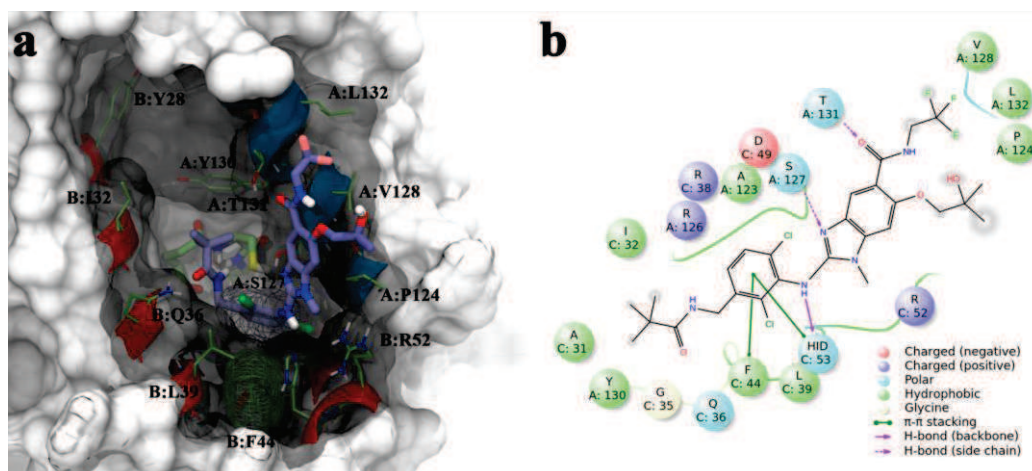
**Figure 3.6** (*a*) *3D model of LVJ in the mPGES-1 binding site (PDB code: 4BPM); residues in the active site represented in licorice and related molecular surfaces depicted in transparent silver; molecular surfaces of the interacting chemical groups of LVJ and B:PHE44 (edge-to-face π-π interaction) are highlighted in wireframes. (**b**) 2D panel representing interactions between LVJ and residues in mPGES-1 binding site.*

Importantly, LVJ adopts a peculiar slumped shape in the binding site, and this is mainly due to a strong edge-to-face π-π interaction between its dichlorophenyl moiety and the phenyl group in the side chain of B:PHE44, and similarly with B:HIS53. Moreover, the substituted benzimidazole moiety interacts with the external part of the binding site toward chain A, and the smaller (2,2-dimethylpropanoylamino)-methyl linear substituent partially occupies the binding groove in the upper portion of the active site (**Figure 3.6**). In light of the new elucidated structural insights, the binding mode of our lead compound **48** (**Scheme 3.2**) was re-evaluated with this new X-ray mPGES-1 structure (**Figure 3.7**). In particular, in our previous model, it was underlined the importance of the 4-methoxybenzoyl group at C5 on the central DHPM core that, when absent, dropped the inhibitory activity due to the lack of key-interactions with the receptor counterpart. Moreover, a fundamental face-to-face π-π interaction emerged between this aromatic moiety and the A:TYR130, the latter being normally involved in a stable contact with the cofactor GSH promoting the catalytic process.[212] In the new model here proposed, the binding mode of **48** was evaluated in presence of GSH, in

comparison with LVJ-protein interaction, revealing that the main feature of these two models is the different orientation of the 4-methoxybenzoyl group at C5 (**Figure 3.7**). In particular, while the 5-(3-(trifluoromethyl)phenyl)furan-2-yl group at C4 occupies the binding groove in a similar manner, in our new model the aromatic ring at C5 is oriented toward the shallow binding groove on the cytoplasmic part of the protein, close to the B:PHE44.
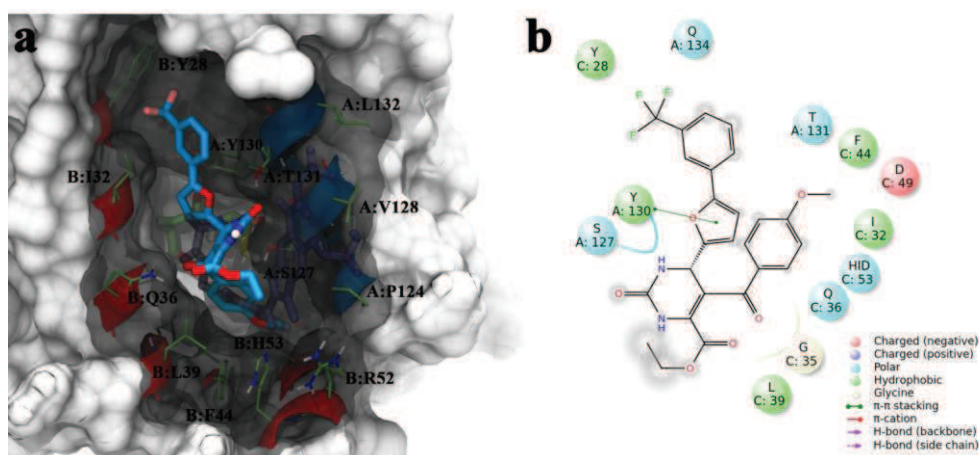


**Figure 3.7** (*a*) *3D model of **48** in docking with mPGES-1 (PDB code: 4BPM); residues in the active site represented in licorice and related molecular surfaces depicted in transparent silver; superimposed structure of LVJ is depicted in transparent iceblue licorice. (**b**) 2D panel representing interactions between **48** and residues in mPGES-1 binding site.*

Nevertheless, although the compound is able to occupy the binding site by establishing a large pattern of contacts, the strong edge-to-face π-π interaction with B:PHE44, observed for LVJ, was not detectable in this case (**Figure 3.7**).

In an effort to improve the activity of our lead compound, three structural related analogues of **48** (compounds **51-53**, **Scheme 3.3**), considered as reference compound, were designed and synthesized, by making precise and accurate slight modifications. In particular, the 5-(3-(trifluoromethyl)phenyl)-furan-2-yl group at C4 was preserved in light of its good shape complementarity with the enzyme, the aromatic substituent at C5 was modified in order to reach B:PHE44, and finally the C6 position of the DHPM core was simplified, as it showed to be not essential for the protein inhibition.

**Scheme 3.3** *Structures of compounds 51-53 and synthetic strategy.*
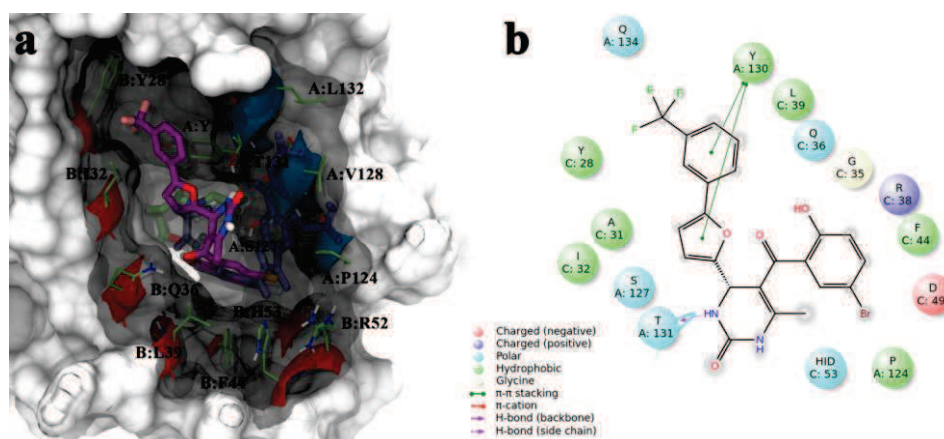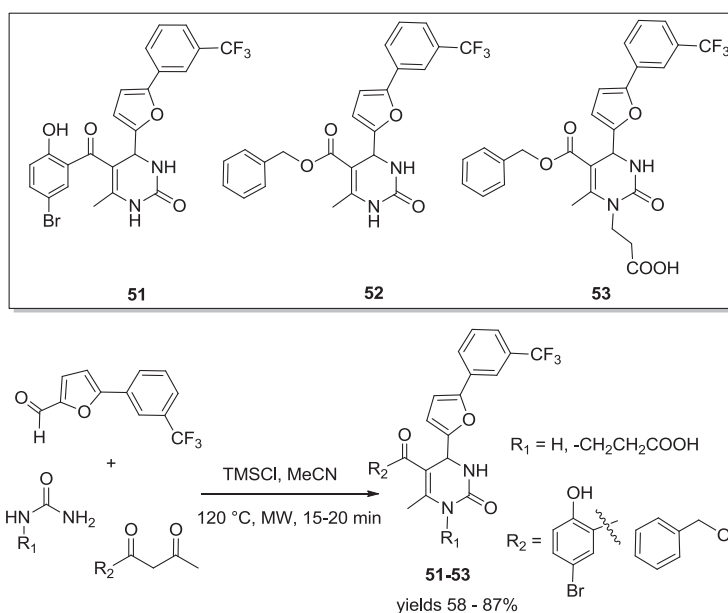




**Figure 3.8** (*a*) *3D model of 51 in docking with mPGES-1 (PDB code: 4BPM); residues in the active site represented in licorice and related molecular surfaces depicted in transparent silver; superimposed structure of LVJ is depicted in transparent iceblue licorice.* (*b*) *2D panel representing interactions between 51 and residues in mPGES-1 binding site.*

Three commercially available Biginelli building blocks were used in the microwave-assisted procedure, which yielded compounds **51-53** in good yields and short reaction times, as outlined in **Scheme 3.3**. At first, compound **51** was synthesized, employing 1-(5-bromo-2-hydroxyphenyl)-1,3-butanedione as 1,3-dicarbonyl synthon in the Biginelli reaction, to verify whether substitutions on

the aromatic ring with H-bond acceptors/donors type (Br and OH) at the C5 of the DHPM core could gain favourable interactions with B:PHE44, also in consideration that, in virtual screening predictions, the meta bromine showed to mimic the chlorine of LVJ inserting deeply in mPGES-1 binding cavity, and showed to be more effective than meta chloro and meta hydroxy analogues. Moreover, since in the proposed 3D model of **48** the 6-ethylcarboxylate function was not involved in fundamental contacts in the binding site, this chemical function was replaced with the smaller 6-methyl group.

Docking studies on **51** showed a slightly better interaction of the (5-bromo-2-hydroxyphenyl)-oxo substituent at the C5 with B:PHE44 even if, also in this case, the moiety revealed to be not perfectly superimposed with that of LVJ involved in the π-π with B:PHE44. In vitro biological tests confirmed these computational outcomes, with an $IC_{50} = 5.6 \pm 0.4$ μM, comparable with that of **48** ($IC_{50} = 4.16 \pm 0.47$ μM). On the basis of these results, in order to achieve a more favourable orientation of the C5 linked moiety in the binding site, an unsubstituted aromatic ring was inserted at C5, more spaced from the dihydropryrimidine core through the introduction of an oxymethylene linker (**Scheme 3.3**). For this purpose, benzyl acetoacetate was used as 1,3 dicarbonyl synthon for the synthesis of compound **52**. Docking experiments supported our hypothesis, revealing a perfect superimposition of the benzyl-oxy-carbonyl portion at the C5 of **52** with the dichlorophenyl moiety of LVJ and showing to establish the key edge-to-face π-π with B:PHE44 (**Figure 3.9**). As expected, the inhibitory activity of **52** on mPGES-1 was improved, with an $IC_{50} = 1.4 \pm 0.6$ μM. After having identified the optimal C5 substituent on the DHPM core, the possibility of modifying the N1 position was also considered, since in **48** this unsubstituted nitrogen was not involved in any key interactions with polar residues. A 2-carboxy-ethyl function was thus inserted at N1 (compound **53**), also in accordance with the suggestion of molecular docking experiments performed on differently N1 substituted compounds.
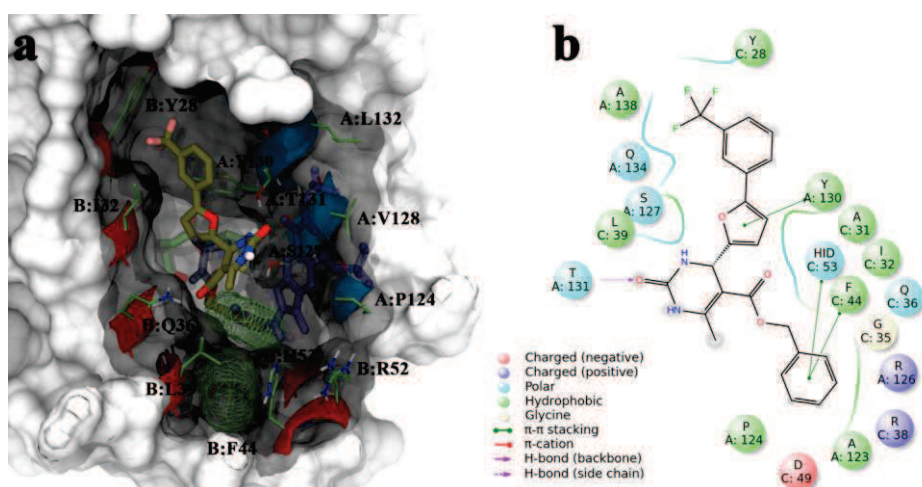
**Figure 3.9** (*a*) *3D model of* **52** *in docking with mPGES-1 (PDB code: 4BPM); residues in the active site represented in licorice and related molecular surfaces depicted in transparent silver; superimposed structure of LVJ is depicted in transparent iceblue licorice. (**b**) 2D panel representing interactions between* **52** *and residues in mPGES-1 binding site.*
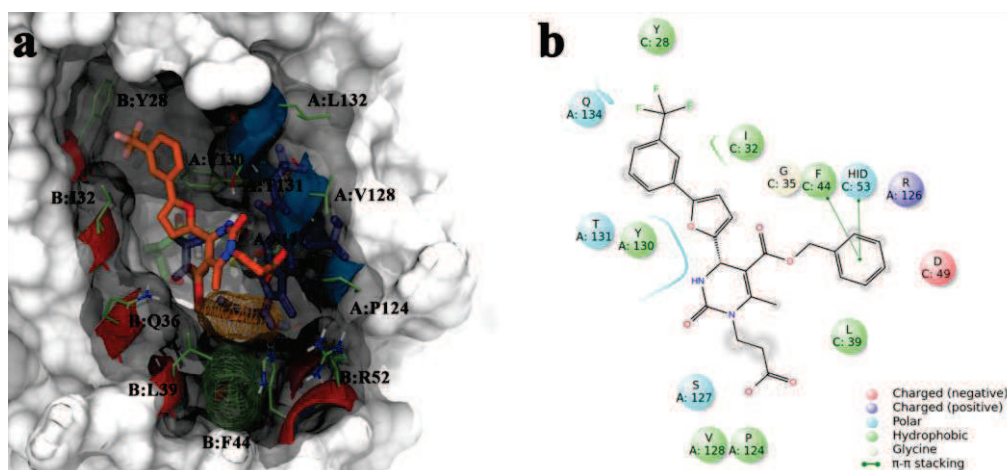


**Figure 3.10** (*a*) *3D model of* **53** *in docking with mPGES-1 (PDB code: 4BPM); residues in the active site represented in and related molecular surfaces depicted in transparent silver; molecular surfaces of the interacting chemical groups of* **53** *and B:PHE44 (edge-to-face π-π interaction) are highlighted in wireframes; superimposed structure of LVJ is depicted in transparent iceblue licorice. (**b**) 2D panel representing interactions between* **53** *and residues in mPGES-1 binding site.*

The significant improvement of the biological profile of **53** ($IC_{50} = 0.41 \pm 0.02$ μM) fully validated our computational approach (**Figure 3.10**), confirming the hypothesis that the additional 2-carboxy-ethyl moiety at N1 gains relevant polar interactions with the key residue A:SER127 that, in turn, contributes to the catalytic isomerization of $PGH_2$ to $PGE_2$.[212]

In consideration that all the molecules have a stereocenter at C4 position of the DHPM core, computational calculations were performed on both the possible enantiomers. Results obtained for **53** showed only slight different binding energy values between them which, however, prompted us to further explore the stereochemical aspect on DHPM chemistry (studies are currently in progress). Anyway, the fulfillment of the key-interactions with the receptor counterpart was found for both the possible enantiomers at C4, albeit a difference in predicted binding energies was observed due to the slightly different orientation of the DHPM core into the mPGES-1 binding cavity (**Figure 3.11**).
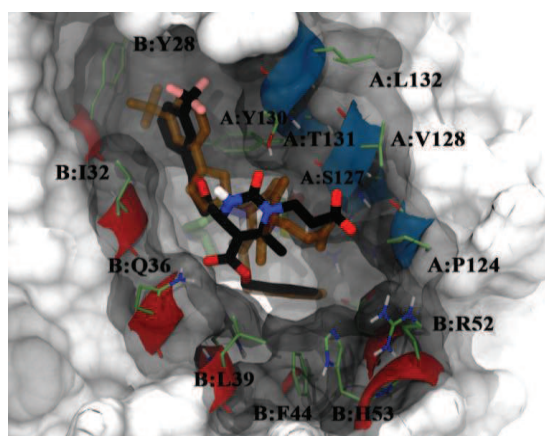


**Figure 3.11** *Superimposition between the two possible enantiomers of 53 at C4 (R enantiomer colored by atom types: C black, N blue, O red, H light gray, F pink; S enantiomer colored in transparent orange) in docking with mPGES-1. Predicted binding affinities, as calculated with Glide software: -7.48 kcal/mol (R enantiomer); -8.83 kcal/mol (S enantiomer).*

In conclusion, the careful analysis of mPGES-1 crystal structure in complex with its known inhibitor LVJ offered precious insight for the structural optimization of our DHPM-based mPGES-1 inhibitor **48**, allowing to disclose the 10-fold more potent analogue **53**. The described structure-activity relationships and the very useful synthetic approach constitute important guidelines for the design of further improved DHPM-based inhibitors of mPGES-1.

# -CHAPTER 4-

Discovery of new Hsp90 C-terminal modulators: synthesis and biological evaluation of 3,4-dihydropyrimidin-2(1H)-one derivatives.

## 4.1 Stressing the discovery of Hsp90 C-terminal inhibitors

In recent years many natural and synthetic Hsp90 N-terminal inhibitors have been developed, some of which show excellent antitumor activity and have entered clinical trials,[348] while only few C-terminal inhibitors have been identified so far.[361] In contrast to N-terminal modulators, which have some drawbacks in clinical application (high concentration for biological effect, poor solubility and toxic side effects),[353-355] the C-terminal inhibitors represent a promising therapeutic alternative for targeting malignant cells, as they do not induce the deleterious pro-survival heat shock response commonly reported for N-terminal ligands.[356, 357] The heat shock response (HSR) is a highly conserved mechanism in all organisms, from yeast to humans, induced by proteotoxic insults such as heat, oxidative stress, toxins, bacterial infections and heavy metals.[460] This ubiquitous reaction suggests that the HSR is crucial for survival in a stressful environment. Expression of the heat shock proteins (HSPs) is increased as a result of HSR induction, which is mediated by the transcription factor heat shock factor 1 (HSF-1).[461, 462] In non-stressed cells, HSF-1 is found as a monomer, bound to Hsp90 (inactive state) in the cytoplasm.[463-465] In case of stress, or upon administration of an N-terminal Hsp90 inhibitor, HSF-1 is released from the heteroprotein complex.[357] As a monomer, HSF-1 is unable to bind to DNA but, once dissociated from Hsp90, it trimerizes, undergoes hyperphosphorylation and translocates to the nucleus.[466] As an activated trimer, HSF-1 is able to bind the so-called heat shock element sequence on the DNA and directs transcription, resulting in the expression of HSPs.[467] N-terminal Hsp90 inhibitors induce the dissociation of HSF-1 from Hsp90 and trigger the pro-survival heat shock response, which results in increased levels of HSPs, giving rise to a cytoprotective mechanism that allows cancer cells to escape the cytotoxic effect (**Figure 4.1**).[358] In addition, Hsp90 levels are remarkably increased, producing dosing and scheduling issues.[468, 469]
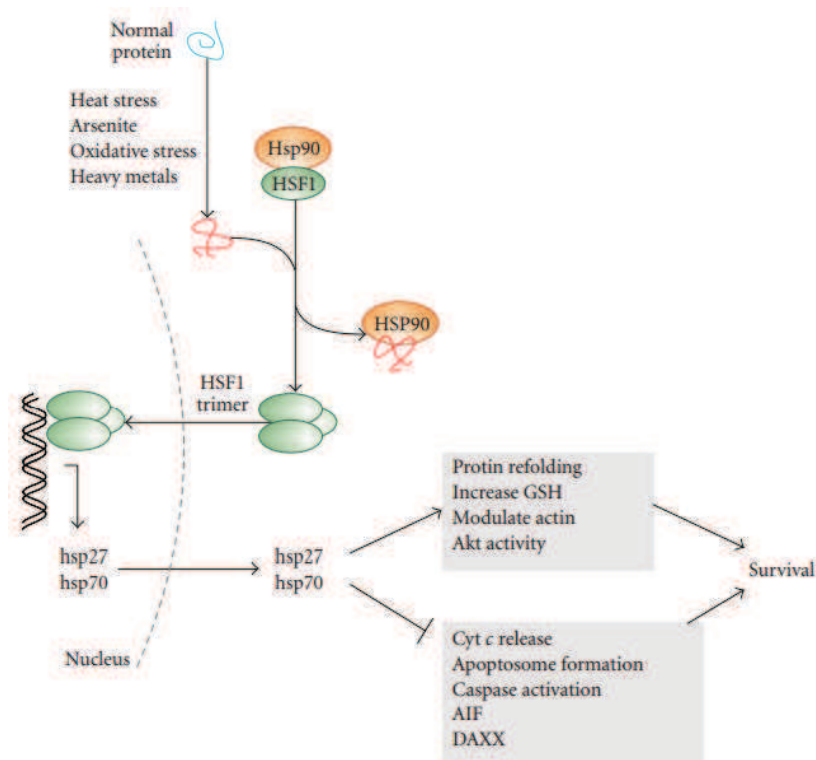
**Figure 4.1** *Heat shock response.*[462]

Conversely, C-terminal Hsp90 inhibitors have an opposite effect, as they lock HSF-1 into its inactive Hsp90-bound state and promote its degradation *via* the proteasome.[359, 470, 471] This aspect of C-terminal inhibition is particularly relevant, due to the possibility of overcoming the limitations associated with N-terminal inhibition. The first identified C-terminal ligand was novobiocin ($IC_{50}$ = 700 µM against Hsp90 in SKBr3), a natural coumarin antibiotic which inhibits type II topoisomerases.[362] Since novobiocin's discovery, only few other C-terminal inhibitors have been found, including taxol,[374] epigallocatechin-3-gallate,[372] cisplatin,[373] sansalvamide A derivatives,[377] and novobiocin's structural related synthetic analogues (novologues).[367, 368, 389] Although the binding mode of Hsp90 N-terminal inhibitors has been well defined,[472] the structural elements required for interaction with Hsp90 C-terminus are currently poorly characterized, due to the absence of a co-crystal structure of this site with any inhibitor. A recent

work on novobiocin analogues, by molecular dynamics approaches, has provided additional information on structural variations of Hsp90 C-terminal binding site;[473] however, the vast conformational space of this flexible chaperone is still a strong limitation for the rational design of selective inhibitors of this domain.

### 4.2 Targeting Hsp90 C-terminal domain by DHPM-based derivatives

In an attempt to identify non-natural inspired modulators as new molecular templates for the inhibition of Hsp90 C-terminal domain, published data were used as starting assumptions. Csermely *et al.*[335, 337] reported that this domain is able to interact with both purine and pyrimidine nucleotides (GTP and UTP preferentially), unlike the N-terminus which is highly specific for adenine nucleotides. On the basis of the structural analogy between UTP and the privileged heterocyclic core 3,4-dihydropyrimidin-2-(1H)-one (DHPM), a collection of different decorated DHPM derivatives  was synthesized (compounds **54-85**, **Figure 4.2** and **4.3**), by a microwave-assisted Biginelli multicomponent reaction[418] through the combination of the following synthons (**Scheme 4.1**):

- seven different aldehydes (**A-G**);
- four urea derivatives (**i-iv**);
- two 1,3-dicarbonyl compounds (**a-b**).

In most cases, compounds were obtained by using chlorotrimethylsilylane (TMSCl) as the mediator of the microwave-assisted Biginelli reaction but, for some compounds, TMSCl was replaced by the Lewis acids ytterbium(III) trifluoromethanesulfonate [$Yb(OTf)_3$] and iron(III) chloride [$Fe(Cl)_3$] (see Experimental Section).

Biological screening on some of the synthesized compounds is still in progress (**71-85**, **Figure 4.3**), while activity of **54-70** (**Figure 4.2**) has already been investigated and will be here discussed.

**Scheme 4.1** *General synthetic procedure for the synthesis of compounds **54-85** and structures of the building blocks used to generate the collection of DHPMs.*



Regents and conditions: **a)** TMSCl (1 equiv), MeCN **b)** Yb(OTf)3 (10 mol %), AcOH/EtOH (3:1) **c)** FeCl3 (10 mol %), AcOH/EtOH (3:1).
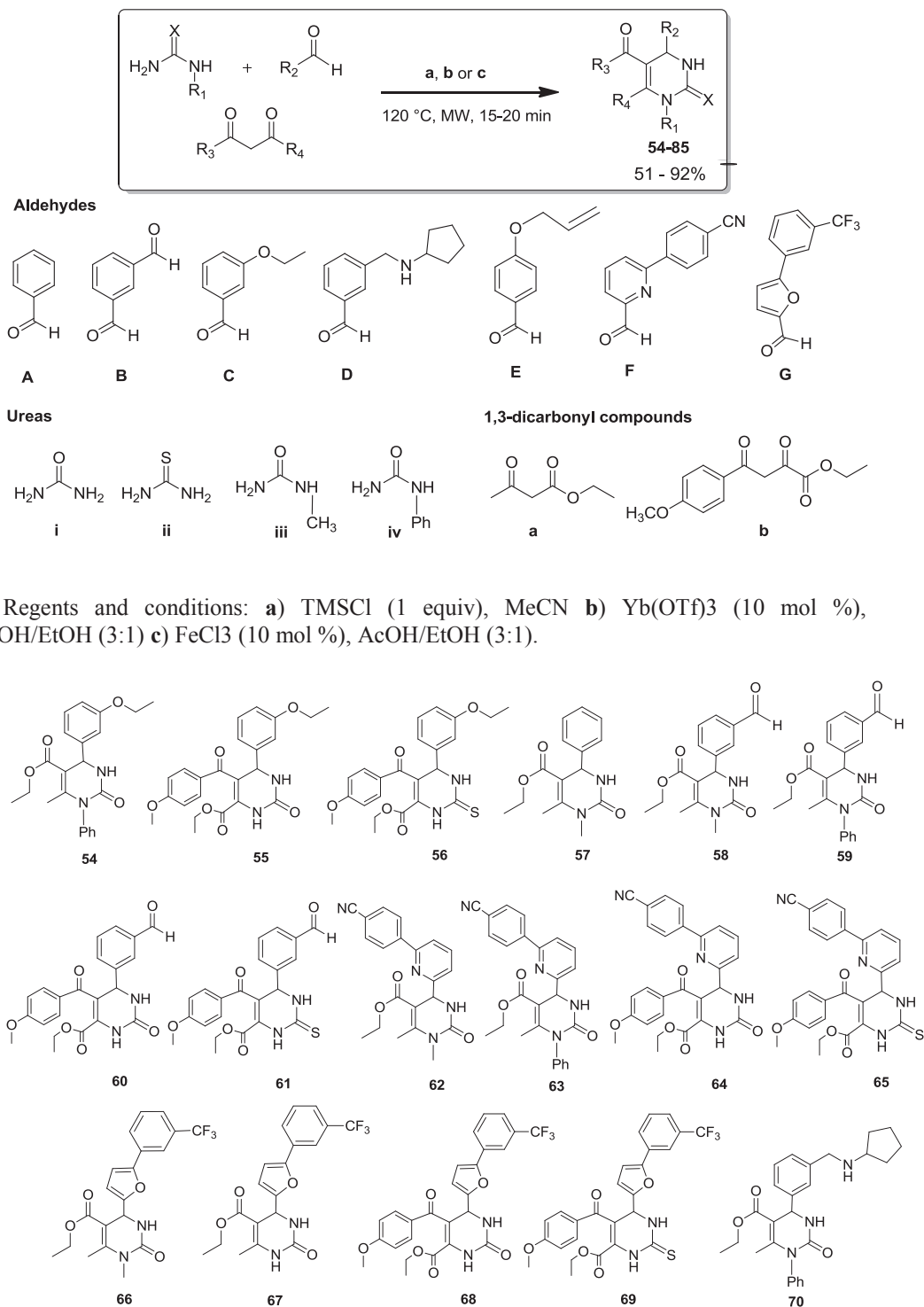


**Figure 4.2** *Structures of compounds **54-70** (preliminary screened compounds).*
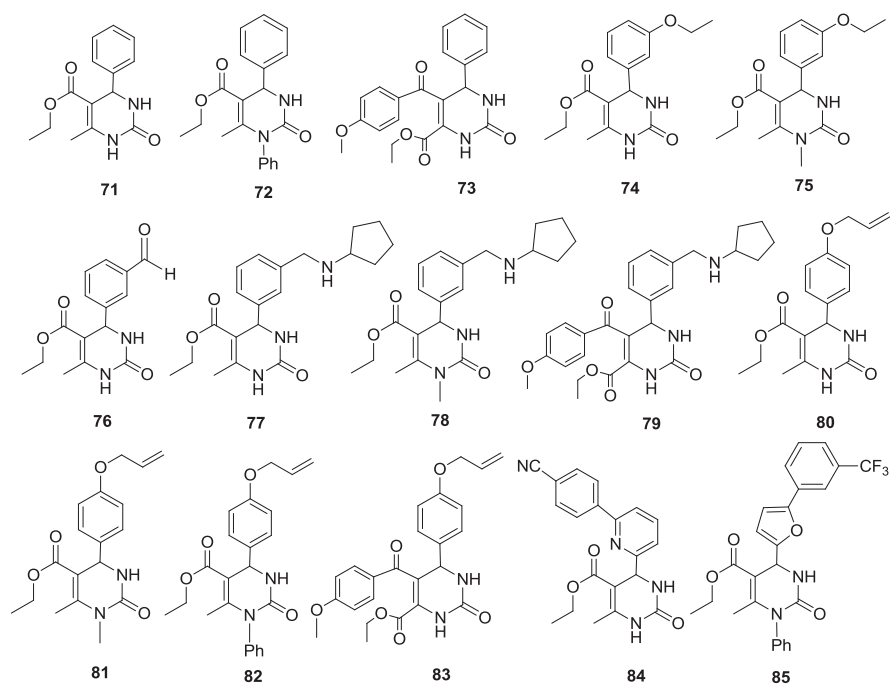
**Figure 4.3** *Structures of compounds 76-85 (biological evaluation in progress).*

Biological evaluation has been accomplished in collaboration with Professor Antonietta Leone and Fabrizio Dal Piaz of Salerno University. Once synthesized, compounds **54-70** were evaluated for the putative binding to the recombinant Hsp90α, by a Surface Plasmon Resonance (SPR)-based approach.[474] On the basis of this preliminary screening, 7 out of 17 tested molecules with low $K_D$ values were identified (**Table 4.1** and **Figure 4.4**). Among these, there are compounds with the less bulky 3-ethoxyphenyl and 3-formylphenyl substituents at $R_2$ of the DHPM ring (**54**, **55**, and **59-61** respectively), one molecule with a bulkier group at this position (**65**) and compound **70**, obtained from derivatisation of **59** by reductive amination.

Actually, the results obtained on this small collection of compounds do not allow to draw a clear SAR profile. In any case, beyond the identification of DHPM as a suitable scaffold for the development of new promising Hsp90 inhibitors, some speculations can be argued. In particular, all the compounds with a N-phenyl at N-1 position were shown to bind to the immobilized

protein with nanomolar ($K_D$ values of $76 \pm 7$ and $30 \pm 1$ nM for **54** and **70**, respectively) or micromolar affinity ($K_D = 3.86 \pm 0.33$ µM for **59**), with the exception of compound **63** which did not exhibit any binding to Hsp90α, probably due to the presence of the bulkier (4-cyanophenyl)pyridin-2-yl group.

**Table 4.1** *Thermodynamic constants measured by SPR for the interaction between tested compounds and immobilized Hsp90α.*

| Entry | $K_D$ (µM) |
|---|---|
| 54 | $0.0756 \pm 0.0071$ |
| 55 | $0.0137 \pm 0.0017$ |
| 56 | No Binding |
| 57 | No Binding |
| 58 | No Binding |
| 59 | $3.860 \pm 0.331$ |
| 60 | $0.176 \pm 0.0089$ |
| 61 | $0.3626 \pm 0.0289$ |
| 62 | No Binding |
| 63 | No Binding |
| 64 | No Binding |
| 65 | $1.1475 \pm 0.098$ |
| 66 | No Binding |
| 67 | No Binding |
| 68 | No Binding |
| 69 | No Binding |
| 70 | $0.0295 \pm 0.0014$ |
| 17-AAG | $0.388 \pm 0.089$ |

Neither the effect of a sulfur atom at the C-2 position of the ring could be clearly rationalized. Indeed, while the thio-analogue of **55**, compound **56**, showed no affinity for the immobilized protein, on the contrary compound **65**, the thio-derivative of **64**, was the only (4-cyanophenyl)pyridin-2-yl-containing molecule able to interact with Hsp90α; furthermore, compounds **60** and **61**,

more related to **55** and obtained utilizing respectively urea and thiourea in the multicomponent reaction, were both tight binders ($K_D$ values of $176 \pm 9$ and $363 \pm 29$ nM, respectively). Finally, the 5-(3-(trifluoromethyl)phenyl)furan-2-yl substituent at C-4 showed to be not effective, since compounds **66-69** did not bind at all to the immobilized target protein.
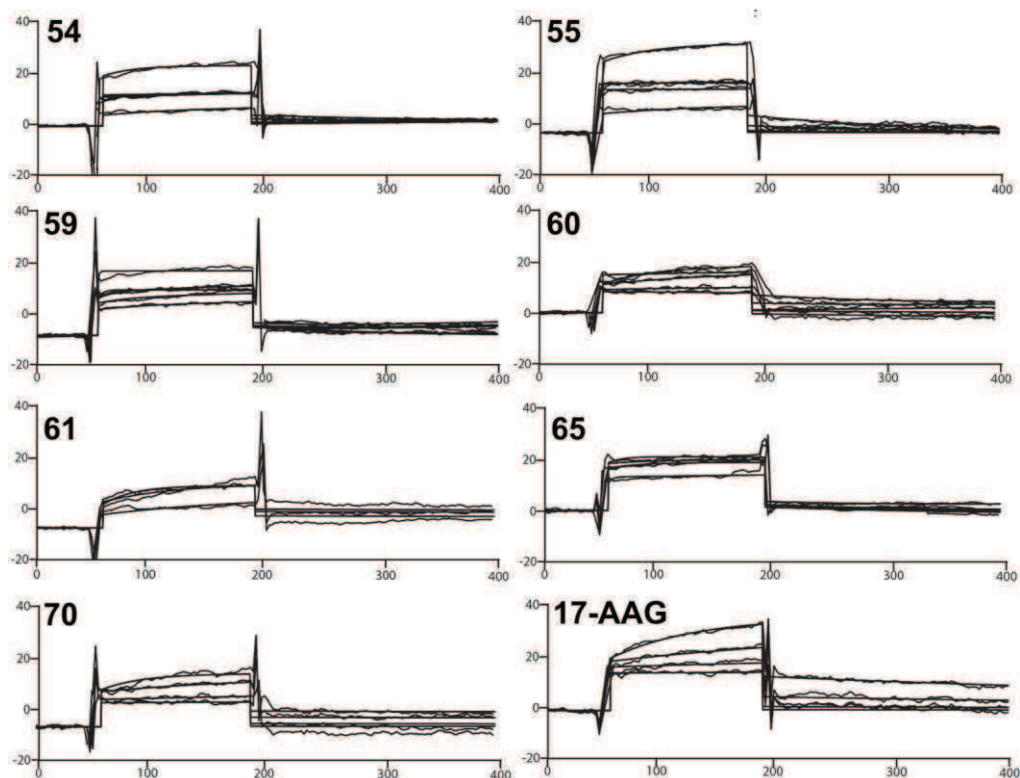


**Figure 4.4** *Surface Plasmon Resonance sensorgrams acquired for compounds interacting with Hsp90α and for the positive control 17-AAG. Each compound was injected onto an Hsp90α modified sensor chip at 6 different concentrations in the range 0.025–1 μM.*

## 4.3 Antiproliferative assays, western blot analysis and effect on cell cycle progression

The seven identified Hsp90α binders (**54**, **55**, **59-61**, **65**, **70**) were tested for their potential antiproliferative effect in A375 (human melanoma) and Jurkat (human leukemic) cell lines. Compound **70** exhibited $IC_{50}$ values of $150 \pm 0.3$ μM in both cancer cell lines, while **55**, **59-61** and **65** had no cytotoxicity. The

best result was reported for compound **54**, which showed moderate cytotoxic effects at micromolar concentration, with $IC_{50}$ values of $50.8 \pm 0.2$ and $20.8 \pm 0.3$ µM in A375 and Jurkat, respectively. Under the same experimental conditions, $IC_{50}$ values for 17-AAG treatment were $2.1 \pm 0.3$ µM in A375 and $9.6 \pm 0.15$ µM in Jurkat cell lines, in agreement with those reported by Dal Piaz *et al.*[475] and Liu *et al.*[476] Interestingly, the cytotoxic effect found for compound **54** was in line with SPR analyses, in which **54** resulted as one of the most efficient binder to the immobilized recombinant Hsp90α ($K_D$ of $76 \pm 7$ nM). Furthermore this compound had no negative effect on PHA-stimulated proliferating PBMC, a non-tumour cell line utilised as control (the percentage of non-viable cells after 24 h of treatment with 50 µM of compound **54** (about $8\% \pm 0.7$) was similar to that observed control cells (about $7\% \pm 0.5$) treated with DMSO). To ascertain that the cytotoxic activity of compound **54** was associated with changes in Hsp90 modulation, the level of expression of some Hsp90 client oncoproteins was verified in treated and untreated cancer cell lines, by western blot analysis (**Figure 4.5**).
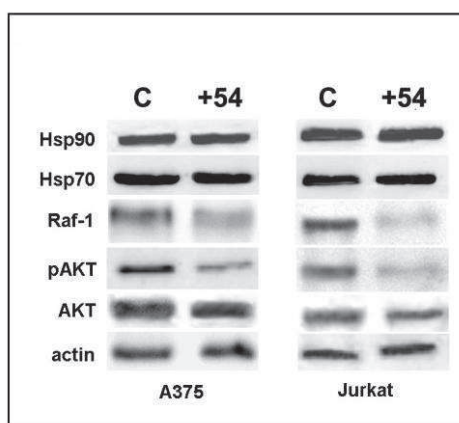


**Figure 4.5** *Effect of compound 54 on Hsp90 client protein levels in A375 and Jurkat cells. The shown blots are representative of three different experiments with similar results.*

Following 24-h exposure to compound **54**, the levels of Hsp90 and Hsp70 proteins were unaffected, while the level of the client proteins Raf-1 and p-Akt was strongly down-regulated (about 50-70% less compared to untreated cells,

by densitometric estimation) in A375 and Jurkat cell lines. These data suggested that the binding of compound **54** might cause conformational changes of Hsp90 structure, thus preventing its chaperone activity, necessary for stabilizing the oncoproteins, which are therefore subsequently addressed to the proteolytic degradation.[289] It is worth to note that exposure to compound **54** did not cause any significant increase in the level of Hsp90 and Hsp70 in both cancer cell lines, evidencing that the undesired HSR was not induced.

To further investigate the cytotoxic effects induced by compound **54**, the cell cycle progression of treated cancer cells versus normal cell PHA-stimulated PBMC was analyzed, using flow cytometric analysis.[477] The A375, Jurkat and PBMC cells were incubated for 24 h with concentrations close to IC$_{50}$ values of **54** or 17-AAG. Cell cycle distribution analysis indicates that, unlike 17-AAG, compound **54** affects the cell cycle inducing a G2/M arrest in both cancer cell lines, and a consequent increase of subG0/G1 DNA content, indicative of apoptotic/necrotic cell death, in the Jurkat cells (**Figure 4.6**). Compound **54** did not exhibit any pro-death or cytostatic activity in PHA-stimulated proliferating PBMC (data not shown).
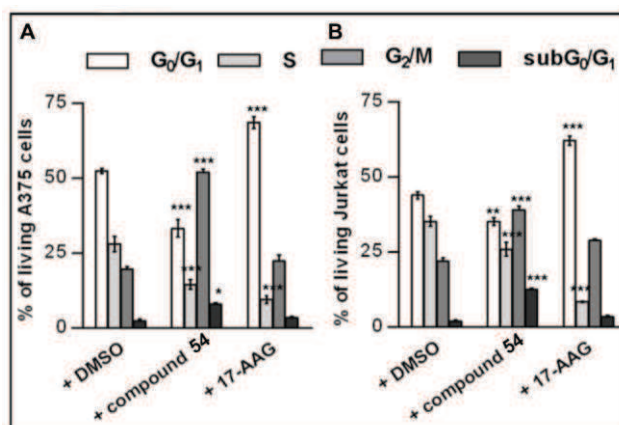


**Figure 4.6** *Quantification of cell cycle distribution of viable A375 (A) or Jurkat (B) cells treated with DMSO, compound **54** (50 or 20 µM, respectively) or 17-AAG (2 or 10 µM, respectively) for 24 h, evaluated by PI staining. Results are expressed as means ± SD of three independent experiments, performed in duplicate (\*\*\*P < 0.001, \*\* P < 0.01, \*P < 0.05 versus control).*

### 4.4 Study of Hsp90α/54 interaction

With the aim of identifying the Hsp90α region involved in the binding of **54**, a limited proteolysis-mass spectrometry-based approach was employed out for the structural analysis of the Hsp90α/**54** complex. The efficiency of this approach, in the investigation of Hsp90α/inhibitor interaction, relies on the evidence that exposed, weakly structured and flexible regions of a target protein can be recognized by a proteolytic enzyme and, therefore, the observed differences in the proteolytic patterns, in the presence or in the absence of a putative protein ligand, can be useful to identify the protein regions involved in the molecular interactions.[475, 478] The proteolytic patterns obtained both on Hsp90α and on the Hsp90α/**54** complex, using trypsin or chymotrypsin as proteolytic agents, are summarized in **Figure 4.7**. A comparison between them confirmed a direct interaction between **54** and the chaperone. Indeed, it was observed that the peptide bonds following Lys435 and Lys614, preferential cleavage sites of the native chaperone in absence of **54**, were protected in the complex, thus indicating that the middle and C-terminal domain of Hsp90α are likely involved in the ligand binding.
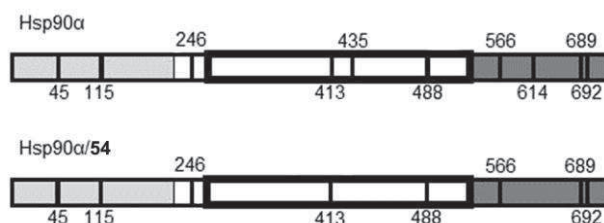


**Figure 4.7** *Schematic representation of limited proteolysis experiments. The preferential cleavage sites detected on recombinant Hsp90α and on the Hsp90α/**54** complex are indicated in black. The Hsp90α N-terminal domain is highlighted in light grey, while the middle domain is boxed and the C-terminal domain is highlighted in grey*.

The conformational changes of Hsp90 induced by compound **54**, through a likely interaction with its C-terminus encouraged to evaluate whether this binding could affect also Hsp90α oligomerisation, as previously reported for other C-terminal inhibitors, such as some novobiocin-related compounds[366] or

(-)-epigallocatechin-3-gallate.[372] To evaluate this hypothesis, an Hsp90α dimerisation experiment, using a chemical cross-linking agent on both the full-length protein and on the Hsp90α/**54** complex, was carried out.[372]
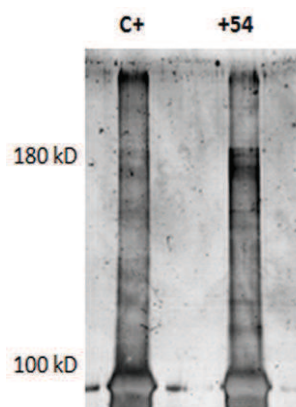


**Figure 4.8** *Inhibition of Hsp90α oligomerisation by compound **54**.*

Compound **54** showed to inhibit the chemically-induced oligomerisation of the full-length Hsp90 (**Figure 4.8**). Under the experimental conditions used, and in the presence of the cross-linking agent, the protein tended to form tetramers, while incubation of Hsp90α with **54** clearly prevented protein tetramer formation. These effects on Hsp90α oligomerisation closely resemble those observed for (-)-epigallocatechin-3-gallate,[372] thus confirming a similar interaction of **54** with Hsp90α. Taken together, the experimental data from limited proteolysis and those from oligomerisation assays indicated that compound **54** interacts with the C-terminal domain of Hsp90α. Finally, molecular docking was performed in the attempt to obtain a binding mode of **54** in the C-terminal pocket. The chosen model receptor for computational analyses was the ATP-bound active state of Hsp82, yeast homolog of Hsp90α (PDB code: 2CG9),[341] and its sequence alignment with the human protein, reported by Lee *et al.*[479] As recently reported by Colombo *et al.*,[473] the most frequent residues interacting with inhibitors are represented by Arg591, Asp503, Lys423, Gln596, and Arg599 of chain B, and Lys594 and Glu477 of chain A (Hsp90 residue numbering as in the PDB entry 2CG9).[341] **Figure 4.9**

clearly shows the interactions of **54** with the region located at the dimerisation site interface (residues 587-594, chain A).
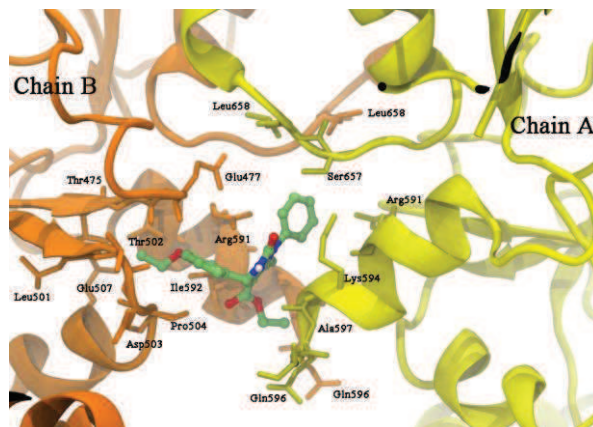


**Figure 4.9** *Three dimensional model of 54 at interface of C-terminal domain of chain B (orange ribbon) and chain A (yellow ribbon) of the Hsp82, yeast homolog of Hsp90α.*

In more detail, the contemporary π-cation interaction with Arg591 of chain B and Lys594 of chain A, together with the hydrophobic contacts with the key residues, such as Gln596, Asp503, Glu477, can account for its inhibitory activity. These results are consistent with the data obtained from limited proteolysis and oligomerisation assays, confirming that the C-terminal domain of Hsp90α (Lys614$_{Hsp90}$ (Lys594$_{Hsp82}$)) is involved in the ligand binding responsible for its inhibitory activity.

In **Table 4.2**, the most representative properties of compounds **54-70** are reported and, among them, predicted apparent Caco-2 cell permeability (nm/sec) was considered with particular attention.[480, 481]

Interestingly, **54** shows the highest predicted Caco-2 cell permeability with respect to the other Hsp90α binders (**55**, **59-61**, **65** and **70**) emerged from the SPR assay. The presence of a 3-ethoxyphenyl group in **54** at R$_2$ position increases the predicted Caco-2 cell permeability of ≈ 4 folds with respect to the strictly related compound **59** which instead contains at R$_2$ the 3-formylphenyl group; this could explain their different in-cell activity, together with the higher K$_D$ value observed for **59**.

**Table 4.2** *Predicted properties of tested compounds calculated by QikProp algorithm.*

| Entry | mol MW[a] | QPPCaco2[b] | metab[c] | RuleOfFive[d] | rtvFG[e] | QPlogPo/w[f] | QPlogS[g] |
|---|---|---|---|---|---|---|---|
| **54** | 380.4 | 1444.6 | 4 | 1 | 1 | 4.28 | -5.33 |
| **55** | 424.5 | 538.0 | 4 | 0 | 2 | 2.98 | -4.56 |
| **56** | 440.5 | 1572.8 | 5 | 1 | 3 | 5.21 | -6.59 |
| **57** | 274.3 | 1012.5 | 3 | 0 | 1 | 3.33 | -4.39 |
| **58** | 302.3 | 244.1 | 3 | 0 | 1 | 5.07 | -6.54 |
| **59** | 364.4 | 344.6 | 3 | 0 | 1 | 3.67 | -5.36 |
| **60** | 408.4 | 88.1 | 3 | 0 | 2 | 5.38 | -6.37 |
| **61** | 424.5 | 295.7 | 4 | 0 | 3 | 3.88 | -6.59 |
| **62** | 376.4 | 204.1 | 3 | 0 | 1 | 6.00 | -6.94 |
| **63** | 438.5 | 232.3 | 3 | 1 | 1 | 5.32 | -7.17 |
| **64** | 482.5 | 71.0 | 3 | 0 | 2 | 3.60 | -6.58 |
| **65** | 498.6 | 340.2 | 4 | 0 | 3 | 5.00 | -8.00 |
| **66** | 408.4 | 936.7 | 4 | 1 | 1 | 2.20 | -3.49 |
| **67** | 394.4 | 566.0 | 4 | 1 | 1 | 3.81 | -5.67 |
| **68** | 514.5 | 261.9 | 4 | 2 | 1 | 4.94 | -7.64 |
| **69** | 530.5 | 1289.1 | 5 | 2 | 2 | 5.15 | -6.32 |
| **70** | 433.5 | 241.0 | 5 | 1 | 1 | 5.10 | -6.88 |

[a] Molecular weight, range 95% of drugs (130/725). [b] Caco2 cell permeability in nm/s, range 95% of drugs (<25 poor, >500 great). [c] Number of primary metabolites. Range 95% of drugs (1/8). [d] Number of violations of Lipinski's rule of five.[35] The rules are: mol_MW < 500, QPlogPo/w < 5, donor HB ≤5, accptHB ≤10. Compounds that satisfy these rules are considered drug-like. [e] Number of reactive functional groups, range 95% of drugs (0 – 2). [f] Log of the octanol/water partition coefficient, range 95% of drugs (2/6.5). [g] Log of aqueous solubility S (mol/L), range 95% of drugs (-6.5/0.5).

Given the promising results on compound **54**, the DHPM collection was further expanded by synthesizing other structural related analogues of this compound has been undertaken in order to get more information and to provide a clear structure-activity relationships profile against Hsp90. The structures of some **54**-derivatives are shown in **Figure 4.10**. Their biological evaluation as well as and the synthesis of further analogues are currently in progress.
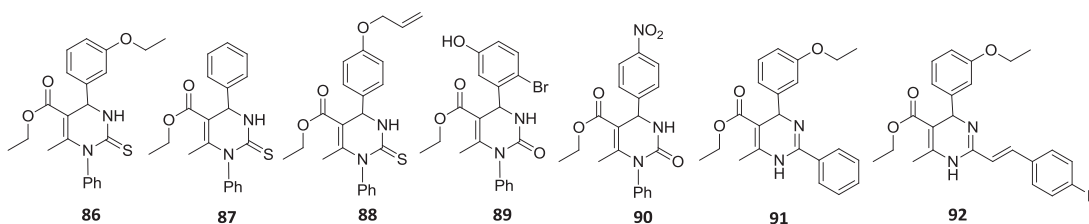
**Figure 4.10** *Synthesized analogues of compound 54 to explore SAR against Hsp90.*

# -CHAPTER 5-

His-tagged human mPGES-1 overexpression in
Lemo21(DE3) *E. coli* strain and 2D-crystallization studies.

During the second year of my PhD, in 2013, I joined Prof. Hans Hebert's research group at the Department of Biosciences and Nutrition of Karolinska Institutet (Sweden), where I spent seven months. During that period, my research was carried out under the supervision of Dr. Caroline Jegerschöld and was addressed to the heterologous expression and two-dimensional crystallization of human mPGES-1. Results of that work are here discussed.

## 5.1 Membrane protein overexpression in *E. coli*

Integral membrane proteins are notoriously difficult to study, as their natural abundance is usually too low to isolate sufficient material for structural and biochemical investigation. Consequently, membrane protein characterization studies can be accomplished only after appropriate overexpression procedures in suitable hosts.[482-486] Membrane proteins are grouped in two main classes: β-barrel and helical bundle membrane proteins.[487] β-barrel membrane proteins can be more easily obtained than helical bundle ones, as they can be readily isolated and refolded after overexpression from inclusion bodies.[488] Conversely, despite remarkable efforts, the refolding of helical bundle membrane proteins after denaturing isolation from inclusion bodies is very challenging and frequently unsuccessful.[489] Therefore, overexpression of helical membrane proteins, through accumulation in a membrane system, is actually the preferred strategy, as it avoids the refolding problems and enables protein purification after detergent extraction. The bacterium *E. coli* is the most widely used host,[490] although membrane protein overexpression is often toxic to prokaryotic cells, hence preventing biomass formation and strongly reducing yields.[482, 491] Toxicity to their over-production host is just one of the problems to deal with: in fact, the unavailability of a systematic, generic, and high-throughput-compatible method, the requirement of lipids for correct folding and function,

and finally the need to use detergents that can destabilise the overexpressed protein are further difficulties to be faced.[492-494]

Bacteriophage T7 RNA polymerase (T7RNAP) is often used to drive recombinant protein expression in *E. coli*.[495] T7RNAP recognizes the T7 promoter, governing the expression of the target protein, and transcribes 8 times faster than *E. coli* RNAP, allowing high yields of produced protein.[496, 497] In *E. coli* BL21(DE3) strain and its derivatives,[498, 499] the gene encoding T7RNAP is under control of the IPTG–inducible, not well–titratable *lac*UV5 promoter, a strong variant of the wild-type *lac* promoter.[497, 500, 501] The rationale behind BL21(DE3) is very simple; the more mRNA is produced, the more protein can be overexpressed. However, this assumption is not always correct, especially in the case of membrane proteins.[502] Indeed, membrane proteins overexpression in BL21(DE3) is typically toxic, resulting in accumulation of cytoplasmic aggregates containing the overexpressed protein, proteases, chaperones, many essential cytoplasmic proteins, and many precursors of periplasmic and outer membrane proteins.[503] Moreover, membrane protein overexpression causes an inefficient ATP production, due to the reduced levels of respiratory chain complexes in the cytoplasmic membrane. These effects are caused by a too fast transcription/translation rate, which leads to saturation of the bacterial membrane protein insertion machinery, the Sec translocon,[504] that has a severe impact both on the composition and on the functioning of the cell envelope, as it is proved by hampered cell division (**Figure 5.1**).[503]

An expedient to harmonise translation and insertion into the membrane of the recombinant membrane protein would be therefore the minimization of the toxic effects derived from overexpression.
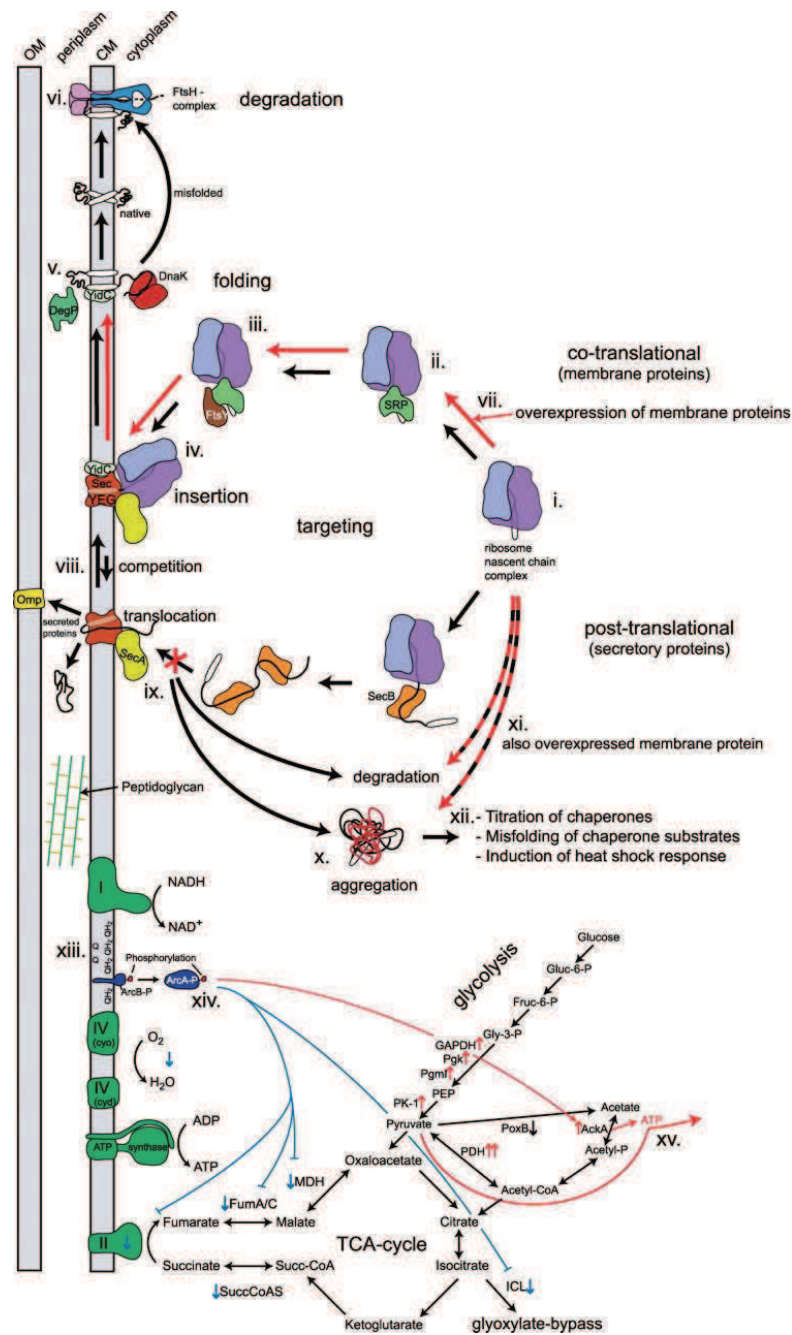
**Figure 5.1** *Consequences of membrane protein overexpression in E. coli.*[503]

BL21(DE3)–derived strains with improved membrane protein overexpression characteristics were isolated in the laboratory of John Walker: BL21(DE3) cells, able to cope with the toxic effects of membrane protein

overexpression, were selected and led to the C41(DE3) and C43(DE3) strains, commonly known as the Walker strains, which are often used to overexpress membrane proteins.[505] However, they do not always allow to get improved yields for all tested membrane proteins.[506] Mutations in the *lac*UV5 promoter, governing expression of the T7 RNAP, play a key role in the improved membrane protein overexpression observed with the Walker strains.[506] As a consequence of these mutations, much lower amounts of T7 RNAP are produced upon the addition of IPTG, when compared to BL21(DE3). Therefore, the risk of saturating the Sec translocon capacity upon membrane protein overexpression is diminished.

## 5.2 Lemo21(DE3) *E. coli* strain

The mutations in the *lac*UV5 promoters in the Walker strains can be mimicked in BL21(DE3) by dampening T7RNAP activity through its natural inhibitor, T7 lysozyme (T7Lys).[507] Expression of T7Lys is under the control of a rhamnose promoter, which is extremely well titratable, meaning that the amount of rhamnose added correlates with the amount of protein expressed.[508]

T7Lys was placed under the control of an L-rhamnose inducible promoter (*rha*BAD) on a pACYC derived plasmid, designated pLemo. The *rha*BAD promoter has some features that make it extremely well suitable for expression of the T7RNAP inhibitor T7Lys: it is exceptionally well titratable, covers a broad window of expression intensities, and finally it functions independently of strain background (**Figure 5.2**).[508] BL21(DE3) transformed with pLemo is referred to as Lemo21(DE3).[506] In Lemo21(DE3) strain a clear correlation between the L-rhamnose concentration, growth, and protein production was observed. Upon increase of L-rhamnose concentrations, overgrowth of the culture, by nonexpressing cells and aggregate formation, were prevented. Moreover, at the optimal concentration of L-rhamnose, only mild induction of bacterial chaperones was detected and oxygen consumption was not affected.

Interestingly, screening the overexpression of various membrane proteins in Lemo21(DE3) in the presence of different amounts of rhamnose suggested that this strain may be very well suitable for optimizing the *E. coli*-based production of membrane proteins.[506, 509-511]

Given the tunable characteristics of the Lemo21(DE3) for membrane protein overexpression, this strain has been employed for the heterologous expression of the human homotrimeric membrane protein mPGES-1, with the aim of performing 2D-crystallization studies in order to evaluate the interaction of our identified DHPM inhibitors with this enzyme.
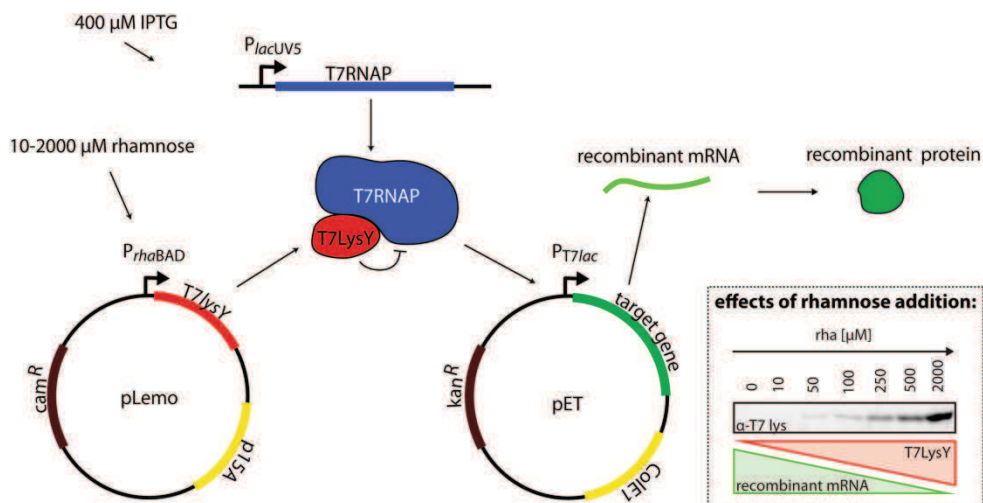


**Figure 5.2** *Optimizing membrane protein overexpression in Lemo21(DE3) strain.*[510]

## 5.3 mPGES-1 overexpression in Lemo21(DE3) strain

Human mPGES-1 had been previously overexpressed in *E. coli* BL21(DE3)pLysS competent cells.[446] In that case, the electron crystallographic structure of the enzyme was elucidated at 3.5 Å in-plane resolution. However, the protein was in its closed conformation, while only its open active form represents the suitable state for ligand/protein interaction studies. In an attempt to isolate mPGES-1 from a different host for further structural studies finalized to investigate the interaction between this

membrane protein and its ligands, an expression in a bacterial strain, more suitable for membrane protein overexpression, was carried out. Preliminary screenings pointed out that the Walker strains, C41(DE3) and C43(DE3), often used for overexpression of membrane proteins, resulted inappropriate in the case of mPGES-1. Therefore, a strain more similar to the previously used BL21(DE3)pLysS, but engineered for the production of proteins considered as "difficult" to be overexpressed, was employed: the Lemo21(DE3) strain.[486]
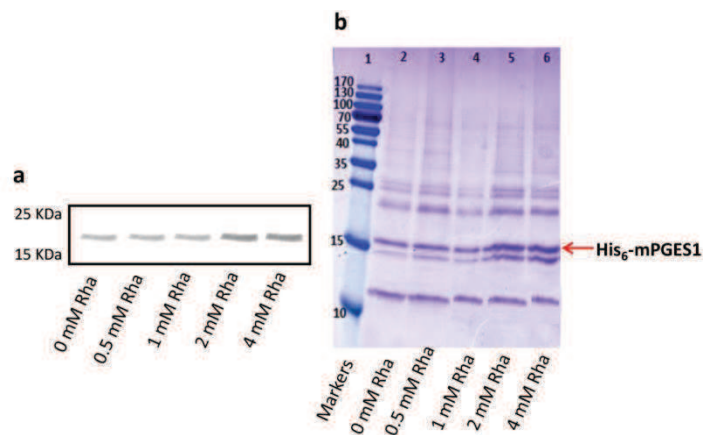


**Figure 5.3** *Screening of the optimal overexpression condition of His$_6$-mPGES-1 in Lemo21(DE3) cells. Results are shown in the case of induced protein expression in LB medium at 30 °C.(**a**) Western Blot analyses of overexpressed protein at different L-rhamnose concentrations. (**b**) SDS-PAGE of samples from Western Blot experiments.*

Lemo21(DE3) competent cells were transformed with pSP19T7LT-His$_6$-mPGES1 vector, expressing the protein with a hexahistidine tag (His$_6$-mPGES1) at the N-terminal portion. Initial expression screening was carried out by inoculating a starter culture of transformed Lemo21(DE3) cells in 20 ml of Luria-Bertani (LB) or Terrific broth (TB) at different L-rhamnose concentrations (0 – 4 mM), by inducing protein expression with the addition of 0.4 mM Isopropyl β-D-1-thiogalactopyranoside (IPTG) at different temperatures (in a range between 20 and 37 °C). Purification of cell lysates on nickel magnetic beads (Dynabeads® Life Technologies) and analysis by SDS-PAGE, followed by Western Blot, highlighted that a major amount of

overexpressed protein was obtained in LB medium at 2 or 4 mM of L-rhamnose by inducing protein expression at 30 °C (**Figure 5.3**).

The optimal identified conditions were employed to scale-up mPGES-1 overexpression in 1 liter culture of Lemo21(DE3) cells in LB medium at 2 mM L-rhamnose concentration. Cells were grown at 37 °C until an appropriate value of optical density was reached ($OD_{600}$ = 0.4–0.6), afterwards temperature was cooled to 30 °C and protein expression was induced by the addition of IPTG. Cells continued to grow over-night at 30 °C and were subsequently harvested by centrifugation and lysed by sonication. His$_6$-mPGES1 was purified from the whole cell extract, after detergent solubilisation of membrane proteins (4% Triton X-100), by a two-step combination of hydroxyapatite followed by immobilized metal ion affinity chromatography on a chelating Sepharose column charged with Ni$^{2+}$. The solubilised extract was mixed with hydroxyapatite resin and the unbound fraction was loaded on the nickel column. All His$_6$-mPGES-1 was retained on the column, and the unspecifically bound proteins were removed by a wash step of 60 mM imidazole. Pure His$_6$-mPGES-1 was then eluted by the addition of 350 mM imidazole (**Figure 5.4a**). The eluted protein was instantly loaded on a desalting column to avoid any possible damage by the high imidazole concentration. A 17,500 purified protein on Comassie-staining SDS-PAGE gels was identified. The molecular weight of the purified protein was calculated to 17,500 from its electrophoretic mobility relative to standards used for SDS-PAGE gel. This value is in agreement with the theoretical molecular weight of human His$_6$-mPGES1 (17,900) (**Figure 5.4a**). The yield was 0.2–0.5 mg of purified protein per 1 liter of Lemo21(DE3) expression culture. The purified protein was identified as mPGES-1 by immunoblot analysis, using rabbit polyclonal antibody directed against mPGES-1. Moreover, the correct assembly in its native trimeric form was confirmed by High Resolution Clear Native Electrophoresis (hrCNE),[512] which revealed a

band at 66,000 perfectly compatible with the native molecular weight of trimeric His$_6$-mPGES1 (53,700) solubilised in detergent micelles (**Figure 5.4b**).
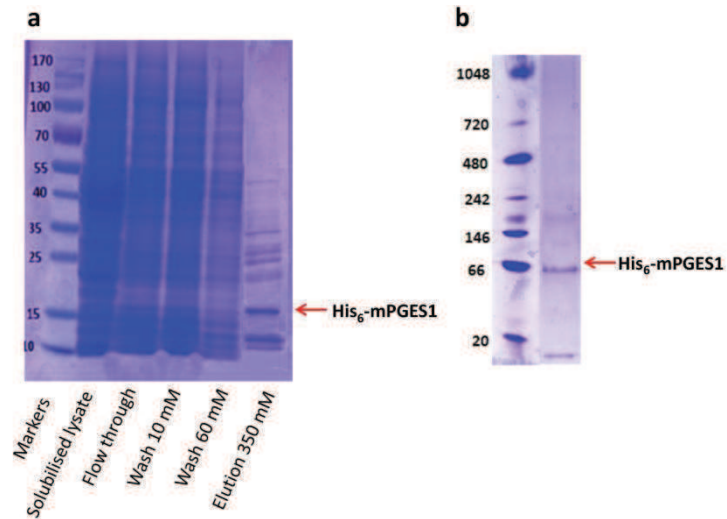


**Figure 5.4** *Large scale expression of human His$_6$-mPGES1.* (**a**) *SDS-PAGE from large scale purification of His$_6$-mPGES1 overexpressed in the Lemo21(DE3) strain in the presence of 2.0 mM L-rhamnose.*(**b**) *High-resolution clear native electrophoresis (hrCNE) of the purified protein.*
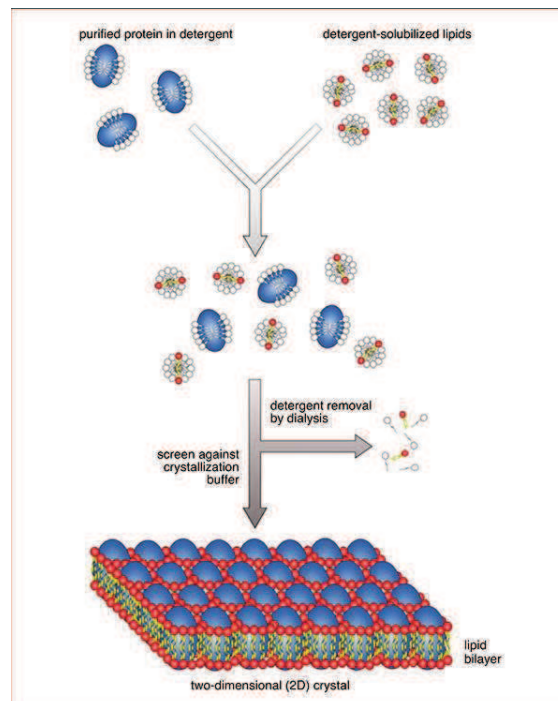


**Figure 5.5** *Two-dimensional crystallisation of membrane proteins.*[513]

Purified His$_6$-mPGES1 was subsequently subjected to two-dimensional crystallographic experiments in order to proceed with structural characterization by electron microscopy studies. Electron crystallography is the only structural biology branch in which a membrane protein is crystallized within the context of a membrane and from which atomic resolution structures of both protein and lipid can emerge.[513] Two-dimensional crystals are prepared by slow dialysis, which allows reconstitution of the membrane protein into a lipid bilayer. This is accomplished by mixing the detergent-solubilised protein with detergent-solubilised lipids. The detergent is then removed by slow dialysis and its removal induces the lipids to begin to form membranes in which the protein is integrated (**Figure 5.5**). This process must be optimized with the aim of inducing the formation of large and very well ordered crystalline sheets or vesicles.
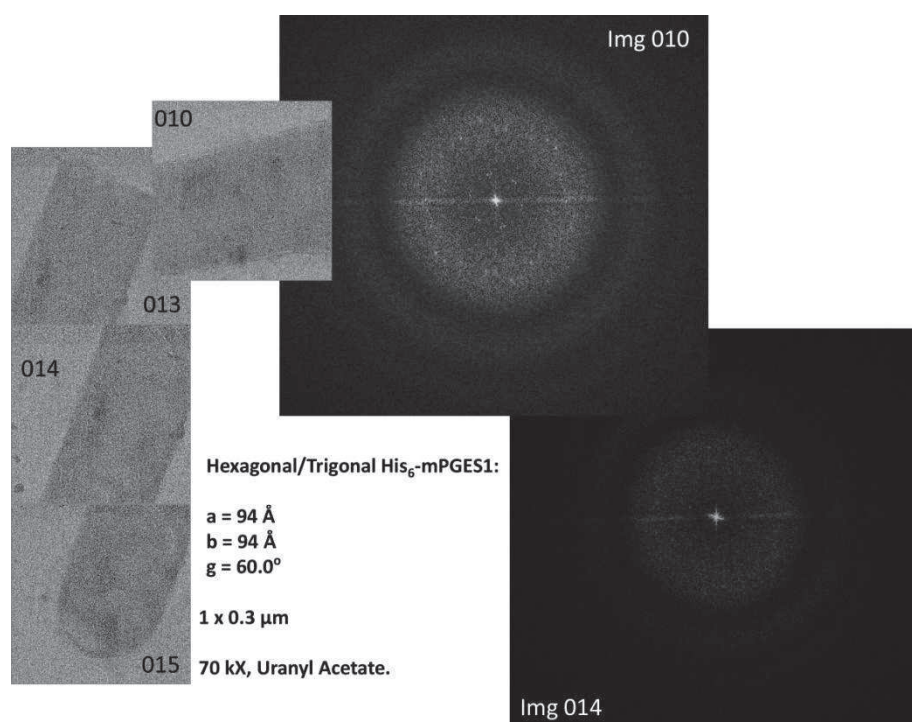


**Figure 5.6** *Two-dimensional crystals of human His$_6$-mPGES1 overexpressed in Lemo21(DE3) cells.*

In the case of His$_6$-mPGES1, two-dimensional crystals were grown by adding to the protein, solubilised in 1% Triton X-100, the lipid (bovine liver lecithin) at a low molar lipid to protein ratio of 9. The protein-lipid-detergent mixture was subsequently subjected to slow dialysis, by using a buffer as the one used for protein storage, but with 20% glycerol and lacking the detergent. Negatively stained samples, analysed by transmission electron microscopy, disclosed 1 x 0.3 µm crystals with a hexagonal symmetry in two layers (**Figure 5.6**). Unfortunately, crystals were not suitable for electron diffraction studies due to their small size. Several attempts were made to improve the quality of mPGES-1 crystals, such as repurification on magnetic beads of the eluate from Ni-NTA column, washes/elution of Ni-NTA column charged with His$_6$-mPGES1 at different imidazole concentrations, performing size exclusion chromatography on the samples from hydroxyapatite/IMAC purification, and finally isolation of the recombinant protein from the membrane fraction of bacterial cells, rather than from the whole cell lysates. Nevertheless, none of these trials enabled a better quality of the crystals suitable for structural studies.

In conclusion, in the field of bacterial overexpression of human mPGES-1 the best results have been achieved with BL21(DE3)pLysS until now.[446] However, the two mPGES-1 X-ray crystal structures, published in 2013[212] and 2014[448] respectively, display that high-resolution crystal structures of mPGES-1 can be elucidated when this membrane protein is expressed in *Spodoptera frugiperda* Sf9 cells, that represents a precious insight in the field and paves the way for next more efficient experiments of membrane protein expression by the use of eukaryotic cells instead of bacterial host.

# -CONCLUSIONS-

**Conclusions**

The crosstalk between cancer cells and inflammatory mediators has been known for a long time, even though the complex pathways and correlations between these two pathological processes have not been fully clarified yet. In this research field, considerable efforts have been carried out leading to the identification of new emerging molecular targets involved at different levels in cancer and inflammatory-related diseases. Among these, bromodomain (BRD) containing proteins, microsomal Prostaglandin $E_2$ Synthase-1 (mPGES-1) and Heat shock protein 90 (Hsp90) are of relevant interest, as they are main players both in inflammatory and in malignant processes. Considered their biological importance and their potential for therapeutic applications, this research project has been mainly addressed to the discovery of new modulators of these three biological targets.

In order to find new BRDs modulators, a combination of structure-guided and computational approaches was employed, allowing to identify some 9*H*-purine-based compounds (e.g., **7d** and **11)** which showed nanomolar affinity towards BRD9, with lower activity towards BRD4. The interaction between the two emerged 6-aryl-9*H*-purine inhibitors (**7d** and **11**) and the bromodomain cavities of BRD9 and BRD4 has been fully elucidated by crystallography and docking experiments. Finally, their efficiency in a cellular environment was validated by performing BRET assays. These outcomes validate the hypothesis of using 2-amino-9*H*-purines as a starting point to develop new compounds targeting BRDs outside the BET family, with compound **11** representing a promising tool in the case of BRD9.

The use of a proper qualitative structure-based filter, together with the docking binding predicted affinities, represented an excellent approach for the discovery of new mPGES-1 inhibitors. This strategy allowed to identify the 3,4-dyhidropyrimidin-2(1H)-one (DHPM) core as new molecular platform for mPGES-1 modulation, yielding compounds **48** and **49** which exhibited $IC_{50}$

values in the low micromolar range. Subsequently, the study of mPGES-1 crystal structure in complex with its known inhibitor LVJ offered new insights for the structural optimization of compound **48** ($IC_{50}$ = 4.16 ± 0.47 μM), leading to a 10-fold more potent analogue (compound **53**, $IC_{50}$ = 0.41 ± 0.02 μM).

The assumption that the DHPM core may also represent a new template to target Hsp90 C-terminal domain derived from the structural analogy between the DHPM core and uridine triphosphate (UTP), a nucleotide that selectively interacts with Hsp90 C-terminus. A collection of differently decorated DHPMs has been synthesized and, to date, deep biological investigation has been carried out on a group of 17 compounds. Our outcomes disclosed compound **54** as a new promising antiproliferative agent, exerting its activity through inhibition of Hsp90 upon binding to its C-terminal region.

# EXPERIMENTAL SECTION

# -CHAPTER 6-

Synthesis of purine derivatives as new modulators of human

bromodomains: Experimental procedures

## 6.1 General synthetic methods

All commercially available starting materials were purchased from Sigma-Aldrich and were used as received. Solvents used for the synthesis were of HPLC grade and were purchased from Sigma-Aldrich or Carlo Erba Reagenti. NMR spectra were recorded on Bruker Avance 600 or 300 MHz instruments. Compounds were dissolved in 0.5 ml of MeOD, CDCl$_3$, or DMSO-$d_6$. Coupling constants (*J*) are reported in Herz, and chemical shifts are expressed in parts per million (ppm) on the delta (δ) scale relative to the solvent peak as internal reference. Multiplicities are reported as follows: s, singlet; d, doublet; t, triplet; m, multiplet; dd, doublet of doublets. Electrospray mass spectrometry (ESI-MS) was performed on a LCQ DECA TermoQuest (San Josè, California, USA) mass spectrometer. Chemical reactions were monitored on silica gel 60 F$_{254}$ plates (Merck) and spots were visualized under UV light. Analytical and semi-preparative reversed-phase HPLC were performed on an Agilent Technologies 1200 Series high performance liquid chromatography system using Jupiter Proteo C$_{18}$ reversed-phase columns ((a) 250 x 4.60mm, 4 μ, 90 Å, flow rate = 1 ml/min; (b) 250 x 10.00 mm, 10 μ, 90 Å, flow rate = 4 ml/min respectively, Phenomenex®). The binary solvent system (A/B) was as follows: 0.1% TFA in water (A) and 0.1% TFA in CH$_3$CN (B). Absorbance was detected at 240 nm. The purity of all tested compound (> 95%) was determined by HPLC analysis. Microwave irradiation reactions were carried out in a dedicated CEM-Discover® Focused Microwave Synthesis apparatus, operating with continuous irradiation power from 0 to 300 W utilizing the standard absorbance level of 300 W maximum power. Reactions were carried out in 10 ml sealed microwave glass vials. The Discover™ system also included controllable ramp time, hold time (reaction time) and uniform stirring. After the irradiation period, reaction vessels were cooled rapidly (60-120 s) to ambient temperature by air jet cooling.

## 6.2 Methods and materials

Fragments **1** (2,6-dichloro-9*H*-purine) and **2a** (2-amino-6-bromo-9*H*-purine) were purchased from Sigma Aldrich and used as received. Fragment **2b** (2-amino-6-bromo-9-methylpurine) was synthesized from **2a** by a TBAF-assisted alkylation procedure with iodomethane (See *6.2.2*).

### 6.2.1 General procedure for the Suzuki-Miyaura cross-coupling of free halo-purines (3a-b, 3d, 3f-h, 4a-d, 5a, 6a-c, 7a-e, 8a, 9a-b, 10, 11)

2-amino-6-bromopurine (50.0 mg, 0.23 mmol), commercially available boronic acids (**A-U**, 0.29 mmol), Pd(OAc)$_2$ (2.70 mg, 0.012 mmol), P(C$_6$H$_4$SO$_3$Na)$_3$ (34.0 mg, 0.06 mmol) and Cs$_2$CO$_3$ (228.0 mg, 0.70 mmol) were added to a 10 ml microwave vial equipped with a magnetic stirrer. The vial was evacuated and backfilled with nitrogen three times. Degassed acetonitrile (0.5 ml) and degassed water (1.0 ml) were added by means of an air-tight syringe. The mixture was heated under microwave irradiation at 150 ºC for 5-15 min. After irradiation, the vial was cooled to ambient temperature by air jet cooling and a mixture of cold water and 1.5 M HCl were added (5.0 and 2.0 ml, respectively). The mixture was subsequently poured into crushed ice and then left at 4 ºC overnight. The resulting precipitate was filtered and purified by HPLC to give the desired product in good yields (53-90%). HPLC purification was performed by semi-preparative reversed-phase HPLC using the gradient conditions reported below for each compound.
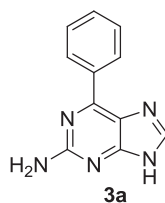


**2-amino-6-phenyl-9*H*-purine (3a)**: was obtained as a white powder in 90% yield from **2a** and phenylboronic acid (**A**). RP-HPLC t$_R$ = 12.1 min,

gradient condition: from 5% B to 100% B in 60 min, flow rate of 4 ml/min, $\lambda$ = 240 nm. Spectral data were in accord with previously published data.[514]
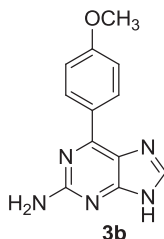


**2-amino-6-(4-methoxyphenyl)-9*H*-purine (3b)** was obtained as a pale yellow powder in 86% yield from **2a** and 4-methoxyphenylboronic acid (**B**). RP-HPLC $t_R$ = 14.6 min, gradient condition: from 5% B to 100% B in 65 min, flow rate of 4 ml/min, $\lambda$ = 240 nm. Spectral data were in accord with previously published data.[395]
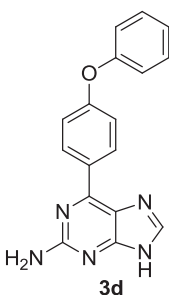


**2-amino-6-(4-phenoxyphenyl)-9*H*-purine (3d)** was obtained as a pale yellow powder in 90% yield from **2a** and 4-phenoxyphenylboronic acid (**O**). RP-HPLC $t_R$ = 24.1 min, gradient condition: from 5% B to 100% B in 65 min, flow rate of 4 ml/min, $\lambda$ = 240 nm. ^{1}H NMR (300 MHz, MeOD): $\delta$ = 7.10-7.20 (m, 4H), 7.25 (t, $J$ = 7.1 Hz, 1H), 7.46 (t, $J$ = 7.5 Hz, 2H), 8.36 (br s, 3H). ESI-MS, calcd for $C_{17}H_{13}N_5O$ 303.1; found m/z = 304.3 [M + H]$^+$.

**3f**
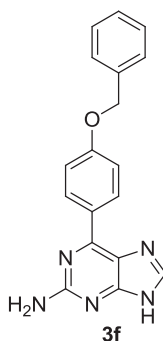
**2-amino-6-(4-(benzyloxy)phenyl)-9*H*-purine (3f)** was obtained as a yellow powder in 77% yield from **2a** and 4-(benzyloxy)phenylboronic acid (**R**). RP-HPLC $t_R$ = 17.4 min, gradient condition: from 5% B to 100% B in 40 min, flow rate of 4 ml/min, λ = 240 nm. $^1$H NMR (300 MHz, MeOD): δ = 5.28 (s, 2H), 7.30 (d, *J* = 8.8 Hz, 2H), 7.36-7.46 (m, 3H), 7.50 (br s, 2H), 8.37-8.45 (m, 3H). ESI-MS, calcd for $C_{18}H_{15}N_5O$ 317.1; found m/z = 318.1 [M + H]$^+$.



**3g**
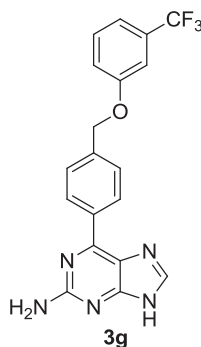
**2-amino-6-(4-(3'-(trifluoromethyl)phenoxymethyl)phenyl)-9*H*-purine (3g)** was obtained as a yellow powder in 79% yield from **2a** and 4-(3'-(trifluoromethyl)phenoxymethyl)phenylboronic acid (**S**). RP-HPLC $t_R$ = 25.0 min, gradient condition: from 5% B to 100% B in 50 min, flow rate of 4 ml/min, λ = 240 nm. $^1$H NMR (300 MHz, MeOD): δ = 5.31 (s, 2H), 7.22-7.33 (m, 3H), 7.48 (t, *J* = 7.9 Hz, 1H), 7.73 (d, *J* = 8.1 Hz, 2H), 8.37 (br s, 3H). ESI-MS, calcd for $C_{19}H_{14}F_3N_5O$ 385.1; found m/z = 386.1 [M + H]$^+$.

**3h**
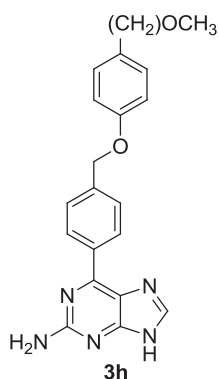
**2-amino-6-(4-((4'-(2-methoxyethyl)phenoxy)methyl)phenyl)-9*H*-purine (3h)** was obtained as a yellow powder in 77% yield from **2a** and 4-((4'-(2-methoxyethyl)phenoxy)methyl)phenylboronic acid (**T**). RP-HPLC $t_R$ = 17.9 min, gradient condition: from 5% B to 100% B in 40 min, flow rate of 4 ml/min, $\lambda$ = 240 nm. ^{1}H NMR (300 MHz, MeOD): $\delta$ = 2.80 (t, $J$ = 6.9 Hz, 2H), 3.33 (s, 3H) , 3.57 (t, $J$ = 6.9 Hz, 2H), 5.22 (s, 2H), 6.96 (d, $J$ = 8.7 Hz, 2H), 7.16 (d, $J$ = 8.6 Hz, 2H), 7.70 (d, $J$ = 8.1 Hz, 2H), 8.33 (s, 1H), 8.40 (d, $J$ = 8.3 Hz, 2H). ESI-MS, calcd for $C_{21}H_{21}N_5O_2$ 375.2; found m/z = 376.1 [M + H]$^+$.



**4a**
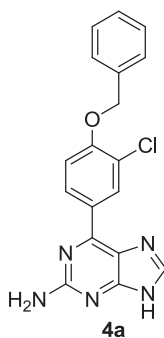
**2-amino-6-(4-benzyloxy-3-chlorophenyl)-9*H*-purine (4a)** was obtained as a yellow powder in 84% yield from **2a** and 4-benzyloxy-3-chlorophenylboronic acid (**P**). RP-HPLC $t_R$ = 20.4 min, gradient condition: from 5% B to 100% B in 40 min, flow rate of 4 ml/min, $\lambda$ = 240 nm. ^{1}H NMR (300 MHz, MeOD): $\delta$ = 5.32 (s, 2H), 7.33-7.44 (m, 4H), 7.50 (br s, 2H), 8.34

(br s, 2H), 8.50 (s, 1H). ESI-MS, calcd for $C_{18}H_{14}ClN_5O$ 351.1; found m/z = 352.1 $[M + H]^+$.



**4b**
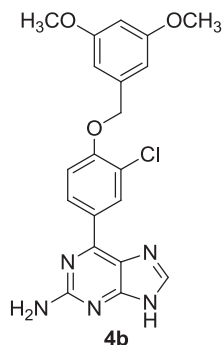
**2-amino-6-(3-chloro-4-(3',5'-dimethoxybenzyloxy)phenyl)-9*H*-purine**

**(4b)** was obtained as a yellow powder in 86% yield from **2a** and 3-chloro-4-(3',5'-dimethoxybenzyloxy)phenylboronic acid (**U**). RP-HPLC $t_R$ = 20.5 min, gradient condition: from 5% B to 100% B in 40 min, flow rate of 4 ml/min, λ = 240 nm. $^1$H NMR (600 MHz, MeOD): δ = 3.76 (s, 6H), 5.28 (s, 2H), 6.48 (s, 1H), 6.68 (s, 2H), 7.32 (d, *J* = 8.8 Hz, 1H), 8.18 (s, 1H), 8.47 (br s, 1H), 8.61 (s, 1H). $^{13}$C NMR (150 MHz, MeOD): δ = 56.2, 71.6, 100.7, 106.2, 115.6, 123.2, 127.0, 128.7, 132.1, 139.7, 143.1, 149.5, 150.3, 155.7, 157.2, 160.4, 161.8. ESI-MS, calcd for $C_{20}H_{18}ClN_5O_3$ 411.1; found m/z = 412.1 $[M + H]^+$.



**4c**
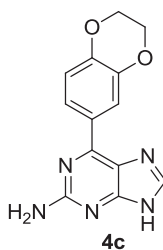
**2-amino-6-(2,3-dihydrobenzo[b][1,4]dioxin-6-yl)-9*H*-purine** **(4c)** was obtained as a pale yellow powder in 84% yield from **2a** and 1,4-benzodioxane-6-boronic acid (**N**). RP-HPLC $t_R$ = 11.6. min, gradient condition: from 5% B to 100% B in 50 min, flow rate of 4 ml/min, λ = 240 nm. $^1$H NMR (300 MHz, MeOD): δ = 4.34-4.40 (m, 4H), 7.09 (d, *J* = 8.5 Hz, 1H), 7.89-7.98 (m, 2H),

8.34 (s, 1H). ESI-MS, calcd for $C_{13}H_{11}N_5O_2$ 269.1; found m/z = 270.2 [M + H]$^+$.



**4d**
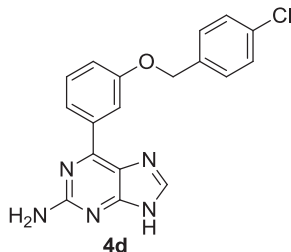
**2-amino-6-(3-(4'-chlorobenzyloxy)phenyl)-9*H*-purine (4d)** was obtained as a yellow powder in 78% yield from **2a** and 3-(4'-chlorobenzyloxy)-phenylboronic acid (**Q**). RP-HPLC $t_R$ = 29.8 min, gradient condition: from 5% B to 100% B in 70 min, flow rate of 4 ml/min, λ = 240 nm. $^1$H NMR (300 MHz, MeOD): δ = 5.19 (s, 2H), 7.29 (d, *J* = 7.6 Hz, 1H), 7.40 (d, *J* = 8.4 Hz, 2H), 7.45-7.58 (m, 3H), 7.90 (d, *J* = 6.9 Hz, 1H), 8.01 (s, 1H), 8.37 (s, 1H). ESI-MS, calcd for $C_{18}H_{14}ClN_5O$ 351.1; found m/z = 352.2 [M + H]$^+$.



**5a**
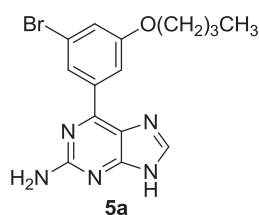
**2-amino-6-(3-bromo-5-butoxyphenyl)-9*H*-purine (5a)** was obtained as a white powder in 83% yield from **2a** and 3-bromo-5-butoxyphenylboronic acid (**I**). RP-HPLC $t_R$ = 26.7 min, gradient condition: from 5% B to 100% B in 50 min, flow rate of 4 ml/min, λ = 240 nm. $^1$H NMR (600 MHz, DMSO-$d_6$): δ = 0.93 (t, *J* = 7.3 Hz, 3H), 1.39-1.51 (m, 2H), 1.68-1.76 (m, 2H), 4.06 (t, *J* = 6.3 Hz, 2H), 6.46 (s, 2H), 7.28 (s, 1H), 8.16 (s, 1H), 8.37 (s, 1H), 8.50 (s, 1H), 12.72 (s, 1H). $^{13}$C NMR (150 MHz, DMSO-$d_6$): δ = 14.9, 20.1, 32.1, 69.5, 115.8, 120.9, 124.4, 125.8, 138.7, 142.2, 148.1, 151.3, 157.2, 161.3. ESI-MS, calcd for $C_{15}H_{16}BrN_5O$ 361.1; found m/z = 362.3 [M + H]$^+$.
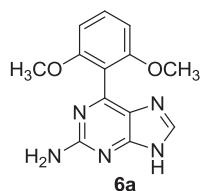
**2-amino-6-(2,6-dimethoxyphenyl)-9*H*-purine (6a)** was obtained as a white powder in 53% yield from **2a** and 2,6-dimethoxyphenylboronic acid (**J**). RP-HPLC $t_R$ = 13.0 min, gradient condition: from 5% B to 100% B in 80 min, flow rate of 4 ml/min, $\lambda$ = 240 nm. $^1$H NMR (300 MHz, MeOD): $\delta$ = 3.82 (s, 6H), 6.87 (d, *J* = 8.5 Hz, 2H), 7.60 (t, *J* = 8.5 Hz, 1H), 8.44 (s, 1H). ESI-MS, calcd for $C_{13}H_{13}N_5O_2$ 271.1; found m/z = 272.2 $[M + H]^+$.
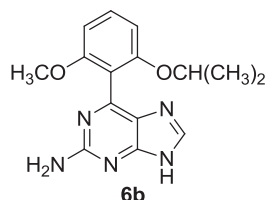


**2-amino-6-(2-isopropoxy-6-methoxyphenyl)-9*H*-purine (6b)** was obtained as a white powder in 62% yield from **2a** and 2-isopropoxy-6-methoxyphenylboronic acid (**K**). RP-HPLC $t_R$ = 18.1 min, gradient condition: from 5% B to 100% B in 40 min, flow rate of 4 ml/min, $\lambda$ = 240 nm. $^1$H NMR (300 MHz, MeOD): $\delta$ = 1.18 (s, 6H), 3.80 (s, 3H), 4.60-4.71 (m, 1H), 6.80-6.88 (m, 2H), 7.56 (t, *J* = 8.5 Hz, 1H), 8.43 (s, 1H). ESI-MS, calcd for $C_{15}H_{17}N_5O_2$ 299.1; found m/z = 300.1 $[M + H]^+$.



**2-amino-6-(2-isobutoxy-6-methoxyphenyl)-9*H*-purine (6c)** was obtained as a white powder in 76% yield from **2a** and 2-isobutoxy-6-methoxy-phenylboronic acid (**L**). RP-HPLC $t_R$ = 14.2 min, gradient condition: from 5% B to 100% B in 40 min, flow rate of 4 ml/min, $\lambda$ = 240 nm. $^1$H NMR (600

MHz, DMSO-$d_6$): δ = 0.69 (s, 6H), 1.72-1.79 (m, 1H), 3.71 (br s, 5H), 6.81-6.86 (m, 2H), 7.52 (t, $J$ = 8.1 Hz, 1H), 8.47 (s, 1H). $^{13}$C NMR (150 MHz, MeOD): δ = 20.3, 29.0, 57.6, 76.1, 106.2, 118.6, 125.8, 134.7, 137.4, 142.7, 154.9, 159.3, 160.8, 173.0. ESI-MS, calcd for $C_{16}H_{19}N_5O_2$ 313.2; found m/z = 314.1 $[M + H]^+$.



**2-amino-6-(2-methoxyphenyl)-9*H*-purine (7a)** was obtained as a pale yellow powder in 78% yield from **2a** and 2-methoxyphenylboronic acid (**C**). RP-HPLC $t_R$ = 14.9 min, gradient condition: from 5% B to 100% B in 80 min, flow rate of 4 ml/min, λ = 240 nm. $^1$H NMR (300 MHz, MeOD): δ = 3.97 (s, 3H), 7.21 (t, $J$ = 7.5 Hz, 1H), 7.30 (d, $J$ = 8.4 Hz, 1H), 7.67 (t, $J$ = 7.8 Hz, 1H), 8.10 (d, $J$ = 7.4 Hz, 1H), 8.45 (s, 1H). ESI-MS, calcd for $C_{12}H_{11}N_5O$ 241.1; found m/z = 242.2 $[M + H]^+$.
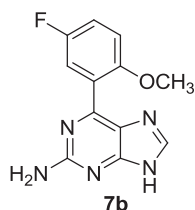


**2-amino-6-(5-fluoro-2-methoxyphenyl)-9*H*-purine (7b)** was obtained as a pale yellow powder in 70% yield from **2a** and 5-fluoro-2-methoxy-phenylboronic acid (**D**). RP-HPLC $t_R$ = 14.0 min, gradient condition: from 5% B to 100% B in 60 min, flow rate of 4 ml/min, λ = 240 nm. $^1$H NMR (300 MHz, MeOD): δ = 3.95 (s, 3H), 7.29 (d, $J$ = 8.9 Hz, 1H), 7.41 (dd, $J$ = 8.9, 2.4 Hz, 1H), 7.92 (br s, 1H), 8.54 (s, 1H). ESI-MS, calcd for $C_{12}H_{10}FN_5O$ 259.1; found m/z = 260.1 $[M + H]^+$.
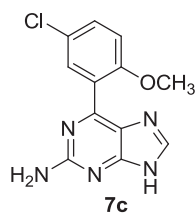
**2-amino-6-(5-chloro-2-methoxyphenyl)-9H-purine (7c)** was obtained as a pale yellow powder in 78% yield from **2a** and 5-chloro-2-methoxy-phenylboronic acid (**E**). RP-HPLC $t_R$ = 18.1 min, gradient condition: from 5% B to 100% B in 80 min, flow rate of 4 ml/min, $\lambda$ = 240 nm. $^1$H NMR (300 MHz, MeOD): $\delta$ = 3.95 (s, 3H), 7.28 (d, $J$ = 8.9 Hz, 1H), 7.63 (dd, $J$ = 8.9, 2.5 Hz, 1H), 8.03 (br s, 1H), 8.53 (s, 1H). ESI-MS, calcd for $C_{12}H_{10}ClN_5O$ 275.1; found m/z = 276.1 $[M + H]^+$.



**2-amino-6-(5-bromo-2-methoxyphenyl)-9*H*-purine (7d)** was obtained as a yellow powder in 77% yield from **2a** and 5-bromo-2-methoxyphenylboronic acid (**F**). RP-HPLC $t_R$ = 17.3 min, gradient condition: from 5% B to 100% B in 60 min, flow rate of 4 ml/min, $\lambda$ = 240 nm. $^1$H NMR (600 MHz, MeOD): $\delta$ = 3.95 (s, 3H), 7.23 (d, $J$ = 9.0 Hz, 1H), 7.76 (dd, $J$ = 8.9, 2.4 Hz, 1H), 8.14 (br s, 1H), 8.53 (s, 1H). $^{13}$C NMR (150 MHz, MeOD): $\delta$ = 56.3, 113.3, 114.4, 123.7, 126.4, 135.4, 135.9, 142.6, 149.5, 155.1, 157.8, 160.9. ESI-MS, calcd for $C_{12}H_{10}BrN_5O$ 319.0; found m/z = 320.3 $[M + H]^+$.
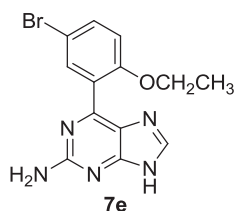
**2-amino-6-(5-bromo-2-ethoxyphenyl)-9*H*-purine (7e)** was obtained as a yellow powder in 82% yield from **2a** and 5-bromo-2-ethoxyphenylboronic acid (**G**). RP-HPLC $t_R$ = 21.6 min, gradient condition: from 5% B to 100% B in 80 min, flow rate of 4 ml/min, $\lambda$ = 240 nm. $^1$H NMR (300 MHz, MeOD): $\delta$ = 1.31 (t, *J* = 6.9 Hz, 3H), 4.13-4.24 (m, 2H), 7.19 (d, *J* = 8.9 Hz, 1H), 7.72 (dd, *J* = 8.9, 2.3 Hz, 1H), 7.98 (brs, 1H), 8.53 (s, 1H). ESI-MS, calcd for $C_{13}H_{12}BrN_5O$ 333.0; found m/z = 334.1 $[M + H]^+$.



8a

**6-(5-bromo-2-methoxyphenyl)-2-chloro-9*H*-purine (8a)** was obtained following the general procedure (**a**) as a yellow powder in 68% yield from **1** and 5-bromo-2-methoxyphenylboronic acid (**E**). RP-HPLC $t_R$ = 24.3 min, gradient condition: from 5% B to 100% B in 45 min, flow rate of 4 ml/min, $\lambda$ = 240 nm. $^1$H NMR (300 MHz, CDCl3): $\delta$ = 3.91 (s, 3H), 7.00 (d, *J* = 8.8 Hz, 1H), 7.23 (br s, 1H) 7.63 (d, *J* = 8.1 Hz, 1H), 8.04 (s, 1H). ESI-MS, calcd for $C_{12}H_8BrClN_4O$ 338.0; found m/z = 339.2 $[M + H]^+$.



9a
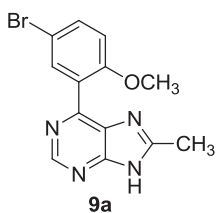
**6-(5-bromo-2-methoxyphenyl)-8-methyl-9*H*-purine (9a)** was obtained as a pale yellow powder in 70% yield from 6-chloro-8-methyl-9*H*-purine **12** and 5-bromo-2-methoxyphenylboronic acid (**E**). RP-HPLC $t_R$ = 21.7 min, gradient condition: from 5% B to 100% B in 70 min, flow rate of 4 ml/min, $\lambda$ = 240 nm. $^1$H NMR (300 MHz, DMSO-$d_6$): $\delta$ = 2.69 (s, 3H), 3.87 (s, 3H), 7.20 (d, *J*

= 9.0 Hz, 1H), 7.71 (dd, $J$ = 8.9, 2.4 Hz, 1H), 7.82 (s, 1H), 8.95 (s, 1H). ESI-MS, calcd for $C_{13}H_{11}BrN_4O$ 318.0; found m/z = 319.2 $[M + H]^+$.



**9b**
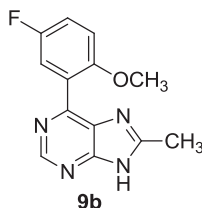
**6-(5-fluoro-2-methoxyphenyl)-8-methyl-9*H*-purine (9b)** was obtained as a pale yellow powder in 81% yield from 6-chloro-8-methyl-9H-purine **12** and 5-fluoro-2-methoxyphenylboronic acid (**D**). RP-HPLC $t_R$ = 15.6 min, gradient condition: from 5% B to 100% B in 60 min, flow rate of 4 ml/min, $\lambda$ = 240 nm. $^1$H NMR (300 MHz, MeOD): $\delta$ = 2.76 (s, 3H), 3.90 (s, 3H), 7.27 (d, $J$ = 9.0 Hz, 1H), 7.39 (br s, 1H), 7.67 (dd, $J$ = 8.9, 2.4 Hz, 1H), 9.04 (s, 1H). $^{13}$C NMR (75 MHz, MeOD): $\delta$ = 14.1, 56.2, 113.5, 117.9, 118.3, 119.2, 126.9, 147.7, 151.3, 154.5, 155.9, 158.2, 159.2. ESI-MS, calcd for $C_{13}H_{11}FN_4O$ 258.1; found m/z = 259.1 $[M + H]^+$.



**10**
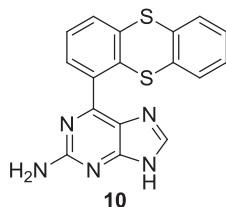
**2-amino-6-thianthrenyl-9*H*-purine (10)** was obtained as a yellow powder in 82% yield from **2a** and 1-thianthrenylboronic acid (**M**). RP-HPLC $t_R$ = 18.5 min, gradient condition: from 5% B to 100% B in 40 min, flow rate of 4 ml/min, $\lambda$ = 240 nm. $^1$H NMR (300 MHz, MeOD): $\delta$ = 7.22-7.37 (m, 3H), 7.51 (t, $J$ = 7.5 Hz, 2H), 7.65 (d, $J$ = 7.4 Hz, 1H), 7.75 (d, $J$ = 7.7 Hz, 1H), 8.37 (s, 1H). ESI-MS, calcd for $C_{17}H_{11}N_5S_2$ 349.0; found m/z = 350.1 $[M + H]^+$.
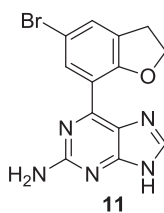
**2-amino-6-(5-bromo-2,3-dihydrobenzo[b]furan-7-yl)-9*H*-purine** **(11)** was obtained as a pale yellow powder in 79% yield from **2a** and 5-bromo-2,3-dihydrobenzo[*b*]furan-7-boronic acid (**H**). RP-HPLC $t_R$ = 15.2 min, gradient condition: from 5% B to 100% B in 40 min, flow rate of 4 ml/min, $\lambda$ = 240 nm. $^1$H NMR (600 MHz, MeOD): $\delta$ = 3.35-3.42 (m, 2H), 4.87-4.93 (m, 2H), 7.65 (s, 1H), 8.50 (s, 1H), 8.57 (s, 1H). $^{13}$C NMR (150 MHz, MeOD): $\delta$ = 29.1, 74.3, 113.6, 121.2, 125.8, 131.5, 132.1, 134.0, 146.1, 154.9, 158.8, 159.9, 160.7. ESI-MS, calcd for $C_{13}H_{10}BrN_5O$ 331.0; found m/z = 332.2 [M + H]$^+$.

### 6.2.2 General procedure for TBAF-assisted N9-alkylation of purine rings (2b, 3c, 3e, 4e, 5b, 8b, 8c)

The opportune 2-amino-6-arylpurine (0.1 mmol) was dissolved in 0.4 ml THF at room temperature. To this mixture 0.2 ml (0.2 mmol) TBAF (1.0 M solution in THF) and iodomethane (12.5 μL, 0.2 mmol) or chloro-acetone (16.0 μL, 0.2 mmol) were added. The reaction was stirred at room temperature for 10 min. Water was added and the aqueous layer was extracted three times with dichloromethane. The combined organic layers were washed with water, dried with anhydrous $Na_2SO_4$ and concentrated under vacuum. The crude mixture was purified by semi-preparative reversed-phase HPLC using the gradient conditions reported below for each compound. Compounds were obtained in good yields (50-88%) and high purity (> 95%).

**2b**
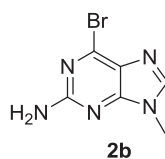
**2-amino-6-bromo-9-methylpurine (2b)** was obtained from **2a** and iodomethane as a yellow powder in 85% yield. RP-HPLC: $t_R$ = 12.4 min, gradient condition: from 5% B to 100% B in 95 min, flow rate of 4 ml/min, $\lambda$ = 240 nm. ^{1}H NMR (600 MHz, MeOD): $\delta$ = 3.74 (s, 3H), 8.25 (s, 1H). ^{13}C NMR (150 MHz, MeOD): $\delta$ = 30.6, 126.3, 142.5, 149.4, 155.62, 160.8. ESI-MS, calcd for $C_6H_6BrN_5$ 227.0; found m/z = 228.1 $[M + H]^+$.



**3c**
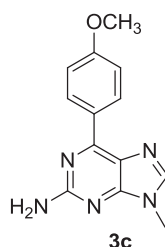
**2-amino-6-(4-methoxyphenyl)-9-methylpurine (3c)** was obtained following from **3b** and iodomethane as a yellow powder in 88% yield. RP-HPLC $t_R$ = 15.5 min, gradient condition: from 5% B to 100% B in 65 min, flow rate of 4 ml/min, $\lambda$ = 240 nm. ^{1}H NMR (300 MHz, CDCl3): $\delta$ = 3.79 (s, 3H), 3.94 (s, 3H), 7.12 (d, $J$ = 8.6 Hz, 2H), 7.95 (s, 1H), 8.55 (d, $J$ = 8.5 Hz, 2H). ESI-MS, calcd for $C_{13}H_{13}N_5O$ 255.1; found m/z = 256.3 $[M + H]^+$.



**3e**
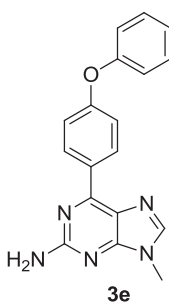
**2-amino-6-(4-phenoxyphenyl)-9-methylpurine (3e)** was obtained from **3d** and iodomethane as a yellow powder in 82% yield. RP-HPLC $t_R$ = 27.5 min, gradient condition: from 5% B to 100% B in 75 min, flow rate of 4

mL/min, $\lambda$ = 240 nm. $^1$H NMR (600 MHz, CDCl3): $\delta$ = 3.77 (s, 3H), 7.05-7.18 (m, 5H), 7.37 (t, J = 7.8 Hz, 2H), 7.79 (s, 1H), 8.70 (br s, 2H). $^{13}$C NMR (150 MHz, CDCl3): $\delta$ = 30.6, 118.3, 121.6, 124.8, 125.7, 127.1, 131.2, 133.9, 142.8, 147.6, 150.7, 156.3, 157.8, 163.3. ESI-MS, calcd for $C_{18}H_{15}N_5O$ 317.1; found m/z = 318.2 [M + H]+.



**4e**
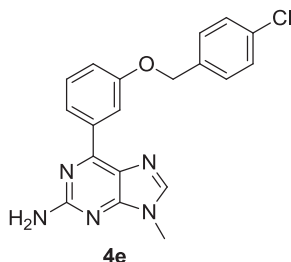
**2-amino-6-(3-(4'-chlorobenzyloxy)phenyl)-9-methylpurine** **(4e)** was obtained from **4d** and iodomethane as a yellow powder in 63% yield. RP-HPLC $t_R$ = 28.3 min, gradient condition: from 5% B to 100% B in 60 min, flow rate of 4 ml/min, $\lambda$ = 240 nm. $^1$H NMR (300 MHz, CDCl3): $\delta$ = 3.77 (s, 3H), 5.20 (s, 2H), 7.13 (d, J = 7.8 Hz, 1H), 7.36 (d, J = 8.2 Hz, 2H), 7.41-7.51 (m, 3H), 7.83 (s, 1H), 8.31-8.42 (m, 2H). ESI-MS, calcd for $C_{19}H_{16}ClN_5O$ 365.1; found m/z = 366.2 [M + H]$^+$.



**5b**
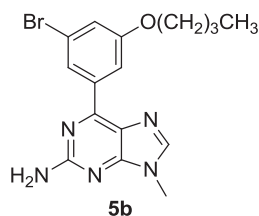
**2-amino-6-(3-bromo-5-butoxyphenyl)-9-methylpurine (5b)** was obtained from **5a** and iodomethane as a yellow powder in 85% yield. RP-HPLC $t_R$ = 27.9 min, gradient condition: from 5% B to 100% B in 45 min, flow rate of 4 ml/min, $\lambda$ = 240 nm. $^1$H NMR (300 MHz, CDCl3): $\delta$ = 0.97 (t, J = 7.3 Hz, 3H), 1.46-1.55 (m, 2H), 1.73-1.83 (m, 2H), 3.79 (s, 3H), 4.11 (t, J = 6.2 Hz, 2H), 7.29 (s, 1H), 7.92 (s, 1H), 7.97 (s, 1H), 8.33 (s, 1H). ESI-MS, calcd for $C_{16}H_{18}BrN_5O$ 375.1; found m/z = 376.2 [M + H]$^+$.

**8b**
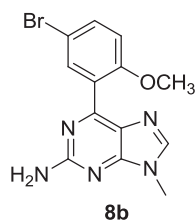
**2-amino-6-(5-bromo-2-methoxyphenyl)-9-methylpurine** **(8b)** was obtained from **7d** and iodomethane as a yellow powder in 87% yield. RP-HPLC $t_R$ = 18.9 min, gradient condition: from 5% B to 100% B in 70 min, flow rate of 4 ml/min, λ = 240 nm. $^1$H NMR (300 MHz, CDCl3): δ = 3.79 (s, 3H), 3.87 (s, 3H), 6.94-7.01 (m, 1H), 7.24 (br s, 1H), 8.02 (s, 1H). ESI-MS, calcd for $C_{13}H_{12}BrN_5O$ 333.0; found m/z = 334.2 $[M + H]^+$.



**8c**
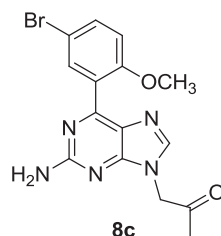
**2-amino-6-(5-bromo-2-methoxyphenyl)-9-(2-oxopropyl)-purine** **(8c)** was obtained from **7d** and chloro-acetone as a yellow powder in 50% yield. RP-HPLC $t_R$ = 22.9 min, gradient condition: from 5% B to 100% B in 80 min, flow rate of 4 ml/min, λ = 240 nm. $^1$H NMR (600 MHz, CDCl$_3$): δ = 2.40 (s, 3H), 4.01 (s, 3H), 5.00 (s, 2H), 7.03 (d, $J$ = 8.9 Hz, 1H), 7.70 (dd, $J$ = 8.9, 2.4 Hz, 1H), 8.02 (s, 1H), 8.19 (s, 1H). $^{13}$C NMR (150 MHz, CDCl$_3$): δ = 27.3, 52.5, 57.1, 114.3, 118.8, 125.1, 126.9, 136.3, 138.4, 143.3, 148.2, 154.3, 156.7, 158.4, 199.2. ESI-MS, calcd for $C_{15}H_{14}BrN_5O_2$ 375.0; found m/z = 376.1 $[M + H]^+$.

### 6.2.3 General procedure for the synthesis of 2-hydroxy-6-arylpurines (8d-f)

A three-necked flask was charged with the 2-amino-6-arylpurine derivative (**7b-d**, 0.5 mmol) and 50% $H_2SO_4$ (2.0 ml). The mixture was stirred at room temperature for 30 min and then cooled to -5 ºC. A solution of NaNO$_2$ (48.3

mg, 0.7 mmol) in $H_2O$ (200 μL) was added dropwise and the release of nitrogen gas was immediately observed. The reaction mixture was then stirred at -10 ºC for 2 h and urea (24.0 mg, 0.4 mmol) was added to decompose the excess of $NaNO_2$. The mixture was then stirred at 50 ºC for 1 h and neutralized with 50% NaOH solution, diluted with water and extracted three times with EtOAc. The combined organic layers were dried with anhydrous $Na_2SO_4$ and concentrated under vacuum. The crude mixture was purified by semi-preparative reversed-phase HPLC to get the pure products in good yields (47-63%).



**8d**

**6-(5-fluoro-2-methoxyphenyl)-2-hydroxy-9*H*-purine** (**8d**) was obtained from **7b** as a white powder in 47% yield. RP-HPLC $t_R$ = 13.9 min, gradient condition: from 5% B to 100% B in 50 min, flow rate of 4 ml/min, λ = 240 nm. $^1$H NMR (300 MHz, DMSO-$d_6$): δ = 3.93 (s, 3H), 7.31 (d, $J$ = 8.9 Hz, 1H), 7.40 (dd, $J$ = 8.9, 2.4 Hz, 1H), 7.89 (br s, 1H), 8.54 (s, 1H). ESI-MS, calcd for $C_{12}H_9FN_4O_2$ 260.1; found m/z = 261.1 $[M + H]^+$.



**8e**
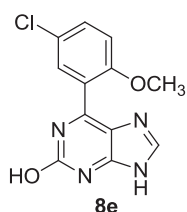
**6-(5-chloro-2-methoxyphenyl)-2-hydroxy-9*H*-purine** (**8e**) was obtained from **7c** as a white powder in 63% yield. RP-HPLC $t_R$ = 14.8 min, gradient condition: from 5% B to 100% B in 50 min, flow rate of 4 ml/min, λ = 240 nm. $^1$H NMR (300 MHz, DMSO-$d_6$): δ = 3.94 (s, 3H), 7.26 (d, $J$ = 8.9 Hz,

1H), 7.63 (dd, *J* = 8.9, 2.5 Hz, 1H), 8.03 (br s, 1H), 8.53 (s, 1H). ESI-MS, calcd for $C_{12}H_9ClN_4O_2$ 276.0; found m/z = 277.1 $[M + H]^+$.
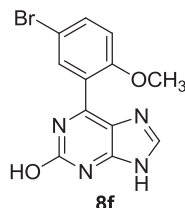


**6-(5-bromo-2-methoxyphenyl)-2-hydroxy-9*H*-purine (8f)** was obtained from **7d** as a white powder in 55% yield. RP-HPLC $t_R$ = 15.8 min, gradient condition: from 5% B to 100% B in 50 min, flow rate of 4 ml/min, λ = 240 nm. $^1$H NMR (300 MHz, DMSO-$d_6$): δ = 3.97 (s, 3H), 7.25 (d, *J* = 9.0 Hz, 1H), 7.76 (dd, *J* = 8.9, 2.4 Hz, 1H), 8.14 (br s, 1H), 8.53 (s, 1H). ESI-MS, calcd for $C_{12}H_9BrN_4O_2$ 320.0; found m/z = 321.1$[M + H]^+$.

### 6.2.4 THP-protection of 2-amino-6-bromo-9H-purine
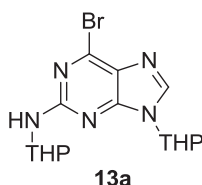


**6-Bromo-9-(tetrahydropyran-2-yl)-2-[(tetrahydropyran-2-yl)amino]purine (13a):** a mixture of 2-amino-6-bromo-9*H*-purine **2a** (500 mg, 2.34 mmol), 1.0 M HCl in DMF (0.1 ml) and anhydrous DMF (18 ml) was stirred at 60 °C under nitrogen. 3,4-dihydro-2*H*-pyran (1.0 ml, 11.7 mmol) was added dropwise through a septum. The stirring at 60 °C was continued for another 6 h and then the solvent was evaporated under reduced pressure. The dark yellow oily residue was dissolved in ethyl acetate and extracted with saturated aqueous $Na_2S_2O_3$. The aqueous layer was washed with ethyl acetate and the combined organic layers were dried with $Na_2SO_4$ and evaporated. Column chromatography of the residue on silica gel (ethyl acetate–light petroleum 1:1) afforded the product **13a** as yellowish powder in

57% yield. RP-HPLC $t_R$ = 32.1 min, gradient condition: from 5% B to 100% B in 40 min, flow rate of 1 ml/min, $\lambda$ = 240 nm. ^{1}H NMR (300 MHz, CDCl$_3$): $\delta$ = 1.47–1.74 (m, 10H), 1.86 (br s, 1H), 2.02 (br s, 1H), 3.58–3.73 (m, 2 H); 3.92–4.12 (m, 2 H); 5.27–5.36 (m, 1 H); 5.49–5.59 (m, 1 H); 7.97 (s, 1H). ESI-MS, calcd for C$_{15}$H$_{20}$BrN$_5$O$_2$ 381.1; found m/z = 382.0[M + H]$^+$.

### 6.2.5 Attempt of C-8 electrophilic fluorination reaction on the bis(THP)-protected purine 13a



**13c**
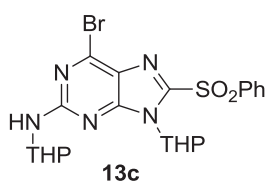
**6-bromo-8-(phenylsulfonyl)-9-(tetrahydropyran-2-yl)-2-[(tetrahydro-pyran-2-yl)amino]purine (13c)**: a stirring solution of bis(THP)-protected purine 1**3a** (150 mg, 0.4 mmol) in dry THF (4.0 ml) was cooled to -78 °C (dry ice/*i*-PrOH) under nitrogen. LDA 2.0 M solution in heptane/THF/EtPh (2.0 mmol, 1.0 ml) was added and the mixture was allowed to stir at -78 °C for 2 h. After that time, solid NFSI (380 mg, 1.2 mmol) was added. The mixture was allowed to stir at -78 °C for 90 min, then warmed to 0 °C with continued stirring for additional 30 min. Sat aq NH$_4$Cl was added to the mixture, and the layers were separated. The aqueous layer was extracted three times with EtOAc, and the combined organic layer was washed with sat aq NaHCO$_3$ and brine. The organic layer was dried over Na$_2$SO$_4$, and the solvent was evaporated under reduced pressure. The crude reaction mixture was purified by HPLC to give the corresponding 8-phenylsulfonyl product **13c** in 69% yield. RP-HPLC $t_R$ = 35.7 min, gradient condition: from 5% B to 100% B in 40 min, flow rate of 4 ml/min, $\lambda$ = 240 nm. ^{1}H NMR (300 MHz, MeOD): $\delta$ = 1.45–2.10 (m, 12H); 3.55–3.68 (m, 2 H); 3.87–3.99 (m, 2 H); 5.23 (br s, 1 H);

6.03–6.12 (m, 1 H); 7.61–7.78 (m, 3H); 8.01–8.14 (m, 2H). ESI-MS, calcd for $C_{21}H_{24}BrN_5O_4S$ 521.1; found m/z = 544.0$[M + Na]^+$.

# -CHAPTER 7-

Synthesis of DHPM-based inhibitors of mPGES-1 and

Hsp90: Experimental procedures

### 7.1 General synthetic methods

All commercially available starting materials were purchased from Sigma-Aldrich and were used as received. All solvents used for the synthesis were of HPLC grade; they were purchased from Sigma-Aldrich and Carlo Erba Reagenti. All NMR spectra were recorded on a Bruker Avance 300, 500 or 600 MHz instrument. All compounds were dissolved in 0.5 mL of 99.95% $CDCl_3$ (Carlo Erba, 99.95 Atom % D). Coupling constants (*J*) are reported in Herz, and chemical shifts are expressed in parts per million (ppm) on the delta (δ) scale relative to $CHCl_3$ (7.26 ppm for $^1H$ and 77.2 ppm for $^{13}C$) as internal reference. Multiplicities are reported as follows: s, singlet; d, doublet; t, triplet; m, multiplet; dd, doublet of doublets. Electrospray mass spectrometry (ESI-MS) was performed on a LCQ DECA TermoQuest (San Josè, California, USA) mass spectrometer. High resolution mass spectra were acquired on a LTQ Orbitrap XL (Thermo Scientific).

Reactions were monitored on silica gel 60 $F_{254}$ plates (Merck) and the spots were visualized under UV light. Analytical and semi-preparative reversed-phase HPLC was performed on Agilent Technologies 1200 Series high performance liquid chromatography using a Jupiter Proteo $C_{18}$ reversed-phase column (250 x 4.60mm, 4μ, 90 Å, flow rate = 1 mL/min; 250 x 10.00mm, 10μ, 90 Å, flow rate = 4 mL/min respectively, Phenomenex®). The binary solvent system (A/B) was as follows: 0.1% TFA in water (A) and 0.1% TFA in $CH_3CN$ (B). The absorbance was detected at 280 nm.The purity of all tested compound (>95%) was determined by HPLC analysis.

All microwave irradiation experiments were carried out in a dedicated CEM-Discover® Focused Microwave Synthesis apparatus, operating with continuous irradiation power from 0 to 300 W utilizing the standard absorbance level of 300 W maximum power. The reactions were carried out in 10 mL sealed microwave glass vials. The Discover$^{TM}$ system also offers controllable ramp time, hold time (reaction time) and uniform stirring. The

temperature was monitored using the CEM-Discover built-in-vertically-focused IR temperature sensor. After the irradiation period, the reaction vessel was cooled rapidly (60-120 s) to ambient temperature by air jet cooling.

## 7.2 Methods and materials

### 7.2.1 General procedure for microwave-assisted Biginelli reaction

A mixture of the appropriate aldehyde (1.0 mmol), urea or its derivative (1.5 mmol), 1,3-dicarbonyl compound (1.0 mmol) in acetonitrile (1.5 mL) was placed in a 10 mL microwave glass vial equipped with a small magnetic stirring bar. TMSCl (1.0 mmol) was added and the mixture was then stirred under microwave irradiation at 120°C for 10-20 min.

In a few cases, TMSCl (procedure **a**) was replaced by 10 mol % Yb(OTf)$_3$ (procedure **b**) or FeCl$_3$ (procedure **c**) as Lewis acid catalysts, as needed. In these cases, also reaction solvent (acetonitrile) was replaced by 1.5 ml of a mixture of EtOH/AcOH (1:3). After irradiation, the reaction mixture was cooled to ambient temperature by air jet cooling, cold water was added and the vial was poured into crushed ice and then left at 4°C overnight. The resulting precipitate was filtered and washed with a cold mixture of ethanol/water (1:1) (3x3 mL), to give the desired product in good yields. HPLC purification was performed by semi-preparative reversed-phase HPLC (on a Jupiter Proteo C18 column: 250 x 10.00mm, 10μ, 90 Å, flow rate = 4 mL/min) using the gradient conditions reported below for each compound. The final products were obtained with high purity (>95%) as detected by HPLC analysis and were fully characterized by ESI-MS and NMR spectra.



**14a**
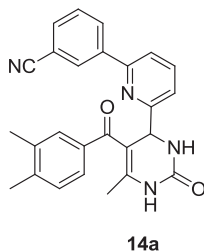
**3-(6-(5-(3,4-dimethylbenzoyl)-6-methyl-2-oxo-1,2,3,4-tetrahydro-pyrimidin-4-yl)pyridin-2-yl)benzonitrile (14a)** was obtained by following the general procedure **a** as a brownish solid in 86% yield. RP-HPLC $t_R$ = 35.3 min, gradient condition: from 5% B to 100% B in 65 min, flow rate of 4 ml/min, $\lambda$ = 280 nm. ^{1}H NMR (300 MHz, CDCl$_3$): $\delta$ = 1.82 (s, 3H); 2.24 (s, 3H); 2.29 (s, 3H); 5.70 (s, 1H); 7.09-7.17 (m, 1H); 7.34-7.50 (m, 4H); 7.64 (br s, 2H), 7.82 (br s, 1H); 8.03-8.17 (m, 2H). ESI-MS, calcd for C$_{26}$H$_{22}$N$_4$O$_2$ 422.2; found m/z = 423.1 [M + H]$^+$.



**14b**
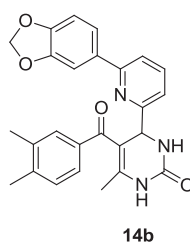
**4-(6-(benzo[d][1,3]dioxol-5-yl)pyridin-2-yl)-5-(3,4-dimethylbenzoyl)-6-methyl-3,4-dihydropyrimidin-2(1H)-one (14b)** was obtained by following the general procedure **a** as a yellow solid in 82% yield. RP-HPLC $t_R$ = 26.0min, gradient condition: from 5% B to 25% B in 10 min, increased to 100% B in 50 min, flow rate of 4 ml/min, $\lambda$ = 280 nm. ^{1}H NMR (300 MHz, DMSO-*d6*): 1.71 (s, 3H); 2.20 (s, 3H); 2.26 (s, 3H); 5.35 (s, 1H); 6.08 (s, 2H); 6.97 (d, *J* = 8.6 Hz, 1H); 7.11 (br s, 1H); 7.18 (d, *J* = 8.0 Hz, 1H); 7.36 (s, 1H), 7.54 (br s, 2H); 7.75-7.80 (m, 3H). ESI-MS, calcd for C$_{26}$H$_{23}$N$_3$O$_4$ 441.2; found m/z = 442.0 [M + H]$^+$.



**14c**
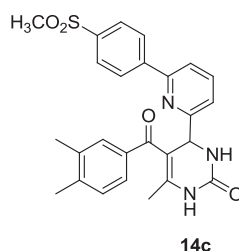
**5-(3,4-dimethylbenzoyl)-6-methyl-4-(6-(4-(methylsulfonyl)phenyl)-pyridin-2-yl)-3,4-dihydropyrimidin-2(1H)-one (14c)** was obtained by

following the general procedure **a** as a yellow gelatinous solid in 83% yield. RP-HPLC $t_R$ = 36.5 min, gradient condition: from 5% B to 100% B in 50 min, flow rate of 4 ml/min, $\lambda$ = 280 nm. $^1$H NMR (300 MHz, DMSO-*d6*): $\delta$ = 1.69 (s, 3H); 2.16 (s, 3H); 2.25 (s, 3H); 3.27 (s, 3H); 5.42 (s, 1H); 7.19 (d, *J* = 7.9 Hz, 1H); 7.25-7.33 (m, 2H); 7.84 (br s, 1H), 7.92-7.99 (m, 2H); 8.20 (d, *J* = 8.4 Hz, 1H). ESI-MS, calcd for $C_{26}H_{25}N_3O_4S$ 475.2; found m/z = 476.0 [M + H]$^+$.



**14d**
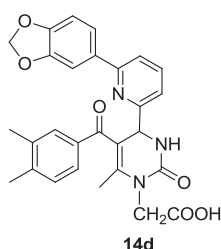
**2-(4-(6-(benzo[d][1,3]dioxol-5-yl)pyridin-2-yl)-5-(3,4-dimethylbenzoyl)-6-methyl-2-oxo-3,4-dihydropyrimidin-1(2H)-yl)acetic acid (14d)** was obtained by following the general procedure **a** as a reddish solid in 61% yield. RP-HPLC $t_R$ = 40.6 min, gradient condition: from 5% B to 20% B in 10 min, increased to 65% B in 50 min, $\lambda$ = 280 nm. $^1$H NMR (300 MHz, DMSO-*d6*): $\delta$ = 1.68 (s, 3H); 2.18 (s, 3H); 2.25 (s, 3H); 5.60 (s, 1H); 5.98 (s, 2H); 6.98 (d, *J* = 8.6 Hz, 1H); 7.09 (br s, 1H); 7.15 (d, *J* = 8.0 Hz, 1H); 7.34 (s, 1H), 7.53 (br s, 2H); 7.74-7.81 (m, 3H). ESI-MS, calcd for $C_{28}H_{25}N_3O_6$ 499.2; found m/z = 500.1 [M + H]$^+$.



**14e**
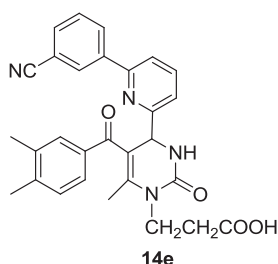
**3-(4-(6-(3-cyanophenyl)pyridin-2-yl)-5-(3,4-dimethylbenzoyl)-6-methyl-2-oxo-3,4-dihydropyrimidin-1(2H)-yl)propanoic acid (14e)** was obtained by following the general procedure **a** as a yellow gelatinous solid in 56% yield.

RP-HPLC $t_R$ = 35.5 min, gradient condition: from 5% B to 25% B in 10 min, increased to 80% B in 50 min, flow rate of 4 ml/min, $\lambda$ = 280 nm. ^{1}H NMR (300 MHz, CDCl$_3$): $\delta$ = 1.88 (s, 3H); 2.20 (s, 3H); 2.25 (s, 3H); 2.40-2.48 (m, 2H); 3.87-3.97 (m, 2H); 5.41 (s, 1H); 7.09-7.16 (m, 1H); 7.37-7.52 (m, 4H); 7.67 (br s, 2H), 7.83 (br s, 1H); 8.01-8.15 (m, 2H). ESI-MS, calcd for C$_{29}$H$_{26}$N$_4$O$_4$ 494.2; found m/z = 495.0 [M + H]$^+$.



**14m**
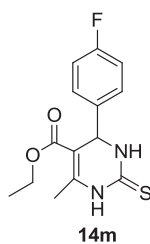
**Ethyl 4-(4-fluorophenyl)-6-methyl-2-thioxo-1,2,3,4-tetrahydro-pyrimidine-5-carboxylate (14m)** was obtained by following the general procedure **a** as a yellow solid in 92% yield. RP-HPLC $t_R$ = 28.7 min, gradient condition: from 5% B to 100% B in 50 min, flow rate of 1 mL/min, $\lambda$ = 280 nm. Spectral data were in accord with previously published data.[515]

^{1}H NMR (300 MHz, CDCl$_3$): $\delta$ = 1.14 (t, $J$ = 7.1 Hz, 3H); 2.47 (s, 3H); 3.95-4.12 (m, 2H); 5.65 (s, 1H); 6.95 (br s, 2H); 7.25 (br s, 2H). ESI-MS, calcd for C$_{14}$H$_{15}$FN$_2$O$_2$S 294.1; found m/z = 295.0 [M + H]$^+$.



**14n**
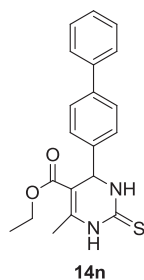
**Ethyl 4-([1,1'-biphenyl]-4-yl)-6-methyl-2-thioxo-1,2,3,4-tetrahydro-pyrimidine-5-carboxylate (14n)** was obtained by following the general procedure **a** as a pale yellow solid in 94% yield. RP-HPLC $t_R$ = 30.9 min, gradient condition: from 5% B to 100 % B in 50 min, flow rate of 1 mL/min, $\lambda$ = 280 nm. ^{1}H NMR (300 MHz, CDCl$_3$): $\delta$ = 1.20 (t, $J$ = 7.1 Hz, 3H); 2.54 (s,

3H); 4.13-4.21 (m, 2H); 5.65 (s, 1H); 7.38-7.46 (m, 7H); 7.65 (br s, 1H); 7.79 (br s, 2H). ESI-MS, calcd for $C_{20}H_{20}N_2O_2S$ 352.1; found m/z = 353.0 [M + H]$^+$.



**14o**
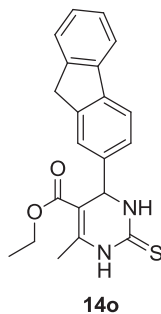
**Ethyl 4-(9H-fluoren-2-yl)-6-methyl-2-thioxo-1,2,3,4-tetrahydro-pyrimidine-5-carboxylate (14o)** was obtained by following the general procedure **a** as a yellow gelatinous solid in 87% yield. RP-HPLC $t_R$ = 35.1 min, gradient condition: from 5% B to 100 % B in 50 min, flow rate of 1 mL/min, λ = 280 nm. $^1$H NMR (300 MHz, CDCl$_3$): δ = 1.13 (t, *J* = 7.1 Hz, 3H); 2.70 (s, 3H); 4.07-4.18 (m, 2H); 5.75 (s, 1H); 7.45-7.57 (m, 4H); 7.70-7.79 (m, 3H); 7.79 (br s, 2H). ESI-MS, calcd for $C_{21}H_{20}N_2O_2S$ 364.1; found m/z = 365.0 [M + H]$^+$.



**14p**
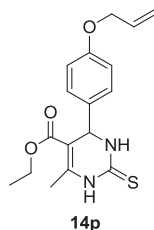
**Ethyl 4-(4-(allyloxy)phenyl)-6-methyl-2-thioxo-1,2,3,4-tetrahydro-pyrimidine-5-carboxylate (14p)** was obtained by following the general procedure **a** as a pale reddish solid in 91% yield. RP-HPLC $t_R$ = 30.4 min, gradient condition: from 5% B to 20% B in 5 min, increased to 100 % B in 55 min, flow rate of 1 mL/min, λ= 280 nm. $^1$H NMR (300 MHz, CDCl$_3$): δ = 1.15 (t, *J* = 7.1 Hz, 3H); 2.48 (s, 3H); 4.05-4.17 (m, 2H); 4.54 (d, *J* = 5.2 Hz, 2H); 5.31-5.45 (m, 2H); 5.60 (s, 1H), 5.97-6.12 (m, 1H), 6.88 (d, *J* = 8.6 Hz, 2H);

7.22 (d, $J$ = 8.6 Hz, 2H). ESI-MS, calcd for $C_{17}H_{20}N_2O_3S$ 332.1; found m/z = 333.0 $[M + H]^+$.



**14q**
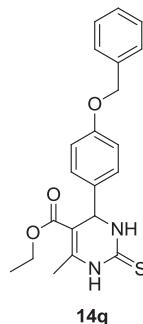
**Ethyl 4-(4-(benzyloxy)phenyl)-6-methyl-2-thioxo-1,2,3,4-tetrahydro-pyrimidine-5-carboxylate (14q)** was obtained by following the general procedure **a** as a pale yellow solid in 76% yield. RP-HPLC $t_R$ = 32.6 min, gradient condition: from 5% B to 100 % B in 50 min, flow rate of 1 mL/min, $\lambda$= 280 nm. $^1$H NMR (300 MHz, CDCl$_3$): $\delta$ = 1.13 (t, $J$ = 7.1 Hz, 3H); 2.30 (s, 3H); 4.04-4.15 (m, 2H); 5.15 (s, 2H); 5.65 (s, 1H); 6.92 (d, $J$ = 8.3 Hz, 2H); 7.29-7.41 (m, 7H). ESI-MS, calcd for $C_{21}H_{22}N_2O_3S$ 382.1; found m/z = 383.0 $[M + H]^+$.



**24**
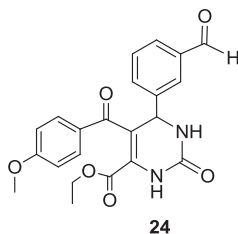
**Ethyl 6-(3-formylphenyl)-5-(4-methoxybenzoyl)-2-oxo-1,2,3,6-tetrahydropyrimidine-4-carboxylate (24)** was obtained by following the general procedure **a** as a yellow gelatinous solid in 85% yield. RP-HPLC $t_R$ = 24.7 min, gradient condition: from 5% B to 25% B in 10 min, increased to 100 % B in 45 min, flow rate of 4 mL/min, $\lambda$= 280 nm. $^1$H NMR (500 MHz, CDCl$_3$): $\delta$ = 0.85 (t, $J$ = 7.1 Hz, 3H), 3.81 (s, 3H), 3.88-4.01 (m, 4H), 5.59 (s, 1H), 6.77 (d, $J$ = 8.9 Hz, 2H), 7.44 (t, $J$ = 7.8 Hz, 1H), 7.53-7.61 (m, 3H), 7.76 (br s, 2H), 9.92 (s, 1H); $^{13}$C NMR (125 MHz, CDCl$_3$): $\delta$ = 13.7, 54.6, 57.8,

61.9, 112.7, 113.3, 128.4, 128.8, 130.7, 131.6, 132.0, 133.2, 190.7. ESI-MS, calcd for $C_{22}H_{20}N_2O_6$ 408.13; found m/z = 409.1 [M + H]$^+$. HRMS, calcd for $C_{22}H_{21}N_2O_6$ [ M+H]$^+$ 409.1400, found 409.1388.
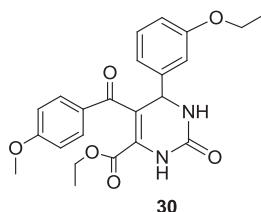


**30**

**Ethyl 6-(3-ethoxyphenyl)-5-(4-methoxybenzoyl)-2-oxo-1,2,3,6-tetrahydropyrimidine-4-carboxylate (30)** was obtained by following the general procedure **a** as a brown gelatinous solid in 78% yield. RP-HPLC $t_R$ = 22.9 min, gradient condition: from 5% B to 30% B in 10 min, increased to 100 % B in 40 min, flow rate of 4 mL/min, λ= 280 nm. $^1$H NMR (500 MHz, CDCl$_3$): δ = 0.85 (t, $J$ = 7.1 Hz, 3H), 1.33 (t, $J$ = 7.1 Hz, 3H), 3.79 (s, 3H), 3.85-3.98 (m, 4H), 5.46 (s, 1H), 6.72-6.82 (m, 4H), 7.13 (t, $J$ = 7.8 Hz, 1H), 7.35 (br s, 1H), 7.57 (d, $J$ = 8.8 Hz, 2H); $^{13}$C NMR (125 MHz, CDCl$_3$): δ = 13.2, 14.2, 56.1, 55.9, 56.1, 59.6, 113.4, 113.9, 114.2, 119.6, 119.8, 130.7, 131.4, 131.7. ESI-MS, calcd for $C_{23}H_{24}N_2O_6$ 424.16; found m/z = 425.2 [M + H]$^+$. HRMS calcd for $C_{23}H_{25}N_2O_6$ [ M+H]$^+$ 425.1713, found 425.1692.
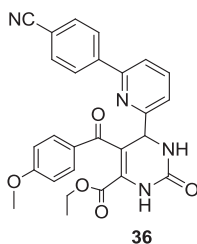


**36**

**Ethyl 6-(6-(4-cyanophenyl)pyridin-2-yl)-5-(4-methoxybenzoyl)-2-oxo-1,2,3,6-tetrahydropyrimidine-4-carboxylate (36)** was obtained by following the general procedure **a** as a yellow powder in79 % yield; RP-HPLC $t_R$ = 20.8 min, gradient condition: from 20% B to 100% B in 45 min, flow rate of 4 mL/min, λ= 280 nm. $^1$H NMR (500 MHz, CDCl$_3$): δ = 0.83 (t, $J$ = 7.1 Hz, 3H), 3.74 (s, 3H), 3.84-3.99 (m, 2H), 5.62 (s, 1H), 6.71 (d, $J$ = 9.0 Hz, 2H),

7.24-7.37 (m, 1H), 7.60-7.63 (m, 4H), 7.74-7.88 (m, 4H); $^{13}$C NMR (125 MHz, CDCl$_3$): δ = 13.4, 55.6, 59.7, 62.9, 113.5, 114.0, 120.1, 120.3, 127.3, 127.7, 129.8, 131.4, 141.4. ESI-MS, calcd for C$_{27}$H$_{22}$N$_4$O$_5$ 482.16; found m/z = 483.1 [M + H]$^+$. HRMS calcd for C$_{27}$H$_{23}$N$_4$O$_5$ [ M+H]$^+$ 483.1668, found 483.1636.



**42**
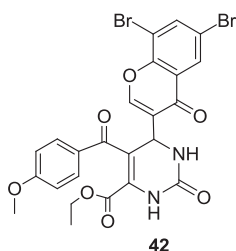
**Ethyl 6-(6,8-dibromo-4-oxo-4H-chromen-3-yl)-5-(4-methoxybenzoyl)-2-oxo-1,2,3,6-tetrahydropyrimidine-4-carboxylate (42)** was obtained by following the general procedure **a** as a yellow powder in 75% yield; RP-HPLC t$_R$ = 26.4 min, gradient condition: from 5% B to 30% B in 5 min, increased to 100 % B in 45 min, flow rate of 4 mL/min, λ= 280 nm. $^1$H NMR (500 MHz, CDCl$_3$): δ = 0.98 (t, *J* = 7.1 Hz, 3H), 3.88 (s, 3H), 4.02-4.12 (m, 2H), 5.42 (s, 1H), 6.98 (d, *J* = 8.7 Hz, 2H), 7.10 (s, 1H), 7.92 (d, *J* = 8.7 Hz, 2H), 8.03 (br s, 1H), 8.25 (br s, 1H); $^{13}$C NMR (125 MHz, CDCl$_3$): δ = 13.0, 61.7, 62.7, 75.3, 112.5, 127.4, 130.7, 135.3, 136.3, 148.5, 157.4. ESI-MS, calcd for C$_{24}$H$_{18}$Br$_2$N$_2$O$_7$ 606.22; found m/z = 606.8 [M + H]$^+$. HRMS, calcd for C$_{24}$H$_{19}$Br$_2$N$_2$O$_7$ [ M+H]$^+$ 604.9559, found 604.9533.
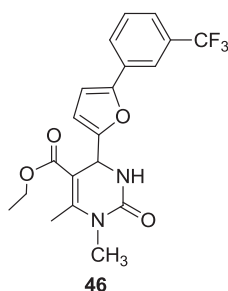


**46**

**Ethyl 1,6-dimethyl-2-oxo-4-(5-(3-(trifluoromethyl)phenyl)furan-2-yl)-1,2,3,4-tetrahydropyrimidine-5-carboxylate (46)** was obtained by following

the general procedure **a** as a reddish solid in 75% yield; RP-HPLC $t_R$ = 26.7 min, gradient condition: from 5% B to 40% B in 10 min, increased to 100 % B in 40 min, flow rate of 4 mL/min, $\lambda$= 280 nm. $^1$H NMR (500 MHz, CDCl$_3$): $\delta$ = 1.29 (t, $J$ = 7.1 Hz, 3H), 2.55 (s, 3H), 3.26 (s, 3H), 4.10-4.20 (m, 2H), 5.52 (s, 1H), 6.21 (d, $J$ = 3.3 Hz, 1H), 6.62 (d, $J$ = 3.3 Hz, 1H), 7.45-7.52 (m, 3H), 7.81 (br s, 1H); $^{13}$C NMR (125 MHz, CDCl$_3$): $\delta$ = 13.7, 14.8, 32.6, 56.0, 60.2, 108.0, 110.8, 127.4, 128.6, 130.3, 133.5. ESI-MS, calcd for C$_{20}$H$_{19}$F$_3$N$_2$O$_4$ 408.13.; found m/z = 409.1 [M + H]$^+$. HRMS, calcd for C$_{20}$H$_{20}$F$_3$N$_2$O$_4$ [M + H]$^+$ 409.1375, found 409.1354.
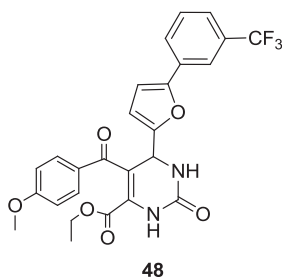


**48**

**Ethyl 5-(4-methoxybenzoyl)-2-oxo-6-(5-(3-(trifluoromethyl)phenyl)-furan-2-yl)-1,2,3,6-tetrahydropyrimidine-4-carboxylate (48)** was obtained by following the general procedure **a** as a reddish gelatinous solid in 88% yield; RP-HPLC $t_R$ = 34.2 min, gradient condition: from 5% B to 35% B in15 min, increased to 100 % B in 40 min, flow rate of 4 mL/min, $\lambda$= 280 nm. $^1$H NMR (500 MHz, CDCl$_3$): $\delta$ = 0.85 (t, $J$ = 7.1 Hz, 3H), 3.74 (s, 3H), 3.85-4.00 (m, 2H), 5.59 (s, 1H), 6.37 (d, $J$ = 3.3 Hz, 1H), 6.57 (d, $J$ = 3.3 Hz, 1H), 6.75 (d, $J$ = 8.4 Hz, 2H), 7.41-7.47 (m, 2H), 7.60 (br s, 2H), 7.73 (d, $J$ = 8.4 Hz, 2H); $^{13}$C NMR (125 MHz, CDCl$_3$): $\delta$ = 13.7, 52.7, 55.4, 63.0, 107.5, 109.7, 111.6, 116.8, 121.7, 124.4, 127.0, 129.5, 130.8, 131.7. ESI-MS, calcd for C$_{26}$H$_{21}$F$_3$N$_2$O$_6$ 514.14; found m/z = 515.1 [M + H]$^+$. HRMS, calcd for C$_{26}$H$_{22}$F$_3$N$_2$O$_6$ [ M+H]$^+$ 515.1430, found 515.1403.

**49**
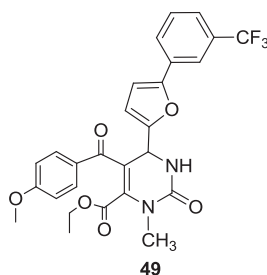
**Ethyl 5-(4-methoxybenzoyl)-3-methyl-2-oxo-6-(5-(3-(trifluoromethyl)-phenyl)furan-2-yl)-1,2,3,6-tetrahydropyrimidine-4-carboxylate (49)** was obtained by following the general procedure **a** as a red gelatinous solid in 76% yield; RP-HPLC $t_R$ = 30.3 min, gradient condition: from 5% B to 40% B in 10 min, increased to 100 % B in 40 min, flow rate of 4 mL/min, λ= 280 nm. $^1$H NMR (500 MHz, CDCl$_3$): δ = 1.05 (t, $J$ = 7.1 Hz, 3H), 3.20 (s, 3H), 3.82 (s, 3H), 3.76-3.88 (m, 2H), 5.54 (s, 1H), 6.40 (d, $J$ = 3.3 Hz, 1H), 6.60 (d, $J$ = 3.3 Hz, 1H), 6.87 (d, $J$ = 8.7 Hz, 2H), 7.48 (br s, 2H), 7.66-7.73 (m, 4H); $^{13}$C NMR (125 MHz, CDCl$_3$): δ = 13.7, 32.6, 50.8, 56.0, 63.5, 108.0, 110.8, 114.6, 120.7, 121.2, 121.7 127.4, 128.6, 130.3, 133.5. ESI-MS, calcd for C$_{27}$H$_{23}$F$_3$N$_2$O$_6$ 528.15; found m/z = 529.1 [M + H]$^+$. HRMS, calcd for C$_{27}$H$_{24}$F$_3$N$_2$O$_6$ 529.1586, found 529.1564.
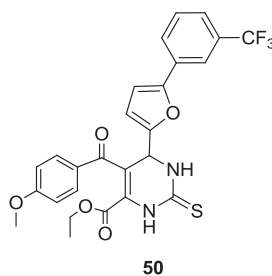


**50**

**Ethyl 5-(4-methoxybenzoyl)-2-thioxo-6-(5-(3-(trifluoromethyl)phenyl)-furan-2-yl)-1,2,3,6-tetrahydropyrimidine-4-carboxylate (50)** was obtained by following the general procedure **a** as a pale red solid in 90% yield; RP-HPLC $t_R$ = 32.3 min, gradient condition: from 5% B to 35% B in 10 min, increased to 100 % B in 40 min, flow rate of 4 mL/min, λ= 280 nm. $^1$H NMR (500 MHz, CDCl$_3$): δ = 0.85 (t, $J$ = 7.1 Hz, 3H), 3.75 (s, 3H), 3.85-4.00 (m,

2H), 5.58 (s, 1H), 6.42 (d, $J$ = 3.3 Hz, 1H), 6.58 (d, $J$ = 3.3 Hz, 1H), 6.78 (d, $J$ = 8.7 Hz, 2H), 7.43-7.51 (m, 2H), 7.60 (br s, 2H), 7.74 (d, $J$ = 8.7 Hz, 2H); $^{13}$C NMR (125 MHz, CDCl$_3$): δ = 13.7, 52.2, 55.1, 62.8, 107.4, 110.7, 113.6, 113.8, 120.4, 124.0, 126.8, 128.9, 129.2, 131.1. ESI-MS, calcd for C$_{26}$H$_{21}$F$_3$N$_2$O$_5$S 530.11; found m/z = 531.1 [M + H]$^+$. HRMS, calcd for C$_{26}$H$_{22}$F$_3$N$_2$O$_5$S [M + H]$^+$ 531.1202, found 531.1172.
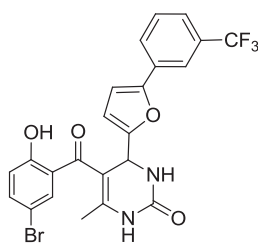


**51**

**5-(5-bromo-2-hydroxybenzoyl)-6-methyl-4-(5-(3-(trifluoromethyl)-phenyl)furan-2-yl)-3,4-dihydropyrimidin-2(1H)-one (51)** was obtained by following the general procedure **a** as a red gelatinous solid in 65% yield. RP-HPLC t$_R$ = 34.9 min, gradient condition: from 5% B to 35% B in 15 min, increased to 100 % B in 40 min, flow rate of 4 mL/min, λ= 280 nm. $^1$H NMR (600 MHz, CDCl$_3$): δ = 3.20 (s, 3H), 5.53 (s, 1H), 6.37 (brs, 1H), 6.64 (brs, 1H), 7.49 (br s, 2H), 7.62-7.69 (m, 3H), 7.79 (s, 1H), 8.06 (s, 1H); $^{13}$C NMR (150 MHz, CDCl$_3$): δ = 19.5, 50.0, 108.1, 109.7, 121.5, 124.6, 126.3, 129.5, 130.7, 133.7. ESI-MS, calcd for C$_{23}$H$_{16}$BrF$_3$N$_2$O$_4$ 521.29; found m/z = 522.7 [M + H]$^+$. HRMS, calcd for C$_{23}$H$_{17}$BrF$_3$N$_2$O$_4$ [M+H]$^+$ 521,03183, found 522.03227.
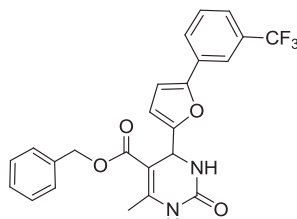


**52**

**Benzyl 6-methyl-2-oxo-4-(5-(3-(trifluoromethyl)phenyl)furan-2-yl)-1,2,3,4-tetrahydropyrimidine-5-carboxylate (52)** was obtained by following the general procedure **a** as a yellow gelatinous solid in 87% yield. RP-HPLC $t_R$ = 32.7 min, gradient condition: from 5% B to 25% B in 5 min, increased to 85% B in 40 min, flow rate of 4 mL/min, λ= 280 nm. $^1$H NMR (600 MHz, CDCl$_3$): δ = 2.40 (s, 3H), 5.13 (dd, *J*= 25.5, 12.5 Hz, 2H), 5.58 (s, 1H), 6.12 (brs, 1H), 6.18 (br s, 1H), 6.57 (br s, 1H), 7.21 (br s, 2H), 7.24 (br s, 1H) 7.44-7.48 (m, 2H), 7.71 (br s, 1H), 7.81 (br s, 1H), 8.05 (s, 1H); $^{13}$C NMR (150 MHz, CDCl$_3$): δ = 19.7, 50.1, 66.4, 108.1, 109.7, 121.5, 124.6, 126.3, 128.1, 129.5, 130.7. ESI-MS, calcd for C$_{24}$H$_{19}$F$_3$N$_2$O$_4$ 456.42; found m/z = 457.1 [M + H]$^+$. HRMS, calcd for C$_{24}$H$_{20}$F$_3$N$_2$O$_4$ [ M+H]$^+$ 457.13697, found 457.13765.



**53**
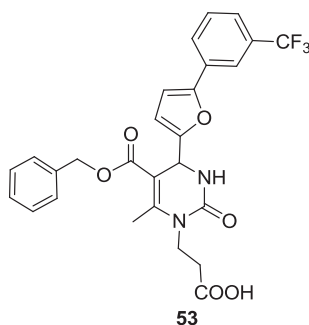
**3-(5-((benzyloxy)carbonyl)-6-methyl-2-oxo-4-(5-(3-(trifluoromethyl)-phenyl)furan-2-yl)-3,4-dihydropyrimidin-1(2H)-yl)propanoic acid (53)** was obtained by following the general procedure **a** as a red gelatinous solid in 58% yield. RP-HPLC $t_R$ = 29.6 min, gradient condition: from 5% B to 30% B in 5 min, increased to 100 % B in 45 min, flow rate of 4 mL/min, λ= 280 nm. $^1$H NMR (600 MHz, CDCl$_3$): δ = 2.55 (s, 3H), 2.74-2.79 (m, 2H), 3.91-4.12 (m, 2H), 5.15 (s, 2H), 5.53 (s, 1H), 6.12 (brs, 1H), 6.33 (d, *J*=3.3Hz, 1H), 6.57 (d, *J*= 3.4Hz, 1H), 7.28 (br s, 4H), 7.44 (br s, 2H), 7.66-7.70 (m, 1H), 7.78 (s, 1H); $^{13}$C NMR (150 MHz, CDCl$_3$): δ = 19.3, 36.6, 50.3, 66.2, 108.1, 109.6, 121.5, 124.4, 126.3, 128.1, 129.5, 130.8. ESI-MS, calcd for C$_{27}$H$_{23}$F$_3$N$_2$O$_6$ 528.48; found m/z = 529.0 [M + H]$^+$. HRMS, calcd for C$_{27}$H$_{24}$F$_3$N$_2$O$_6$ [ M+H]$^+$ 529.15810, found 529.15826.

**54**
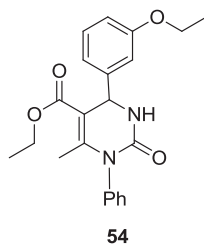
**Ethyl 4-(3-ethoxyphenyl)-6-methyl-2-oxo-1-phenyl-1,2,3,4-tetrahydro-pyrimidine-5-carboxylate (54)** was obtained by following the general procedure **a** as a yellow gelatinous solid in 73% yield. RP-HPLC $t_R$ = 30.6 min, gradient condition: from 5% B to 100% B in 45 min, flow rate of 4 mL/min, λ= 280 nm. $^1$H NMR (600 MHz, CDCl$_3$): δ = 1.21 (t, $J$ = 7.1 Hz, 3H), 1.42 (t, $J$ = 6.9 Hz, 3H), 2.10 (s, 3H), 4.03 (q, $J$ = 7.0 Hz, 2H), 4.15 (q, $J$ = 7.1 Hz, 2H), 5.46 (s, 1H), 6.84 (dd, $J$ = 8.2, 2.1 Hz, 1H), 6.93 (s, 1H), 6.95 (d, $J$ = 7.6 Hz, 1H), 7.25-7.29 (m, 2H), 7.41-745 (m, 4H); $^{13}$C NMR (150 MHz, CDCl$_3$): δ = 14.9, 15.1, 19.0, 54.5, 60.5, 64.4, 112.5, 114.2, 115.1, 118.3, 117.9, 129.2, 129.5, 130.1, 131.3, 141.7, 145.1, 148.2, 158.2, 161.2, 168.4. ESI-MS, calcd for C$_{22}$H$_{24}$N$_2$O$_4$ 380.4; found m/z = 381.8 [M + H]$^+$.

**Ethyl 6-(3-ethoxyphenyl)-5-(4-methoxybenzoyl)-2-oxo-1,2,3,6-tetrahydropyrimidine-4-carboxylate (55):** see compound **30**.
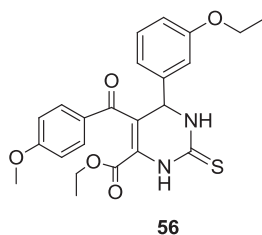


**56**

**Ethyl 6-(3-ethoxyphenyl)-5-(4-methoxybenzoyl)-2-thioxo-1,2,3,6-tetrahydropyrimidine-4-carboxylate (56)** was obtained by following the general procedure **a** as a yellow powder in 78% yield. RP-HPLC $t_R$ = 31.8 min, gradient condition: from 5% B to 35% B in 10 min, increased to 100 % B in 65 min, flow rate of 4 mL/min, λ= 280 nm. $^1$H NMR (600 MHz, CDCl$_3$): δ

= 0.84 (t, *J* = 7.1 Hz, 3H), 1.33 (t, *J* = 6.9 Hz, 3H), 3.82 (s, 3H), 3.85-3.97 (m, 4H), 5.41 (s, 1H), 6.70 (s, 1H), 6.78 (d, *J* = 8.5 Hz, 3H), 7.16 (t, *J* = 7.9 Hz, 1H), 7.38 (br s, 1H), 7.58 (d, *J* = 8.6 Hz, 2H);^{13}C NMR (150 MHz, CDCl$_3$): δ = 13.2, 14.5, 56.7, 55.9, 56.3, 59.8, 113.4, 113.8, 114.2, 119.6, 119.9, 120.5, 130.9, 131.5, 131.8, 144.7, 159.7, 165.5, 180.1, 192.3. ESI-MS, calcd for C$_{23}$H$_{24}$N$_2$O$_5$S 440.5; found m/z = 441.2 [M + H]$^+$.



**57**
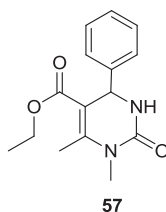
**Ethyl 1,6-dimethyl-2-oxo-4-phenyl-1,2,3,4-tetrahydropyrimidine-5-carboxylate (57)** was obtained by following the general procedure **a** as a yellow gelatinous solid in 89% yield. RP-HPLC t$_R$ = 23.6 min, gradient condition: from 5% B to 30% B in 10 min, increased to 90 % B in 50 min, flow rate of 4 mL/min, λ= 280 nm. All spectral data were in accord with previously published data.[516]



**58**
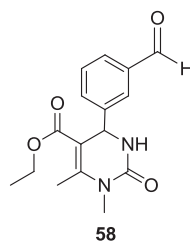
**Ethyl 4-(3-formylphenyl)-1,6-dimethyl-2-oxo-1,2,3,4-tetrahydro-pyrimidine-5-carboxylate (58)** was obtained by following the general procedure **b** as a yellow gelatinous solid in 60% yield. RP-HPLC t$_R$ = 23.9 min, gradient condition: from 5% B to 25% B in 10 min, increased to 95 % B in 50 min, flow rate of 4 mL/min, λ= 280 nm. ^{1}H NMR (600 MHz, CDCl$_3$): δ = 1.18 (t, *J* = 7.1 Hz, 3H), 2.53 (s, 3H), 3.26 (s, 3H), 4.10 (q, *J* = 7.1 Hz, 2H), 5.45 (s, 1H), 7.47-7.55 (m, 2H),7.77 (br s, 2H), 9.98 (s, 1H);^{13}C NMR (150 MHz, CDCl$_3$): δ = 14.3, 19.0, 30.3, 54.1, 61.0, 105.9, 129.9, 130.3, 132.5,

137.8, 143.6, 147.9, 156.7, 166.4, 192.1. ESI-MS, calcd for $C_{16}H_{18}N_2O_4$ 302.3; found m/z = 303.1 $[M + H]^+$.



**59**
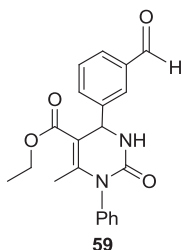
**Ethyl 4-(3-formylphenyl)-6-methyl-2-oxo-1-phenyl-1,2,3,4-tetrahydro-pyrimidine-5-carboxylate (59)** was obtained by following the general procedure **c** as a pale orange gelatinous solid in 62% yield. RP-HPLC $t_R$ = 27.3 min, gradient condition: from 5% B to 100% B in 40 min, flow rate of 4 mL/min, λ = 280 nm. $^1$H NMR (600 MHz, CDCl$_3$): δ = 1.19 (t, $J$ = 7.1 Hz, 3H), 2.14 (s, 3H), 4.13 (q, $J$ = 7.1 Hz, 2H), 5.59 (s, 1H), 7.30 (br s, 1H), 7.42-7.51 (m, 4H), 7.58 (t, $J$ = 7.9 Hz, 1H), 7.71 (d, $J$ =7.6 Hz, 1H), 7.86 (d, $J$ = 7.4 Hz, 1H), 10.05 (s, 1H); $^{13}$C NMR (150 MHz, CDCl$_3$): δ = 14.7, 19.2, 54.8, 60.4, 106.8, 120.6, 124.0, 127.7, 130.4, 132.8, 138.1, 140.9, 141.7, 145.1, 148.2, 158.2, 168.4, 192.4. ESI-MS, calcd for $C_{21}H_{20}N_2O_4$ 364.4; found m/z = 365.3 $[M + H]^+$.

**Ethyl 6-(3-formylphenyl)-5-(4-methoxybenzoyl)-2-oxo-1,2,3,6-tetrahydropyrimidine-4-carboxylate (60)**: see compound **24**.
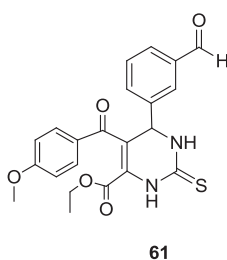


**61**

**Ethyl 6-(3-formylphenyl)-5-(4-methoxybenzoyl)-2-thioxo-1,2,3,6-tetrahydropyrimidine-4-carboxylate (61)** was obtained by following the general procedure **a** as a yellow powder in 85% yield. RP-HPLC $t_R$ = 28.3

min, gradient condition: from 5% B to 25% B in 10 min, increased to 90 % B in 50 min, flow rate of 4 mL/min, λ= 280 nm. $^1$H NMR (600 MHz, CDCl$_3$): δ = 0.85 (t, *J* = 7.1 Hz, 3H), 3.82 (s, 3H), 3.92-4.03 (m, 2H), 5.53 (s, 1H), 6.79 (d, *J* = 8.8 Hz, 2H), 7.33 (br s, 1H), 7.44-7.54 (m, 2H), 7.60 (d, *J* = 8.7 Hz, 1H), 7.71 (s, 1H), 7.78 (d, *J* = 7.3 Hz, 1H), 9.91 (s, 1H); $^{13}$C NMR (150 MHz, CDCl$_3$): δ = 13.5, 54.8, 57.4, 61.9, 112.5, 113.6, 128.7, 129.0, 130.7, 131.4, 132.1, 133.5, 159.8, 165.6, 180.3, 190.8, 192.6. ESI-MS, calcd for C$_{22}$H$_{20}$N$_2$O$_5$S 424.5; found m/z = 425.2 [M + H]$^+$.



**62**
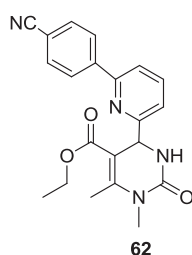
**Ethyl 4-(6-(4-cyanophenyl)pyridin-2-yl)-1,6-dimethyl-2-oxo-1,2,3,4-tetrahydropyrimidine-5-carboxylate (62)** was obtained by following the general procedure **a** as a yellow gelatinous solid in 90% yield. RP-HPLC t$_R$ = 21.5 min, gradient condition: from 5% B to 40% B in 10 min, increased to 100 % B in 50 min, flow rate of 4 mL/min, λ = 280 nm. $^1$H NMR (600 MHz, CDCl$_3$): δ = 1.24 (t, *J* = 7.1 Hz, 3H), 2.51 (s, 3H), 3.22 (s, 3H), 4.18 (q, *J* = 7.0 Hz, 2H), 5.50 (s, 1H), 7.22 (d, *J* = 7.5 Hz, 1H), 7.67 (d, *J* = 7.7 Hz, 1H), 7.71-7.76 (m, 3H), 8.11 (d, *J* = 7.0 Hz, 2H); $^{13}$C NMR (150 MHz, CDCl$_3$): δ = 14.4, 16.6, 30.4, 54.6, 60.4, 103.7, 119.6, 119.9, 120.9, 122.3, 127.4, 132.7, 138.1, 143.7, 151.3, 155.9, 162.8, 166.5. ESI-MS, calcd for C$_{21}$H$_{20}$N$_4$O$_3$ 376.4; found m/z = 377.1 [M + H]$^+$.



**63**
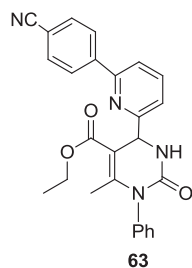
**Ethyl      4-(6-(4-cyanophenyl)pyridin-2-yl)-6-methyl-2-oxo-1-phenyl-1,2,3,4-tetrahydropyrimidine-5-carboxylate (63)** was obtained by following the general procedure **a** as a brownish gelatinous solid in 67% yield. RP-HPLC $t_R$ = 31.2 min, gradient condition: from 5% B to 35% B in 10 min, increased to 100 % B in 45 min, flow rate of 4 mL/min, λ= 280 nm. ^{1}H NMR (600 MHz, CDCl$_3$): δ = 1.27 (t, $J$ = 7.1 Hz, 3H), 2.07 (s, 3H), 4.22 (q, $J$ = 7.0 Hz, 2H), 5.66 (s, 1H), 6.99 (br s, 1H), 7.33-7.42 (m, 4H), 7.67-7.77 (m, 4H), 7.81(d, $J$ = 7.5 Hz, 1H), 8.08 (d, $J$ = 8.2 Hz, 1H);^{13}C NMR (150 MHz, CDCl$_3$): δ = 14.4, 16.6, 54.6, 60.4, 103.7, 119.6, 119.9, 120.9, 122.3, 127.4, 129.3, 130.0, 132.7, 138.1, 141.6, 143.7, 151.3, 155.9, 162.8, 166.5. ESI-MS, calcd for C$_{26}$H$_{22}$N$_4$O$_3$ 438.5; found m/z = 439.1 [M + H]$^+$.

**Ethyl    6-(6-(4-cyanophenyl)pyridin-2-yl)-5-(4-methoxybenzoyl)-2-oxo-1,2,3,6-tetrahydropyrimidine-4-carboxylate (64)**: see compound **38**.
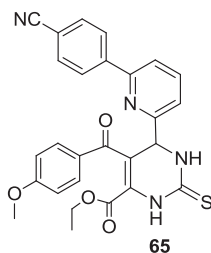


**65**

**Ethyl        6-(6-(4-cyanophenyl)pyridin-2-yl)-5-(4-methoxybenzoyl)-2-thioxo-1,2,3,6-tetrahydropyrimidine-4-carboxylate (65)** was obtained by following the general procedure **a** as a red gelatinous solid in 70% yield. RP-HPLC $t_R$ = 30.0 min, gradient condition: from 5% B to 100% B in 45min, flow rate of 4 mL/min, λ= 280 nm. ^{1}H NMR (600 MHz, CDCl$_3$): δ = 0.85 (t, $J$ = 7.1 Hz, 3H), 3.78 (s, 3H), 3.89-4.00 (m, 2H), 5.62 (s, 1H), 6.72 (d, $J$ = 8.7 Hz, 2H), 7.33 (br s, 1H), 7.61-7.70 (m, 5H), 7.81 (br s, 1H), 7.87 (d, $J$ = 8.3 Hz, 2H); ^{13}C NMR (150 MHz, CDCl$_3$):δ = 13.8, 55.4, 59.9, 62.7, 113.4, 114.1, 119.5, 120.3, 120.5, 122.4, 127.2, 127.6, 129.8, 131.5, 141.4, 143.6, 151.6,

155.8, 159.5, 163.0, 165.7, 192.3. ESI-MS, calcd for $C_{27}H_{22}N_4O_4S$ 498.6; found m/z = 499.4 $[M + H]^+$.

**Ethyl 1,6-dimethyl-2-oxo-4-(5-(3-(trifluoromethyl)phenyl)furan-2-yl)-1,2,3,4-tetrahydropyrimidine-5-carboxylate (66)**: see compound **46**.



**67**
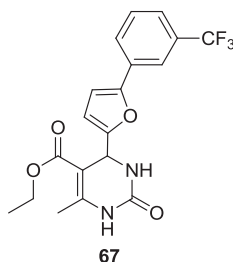
**Ethyl 6-methyl-2-oxo-4-(5-(3-(trifluoromethyl)phenyl)furan-2-yl)-1,2,3,4-tetrahydropyrimidine-5-carboxylate (67)** was obtained by following the general procedure **a** as a brownish gelatinous solid in 78% yield. RP-HPLC $t_R$ = 25.6 min, gradient condition: from 5% B to 40% B in 10 min, increased to 100 % B in 50 min, flow rate of 4 mL/min, λ= 280 nm. $^1$H NMR (600 MHz, CDCl$_3$): δ = 1.24 (t, $J$ = 7.1 Hz, 3H), 2.37 (s, 3H), 4.17 (q, $J$ = 7.0 Hz, 2H), 5.56 (s, 1H), 6.22 (d, $J$ = 3.3 Hz, 1H), 6.59 (d, $J$ = 3.3 Hz, 1H), 7.43-7.51 (m, 2H), 7.73 (br s, 1H), 7.81 (s, 1H); $^{13}$C NMR (150 MHz, CDCl$_3$):δ = 13.7, 14.8, 56.0, 60.2, 102.9, 108.0, 110.8, 123.7, 127.4, 128.6, 130.3, 133.5, 136.4, 151.6, 155.4, 156.0, 166.8. ESI-MS, calcd for $C_{19}H_{17}F_3N_2O_4$ 394.3; found m/z = 395.1 $[M + H]^+$.

**Ethyl 5-(4-methoxybenzoyl)-2-oxo-6-(5-(3-(trifluoromethyl)phenyl)-furan-2-yl)-1,2,3,6-tetrahydropyrimidine-4-carboxylate (68)**: see compound **48**.

**Ethyl 5-(4-methoxybenzoyl)-2-thioxo-6-(5-(3-(trifluoromethyl)phenyl)-furan-2-yl)-1,2,3,6-tetrahydropyrimidine-4-carboxylate (69)**: see compound **50**.

**71**
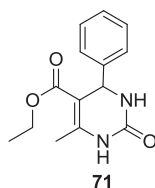
**Ethyl          6-methyl-2-oxo-4-phenyl-1,2,3,4-tetrahydropyrimidine-5-carboxylate (71)** was obtained by following the general procedure **a** as a white solid in 92% yield. RP-HPLC $t_R$ = 18.9 min, gradient condition: from 5% B to 100% B in 40 min, flow rate of 4 mL/min, λ= 280 nm. Spectral data were in accord with previously published data.[517]



**72**
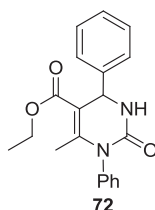
**Ethyl          6-methyl-2-oxo-1,4-diphenyl-1,2,3,4-tetrahydropyrimidine-5-carboxylate (72)** was obtained by following the general procedure **a** as a yellow gelatinous solid in 58% yield. RP-HPLC $t_R$ = 24.0 min, gradient condition: from 5% B to 100 % B in 55 min, flow rate of 4 mL/min, λ= 280 nm. Spectral data were in accord with previously published data.[422]

$^1$H NMR (300 MHz, CDCl$_3$): δ = 1.22 (t, *J* = 7.1 Hz, 3H), 2.13 (s, 3H), 4.15 (q, *J* = 6.9 Hz, 2H), 5.56 (s, 1H), 7.17-7.25 (m, 2H), 7.36-7.48 (m, 8H). ESI-MS, calcd for C$_{20}$H$_{20}$N$_2$O$_3$ 336.1; found m/z = 337.1 [M + H]$^+$.



**73**
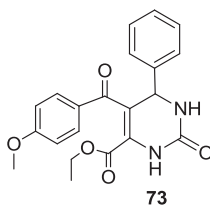
**Ethyl          5-(4-methoxybenzoyl)-2-oxo-6-phenyl-1,2,3,6-tetrahydro-pyrimidine-4-carboxylate (73)** was obtained by following the general procedure **a** as a colourless gelatinous solid in 81% yield. RP-HPLC $t_R$ = 16.4 min, gradient condition: from 5% B to 35% B in 5 min, increased to 100% B

in 45 min, flow rate of 4 mL/min, λ= 280 nm. $^1$H NMR (300 MHz, CDCl$_3$): δ = 0.88 (t, $J$ = 6.8 Hz, 3H), 3.81 (s, 3H), 3.91-4.05 (m, 2H), 5.54 (s, 1H), 6.78 (d, $J$ = 8.1 Hz, 2H), 7.30 (brs, 4H), 7.58 (d, $J$ = 8.1 Hz, 2H), 7.77 (br s, 1H). ESI-MS, calcd for C$_{21}$H$_{20}$N$_2$O$_5$ 380.1; found m/z = 381.0 [M + H]$^+$.



**74**
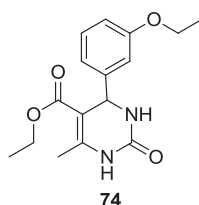
**Ethyl 4-(3-ethoxyphenyl)-6-methyl-2-oxo-1,2,3,4-tetrahydro-pyrimidine-5-carboxylate (74)** was obtained by following the general procedure **a** as a white powder in 86% yield. RP-HPLC t$_R$ = 17.5 min, gradient condition: from 5% B to 30% B in 5 min, increased to 100 % B in 40 min, flow rate of 4 mL/min, λ= 280 nm. $^1$H NMR (300 MHz, CDCl$_3$): δ = 1.19 (t, $J$ = 7.1 Hz, 3H), 1.42 (t, $J$ = 6.9 Hz, 3H), 2.37 (s, 3H), 3.99-4.15 (m, 4H), 5.59 (s, 1H), 6.77-6.93 (m, 3H); 7.23 (t, $J$ = 8.0 Hz, 1H). ESI-MS, calcd for C$_{16}$H$_{20}$N$_2$O$_4$ 304.1; found m/z = 304.0 [M + H]$^+$.



**75**
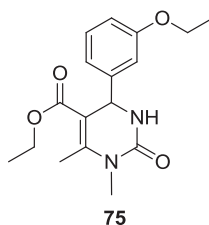
**Ethyl 4-(3-ethoxyphenyl)-1,6-dimethyl-2-oxo-1,2,3,4-tetrahydro-pyrimidine-5-carboxylate (75)** was obtained by following the general procedure **b** as a white solid in 88% yield. RP-HPLC t$_R$ = 18.6 min, gradient condition: from 5% B to 35% B in 5 min, increased to 100 % B in 40 min, flow rate of 4 mL/min, λ= 280 nm. $^1$H NMR (300 MHz, CDCl$_3$): δ = 1.21 (t, $J$ = 7.1 Hz, 3H), 1.42 (t, $J$ = 7.0 Hz, 3H), 2.53 (s, 3H), 4.02 (q, $J$ = 7.0 Hz, 2H), 4.13 (q, $J$ = 7.1 Hz, 2H), 5.40 (s, 1H), 6.77-6.87 (m, 3H); 7.23 (br s, 1H). ESI-MS, calcd for C$_{17}$H$_{22}$N$_2$O$_4$ 318.2; found m/z = 319.1 [M + H]$^+$.

**76**
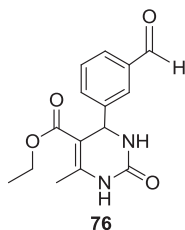
**Ethyl 4-(3-formylphenyl)-6-methyl-2-oxo-1,2,3,4-tetrahydro-pyrimidine-5-carboxylate (76)** was obtained by following the general procedure **c** as a yellow gelatinous solid in 87% yield. RP-HPLC $t_R$ = 21.6 min, gradient condition: from 5% B to 100 % B in 50 min, flow rate of 4 mL/min, λ= 280 nm. $^1$H NMR (300 MHz, CDCl$_3$): δ = 1.18 (t, $J$ = 7.1 Hz, 3H), 2.37 (s, 3H), 4.02-4.17 (m, 2H), 5.50 (s, 1H), 7.15 (br s, 1H); 7.50-7.63 (m, 2H); 7.83 (br s, 1H), 10.00 (s, 1H). ESI-MS, calcd for C$_{15}$H$_{16}$N$_2$O$_4$ 288.1; found m/z = 289.0 [M + H]$^+$.



**80**
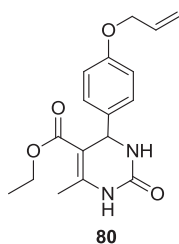
**Ethyl 4-(4-(allyloxy)phenyl)-6-methyl-2-oxo-1,2,3,4-tetrahydro-pyrimidine-5-carboxylate (80)** was obtained by following the general procedure **a** as an orange solid in 74% yield. RP-HPLC $t_R$ = 17.2 min, gradient condition: from 5% B to 35% B in 5 min, increased to 100% B in 45 min, flow rate of 4 mL/min, λ= 280 nm. Spectral data were in accord with previously published data.[517] $^1$H NMR (300 MHz, CDCl$_3$): δ = 1.18 (t, $J$ = 7.1 Hz, 3H); 2.37 (s, 3H); 4.09 (q, $J$ = 7.0 Hz, 2H); 4.53 (d, $J$ = 5.2 Hz, 2H); 5.29-5.42 (m, 2H); 5.70 (s, 1H), 5.95-6.10 (m, 1H), 6.86 (d, $J$ = 8.6 Hz, 2H); 7.23 (d, $J$ = 8.6 Hz, 2H). ESI-MS, calcd for C$_{17}$H$_{20}$N$_2$O$_4$ 316.1; found m/z = 317.0 [M + H]$^+$.

**81**
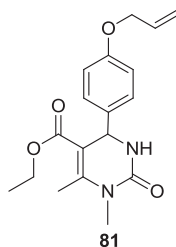
**Ethyl 4-(4-(allyloxy)phenyl)-1,6-dimethyl-2-oxo-1,2,3,4-tetrahydropyrimidine-5-carboxylate (81)** was obtained by following the general procedure **a** as a yellow solid in 80% yield. RP-HPLC $t_R$ = 24.5 min, gradient condition: from 5% B to 30% B in 5 min, increased to 100% B in 55 min, flow rate of 4 mL/min, $\lambda$= 280 nm. $^1$H NMR (300 MHz, CDCl$_3$): $\delta$ = 1.19 (t, $J$ = 7.1 Hz, 3H); 2.51 (s, 3H); 3.26 (s, 3H); 4.12 (q, $J$ = 7.1 Hz, 2H); 4.53 (d, $J$ = 5.2 Hz, 2H); 5.28-5.39 (m, 2H); 5.67 (s, 1H), 5.98-6.11 (m, 1H), 6.86 (d, $J$ = 8.6 Hz, 2H); 7.18 (d, $J$ = 8.6 Hz, 2H). ESI-MS, calcd for C$_{18}$H$_{22}$N$_2$O$_4$ 330.2; found m/z = 331.1 [M + H]$^+$.
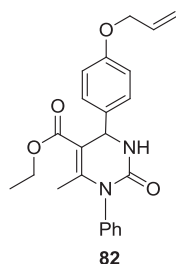


**82**

**Ethyl 4-(4-(allyloxy)phenyl)-6-methyl-2-oxo-1-phenyl-1,2,3,4-tetrahydropyrimidine-5-carboxylate (82)** was obtained by following the general procedure **a** as a yellow gelatinous solid in 63% yield. RP-HPLC $t_R$ = 26.8 min, gradient condition: from 5% B to 40% B in 5 min, increased to 100 % B in 45 min, flow rate of 4 mL/min, $\lambda$= 280 nm. $^1$H NMR (300 MHz, CDCl$_3$): $\delta$ = 1.28 (t, $J$ = 7.1 Hz, 3H); 2.65 (s, 3H); 4.13-4.22 (m, 2H); 4.54 (d, $J$ = 5.2 Hz, 2H); 5.27-5.41 (m, 2H); 5.47 (s, 1H), 5.99-6.13 (m, 1H), 6.90 (d, $J$ = 8.7 Hz, 2H); 7.11-7.25 (m, 7H). ESI-MS, calcd for C$_{23}$H$_{24}$N$_2$O$_4$ 392.2; found m/z = 393.1 [M + H]$^+$.
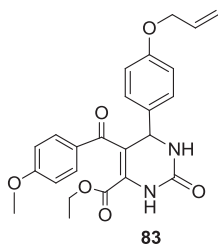
**Ethyl 6-(4-(allyloxy)phenyl)-5-(4-methoxybenzoyl)-2-oxo-1,2,3,6-tetrahydropyrimidine-4-carboxylate (83)** was obtained by following the general procedure **a** as a pale yellow solid in 89% yield. RP-HPLC $t_R$ = 21.0 min, gradient condition: from 5% B to 35% B in 5 min, increased to 100 % B in 45 min, flow rate of 4 mL/min, λ= 280 nm. $^1$H NMR (300 MHz, CDCl$_3$): δ = 0.86 (t, $J$ = 7.2 Hz, 3H); 3.84 (s, 3H); 3.88-4.01 (m, 2H); 4.45 (d, $J$ = 5.2 Hz, 2H); 5.25-5.37 (m, 2H); 5.67 (s, 1H), 5.91-6.09 (m, 1H), 6.75-6.84 (m, 4H); 7.17 (d, $J$ = 8.6 Hz, 2H); 7.61 (d, $J$ = 8.7 Hz, 2H). ESI-MS, calcd for C$_{24}$H$_{24}$N$_2$O$_6$ 436.2; found m/z = 437.1 [M + H]$^+$.
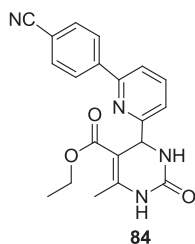


**Ethyl 4-(6-(4-cyanophenyl)pyridin-2-yl)-6-methyl-2-oxo-1,2,3,4-tetrahydropyrimidine-5-carboxylate (84)** was obtained by following the general procedure **a** as a white solid in 80% yield. RP-HPLC $t_R$ = 35.1 min, gradient condition: from 5% B to 100% B in 60 min, flow rate of 4 mL/min, λ = 280 nm. $^1$H NMR (300 MHz, CDCl$_3$): δ = 1.22 (t, $J$ = 7.1 Hz, 3H), 2.40 (s, 3H), 4.19 (q, $J$ = 7.0 Hz, 2H), 5.59 (s, 1H), 7.21 (d, $J$ = 7.5 Hz, 1H), 7.64 (d, $J$ = 7.7 Hz, 1H), 7.72-7.77 (m, 3H), 8.14 (d, $J$ = 7.0 Hz, 2H). ESI-MS, calcd for C$_{20}$H$_{18}$N$_4$O$_3$ 362.1; found m/z = 363.0 [M + H]$^+$.
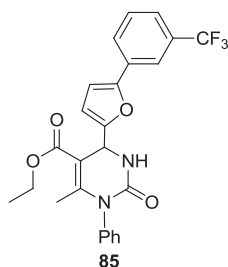
**Ethyl 6-methyl-2-oxo-1-phenyl-4-(5-(3-(trifluoromethyl)phenyl)furan-2-yl)-1,2,3,4-tetrahydropyrimidine-5-carboxylate (85)** was obtained by following the general procedure **a** as a reddish gelatinous solid in 51% yield. RP-HPLC $t_R$ = 31.6 min, gradient condition: from 5% B to 35% B in 5 min, increased to 100 % B in 40 min, flow rate of 4 mL/min, $\lambda$ = 280 nm. $^1$H NMR (300 MHz, CDCl$_3$): $\delta$ = 1.23 (t, $J$ = 7.1 Hz, 3H); 2.42 (s, 3H); 4.48 (q, $J$ = 7.2 Hz, 2H); 5.67 (s, 1H); 7.20-7.25 (m, 2H); 7.39-7.46 (m, 3H); 7.63 (s, 1H); 7.71-7.79 (m, 3H); 8.00 (br s, 2H). ESI-MS, calcd for C$_{25}$H$_{21}$F$_3$N$_2$O$_4$ 470.1; found m/z = 471.0 [M + H]$^+$.
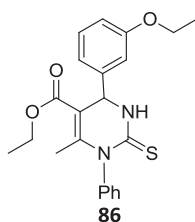


**Ethyl 4-(3-ethoxyphenyl)-6-methyl-1-phenyl-2-thioxo-1,2,3,4-tetrahydropyrimidine-5-carboxylate (86)** was obtained by following the general procedure **a** as a pale yellow powder in 59% yield. RP-HPLC $t_R$ = 30.8 min, gradient condition: from 5% B to 35% B in 5 min, increased to 100% B in 50 min, flow rate of 4 mL/min, $\lambda$= 280 nm. $^1$H NMR (300 MHz, CDCl$_3$): $\delta$ = 1.23 (t, $J$ = 7.1 Hz, 3H), 1.45 (t, $J$ = 6.9 Hz, 3H), 2.14 (s, 3H), 4.06 (q, $J$ = 7.0 Hz, 2H), 4.16 (q, $J$ = 7.1 Hz, 2H), 5.50 (s, 1H), 6.87 (dd, $J$ = 8.2, 2.1 Hz, 1H), 6.95 (s, 1H) 6.97 (d, $J$ = 7.6 Hz, 1H), 7.28-7.31 (m, 2H), 7.43-7.49 (m, 4H). ESI-MS, calcd for C$_{22}$H$_{24}$N$_2$O$_3$S 396.2; found m/z = 397.1 [M + H]$^+$.

**87**
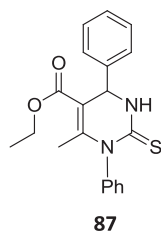
**Ethyl 6-methyl-1,4-diphenyl-2-thioxo-1,2,3,4-tetrahydropyrimidine-5-carboxylate (86)** was obtained by following the general procedure **a** as a yellow gelatinous solid in 62% yield. RP-HPLC $t_R$ = 27.8 min, gradient condition: from 5% B to 40% B in 5 min, increased to 100 % B in 50 min, flow rate of 4 mL/min, λ= 280 nm. Spectral data were in accord with previously published data.[422]

$^1$H NMR (300 MHz, CDCl$_3$): δ = 1.20 (t, *J* = 7.1 Hz, 3H), 2.18 (s, 3H), 4.16 (q, *J* = 6.9 Hz, 2H), 5.58 (s, 1H), 7.14-7.23 (m, 2H), 7.33-7.45 (m, 8H). ESI-MS, calcd for C$_{20}$H$_{20}$N$_2$O$_2$S 352.1; found m/z = 353.0 [M + H]$^+$.
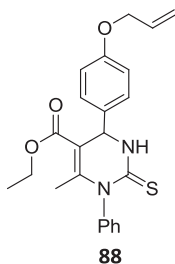


**88**

**Ethyl 4-(4-(allyloxy)phenyl)-6-methyl-1-phenyl-2-thioxo-1,2,3,4-tetrahydropyrimidine-5-carboxylate (88)** was obtained by following the general procedure **a** as a yellow gelatinous solid in 51% yield. RP-HPLC $t_R$ = 34.3 min, gradient condition: from 5% B to 40% B in 5 min, increased to 100% B in 50 min, flow rate of 4 mL/min, λ= 280 nm. $^1$H NMR (300 MHz, CDCl$_3$): δ = 1.25 (t, *J* = 7.1 Hz, 3H); 2.63 (s, 3H); 4.11-4.23 (m, 2H); 4.56 (d, *J* = 5.2 Hz, 2H); 5.25-5.40 (m, 2H); 5.49 (s, 1H), 5.97-6.11 (m, 1H), 6.92 (d, *J* = 8.7 Hz, 2H); 7.13-7.27 (m, 7H). ESI-MS, calcd for C$_{23}$H$_{24}$N$_2$O$_3$S 408.2; found m/z = 409.1 [M + H]$^+$.

**89**
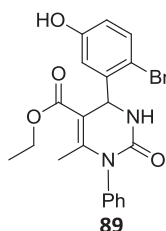
**Ethyl 4-(2-bromo-5-hydroxyphenyl)-6-methyl-2-oxo-1-phenyl-1,2,3,4-tetrahydropyrimidine-5-carboxylate (89)** was obtained by following the general procedure **a** as a pale yellow gelatinous solid in 74% yield. RP-HPLC $t_R$ = 35.0 min, gradient condition: from 5% B to 100% B in 60 min, flow rate of 4 mL/min, λ= 280 nm. $^1$H NMR (300 MHz, CDCl$_3$): δ = 1.10 (t, $J$ = 7.1 Hz, 3H); 2.21 (s, 3H); 3.99-4.16 (m, 2H); 5.83 (s, 1H); 6.60-6.67 (m, 1H); 6.89 (br s, 1H); 7.21 (br s, 1H); 7.38-7.46 (m, 5H). ESI-MS, calcd for C$_{20}$H$_{19}$BrN$_2$O$_4$ 430.1; found m/z = 431.0 [M + H]$^+$.



**90**
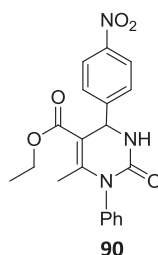
**Ethyl 6-methyl-4-(4-nitrophenyl)-2-oxo-1-phenyl-1,2,3,4-tetrahydropyrimidine-5-carboxylate (90)** was obtained by following the general procedure **a** as a yellow gelatinous solid in 66% yield. RP-HPLC $t_R$ = 22.7 min, gradient condition: from 5% B to 40% B in 5 min, increased to 100 % B in 45 min, flow rate of 4 mL/min, λ= 280 nm. $^1$H NMR (300 MHz, CDCl$_3$): δ = 1.22 (t, $J$ = 7.1 Hz, 3H); 2.12 (s, 3H); 4.16 (q, $J$ = 7.0 Hz, 2H); 5.61 (s, 1H); 7.16 (br s, 2H); 7.40-7.50 (m, 3H); 7.57 (d, $J$ = 8.5 Hz, 2H); 8.22 (d, $J$ = 8.4 Hz, 2H). ESI-MS, calcd for C$_{20}$H$_{19}$N$_3$O$_5$ 381.1; found m/z = 382.0 [M + H]$^+$.

**93**
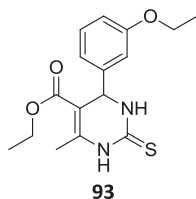
**Ethyl 4-(3-ethoxyphenyl)-6-methyl-2-thioxo-1,2,3,4-tetrahydro-pyrimidine-5-carboxylate (93)** was obtained by following the general procedure **a** as a pale yellow solid in 89% yield. RP-HPLC $t_R$ = 30.5 min, gradient condition: from 5% B to 100 % B in 50 min, flow rate of 4 mL/min, $\lambda$= 280 nm. $^1$H NMR (300 MHz, CDCl$_3$): $\delta$ = 1.18 (t, $J$ = 7.1 Hz, 3H), 1.45 (t, $J$ = 6.9 Hz, 3H), 2.39 (s, 3H), 4.02-4.18 (m, 4H), 5.63 (s, 1H), 6.81-6.95 (m, 3H); 7.26 (t, $J$ = 8.0 Hz, 1H). ESI-MS, calcd for C$_{16}$H$_{20}$N$_2$O$_3$S 320.1; found m/z = 321.0 [M + H]$^+$.

### 7.2.2 General procedure for microwave-assisted Liebeskind-Srogl cross coupling reaction

A dry microwave process vial was charged with the corresponding dihydropyrimidine-2-thione (1.0 equiv), the appropriate arylboronic acid (1.5 equiv), CuTC (3.0 equiv), and Pd(PPh$_3$)$_4$ (10 mol%). The reaction vessel was degassed and backfilled with nitrogen three times. Through the septum degassed dry THF (2.0 mL) was added. The mixture was subsequently heated in a microwave reactor at 100 °C for 60 min. After cooling, the mixture was transferred to a round-bottom flask and dried under reduced pressure. A solution of aqueous ammonia (25%) was added and the mixture was extracted three times with CHCl$_3$. The combined organic layers were dried with anhydrous Na$_2$SO$_4$ and concentrated under vacuum. The crude residue was purified by HPLC to give the pure products in good yields (59-85%) and high purity (>95%).
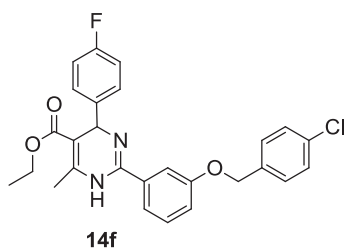
**14f**

**Ethyl 2-(3-((4-chlorobenzyl)oxy)phenyl)-4-(4-fluorophenyl)-6-methyl-1,4-dihydropyrimidine-5-carboxylate (14f)** was obtained from **14m** as a greenish gelatinous solid in 83% yield. RP-HPLC $t_R$ = 27.3 min, gradient condition: from 5% B to 100 % B in 50 min, flow rate of 4 mL/min, $\lambda$ = 280 nm. ^{1}H NMR (300 MHz, CDCl$_3$): $\delta$ = 1.12 (t, $J$ = 7.0 Hz, 3H); 2.49 (s, 3H); 39.98-4.15 (m, 2H); 5.03 (s, 2H); 5.63 (s, 1H); 6.95-7.11 (m, 3H); 7.18-7.54 (m, 9H). ESI-MS, calcd for C$_{27}$H$_{24}$ClFN$_2$O$_3$ 478.1; found m/z = 479.1 [M + H]$^+$.



**14g**
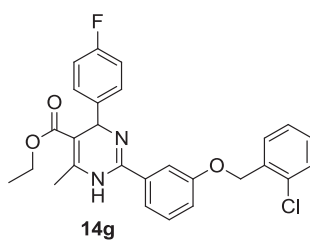
**Ethyl 2-(3-((2-chlorobenzyl)oxy)phenyl)-4-(4-fluorophenyl)-6-methyl-1,4-dihydropyrimidine-5-carboxylate (14g)** was obtained from **14m** as a greenish gelatinous solid in 81% yield. RP-HPLC $t_R$ = 29.5 min, gradient condition: from 5% B to 30% B in 5 min, increased to 100 % B in 75 min, flow rate of 4 mL/min, $\lambda$ = 280 nm. ^{1}H NMR (300 MHz, CDCl$_3$): $\delta$ = 1.13 (t, $J$ = 7.0 Hz, 3H); 2.53 (s, 3H); 4.03-4.17 (m, 2H); 4.97 (s, 2H); 5.61 (s, 1H); 6.96-7.11 (m, 3H); 7.16-7.48 (m, 9H). ESI-MS, calcd for C$_{27}$H$_{24}$ClFN$_2$O$_3$ 478.1; found m/z = 479.0 [M + H]$^+$.

**14h**
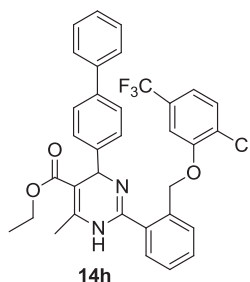
**Ethyl 4-([1,1'-biphenyl]-4-yl)-2-(2-((2-chloro-5-(trifluoromethyl)-phenoxy)methyl)phenyl)-6-methyl-1,4-dihydropyrimidine-5-carboxylate (14h)** was obtained from **14n** as a pale yellow gelatinous solid in 80% yield. RP-HPLC $t_R$ = 36.1 min, gradient condition: from 5% B to 30% B in 5 min, increased to 100 % B in 75 min, flow rate of 4 mL/min, $\lambda$ = 280 nm. $^1$H NMR (300 MHz, CDCl$_3$): $\delta$ = 1.18 (t, $J$ = 7.1 Hz, 3H); 2.52 (s, 3H); 4.02 (s, 2H); 4.10-4.18 (m, 2H); 5.75 (s, 1H); 7.06 (s, 1H); 7.15 (d, $J$ = 8.3 Hz, 1H); 7.38-7.54 (m, 12H); 7.66 (t, $J$ = 7.3 Hz, 1H);. 7.78 (br s, 1H). ESI-MS, calcd for C$_{34}$H$_{28}$ClF$_3$N$_2$O$_3$ 604.2; found m/z = 605.2 [M + H]$^+$.



**14i**
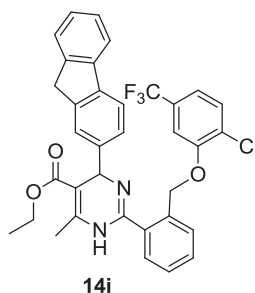
**Ethyl 2-(2-((2-chloro-5-(trifluoromethyl)phenoxy)methyl)phenyl)-4-(9H-fluoren-2-yl)-6-methyl-1,4-dihydropyrimidine-5-carboxylate (14i)** was obtained from **14o** as a yellowish solid in 77% yield. RP-HPLC $t_R$ = 35.3 min, gradient condition: from 5% B to 25% B in 5 min, increased to 100 % B in 65 min, flow rate of 4 mL/min, $\lambda$ = 280 nm. $^1$H NMR (300 MHz, CDCl$_3$): $\delta$ = 1.14 (t, $J$ = 7.0 Hz, 3H); 2.69 (s, 3H); 3.73 (s, 2H); 4.03-4.17 (m, 2H); 5.10 (s, 2H); 5.80 (s, 1H); 7.87 (d, $J$ = 8.1 Hz, 2H); 7.29-7.39 (m, 4H); 7.45-7.55 (m, 4H);. 7.64-7.75 (m, 4H). ESI-MS, calcd for C$_{35}$H$_{28}$ClF$_3$N$_2$O$_3$ 616.2; found m/z = 617.1 [M + H]$^+$.

**14j**
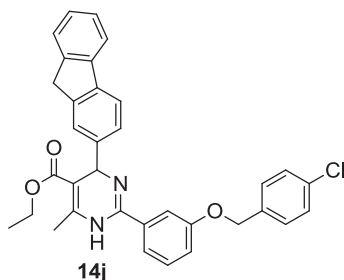
**Ethyl 2-(3-((4-chlorobenzyl)oxy)phenyl)-4-(9H-fluoren-2-yl)-6-methyl-1,4-dihydropyrimidine-5-carboxylate (14j)** was obtained from **14o** as a yellow powder in 74% yield. RP-HPLC $t_R$ = 36.8 min, gradient condition: from 5% B to 25% B in 5 min, increased to 100 % B in 65 min, flow rate of 4 mL/min, λ = 280 nm. ^{1}H NMR (300 MHz, CDCl$_3$): δ = 1.11 (t, $J$ = 7.1 Hz, 3H); 2.69 (s, 3H); 3.82 (s, 2H); 4.01-4.14 (m, 2H); 5.12 (s, 2H); 5.72 (s, 1H); 7.10 (br s, 1H); 7.22 (s, 1H); 7.29-7.42 (m, 8H); 7.53 (br s, 2H);. 7.69-7.77 (m, 3H). ESI-MS, calcd for C$_{34}$H$_{29}$ClN$_2$O$_3$ 548.2; found m/z = 549.1 [M + H]$^+$.



**14k**
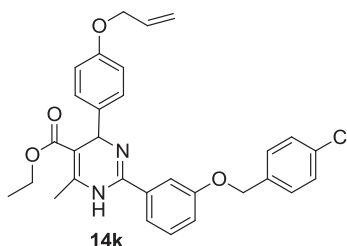
**Ethyl 4-(4-(allyloxy)phenyl)-2-(3-((4-chlorobenzyl)oxy)phenyl)-6-methyl-1,4-dihydropyrimidine-5-carboxylate (14k)** was obtained from **14p** as a yellow solid in 63% yield. RP-HPLC $t_R$ = 37.2 min, gradient condition: from 5% B to 20% B in 5 min, increased to 100 % B in 70 min, flow rate of 4 mL/min, λ = 280 nm. ^{1}H NMR (300 MHz, CDCl$_3$): δ = 1.13 (t, $J$ = 7.1 Hz, 3H); 2.49 (s, 3H); 4.03-4.16 (m, 2H); 4.52 (d, $J$ = 5.2 Hz, 2H); 4.96 (s, 2H); 5.30-5.44 (m, 2H); 5.55 (s, 1H), 5.98-6.10 (m, 1H), 6.86 (d, $J$ = 8.6 Hz, 2H); 7.12 (br s, 1H); 7.22 (d, $J$ = 8.6 Hz, 2H); 7.28-7.34 (m, 5H); 7.44 (br s, 2H). ESI-MS, calcd for C$_{30}$H$_{29}$ClN$_2$O$_4$ 516.2; found m/z = 517.1 [M + H]$^+$.

**14l**
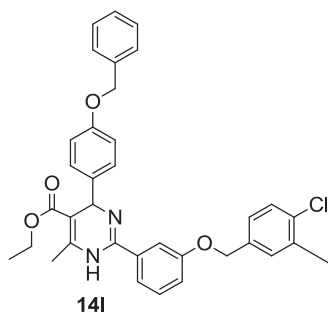
**Ethyl 4-(4-(benzyloxy)phenyl)-2-(3-((4-chloro-3-methylbenzyl)oxy)-phenyl)-6-methyl-1,4-dihydropyrimidine-5-carboxylate (14l)** was obtained from **14q** as a pale yellow solid in 59% yield. RP-HPLC $t_R$ = 34.8 min, gradient condition: from 5% B to 25% B in 5 min, increased to 100 % B in 60 min, flow rate of 4 mL/min, $\lambda$ = 280 nm. $^1$H NMR (300 MHz, CDCl$_3$): $\delta$ = 1.14 (t, $J$ = 7.1 Hz, 3H); 2.29 (s, 3H); 2.67 (s, 3H); 4.05-4.16 (m, 2H); 5.00 (s, 2H); 5.16 (s, 2H); 5.73 (s, 1H), 6.92 (d, $J$ = 8.3 Hz, 2H); 7.08 (d, $J$ = 8.7 Hz, 2H); 7.31-7.45 (m, 10H); 7.84 (d, $J$ = 8.7 Hz, 2H). ESI-MS, calcd for C$_{35}$H$_{33}$ClN$_2$O$_4$ 580.2; found m/z = 581.1 [M + H]$^+$.



**91**
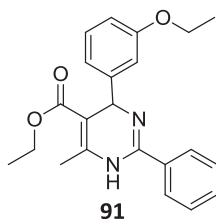
**Ethyl 4-(3-ethoxyphenyl)-6-methyl-2-phenyl-1,4-dihydropyrimidine-5-carboxylate (91)** was obtained from **93** as a colourless gelatinous solid in 85% yield. RP-HPLC $t_R$ = 21.6 min, gradient condition: from 5% B to 100 % B in 50 min, flow rate of 4 mL/min, $\lambda$ = 280 nm. $^1$H NMR (300 MHz, CDCl$_3$): $\delta$ = 1.17 (t, $J$ = 7.1 Hz, 3H); 1.35 (t, $J$ = 7.1 Hz, 3H); 2.50 (s, 3H); 3.93-4.01 (m, 2H); 4.07-4.16 (m, 2H); 5.66 (s, 1H); 6.80-6.90 (m, 3H); 7.19-7.30 (m, 3H); 7.47 (br s, 1H); 7.72 (br s, 2H). ESI-MS, calcd for C$_{22}$H$_{24}$N$_2$O$_3$ 364.2; found m/z = 365.1 [M + H]$^+$.

**92**
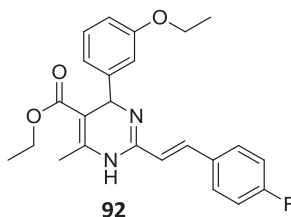
**Ethyl 4-(3-ethoxyphenyl)-2-(4-fluorostyryl)-6-methyl-1,4-dihydropyrimidine-5-carboxylate (92)** was obtained from **93** as a colourless gelatinous solid in 73% yield. RP-HPLC $t_R$ = 20.5 min, gradient condition: from 5% B to 30% B in 5 min, increased to 100 % B in 45 min, flow rate of 4 mL/min, λ = 280 nm. $^1$H NMR (300 MHz, CDCl$_3$): δ = 1.10 (t, $J$ = 7.1 Hz, 3H); 1.36 (t, $J$ = 7.1 Hz, 3H); 2.35 (s, 3H); 3.91-4.09 (m, 4H); 5.30 (s, 1H); 6.74-6.84 (m, 3H); 6.96 (br s, 2H); 7.20 (t, $J$ = 8.0 Hz, 1H); 7.39-7.49 (m, 3H); 7.60 (br s, 1H). ESI-MS, calcd for C$_{24}$H$_{25}$FN$_2$O$_3$ 408.2; found m/z = 409.1 [M + H]$^+$.

### 7.2.3 General procedure for reductive amination

The appropriate aldehyde (1.0 equiv) was dissolved in anhydrous MeOH in a 10 ml round bottom flask. Cyclopentylamine (1.1 equiv) was then added and the reaction mixture was stirred for 3 h at room temperature under nitrogen. Afterwards NaBH$_4$ (1.6 equiv) was added and the mixture was stirred for further 20 min. The mixture was concentrated under reduced pressure, diluted with water and extracted three times with CHCl$_3$. The combined organic layer was dried with anhydrous Na$_2$SO$_4$ and concentrated under vacuum. The pure products were obtained by HPLC purification in good yields (53-90%) and high purity (>95%).
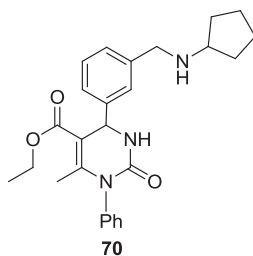
**70**

**Ethyl 4-(3-((cyclopentylamino)methyl)phenyl)-6-methyl-2-oxo-1-phenyl-1,2,3,4-tetrahydropyrimidine-5-carboxylate (70)** was obtained from compound **59** as a yellow powder in 90% yield. RP-HPLC $t_R$ = 19.5 min, gradient condition: from 5% B to 100% B in 45 min, flow rate of 4 mL/min, $\lambda$= 280 nm. $^1$H NMR (600 MHz, CDCl$_3$): $\delta$ = 1.16 (t, $J$ = 7.1 Hz, 3H), 1.49 (br s, 2H), 1.62-1.77 (m, 4H), 1.9 (br s, 2H), 3.30 (s, 1H), 3.88 (s, 2H), 4.05-4.13 (m, 2H), 5.45 (s, 1H), 6.88 (br s,1H), 7.16 (br s, 1H), 7.29-7.35 (m, 3H), 7.37-7.44 (m, 3H), 7.47 (s, 1H); $^{13}$C NMR (150 MHz, CDCl$_3$): $\delta$ = 14.5, 18.9, 23.9, 29.8, 50.3, 53.9, 58.7,60.8, 108.4, 126.8, 129.4, 129.8, 130.6, 139.2, 144.2, 150.5, 156.2, 166.4. ESI-MS, calcd for C$_{26}$H$_{31}$N$_3$O$_3$ 433.5; found m/z = 434.3 [M + H]$^+$.
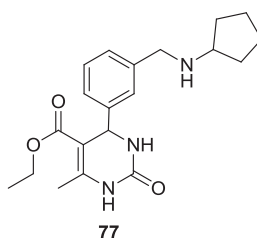


**77**

**Ethyl 4-(3-((cyclopentylamino)methyl)phenyl)-6-methyl-2-oxo-1,2,3,4-tetrahydropyrimidine-5-carboxylate (77)** was obtained from compound **76** as a colourless gelatinous solid in 76% yield. RP-HPLC $t_R$ = 18.6 min, gradient condition: from 5% B to 100% B in 60 min, flow rate of 4 mL/min, $\lambda$= 280 nm. $^1$H NMR (300 MHz, MeOD): $\delta$ = 1.18 (t, $J$ = 7.1 Hz, 3H); 1.62-1.74 (m, 4H); 1.79-1.87 (m, 2H); 2.10-2.20 (m, 2H); 2.37 (s, 3H); 3.51-360 (m, 1H); 4.03-4.11 (m, 2H); 4.20 (br s, 2H); 5.39 (s, 1H); 7.38-7.49 (m, 4H). ESI-MS, calcd for C$_{20}$H$_{27}$N$_3$O$_3$ 357.2; found m/z = 458.1 [M + H]$^+$.

**78**
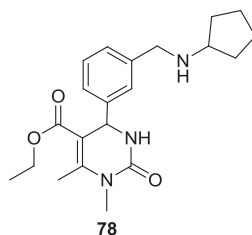
**Ethyl 4-(3-((cyclopentylamino)methyl)phenyl)-1,6-dimethyl-2-oxo-1,2,3,4-tetrahydropyrimidine-5-carboxylate (78)** was obtained from compound **58** as a white solid in 79% yield. RP-HPLC $t_R$ = 18.4 min, gradient condition: from 5% B to 100% B in 50 min, flow rate of 4 mL/min, λ= 280 nm. $^1$H NMR (300 MHz, CDCl$_3$): δ = 1.17 (t, $J$ = 7.1 Hz, 3H); 1.48-1.79 (m, 6H); 1.89-1.98 (m, 2H); 2.55 (s, 3H); 3.21 (s, 3H); 3.28-3.40 (m, 1H); 3.91 (br s, 2H); 4.06-4.15 (m, 2H); 5.36 (s, 1H); 7.16-7.24 (m, 3H); 7.35 (br s, 1H). ESI-MS, calcd for C$_{21}$H$_{29}$N$_3$O$_3$ 371.2; found m/z = 372.1 [M + H]$^+$.



**79**
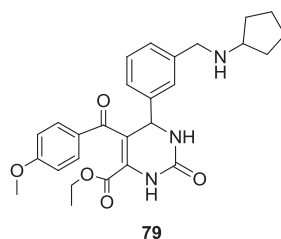
**Ethyl 6-(3-((cyclopentylamino)methyl)phenyl)-5-(4-methoxybenzoyl)-2-oxo-1,2,3,6-tetrahydropyrimidine-4-carboxylate (79)** was obtained from compound **58** as a yellow powder in 53% yield. RP-HPLC $t_R$ = 18.0 min, gradient condition: from 5% B to 100% B in 45 min, flow rate of 4 mL/min, λ= 280 nm. $^1$H NMR (300 MHz, CDCl$_3$): δ = 1.16 (t, $J$ = 7.1 Hz, 3H); 1.45-1.76 (m, 6H); 1.87-1.95 (m, 2H); 3.30-3.40 (m, 1H); 3.84 (s, 3H), 3.92 (br s, 2H); 5.44 (s, 1H), 6.71 (s, 1H), 6.75 (br s, 3H), 7.14 (t, $J$ = 7.9 Hz, 1H), 7.37 (br s, 1H), 7.56 (d, $J$ = 8.6 Hz, 2H). ESI-MS, calcd for C$_{27}$H$_{31}$N$_3$O$_5$ 477.2; found m/z = 478.2 [M + H]$^+$.

# -CHAPTER 8-

His-tagged human mPGES-1 overexpression in
Lemo21(DE3) *E. coli* strain and 2D-crystallization studies:
Experimental procedures

**Materials**

Lemo21(DE3) competent *E. coli* cells were purchased from New Englands BioLabs. Glutathione, Triton X-100 and reduced Triton X-100 were from Sigma. Ni-NTA sepharose gravity flow columns and PD-10 desalting columns were from GE Healthcare Life Sciences. Rabbit mPGES-1 polyclonal antibody was purchased from Cayman Chemicals. Hydroxyapatite (Bio-Gel HTP) and ready-made 18% polyacrylamide gels were from Bio-Rad. Gelcode Blue stain and BCA Protein Assay Reducing Agent Compatible were from Pierce. All other chemicals were of reagent grade and obtained from common commercial sources.

## 8.1 Bacterial Overexpression of Human mPGES-1

The $His_6$-tagged human mPGES-1 ($His_6$-mPGES1) was expressed from the $His_6$-mPGES1-pSP19T7LT vector in *E. coli* Lemo21(DE3) competent cells. An overnight culture of Lemo21(DE3) cells in LB broth containing ampicillin (100 μg/ml) and chloramphenicol (34 μg/ml) was diluted 1:100 into 1–2 liters of Luria Bertani medium containing ampicillin (100 μg/ml), chloramphenicol (34 μg/ml) and L-rhamnose (2.0 mM). The culture was grown at 37 °C with shaking (200 rpm) until the $OD_{600}$ was 0.4–0.6. When the appropriate $OD_{600}$ was reached, expression of $His_6$-mPGES-1 was induced by the addition of 0.4 mM isopropyl β-D-thiogalactopyranoside (IPTG), and the culture was grown over-night at 30 °C. Cells were harvested by centrifugation (7,000 × $g$, 10 min at 4 °C) and washed once with phosphate-buffered saline. The cell pellets were stored frozen at −20 °C until further use.

## 8.2 Preparation and solubilization of whole cell extract

A frozen cell pellet from a 1-liter $His_6$-mPGES-1 was thawed and resuspended in 20 ml of 10 mM sodium phosphate buffer, pH 8.0, 150 mM NaCl, 10% glycerol, 1 mM GSH and lysed by lysozyme addition (1 mg/ml).

DNA was hydrolyzed by the addition of 10 mM $MgCl_2$ and 10 μg/ml DNase and incubation on ice for 30 min. The viscous whole cell lysate was sonicated in an ice water bath by six 15-s sonication pulses until homogeneous from a MSE Soniprep 150 sonicator at 60% power. Then the lysate was solubilized by the addition of an equal volume of 10 mM sodium phosphate buffer, pH 8.0, 150 mM NaCl, 10% glycerol, 1 mM GSH plus 8% Triton X-100 and was gently stirred on ice for 30 min. The remaining cell debris and insoluble material was removed by ultracentrifugation at $100,000 \times g$ for 30 min. The cleared supernatant was filtered through a 0.45-μm filter.

## 8.3 Purification of Human His$_6$-mPGES-1

Recombinant His$_6$-mPGES-1 was purified in a two-step combination of hydroxyapatite followed by immobilized metal ion affinity chromatography. Solubilized whole cell lysate was mixed with hydroxyapatite (1 g/liter expression culture) that had been equilibrated with 10 mM sodium phosphate buffer, pH 8.0, 150 mM NaCl, 1 mM GSH, 10% glycerol, 10 mM imidazole, 0.2% reduced Triton X-100. After a 10-min incubation on ice, the hydroxyapatite was pelleted by a short centrifugation pulse, and the supernatant (unbound fraction) was removed and cleared by centrifugation $(1,500 \times g, 3 \text{ min})$ and filtration (0.45 μm). The cleared, unbound fraction from the hydroxyapatite was immediately loaded on a Ni-NTA Sepharose gravity flow column that had been charged with $NiCl_2$ and equilibrated with 10 mM sodium phosphate buffer, pH 8.0, 150 mM NaCl, 10 mM imidazole, 1 mM GSH, 10% glycerol, 0.2% reduced Triton X-100 (start buffer). After loading, the column was washed with start buffer until all unbound proteins were eluted. Thereafter, 60 mM imidazole was added to wash out unspecifically bound proteins. Finally, the histidine-tagged protein that had bound to the affinity column was eluted by a step addition of 350 mM imidazole and immediately desalted into 20 mM sodium phosphate buffer, pH

7.5, 50 mM NaCl, 10% glycerol, 1 mM GSH, and 0.2% reduced Triton X-100 on a PD-10 desalting column. Protein concentration was determined by BCA Protein Assay Reducing Agent Compatible (Pierce).

### 8.4 Gel Electrophoresis and Western Blotting

SDS-PAGE was performed in 18% polyacrylamide gels. Protein bands were detected by Gelcode Blue Coomassie stain. Western blots and immunodetection using rabbit mPGES-1 polyclonal antibody were performed with GenScript One-hour Western Detection System. High Resolution Clear Native Electrophoresis (hrCNE) was performed on 4-16% Bis-Tris Glycine gels using sodium deoxycholate (0.05%) and Triton X-100 (0.05%) in place of Comassie Brilliant Blue G-250 in cathode buffers.

### 8.5 Electron Crystallography

Purified $His_6$-mPGES1 in 1% Triton X-100 was subjected to two-dimensional crystallization trials by adding phospholipids prior to reduction of the detergent content. Aliquots of 100 μl of protein were incubated with lipids (bovine liver lecithin, BLL) at a molar lipid to protein ratio of 9.

After 1 h incubation, the detergent-protein-lipid mixture was transferred into a dialysis tube (MWCO 12-14 kDa) and dialyzed at room temperature against 500 ml 25 mM Tris-HCl, pH 7.4, 50 mM KCl, 0.1 mM EDTA, 20% glycerol, 1 mM GSH. After 8 days at least, the crystallisation suspension was analysed by electron microscopy (negative staining with 1% uranyl acetate). For electron microscopy, aliquots (2 μl) of the crystallization suspension were adsorbed onto glow discharged carbon-coated copper grids (400 mesh; Analytical Standards), washed twice with a drop of water and stained with a drop of 1% (w/v) uranyl acetate for 30 s before blotting and air-drying. Grids were placed into a Philips CM120 electron microscope operating at an accelerating voltage of 120 kV.

# References

1.      Nicolaou, K. C. Advancing the Drug Discovery and Development Process. *Angewandte Chemie International Edition* **2014,** 53, 9128-9140.

2.      Malik, N. N. Drug discovery: past, present and future. *Drug Discov Today* **2008,** 13, 909-12.

3.      Burley, S. K.; Park, F. Meeting the challenges of drug discovery: a multidisciplinary re-evaluation of current practices. *Genome Biology* **2005,** 6, 330-330.

4.      Whitty, A.; Gelb, M. H. Critical challenges and emerging paradigms in drug discovery. *Curr Opin Chem Biol* **2010,** 14, 437-9.

5.      Laufer, S.; Holzgrabe, U.; Steinhilber, D. Drug Discovery: A Modern Decathlon. *Angewandte Chemie International Edition* **2013,** 52, 4072-4076.

6.      Knowles, J.; Gromo, G. A guide to drug discovery: Target selection in drug discovery. *Nat Rev Drug Discov* **2003,** 2, 63-9.

7.      Plowright, A. T.; Johnstone, C.; Kihlberg, J.; Pettersson, J.; Robb, G.; Thompson, R. A. Hypothesis driven drug design: improving quality and effectiveness of the design-make-test-analyse cycle. *Drug Discov Today* **2012,** 17, 56-62.

8.      Hughes, J. P.; Rees, S.; Kalindjian, S. B.; Philpott, K. L. Principles of early drug discovery. *British Journal of Pharmacology* **2011,** 162, 1239-1249.

9.      Núñez, S.; Venhorst, J.; Kruse, C. G. Target–drug interactions: first principles and their application to drug discovery. *Drug Discovery Today* **2012,** 17, 10-22.

10.     Newman, D. J.; Cragg, G. M. Natural Products as Sources of New Drugs over the 30 Years from 1981 to 2010(). *Journal of natural products* **2012,** 75, 311-335.

11.     MacCoss, M.; Baillie, T. A. Organic chemistry in drug discovery. *Science* **2004,** 303, 1810-3.

12.     Schreiber, S. L. Organic synthesis toward small-molecule probes and drugs. *Proceedings of the National Academy of Sciences* **2011,** 108, 6699-6702.

13.     Leeson, P. Drug discovery: Chemical beauty contest. *Nature* **2012,** 481, 455-456.

14.     Lombardino, J. G.; Lowe, J. A., 3rd. The role of the medicinal chemist in drug discovery--then and now. *Nat Rev Drug Discov* **2004,** 3, 853-62.

15.     Potoski, J. Timely synthetic support for medicinal chemists. *Drug Discov Today* **2005,** 10, 115-20.

16.      Colombo, M.; Peretto, I. Chemistry strategies in early drug discovery: an overview of recent trends. *Drug Discov Today* **2008,** 13, 677-84.

17.      Davies, I. W.; Welch, C. J. Looking forward in pharmaceutical process chemistry. *Science* **2009,** 325, 701-4.

18.      Cheshire, D. R. How well do medicinal chemists learn from experience? *Drug Discov Today* **2011,** 16, 817-21.

19.      Tappe, F. M. J.; Trepohl, V. T.; Oestreich, M. Transition-Metal-Catalyzed C-P Cross-Coupling Reactions. *Synthesis* **2010,** 2010, 3037-3062.

20.      Hulme, C.; Akritopoulou-Zanze, I.; Dai, W.-M.; Beck, B.; Srivastava, S.; Wang, W.; Wang, K.; Czarna, A.; Holak, T.; Meireles, L.; Camacho, C.; Raghavan, B.; Day, B.; Dömling, A.; Qin, C.; Zhang, R.; Wang, Q.; Ren, J.; Tian, L.; Nikulnikov, M.; Krasavin, M.; Krasavin, M.; Parchinsky, V.; Shkavrov, S.; Bukhryakov, K.; Tsirulnikov, S.; Krasavin, M.; Bushkova, E.; Parchinsky, V.; Krasavin, M.; Kalinski, C.; Kysil, V.; Tsirulnikov, S.; Ivachtchenko, A.; Potapov, V.; Kysil, V.; Fetisova, N.; Nikitin, A.; Ivachtchenko, A.; Potapov, V.; Ilyn, A.; Fetisova, N.; Kravchenko, D.; Ivachtchenko, A.; Shilova, O.; Ilyin, A.; Ivachtchenko, A.; Shkirando, A.; Kysil, V.; Potapov, V.; Ivachtchenko, A.; Vaddula, B.; Kumar, D.; Sharad, S.; Dube, U.; Kapur, S. Multi-Component Reactions in Drug Discovery. In *MCR 2009*, Mironov, M. A., Ed. Springer New York: 2011; Vol. 699, pp 75-106.

21.      Kappe, C. O.; Dallinger, D. The impact of microwave synthesis on drug discovery. *Nat Rev Drug Discov* **2006,** 5, 51-63.

22.      Wirth, T. Flow Chemistry: Enabling Technology in Drug Discovery and Process Research. *ChemSusChem* **2012,** 5, 215-216.

23.      Skinner, A. L.; Laurence, J. S. High-field Solution NMR Spectroscopy as a Tool for Assessing Protein Interactions with Small Molecule Ligands. *Journal of pharmaceutical sciences* **2008,** 97, 4670-4695.

24.      Kassel, D. B. The Expanding Role of HPLC in Drug Discovery. In *HPLC for Pharmaceutical Scientists*, John Wiley & Sons, Inc.: 2006; pp 533-575.

25.      Li, H.; Zheng, M.; Luo, X.; Zhu, W.; Jiang, H.; Begley, T. P. Drug Discovery and Development: Computational Approaches. In *Wiley Encyclopedia of Chemical Biology*, John Wiley & Sons, Inc.: 2007.

26.      Lopez-Vallejo, F.; Caulfield, T.; Martinez-Mayorga, K.; Giulianotti, M. A.; Nefzi, A.; Houghten, R. A.; Medina-Franco, J. L. Integrating virtual screening and combinatorial chemistry for accelerated drug discovery. *Comb Chem High Throughput Screen* **2011,** 14, 475-87.

27.      Bleicher, K. H.; Bohm, H. J.; Muller, K.; Alanine, A. I. Hit and lead generation: beyond high-throughput screening. *Nat Rev Drug Discov* **2003,** 2, 369-78.

28.     Acharya, C.; Coop, A.; Polli, J. E.; Mackerell, A. D., Jr. Recent advances in ligand-based drug design: relevance and utility of the conformationally sampled pharmacophore approach. *Curr Comput Aided Drug Des* **2011,** 7, 10-22.

29.     Chen, L.; Morrow, J. K.; Tran, H. T.; Phatak, S. S.; Du-Cuny, L.; Zhang, S. From laptop to benchtop to bedside: structure-based drug design on protein targets. *Curr Pharm Des* **2012,** 18, 1217-39.

30.     Irwin, J. J.; Sterling, T.; Mysinger, M. M.; Bolstad, E. S.; Coleman, R. G. ZINC: a free tool to discover chemistry for biology. *J Chem Inf Model* **2012,** 52, 1757-68.

31.     Hann, M. M. Molecular obesity, potency and other addictions in drug discovery. *MedChemComm* **2011,** 2, 349-355.

32.     Wunberg, T.; Hendrix, M.; Hillisch, A.; Lobell, M.; Meier, H.; Schmeck, C.; Wild, H.; Hinzen, B. Improving the hit-to-lead process: data-driven assessment of drug-like and lead-like screening hits. *Drug Discov Today* **2006,** 11, 175-80.

33.     Jorgensen, W. L. Efficient Drug Lead Discovery and Optimization. *Accounts of chemical research* **2009,** 42, 724-733.

34.     Gleeson, M. P. Generation of a Set of Simple, Interpretable ADMET Rules of Thumb. *Journal of Medicinal Chemistry* **2008,** 51, 817-834.

35.     Lipinski, C. A.; Lombardo, F.; Dominy, B. W.; Feeney, P. J. Experimental and computational approaches to estimate solubility and permeability in drug discovery and development settings. *Adv Drug Deliv Rev* **2001,** 46, 3-26.

36.     Zhang, M. Q.; Wilkinson, B. Drug discovery beyond the 'rule-of-five'. *Curr Opin Biotechnol* **2007,** 18, 478-88.

37.     Kramer, J. A.; Sagartz, J. E.; Morris, D. L. The application of discovery toxicology and pathology towards the design of safer pharmaceutical lead candidates. *Nat Rev Drug Discov* **2007,** 6, 636-649.

38.     Orloff, J.; Douglas, F.; Pinheiro, J.; Levinson, S.; Branson, M.; Chaturvedi, P.; Ette, E.; Gallo, P.; Hirsch, G.; Mehta, C.; Patel, N.; Sabir, S.; Springs, S.; Stanski, D.; Evers, M. R.; Fleming, E.; Singh, N.; Tramontin, T.; Golub, H. The future of drug development: advancing clinical trial design. *Nat Rev Drug Discov* **2009,** 8, 949-57.

39.     Bamberger, M.; Moore, N.; Lechat, P. How to improve the clinical development paradigm and its division into phases I, II and III. *Therapie* **2011,** 66, 331-4, 327-30.

40.     Elinav, E.; Nowarski, R.; Thaiss, C. A.; Hu, B.; Jin, C.; Flavell, R. A. Inflammation-induced cancer: crosstalk between tumours, immune cells and microorganisms. *Nat Rev Cancer* **2013,** 13, 759-71.

41.     Virchow, R. An Address on the Value of Pathological Experiments. *British Medical Journal* **1881,** 2, 198-203.

42.     de Visser, K. E.; Coussens, L. M. The inflammatory tumor microenvironment and its impact on cancer development. *Contrib Microbiol* **2006,** 13, 118-37.

43.     Yaqub, S.; Aandahl, E. M. Inflammation versus adaptive immunity in cancer pathogenesis. *Crit Rev Oncog* **2009,** 15, 43-63.

44.     de Visser, K. E.; Coussens, L. M. The interplay between innate and adaptive immunity regulates cancer development. *Cancer Immunol Immunother* **2005,** 54, 1143-52.

45.     Sansone, P.; Bromberg, J. Environment, inflammation, and cancer. *Curr Opin Genet Dev* **2011,** 21, 80-5.

46.     Sica, A.; Allavena, P.; Mantovani, A. Cancer related inflammation: the macrophage connection. *Cancer Lett* **2008,** 267, 204-15.

47.     Whiteside, T. L. The tumor microenvironment and its role in promoting tumor growth. *Oncogene* **2008,** 27, 5904-12.

48.     Mantovani, A.; Allavena, P.; Sica, A.; Balkwill, F. Cancer-related inflammation. *Nature* **2008,** 454, 436-444.

49.     Porta, C.; Larghi, P.; Rimoldi, M.; Totaro, M. G.; Allavena, P.; Mantovani, A.; Sica, A. Cellular and molecular pathways linking inflammation and cancer. *Immunobiology* **2009,** 214, 761-77.

50.     Mantovani, A. Molecular pathways linking inflammation and cancer. *Curr Mol Med* **2010,** 10, 369-73.

51.     Borrello, M. G.; Alberti, L.; Fischer, A.; Degl'Innocenti, D.; Ferrario, C.; Gariboldi, M.; Marchesi, F.; Allavena, P.; Greco, A.; Collini, P.; Pilotti, S.; Cassinelli, G.; Bressan, P.; Fugazzola, L.; Mantovani, A.; Pierotti, M. A. Induction of a proinflammatory program in normal human thyrocytes by the RET/PTC1 oncogene. *Proceedings of the National Academy of Sciences of the United States of America* **2005,** 102, 14825-14830.

52.     Mantovani, A. Cancer: Inflaming metastasis. *Nature* **2009,** 457, 36-7.

53.     De Marzo, A. M.; Platz, E. A.; Sutcliffe, S.; Xu, J.; Gronberg, H.; Drake, C. G.; Nakai, Y.; Isaacs, W. B.; Nelson, W. G. Inflammation in prostate carcinogenesis. *Nat Rev Cancer* **2007,** 7, 256-69.

54.     Schiffman, M.; Castle, P. E.; Jeronimo, J.; Rodriguez, A. C.; Wacholder, S. Human papillomavirus and cervical cancer. *Lancet* **2007,** 370, 890-907.

55.     Karin, M.; Lawrence, T.; Nizet, V. Innate Immunity Gone Awry: Linking Microbial Infections to Chronic Inflammation and Cancer. *Cell* **2006,** 124, 823-835.

56.     Rius, J.; Guma, M.; Schachtrup, C.; Akassoglou, K.; Zinkernagel, A. S.; Nizet, V.; Johnson, R. S.; Haddad, G. G.; Karin, M. NF-kappaB links innate immunity to the hypoxic response through transcriptional regulation of HIF-1alpha. *Nature* **2008,** 453, 807-11.

57.     Yu, H.; Kortylewski, M.; Pardoll, D. Crosstalk between cancer and immune cells: role of STAT3 in the tumour microenvironment. *Nat Rev Immunol* **2007,** 7, 41-51.

58.     Hanahan, D.; Weinberg, R. A. The Hallmarks of Cancer. *Cell* **2000,** 100, 57-70.

59.     Hanahan, D.; Weinberg, R. A. Hallmarks of cancer: the next generation. *Cell* **2011,** 144, 646-74.

60.     Igney, F. H.; Krammer, P. H. Immune escape of tumors: apoptosis resistance and tumor counterattack. *J Leukoc Biol* **2002,** 71, 907-20.

61.     Croci, D. O.; Zacarias Fluck, M. F.; Rico, M. J.; Matar, P.; Rabinovich, G. A.; Scharovsky, O. G. Dynamic cross-talk between tumor and immune cells in orchestrating the immunosuppressive network at the tumor microenvironment. *Cancer Immunol Immunother* **2007,** 56, 1687-700.

62.     Seliger, B. Strategies of tumor immune evasion. *BioDrugs* **2005,** 19, 347-54.

63.     Dunn, G. P.; Old, L. J.; Schreiber, R. D. The immunobiology of cancer immunosurveillance and immunoediting. *Immunity* **2004,** 21, 137-48.

64.     Smyth, M. J.; Dunn, G. P.; Schreiber, R. D. Cancer immunosurveillance and immunoediting: the roles of immunity in suppressing tumor development and shaping tumor immunogenicity. *Adv Immunol* **2006,** 90, 1-50.

65.     Dunn, G. P.; Bruce, A. T.; Ikeda, H.; Old, L. J.; Schreiber, R. D. Cancer immunoediting: from immunosurveillance to tumor escape. *Nat Immunol* **2002,** 3, 991-8.

66.     Gajewski, T. F.; Schreiber, H.; Fu, Y.-X. Innate and adaptive immune cells in the tumor microenvironment. *Nat Immunol* **2013,** 14, 1014-1022.

67.     Stewart, T. J.; Greeneltch, K. M.; Lutsiak, M. E.; Abrams, S. I. Immunological responses can have both pro- and antitumour effects: implications for immunotherapy. *Expert Rev Mol Med* **2007,** 9, 1-20.

68.     Allavena, P.; Sica, A.; Garlanda, C.; Mantovani, A. The Yin-Yang of tumor-associated macrophages in neoplastic progression and immune surveillance. *Immunol Rev* **2008,** 222, 155-61.

69.     Mellman, I.; Coukos, G.; Dranoff, G. Cancer immunotherapy comes of age. *Nature* **2011,** 480, 480-9.

70.     Drake, C. G. Prostate cancer as a model for tumour immunotherapy. *Nat Rev Immunol* **2010,** 10, 580-93.

71.     Tartour, E.; Sandoval, F.; Bonnefoy, J. Y.; Fridman, W. H. [Cancer immunotherapy: recent breakthroughs and perspectives]. *Med Sci (Paris)* **2011,** 27, 833-41.

72.     Sun, B.; Karin, M. The therapeutic value of targeting inflammation in gastrointestinal cancers. *Trends Pharmacol Sci* **2014,** 35, 349-57.

73.     Aggarwal, B. B.; Vijayalekshmi, R. V.; Sung, B. Targeting inflammatory pathways for prevention and therapy of cancer: short-term friend, long-term foe. *Clin Cancer Res* **2009,** 15, 425-30.

74.     Bernstein, B. E.; Meissner, A.; Lander, E. S. The mammalian epigenome. *Cell* **2007,** 128, 669-81.

75.     Strahl, B. D.; Allis, C. D. The language of covalent histone modifications. *Nature* **2000,** 403, 41-5.

76.     Rothbart, S. B.; Strahl, B. D. Interpreting the language of histone and DNA modifications. *Biochim Biophys Acta* **2014,** 1839, 627-43.

77.     Fullgrabe, J.; Kavanagh, E.; Joseph, B. Histone onco-modifications. *Oncogene* **2011,** 30, 3391-403.

78.     Musselman, C. A.; Lalonde, M. E.; Cote, J.; Kutateladze, T. G. Perceiving the epigenetic landscape through histone readers. *Nat Struct Mol Biol* **2012,** 19, 1218-27.

79.     Patel, D. J.; Wang, Z. Readout of epigenetic modifications. *Annu Rev Biochem* **2013,** 82, 81-118.

80.     Yun, M.; Wu, J.; Workman, J. L.; Li, B. Readers of histone modifications. *Cell Res* **2011,** 21, 564-578.

81.     Ruan, C.; Li, B. Reading Histone Modifications. In *Fundamentals of Chromatin*, Workman, J. L.; Abmayr, S. M., Eds. Springer New York: 2014; pp 355-373.

82.     Kouzarides, T. Chromatin modifications and their function. *Cell* **2007,** 128, 693-705.

83.     Turner, B. M. Reading signals on the nucleosome with a new nomenclature for modified histones. *Nat Struct Mol Biol* **2005,** 12, 110-2.

84.     Tan, M.; Luo, H.; Lee, S.; Jin, F.; Yang, J. S.; Montellier, E.; Buchou, T.; Cheng, Z.; Rousseaux, S.; Rajagopal, N.; Lu, Z.; Ye, Z.; Zhu, Q.; Wysocka, J.; Ye, Y.; Khochbin, S.; Ren, B.; Zhao, Y. Identification of 67 histone marks and histone lysine crotonylation as a new type of histone modification. *Cell* **2011,** 146, 1016-28.

85.    Jenuwein, T.; Allis, C. D. Translating the histone code. *Science* **2001,** 293, 1074-80.

86.    Zentner, G. E.; Henikoff, S. Regulation of nucleosome dynamics by histone modifications. *Nat Struct Mol Biol* **2013,** 20, 259-66.

87.    Tessarz, P.; Kouzarides, T. Histone core modifications regulating nucleosome structure and dynamics. *Nat Rev Mol Cell Biol* **2014,** 15, 703-8.

88.    Bannister, A. J.; Kouzarides, T. Regulation of chromatin by histone modifications. *Cell Res* **2011,** 21, 381-395.

89.    Swygert, S. G.; Peterson, C. L. Chromatin dynamics: interplay between remodeling enzymes and histone modifications. *Biochim Biophys Acta* **2014,** 1839, 728-36.

90.    Marushige, K. Activation of chromatin by acetylation of histone side chains. *Proceedings of the National Academy of Sciences of the United States of America* **1976,** 73, 3937-3941.

91.    Alabert, C.; Groth, A. Chromatin replication and epigenome maintenance. *Nat Rev Mol Cell Biol* **2012,** 13, 153-167.

92.    Tropberger, P.; Pott, S.; Keller, C.; Kamieniarz-Gdula, K.; Caron, M.; Richter, F.; Li, G.; Mittler, G.; Liu, Edison T.; Bühler, M.; Margueron, R.; Schneider, R. Regulation of Transcription through Acetylation of H3K122 on the Lateral Surface of the Histone Octamer. *Cell* **2013,** 152, 859-872.

93.    Steunou, A.-L.; Rossetto, D.; Côté, J. Regulating Chromatin by Histone Acetylation. In *Fundamentals of Chromatin*, Workman, J. L.; Abmayr, S. M., Eds. Springer New York: 2014; pp 147-212.

94.    Venkatesh, S.; Workman, J. L. Histone exchange, chromatin structure and the regulation of transcription. *Nat Rev Mol Cell Biol* **2015,** advance online publication.

95.    Zhao, S.; Xu, W.; Jiang, W.; Yu, W.; Lin, Y.; Zhang, T.; Yao, J.; Zhou, L.; Zeng, Y.; Li, H.; Li, Y.; Shi, J.; An, W.; Hancock, S. M.; He, F.; Qin, L.; Chin, J.; Yang, P.; Chen, X.; Lei, Q.; Xiong, Y.; Guan, K. L. Regulation of cellular metabolism by protein lysine acetylation. *Science* **2010,** 327, 1000-4.

96.    Choudhary, C.; Kumar, C.; Gnad, F.; Nielsen, M. L.; Rehman, M.; Walther, T. C.; Olsen, J. V.; Mann, M. Lysine acetylation targets protein complexes and co-regulates major cellular functions. *Science* **2009,** 325, 834-40.

97.    Henriksen, P.; Wagner, S. A.; Weinert, B. T.; Sharma, S.; Bacinskaja, G.; Rehman, M.; Juffer, A. H.; Walther, T. C.; Lisby, M.; Choudhary, C. Proteome-wide analysis of lysine acetylation suggests its broad regulatory scope in Saccharomyces cerevisiae. *Mol Cell Proteomics* **2012,** 11, 1510-22.

98.	Choudhary, C.; Weinert, B. T.; Nishida, Y.; Verdin, E.; Mann, M. The growing landscape of lysine acetylation links metabolism and cell signalling. *Nat Rev Mol Cell Biol* **2014,** 15, 536-550.

99.	Philp, A.; Rowland, T.; Perez-Schindler, J.; Schenk, S. Understanding the acetylome: translating targeted proteomics into meaningful physiology. *Am J Physiol Cell Physiol* **2014,** 307, C763-73.

100.	Archer, S. Y.; Hodin, R. A. Histone acetylation and cancer. *Curr Opin Genet Dev* **1999,** 9, 171-4.

101.	Marks, P.; Rifkind, R. A.; Richon, V. M.; Breslow, R.; Miller, T.; Kelly, W. K. Histone deacetylases and cancer: causes and therapies. *Nat Rev Cancer* **2001,** 1, 194-202.

102.	Dawson, M. A.; Kouzarides, T. Cancer epigenetics: from mechanism to therapy. *Cell* **2012,** 150, 12-27.

103.	Di Cerbo, V.; Schneider, R. Cancers with wrong HATs: the impact of acetylation. *Briefings in Functional Genomics* **2013,** 12, 231-243.

104.	Sadoul, K.; Boyault, C.; Pabion, M.; Khochbin, S. Regulation of protein turnover by acetyltransferases and deacetylases. *Biochimie* **2008,** 90, 306-12.

105.	Yang, X. J.; Seto, E. HATs and HDACs: from structure, function and regulation to novel strategies for therapy and prevention. *Oncogene* **2007,** 26, 5310-8.

106.	Filippakopoulos, P.; Knapp, S. The bromodomain interaction module. *FEBS Letters* **2012,** 586, 2692-2704.

107.	Li, Y.; Wen, H.; Xi, Y.; Tanaka, K.; Wang, H.; Peng, D.; Ren, Y.; Jin, Q.; Dent, S. Y.; Li, W.; Li, H.; Shi, X. AF9 YEATS domain links histone acetylation to DOT1L-mediated H3K79 methylation. *Cell* **2014,** 159, 558-71.

108.	Filippakopoulos, P.; Picaud, S.; Mangos, M.; Keates, T.; Lambert, J.-P.; Barsyte-Lovejoy, D.; Felletar, I.; Volkmer, R.; Müller, S.; Pawson, T.; Gingras, A.-C.; Arrowsmith, Cheryl H.; Knapp, S. Histone Recognition and Large-Scale Structural Analysis of the Human Bromodomain Family. *Cell* **2012,** 149, 214-231.

109.	Hudson, B. P.; Martinez-Yamout, M. A.; Dyson, H. J.; Wright, P. E. Solution structure and acetyl-lysine binding activity of the GCN5 bromodomain. *J Mol Biol* **2000,** 304, 355-70.

110.	Yang, X.-J.; Ogryzko, V. V.; Nishikawa, J.-i.; Howard, B. H.; Nakatani, Y. A p300/CBP-associated factor that competes with the adenoviral oncoprotein E1A. *Nature* **1996,** 382, 319-324.

111.	Nagy, Z.; Tora, L. Distinct GCN5/PCAF-containing complexes function as co-activators and are involved in transcription factor and global histone acetylation. *Oncogene* **2007,** 26, 5341-57.

112.   Dhalluin, C.; Carlson, J. E.; Zeng, L.; He, C.; Aggarwal, A. K.; Zhou, M. M. Structure and ligand of a histone acetyltransferase bromodomain. *Nature* **1999,** 399, 491-6.

113.   Trotter, K. W.; Archer, T. K. The BRG1 transcriptional coregulator. *Nuclear Receptor Signaling* **2008,** 6, e004.

114.   Cavellán, E.; Asp, P.; Percipalle, P.; Farrants, A.-K. Ö. The WSTF-SNF2h Chromatin Remodeling Complex Interacts with Several Nuclear Proteins in Transcription. *Journal of Biological Chemistry* **2006,** 281, 16264-16271.

115.   Gregory, G. D.; Vakoc, C. R.; Rozovskaia, T.; Zheng, X.; Patel, S.; Nakamura, T.; Canaani, E.; Blobel, G. A. Mammalian ASH1L Is a Histone Methyltransferase That Occupies the Transcribed Region of Active Genes. *Molecular and Cellular Biology* **2007,** 27, 8466-8479.

116.   Malik, S.; Bhaumik, S. R. Mixed lineage leukemia: histone H3 lysine 4 methyltransferases from yeast to human. *FEBS Journal* **2010,** 277, 1805-1821.

117.   Venturini, L.; You, J.; Stadler, M.; Galien, R.; Lallemand, V.; Koken, M. H.; Mattei, M. G.; Ganser, A.; Chambon, P.; Losson, R.; de The, H. TIF1gamma, a novel member of the transcriptional intermediary factor 1 family. *Oncogene* **1999,** 18, 1209-17.

118.   Jacobson, R. H.; Ladurner, A. G.; King, D. S.; Tjian, R. Structure and Function of a Human TAFII250 Double Bromodomain Module. *Science* **2000,** 288, 1422-1425.

119.   Xue, Y.; Canman, J. C.; Lee, C. S.; Nie, Z.; Yang, D.; Moreno, G. T.; Young, M. K.; Salmon, E. D.; Wang, W. The human SWI/SNF-B chromatin-remodeling complex is related to yeast Rsc and localizes at kinetochores of mitotic chromosomes. *Proceedings of the National Academy of Sciences* **2000,** 97, 13015-13020.

120.   Wu, S. Y.; Chiang, C. M. The double bromodomain-containing chromatin adaptor Brd4 and transcriptional regulation. *J Biol Chem* **2007,** 282, 13141-5.

121.   Brès, V.; Yoh, S. M.; Jones, K. A. The multi-tasking P-TEFb complex. *Current Opinion in Cell Biology* **2008,** 20, 334-340.

122.   Tamkun, J. W.; Deuring, R.; Scott, M. P.; Kissinger, M.; Pattatucci, A. M.; Kaufman, T. C.; Kennison, J. A. brahma: A regulator of Drosophila homeotic genes structurally related to the yeast transcriptional activator SNF2SWI2. *Cell* **1992,** 68, 561-572.

123.   Jeanmougin, F.; Wurtz, J. M.; Le Douarin, B.; Chambon, P.; Losson, R. The bromodomain revisited. *Trends Biochem Sci* **1997,** 22, 151-3.

124.   Owen, D. J.; Ornaghi, P.; Yang, J.-C.; Lowe, N.; Evans, P. R.; Ballario, P.; Neuhaus, D.; Filetici, P.; Travers, A. A. The structural basis for the recognition of

acetylated histone H4 by the bromodomain of histone acetyltransferase Gcn5p. *The EMBO Journal* **2000,** 19, 6141-6149.

125.    Huang, D.; Rossini, E.; Steiner, S.; Caflisch, A. Structured water molecules in the binding site of bromodomains can be displaced by cosolvent. *ChemMedChem* **2014,** 9, 573-9.

126.    Lubula, M. Y.; Eckenroth, B. E.; Carlson, S.; Poplawski, A.; Chruszcz, M.; Glass, K. C. Structural insights into recognition of acetylated histone ligands by the BRPF1 bromodomain. *FEBS Letters* **2014,** 588, 3844-3854.

127.    Tallant, C.; Valentini, E.; Fedorov, O.; Overvoorde, L.; Ferguson, F. M.; Filippakopoulos, P.; Svergun, D. I.; Knapp, S.; Ciulli, A. Molecular Basis of Histone Tail Recognition by Human TIP5 PHD Finger and Bromodomain of the Chromatin Remodeling Complex NoRC. *Structure* **2015,** 23, 80-92.

128.    Belkina, A. C.; Denis, G. V. BET domain co-regulators in obesity, inflammation and cancer. *Nat Rev Cancer* **2012,** 12, 465-77.

129.    Lamonica, J. M.; Deng, W.; Kadauke, S.; Campbell, A. E.; Gamsjaeger, R.; Wang, H.; Cheng, Y.; Billin, A. N.; Hardison, R. C.; Mackay, J. P.; Blobel, G. A. Bromodomain protein Brd3 associates with acetylated GATA1 to promote its chromatin occupancy at erythroid target genes. *Proc Natl Acad Sci U S A* **2011,** 108, E159-68.

130.    Shi, J.; Wang, Y.; Zeng, L.; Wu, Y.; Deng, J.; Zhang, Q.; Lin, Y.; Li, J.; Kang, T.; Tao, M.; Rusinova, E.; Zhang, G.; Wang, C.; Zhu, H.; Yao, J.; Zeng, Y. X.; Evers, B. M.; Zhou, M. M.; Zhou, B. P. Disrupting the interaction of BRD4 with diacetylated Twist suppresses tumorigenesis in basal-like breast cancer. *Cancer Cell* **2014,** 25, 210-25.

131.    Huang, B.; Yang, X. D.; Zhou, M. M.; Ozato, K.; Chen, L. F. Brd4 coactivates transcriptional activation of NF-kappaB via specific binding to acetylated RelA. *Mol Cell Biol* **2009,** 29, 1375-87.

132.    Schroder, S.; Cho, S.; Zeng, L.; Zhang, Q.; Kaehlcke, K.; Mak, L.; Lau, J.; Bisgrove, D.; Schnolzer, M.; Verdin, E.; Zhou, M. M.; Ott, M. Two-pronged binding with bromodomain-containing protein 4 liberates positive transcription elongation factor b from inactive ribonucleoprotein complexes. *J Biol Chem* **2012,** 287, 1090-9.

133.    Rahman, S.; Sowa, M. E.; Ottinger, M.; Smith, J. A.; Shi, Y.; Harper, J. W.; Howley, P. M. The Brd4 extraterminal domain confers transcription activation independent of pTEFb by recruiting multiple proteins, including NSD3. *Mol Cell Biol* **2011,** 31, 2641-52.

134.    Filippakopoulos, P.; Qi, J.; Picaud, S.; Shen, Y.; Smith, W. B.; Fedorov, O.; Morse, E. M.; Keates, T.; Hickman, T. T.; Felletar, I.; Philpott, M.; Munro, S.; McKeown, M. R.; Wang, Y.; Christie, A. L.; West, N.; Cameron, M. J.; Schwartz, B.; Heightman, T. D.; La Thangue, N.; French, C. A.; Wiest, O.; Kung, A. L.; Knapp, S.;

Bradner, J. E. Selective inhibition of BET bromodomains. *Nature* **2010,** 468, 1067-1073.

135.    Nicodeme, E.; Jeffrey, K. L.; Schaefer, U.; Beinke, S.; Dewell, S.; Chung, C. W.; Chandwani, R.; Marazzi, I.; Wilson, P.; Coste, H.; White, J.; Kirilovsky, J.; Rice, C. M.; Lora, J. M.; Prinjha, R. K.; Lee, K.; Tarakhovsky, A. Suppression of inflammation by a synthetic histone mimic. *Nature* **2010,** 468, 1119-23.

136.    Moffat, J. G.; Rudolph, J.; Bailey, D. Phenotypic screening in cancer drug discovery - past, present and future. *Nat Rev Drug Discov* **2014,** 13, 588-602.

137.    Papavassiliou, K. A.; Papavassiliou, A. G. Bromodomains: pockets with therapeutic potential. *Trends Mol Med* **2014,** 20, 477-8.

138.    Filippakopoulos, P.; Knapp, S. Targeting bromodomains: epigenetic readers of lysine acetylation. *Nat Rev Drug Discov* **2014,** 13, 337-56.

139.    Brand, M.; Measures, A. M.; Wilson, B. G.; Cortopassi, W. A.; Alexander, R.; Hoss, M.; Hewings, D. S.; Rooney, T. P.; Paton, R. S.; Conway, S. J. Small Molecule Inhibitors of Bromodomain-Acetyl-lysine Interactions. *ACS Chem Biol* **2015,** 10, 22-39.

140.    Ciceri, P.; Müller, S.; O'Mahony, A.; Fedorov, O.; Filippakopoulos, P.; Hunt, J. P.; Lasater, E. A.; Pallares, G.; Picaud, S.; Wells, C.; Martin, S.; Wodicka, L. M.; Shah, N. P.; Treiber, D. K.; Knapp, S. Dual kinase-bromodomain inhibitors for rationally designed polypharmacology. *Nature chemical biology* **2014,** 10, 305-312.

141.    Ember, S. W.; Zhu, J. Y.; Olesen, S. H.; Martin, M. P.; Becker, A.; Berndt, N.; Georg, G. I.; Schonbrunn, E. Acetyl-lysine binding site of bromodomain-containing protein 4 (BRD4) interacts with diverse kinase inhibitors. *ACS Chem Biol* **2014,** 9, 1160-71.

142.    Hay, D. A.; Fedorov, O.; Martin, S.; Singleton, D. C.; Tallant, C.; Wells, C.; Picaud, S.; Philpott, M.; Monteiro, O. P.; Rogers, C. M.; Conway, S. J.; Rooney, T. P.; Tumber, A.; Yapp, C.; Filippakopoulos, P.; Bunnage, M. E.; Muller, S.; Knapp, S.; Schofield, C. J.; Brennan, P. E. Discovery and optimization of small-molecule ligands for the CBP/p300 bromodomains. *J Am Chem Soc* **2014,** 136, 9308-19.

143.    Rooney, T. P.; Filippakopoulos, P.; Fedorov, O.; Picaud, S.; Cortopassi, W. A.; Hay, D. A.; Martin, S.; Tumber, A.; Rogers, C. M.; Philpott, M.; Wang, M.; Thompson, A. L.; Heightman, T. D.; Pryde, D. C.; Cook, A.; Paton, R. S.; Muller, S.; Knapp, S.; Brennan, P. E.; Conway, S. J. A series of potent CREBBP bromodomain ligands reveals an induced-fit pocket stabilized by a cation-pi interaction. *Angew Chem Int Ed Engl* **2014,** 53, 6126-30.

144.    Demont, E. H.; Bamborough, P.; Chung, C. W.; Craggs, P. D.; Fallon, D.; Gordon, L. J.; Grandi, P.; Hobbs, C. I.; Hussain, J.; Jones, E. J.; Le Gall, A.; Michon, A. M.; Mitchell, D. J.; Prinjha, R. K.; Roberts, A. D.; Sheppard, R. J.; Watson, R. J. 1,3-Dimethyl Benzimidazolones Are Potent, Selective Inhibitors of the BRPF1 Bromodomain. *ACS Med Chem Lett* **2014,** 5, 1190-5.

145.    Chaikuad, A.; Petros, A. M.; Fedorov, O.; Xu, J.; Knapp, S. Structure-based approaches towards identification of fragments for the low-druggability ATAD2 bromodomain. *MedChemComm* **2014,** 5, 1843-1848.

146.    Harner, M. J.; Chauder, B. A.; Phan, J.; Fesik, S. W. Fragment-based screening of the bromodomain of ATAD2. *J Med Chem* **2014,** 57, 9687-92.

147.    Ferguson, F. M.; Fedorov, O.; Chaikuad, A.; Philpott, M.; Muniz, J. R.; Felletar, I.; von Delft, F.; Heightman, T.; Knapp, S.; Abell, C.; Ciulli, A. Targeting low-druggability bromodomains: fragment based screening and inhibitor design against the BAZ2B bromodomain. *J Med Chem* **2013,** 56, 10183-7.

148.    Vidler, L. R.; Brown, N.; Knapp, S.; Hoelder, S. Druggability analysis and structural classification of bromodomain acetyl-lysine binding sites. *J Med Chem* **2012,** 55, 7346-59.

149.    Chung, C. W.; Dean, A. W.; Woolven, J. M.; Bamborough, P. Fragment-based discovery of bromodomain inhibitors part 1: inhibitor binding modes and implications for lead discovery. *J Med Chem* **2012,** 55, 576-86.

150.    Jennings, L. E.; Measures, A. R.; Wilson, B. G.; Conway, S. J. Phenotypic screening and fragment-based approaches to the discovery of small-molecule bromodomain ligands. *Future Med Chem* **2014,** 6, 179-204.

151.    Bamborough, P.; Diallo, H.; Goodacre, J. D.; Gordon, L.; Lewis, A.; Seal, J. T.; Wilson, D. M.; Woodrow, M. D.; Chung, C. W. Fragment-based discovery of bromodomain inhibitors part 2: optimization of phenylisoxazole sulfonamides. *J Med Chem* **2012,** 55, 587-96.

152.    Zhao, L.; Cao, D.; Chen, T.; Wang, Y.; Miao, Z.; Xu, Y.; Chen, W.; Wang, X.; Li, Y.; Du, Z.; Xiong, B.; Li, J.; Xu, C.; Zhang, N.; He, J.; Shen, J. Fragment-based drug discovery of 2-thiazolidinones as inhibitors of the histone reader BRD4 bromodomain. *J Med Chem* **2013,** 56, 3833-51.

153.    Zhao, L.; Wang, Y.; Cao, D.; Chen, T.; Wang, Q.; Li, Y.; Xu, Y.; Zhang, N.; Wang, X.; Chen, D.; Chen, L.; Chen, Y. L.; Xia, G.; Shi, Z.; Liu, Y. C.; Lin, Y.; Miao, Z.; Shen, J.; Xiong, B. Fragment-Based Drug Discovery of 2-Thiazolidinones as BRD4 Inhibitors: 2. Structure-Based Optimization. *J Med Chem* **2015**.

154.    Picaud, S.; Da Costa, D.; Thanasopoulou, A.; Filippakopoulos, P.; Fish, P. V.; Philpott, M.; Fedorov, O.; Brennan, P.; Bunnage, M. E.; Owen, D. R.; Bradner, J. E.; Taniere, P.; O'Sullivan, B.; Muller, S.; Schwaller, J.; Stankovic, T.; Knapp, S. PFI-1, a highly selective protein interaction inhibitor, targeting BET Bromodomains. *Cancer Res* **2013,** 73, 3336-46.

155.    Gehling, V. S.; Hewitt, M. C.; Vaswani, R. G.; Leblanc, Y.; Cote, A.; Nasveschuk, C. G.; Taylor, A. M.; Harmange, J. C.; Audia, J. E.; Pardo, E.; Joshi, S.; Sandy, P.; Mertz, J. A.; Sims, R. J., 3rd; Bergeron, L.; Bryant, B. M.; Bellon, S.; Poy, F.; Jayaram, H.; Sankaranarayanan, R.; Yellapantula, S.; Bangalore Srinivasamurthy,

N.; Birudukota, S.; Albrecht, B. K. Discovery, Design, and Optimization of Isoxazole Azepine BET Inhibitors. *ACS Med Chem Lett* **2013,** 4, 835-40.

156.    Picaud, S.; Wells, C.; Felletar, I.; Brotherton, D.; Martin, S.; Savitsky, P.; Diez-Dacal, B.; Philpott, M.; Bountra, C.; Lingard, H.; Fedorov, O.; Müller, S.; Brennan, P. E.; Knapp, S.; Filippakopoulos, P. RVX-208, an inhibitor of BET transcriptional regulators with selectivity for the second bromodomain. *Proceedings of the National Academy of Sciences of the United States of America* **2013,** 110, 19754-19759.

157.    Dawson, M. A.; Prinjha, R. K.; Dittmann, A.; Giotopoulos, G.; Bantscheff, M.; Chan, W. I.; Robson, S. C.; Chung, C. W.; Hopf, C.; Savitski, M. M.; Huthmacher, C.; Gudgin, E.; Lugo, D.; Beinke, S.; Chapman, T. D.; Roberts, E. J.; Soden, P. E.; Auger, K. R.; Mirguet, O.; Doehner, K.; Delwel, R.; Burnett, A. K.; Jeffrey, P.; Drewes, G.; Lee, K.; Huntly, B. J.; Kouzarides, T. Inhibition of BET recruitment to chromatin as an effective treatment for MLL-fusion leukaemia. *Nature* **2011,** 478, 529-33.

158.    Lucas, X.; Wohlwend, D.; Hugle, M.; Schmidtkunz, K.; Gerhardt, S.; Schule, R.; Jung, M.; Einsle, O.; Gunther, S. 4-Acyl pyrroles: mimicking acetylated lysines in histone code reading. *Angew Chem Int Ed Engl* **2013,** 52, 14055-9.

159.    Gosmini, R.; Nguyen, V. L.; Toum, J.; Simon, C.; Brusq, J. M.; Krysa, G.; Mirguet, O.; Riou-Eymard, A. M.; Boursier, E. V.; Trottet, L.; Bamborough, P.; Clark, H.; Chung, C. W.; Cutler, L.; Demont, E. H.; Kaur, R.; Lewis, A. J.; Schilling, M. B.; Soden, P. E.; Taylor, S.; Walker, A. L.; Walker, M. D.; Prinjha, R. K.; Nicodeme, E. The discovery of I-BET726 (GSK1324726A), a potent tetrahydroquinoline ApoA1 up-regulator and selective BET bromodomain inhibitor. *J Med Chem* **2014,** 57, 8111-31.

160.    SGC. PFI-3: Selective chemical probe for SMARCA bromodomains. http://www.thesgc.org/chemical-probes/PFI-3 (13 February 2015).

161.    SGC. GSK2801: A Selective Chemical Probe for BAZ2B/A bromodomains. http://www.thesgc.org/chemical-probes/GSK2801 (13 February 2015).

162.    Stelow, E. B. A Review of NUT Midline Carcinoma. *Head and Neck Pathology* **2011,** 5, 31-35.

163.    Gallagher, S. J.; Mijatov, B.; Gunatilake, D.; Gowrishankar, K.; Tiffen, J.; James, W.; Jin, L.; Pupo, G.; Cullinane, C.; McArthur, G. A.; Tummino, P. J.; Rizos, H.; Hersey, P. Control of NF-kB activity in human melanoma by bromodomain and extra-terminal protein inhibitor I-BET151. *Pigment Cell Melanoma Res* **2014,** 27, 1126-37.

164.    Wienerroither, S.; Rauch, I.; Rosebrock, F.; Jamieson, A. M.; Bradner, J.; Muhar, M.; Zuber, J.; Muller, M.; Decker, T. Regulation of NO synthesis, local inflammation, and innate immunity to pathogens by BET family proteins. *Mol Cell Biol* **2014,** 34, 415-27.

165.    Ceribelli, M.; Kelly, P. N.; Shaffer, A. L.; Wright, G. W.; Xiao, W.; Yang, Y.; Mathews Griner, L. A.; Guha, R.; Shinn, P.; Keller, J. M.; Liu, D.; Patel, P. R.; Ferrer, M.; Joshi, S.; Nerle, S.; Sandy, P.; Normant, E.; Thomas, C. J.; Staudt, L. M. Blockade of oncogenic IkappaB kinase activity in diffuse large B-cell lymphoma by bromodomain and extraterminal domain protein inhibitors. *Proc Natl Acad Sci U S A* **2014,** 111, 11365-70.

166.    Shi, J.; Vakoc, C. R. The mechanisms behind the therapeutic activity of BET bromodomain inhibition. *Mol Cell* **2014,** 54, 728-36.

167.    Belkina, A. C.; Nikolajczyk, B. S.; Denis, G. V. BET protein function is required for inflammation: Brd2 genetic disruption and BET inhibitor JQ1 impair mouse macrophage inflammatory responses. *J Immunol* **2013,** 190, 3670-8.

168.    Xu, Y.; Vakoc, C. R. Brd4 is on the move during inflammation. *Trends Cell Biol* **2014,** 24, 615-6.

169.    Khan, Y. M.; Kirkham, P.; Barnes, P. J.; Adcock, I. M. Brd4 is essential for IL-1beta-induced inflammation in human airway epithelial cells. *PLoS One* **2014,** 9, e95051.

170.    Mele, D. A.; Salmeron, A.; Ghosh, S.; Huang, H.-R.; Bryant, B. M.; Lora, J. M. BET bromodomain inhibition suppresses T(H)17-mediated pathology. *The Journal of Experimental Medicine* **2013,** 210, 2181-2190.

171.    Zou, Z.; Huang, B.; Wu, X.; Zhang, H.; Qi, J.; Bradner, J.; Nair, S.; Chen, L. F. Brd4 maintains constitutively active NF-kappaB in cancer cells by binding to acetylated RelA. *Oncogene* **2014,** 33, 2395-404.

172.    Perkins, N. D. Post-translational modifications regulating the activity and function of the nuclear factor kappa B pathway. *Oncogene* **2006,** 25, 6717-30.

173.    Huang, B.; Yang, X.-D.; Lamb, A.; Chen, L.-F. Posttranslational modifications of NF-κB: another layer of regulation for NF-κB signaling pathway. *Cellular signalling* **2010,** 22, 1282-1290.

174.    Barrett, E.; Brothers, S.; Wahlestedt, C.; Beurel, E. I-BET151 selectively regulates IL-6 production. *Biochim Biophys Acta* **2014,** 1842, 1549-55.

175.    Anand, P.; Brown, J. D.; Lin, C. Y.; Qi, J.; Zhang, R.; Artero, P. C.; Alaiti, M. A.; Bullard, J.; Alazem, K.; Margulies, K. B.; Cappola, T. P.; Lemieux, M.; Plutzky, J.; Bradner, J. E.; Haldar, S. M. BET bromodomains mediate transcriptional pause release in heart failure. *Cell* **2013,** 154, 569-82.

176.    Flemming, A. Cardiology: Bromodomain inhibition halts heart failure. *Nat Rev Drug Discov* **2013,** 12, 740.

177.    Denis, G. V.; Nikolajczyk, B. S.; Schnitzler, G. R. An emerging role for bromodomain-containing proteins in chromatin regulation and transcriptional control of adipogenesis. *FEBS letters* **2010,** 584, 3260-3268.

178.    Weidner-Glunde, M.; Ottinger, M.; Schulz, T. F. WHAT do viruses BET on? *Front Biosci (Landmark Ed)* **2010,** 15, 537-49.

179.    Li, Z.; Guo, J.; Wu, Y.; Zhou, Q. The BET bromodomain inhibitor JQ1 activates HIV latency through antagonizing Brd4 inhibition of Tat-transactivation. *Nucleic Acids Res* **2013,** 41, 277-87.

180.    Boehm, D.; Calvanese, V.; Dar, R. D.; Xing, S.; Schroeder, S.; Martins, L.; Aull, K.; Li, P. C.; Planelles, V.; Bradner, J. E.; Zhou, M. M.; Siliciano, R. F.; Weinberger, L.; Verdin, E.; Ott, M. BET bromodomain-targeting compounds reactivate HIV from latency via a Tat-independent mechanism. *Cell Cycle* **2013,** 12, 452-62.

181.    Jang, M. K.; Shen, K.; McBride, A. A. Papillomavirus genomes associate with BRD4 to replicate at fragile sites in the host genome. *PLoS Pathog* **2014,** 10, e1004117.

182.    Hellert, J.; Weidner-Glunde, M.; Krausze, J.; Richter, U.; Adler, H.; Fedorov, R.; Pietrek, M.; Ruckert, J.; Ritter, C.; Schulz, T. F.; Luhrs, T. A structural basis for BRD2/4-mediated host chromatin interaction and oligomer assembly of Kaposi sarcoma-associated herpesvirus and murine gammaherpesvirus LANA proteins. *PLoS Pathog* **2013,** 9, e1003640.

183.    Wu, X.; Qi, J.; Bradner, J. E.; Xiao, G.; Chen, L. F. Bromodomain and extraterminal (BET) protein inhibition suppresses human T cell leukemia virus 1 (HTLV-1) Tax protein-mediated tumorigenesis by inhibiting nuclear factor kappaB (NF-kappaB) signaling. *J Biol Chem* **2013,** 288, 36094-105.

184.    Wang, X.; Li, J.; Schowalter, R. M.; Jiao, J.; Buck, C. B.; You, J. Bromodomain protein Brd4 plays a key role in Merkel cell polyomavirus DNA replication. *PLoS Pathog* **2012,** 8, e1003021.

185.    Kudo, I.; Murakami, M. Prostaglandin E synthase, a terminal enzyme for prostaglandin E2 biosynthesis. *J Biochem Mol Biol* **2005,** 38, 633-8.

186.    Needleman, P.; Turk, J.; Jakschik, B. A.; Morrison, A. R.; Lefkowith, J. B. Arachidonic acid metabolism. *Annu Rev Biochem* **1986,** 55, 69-102.

187.    Funk, C. D. Prostaglandins and leukotrienes: advances in eicosanoid biology. *Science* **2001,** 294, 1871-5.

188.    Smith, W. L. The eicosanoids and their biochemical mechanisms of action. *Biochemical Journal* **1989,** 259, 315-324.

189.    Samuelsson, B. An Elucidation of the Arachidonic Acid Cascade. *Drugs* **1987,** 33, 2-9.

190.    Calder, P. C. Polyunsaturated fatty acids and inflammation. *Prostaglandins Leukot Essent Fatty Acids* **2006,** 75, 197-202.

191. Calder, P. C.; Grimble, R. F. Polyunsaturated fatty acids, inflammation and immunity. *Eur J Clin Nutr* **2002,** 56 Suppl 3, S14-9.

192. Bos, C. L.; Richel, D. J.; Ritsema, T.; Peppelenbosch, M. P.; Versteeg, H. H. Prostanoids and prostanoid receptors in signal transduction. *Int J Biochem Cell Biol* **2004,** 36, 1187-205.

193. Murakami, M. Lipid mediators in life science. *Exp Anim* **2011,** 60, 7-20.

194. Suzuki, Y. J.; Forman, H. J.; Sevanian, A. Oxidants as stimulators of signal transduction. *Free Radic Biol Med* **1997,** 22, 269-85.

195. Rodriguez, M.; Domingo, E.; Municio, C.; Alvarez, Y.; Hugo, E.; Fernandez, N.; Sanchez Crespo, M. Polarization of the innate immune response by prostaglandin E2: a puzzle of receptors and signals. *Mol Pharmacol* **2014,** 85, 187-97.

196. Garavito, R. M.; DeWitt, D. L. The cyclooxygenase isoforms: structural insights into the conversion of arachidonic acid to prostaglandins. *Biochim Biophys Acta* **1999,** 1441, 278-87.

197. Nugteren, D. H.; Christ-Hazelhof, E. Chemical and enzymic conversions of the prostaglandin endoperoxide PGH2. *Adv Prostaglandin Thromboxane Res* **1980,** 6, 129-37.

198. Smith, W. L.; Urade, Y.; Jakobsson, P.-J. Enzymes of the Cyclooxygenase Pathways of Prostanoid Biosynthesis. *Chemical Reviews* **2011,** 111, 5821-5865.

199. Smith, W. L.; Marnett, L. J.; DeWitt, D. L. Prostaglandin and thromboxane biosynthesis. *Pharmacol Ther* **1991,** 49, 153-79.

200. Park, J. Y.; Pillinger, M. H.; Abramson, S. B. Prostaglandin E2 synthesis and secretion: the role of PGE2 synthases. *Clin Immunol* **2006,** 119, 229-40.

201. Samuelsson, B.; Morgenstern, R.; Jakobsson, P. J. Membrane prostaglandin E synthase-1: a novel therapeutic target. *Pharmacol Rev* **2007,** 59, 207-24.

202. Friesen, R. W.; Mancini, J. A. Microsomal prostaglandin E2 synthase-1 (mPGES-1): a novel anti-inflammatory therapeutic target. *J Med Chem* **2008,** 51, 4059-67.

203. Cho, W.; Kim, J.; Cho, K.-B.; Choe, J. Production of Prostaglandin E(2) and I(2) Is Coupled with Cyclooxygenase-2 in Human Follicular Dendritic Cells. *Immune Network* **2011,** 11, 364-367.

204. Stichtenoth, D. O.; Thoren, S.; Bian, H.; Peters-Golden, M.; Jakobsson, P. J.; Crofford, L. J. Microsomal prostaglandin E synthase is regulated by proinflammatory cytokines and glucocorticoids in primary rheumatoid synovial cells. *J Immunol* **2001,** 167, 469-74.

205.    Claveau, D.; Sirinyan, M.; Guay, J.; Gordon, R.; Chan, C. C.; Bureau, Y.; Riendeau, D.; Mancini, J. A. Microsomal prostaglandin E synthase-1 is a major terminal synthase that is selectively up-regulated during cyclooxygenase-2-dependent prostaglandin E2 production in the rat adjuvant-induced arthritis model. *J Immunol* **2003,** 170, 4738-44.

206.    Frasor, J.; Weaver, A. E.; Pradhan, M.; Mehta, K. Synergistic up-regulation of prostaglandin E synthase expression in breast cancer cells by 17beta-estradiol and proinflammatory cytokines. *Endocrinology* **2008,** 149, 6272-9.

207.    Ackerman, W. E. t.; Summerfield, T. L.; Vandre, D. D.; Robinson, J. M.; Kniss, D. A. Nuclear factor-kappa B regulates inducible prostaglandin E synthase expression in human amnion mesenchymal cells. *Biol Reprod* **2008,** 78, 68-76.

208.    Jakobsson, P.-J.; Thorén, S.; Morgenstern, R.; Samuelsson, B. Identification of human prostaglandin E synthase: A microsomal, glutathione-dependent, inducible enzyme, constituting a potential novel drug target. *Proceedings of the National Academy of Sciences* **1999,** 96, 7220-7225.

209.    Jakobsson, P. J.; Morgenstern, R.; Mancini, J.; Ford-Hutchinson, A.; Persson, B. Common structural features of MAPEG -- a widespread superfamily of membrane associated proteins with highly divergent functions in eicosanoid and glutathione metabolism. *Protein Sci* **1999,** 8, 689-92.

210.    Jakobsson, P. J.; Mancini, J. A.; Ford-Hutchinson, A. W. Identification and characterization of a novel human microsomal glutathione S-transferase with leukotriene C4 synthase activity and significant sequence identity to 5-lipoxygenase-activating protein and leukotriene C4 synthase. *J Biol Chem* **1996,** 271, 22203-10.

211.    Jakobsson, P. J.; Mancini, J. A.; Riendeau, D.; Ford-Hutchinson, A. W. Identification and characterization of a novel microsomal enzyme with glutathione-dependent transferase and peroxidase activities. *J Biol Chem* **1997,** 272, 22934-9.

212.    Sjögren, T.; Nord, J.; Ek, M.; Johansson, P.; Liu, G.; Geschwindner, S. Crystal structure of microsomal prostaglandin E2 synthase provides insight into diversity in the MAPEG superfamily. *Proceedings of the National Academy of Sciences* **2013,** 110, 3806-3811.

213.    Riendeau, D.; Aspiotis, R.; Ethier, D.; Gareau, Y.; Grimm, E. L.; Guay, J.; Guiral, S.; Juteau, H.; Mancini, J. A.; Methot, N.; Rubin, J.; Friesen, R. W. Inhibitors of the inducible microsomal prostaglandin E2 synthase (mPGES-1) derived from MK-886. *Bioorg Med Chem Lett* **2005,** 15, 3352-5.

214.    Cote, B.; Boulet, L.; Brideau, C.; Claveau, D.; Ethier, D.; Frenette, R.; Gagnon, M.; Giroux, A.; Guay, J.; Guiral, S.; Mancini, J.; Martins, E.; Masse, F.; Methot, N.; Riendeau, D.; Rubin, J.; Xu, D.; Yu, H.; Ducharme, Y.; Friesen, R. W. Substituted phenanthrene imidazoles as potent, selective, and orally active mPGES-1 inhibitors. *Bioorg Med Chem Lett* **2007,** 17, 6816-20.

215.    Xu, D.; Rowland, S. E.; Clark, P.; Giroux, A.; Cote, B.; Guiral, S.; Salem, M.; Ducharme, Y.; Friesen, R. W.; Methot, N.; Mancini, J.; Audoly, L.; Riendeau, D. MF63    [2-(6-chloro-1H-phenanthro[9,10-d]imidazol-2-yl)-isophthalonitrile],    a selective microsomal prostaglandin E synthase-1 inhibitor, relieves pyresis and pain in preclinical models of inflammation. *J Pharmacol Exp Ther* **2008,** 326, 754-63.

216.    Wu, T. Y. H.; Juteau, H.; Ducharme, Y.; Friesen, R. W.; Guiral, S.; Dufresne, L.; Poirier, H.; Salem, M.; Riendeau, D.; Mancini, J.; Brideau, C. Biarylimidazoles as inhibitors of microsomal prostaglandin E2 synthase-1. *Bioorganic & Medicinal Chemistry Letters* **2010,** 20, 6978-6982.

217.    Koeberle, A.; Zettl, H.; Greiner, C.; Wurglics, M.; Schubert-Zsilavecz, M.; Werz, O. Pirinixic acid derivatives as novel dual inhibitors of microsomal prostaglandin E2 synthase-1 and 5-lipoxygenase. *J Med Chem* **2008,** 51, 8068-76.

218.    Hieke, M.; Greiner, C.; Dittrich, M.; Reisen, F.; Schneider, G.; Schubert-Zsilavecz, M.; Werz, O. Discovery and biological evaluation of a novel class of dual microsomal prostaglandin E2 synthase-1/5-lipoxygenase inhibitors based on 2-[(4,6-diphenethoxypyrimidin-2-yl)thio]hexanoic acid. *J Med Chem* **2011,** 54, 4490-507.

219.    Hanke, T.; Dehm, F.; Liening, S.; Popella, S. D.; Maczewsky, J.; Pillong, M.; Kunze, J.; Weinigel, C.; Barz, D.; Kaiser, A.; Wurglics, M.; Lammerhofer, M.; Schneider, G.; Sautebin, L.; Schubert-Zsilavecz, M.; Werz, O. Aminothiazole-featured pirinixic acid derivatives as dual 5-lipoxygenase and microsomal prostaglandin E2 synthase-1 inhibitors with improved potency and efficiency in vivo. *J Med Chem* **2013,** 56, 9031-44.

220.    Chiasson, J.-F.; Boulet, L.; Brideau, C.; Chau, A.; Claveau, D.; Côté, B.; Ethier, D.; Giroux, A.; Guay, J.; Guiral, S.; Mancini, J.; Massé, F.; Méthot, N.; Riendeau, D.; Roy, P.; Rubin, J.; Xu, D.; Yu, H.; Ducharme, Y.; Friesen, R. W. Trisubstituted ureas as potent and selective mPGES-1 inhibitors. *Bioorganic & Medicinal Chemistry Letters* **2011,** 21, 1488-1492.

221.    Wang, J.; Limburg, D.; Carter, J.; Mbalaviele, G.; Gierse, J.; Vazquez, M. Selective inducible microsomal prostaglandin E(2) synthase-1 (mPGES-1) inhibitors derived from an oxicam template. *Bioorg Med Chem Lett* **2010,** 20, 1604-9.

222.    Shiro, T.; Kakiguchi, K.; Takahashi, H.; Nagata, H.; Tobe, M. Synthesis and biological evaluation of substituted imidazoquinoline derivatives as mPGES-1 inhibitors. *Bioorg Med Chem* **2013,** 21, 2068-78.

223.    Liedtke, A. J.; Keck, P. R.; Lehmann, F.; Koeberle, A.; Werz, O.; Laufer, S. A. Arylpyrrolizines as inhibitors of microsomal prostaglandin E2 synthase-1 (mPGES-1) or as dual inhibitors of mPGES-1 and 5-lipoxygenase (5-LOX). *J Med Chem* **2009,** 52, 4968-72.

224.    De Simone, R.; Chini, M. G.; Bruno, I.; Riccio, R.; Mueller, D.; Werz, O.; Bifulco, G. Structure-based discovery of inhibitors of microsomal prostaglandin E2 synthase-1, 5-lipoxygenase and 5-lipoxygenase-activating protein: promising hits for the development of new anti-inflammatory agents. *J Med Chem* **2011,** 54, 1565-75.

225. Chini, M. G.; De Simone, R.; Bruno, I.; Riccio, R.; Dehm, F.; Weinigel, C.; Barz, D.; Werz, O.; Bifulco, G. Design and synthesis of a second series of triazole-based compounds as potent dual mPGES-1 and 5-lipoxygenase inhibitors. *European Journal of Medicinal Chemistry* **2012,** 54, 311-323.

226. He, S.; Li, C.; Liu, Y.; Lai, L. Discovery of highly potent microsomal prostaglandin e2 synthase 1 inhibitors using the active conformation structural model and virtual screen. *J Med Chem* **2013,** 56, 3296-309.

227. Arhancet, G. B.; Walker, D. P.; Metz, S.; Fobian, Y. M.; Heasley, S. E.; Carter, J. S.; Springer, J. R.; Jones, D. E.; Hayes, M. J.; Shaffer, A. F.; Jerome, G. M.; Baratta, M. T.; Zweifel, B.; Moore, W. M.; Masferrer, J. L.; Vazquez, M. L. Discovery and SAR of PF-4693627, a potent, selective and orally bioavailable mPGES-1 inhibitor for the potential treatment of inflammation. *Bioorganic & Medicinal Chemistry Letters* **2013,** 23, 1114-1119.

228. Tamblyn, R.; Berkson, L.; Dauphinee, W. D.; Gayton, D.; Grad, R.; Huang, A.; Isaac, L.; McLeod, P.; Snell, L. Unnecessary prescribing of NSAIDs and the management of NSAID-related gastropathy in medical practice. *Ann Intern Med* **1997,** 127, 429-38.

229. Pellicano, R. Gastrointestinal damage by non-steroidal anti-inflammatory drugs: updated clinical considerations. *Minerva Gastroenterol Dietol* **2014,** 60, 255-61.

230. Marco, J. L.; Amariles, P.; Bosca, B.; Castello, A. Risk factors associated with NSAID-induced upper gastrointestinal bleeding resulting in hospital admissions: A cross-sectional, retrospective, case series analysis in valencia, spain. *Curr Ther Res Clin Exp* **2007,** 68, 107-19.

231. Everts, B.; Wahrborg, P.; Hedner, T. COX-2-Specific inhibitors--the emergence of a new class of analgesic and anti-inflammatory drugs. *Clin Rheumatol* **2000,** 19, 331-43.

232. Cannon, C. P.; Curtis, S. P.; FitzGerald, G. A.; Krum, H.; Kaur, A.; Bolognese, J. A.; Reicin, A. S.; Bombardier, C.; Weinblatt, M. E.; van der Heijde, D.; Erdmann, E.; Laine, L. Cardiovascular outcomes with etoricoxib and diclofenac in patients with osteoarthritis and rheumatoid arthritis in the Multinational Etoricoxib and Diclofenac Arthritis Long-term (MEDAL) programme: a randomised comparison. *Lancet* **2006,** 368, 1771-81.

233. McGettigan, P.; Henry, D. Cardiovascular risk and inhibition of cyclooxygenase: a systematic review of the observational studies of selective and nonselective inhibitors of cyclooxygenase 2. *Jama* **2006,** 296, 1633-44.

234. Kearney, P. M.; Baigent, C.; Godwin, J.; Halls, H.; Emberson, J. R.; Patrono, C. Do selective cyclo-oxygenase-2 inhibitors and traditional non-steroidal anti-inflammatory drugs increase the risk of atherothrombosis? Meta-analysis of randomised trials. *Bmj* **2006,** 332, 1302-8.

235. Cheng, Y.; Wang, M.; Yu, Y.; Lawson, J.; Funk, C. D.; Fitzgerald, G. A. Cyclooxygenases, microsomal prostaglandin E synthase-1, and cardiovascular function. *J Clin Invest* **2006,** 116, 1391-9.

236. Trebino, C. E.; Stock, J. L.; Gibbons, C. P.; Naiman, B. M.; Wachtmann, T. S.; Umland, J. P.; Pandher, K.; Lapointe, J. M.; Saha, S.; Roach, M. L.; Carter, D.; Thomas, N. A.; Durtschi, B. A.; McNeish, J. D.; Hambor, J. E.; Jakobsson, P. J.; Carty, T. J.; Perez, J. R.; Audoly, L. P. Impaired inflammatory and pain responses in mice lacking an inducible prostaglandin E synthase. *Proc Natl Acad Sci U S A* **2003,** 100, 9044-9.

237. Kamei, D.; Yamakawa, K.; Takegoshi, Y.; Mikami-Nakanishi, M.; Nakatani, Y.; Oh-Ishi, S.; Yasui, H.; Azuma, Y.; Hirasawa, N.; Ohuchi, K.; Kawaguchi, H.; Ishikawa, Y.; Ishii, T.; Uematsu, S.; Akira, S.; Murakami, M.; Kudo, I. Reduced pain hypersensitivity and inflammation in mice lacking microsomal prostaglandin e synthase-1. *J Biol Chem* **2004,** 279, 33684-95.

238. Saha, S.; Engstrom, L.; Mackerlova, L.; Jakobsson, P. J.; Blomqvist, A. Impaired febrile responses to immune challenge in mice deficient in microsomal prostaglandin E synthase-1. *Am J Physiol Regul Integr Comp Physiol* **2005,** 288, R1100-7.

239. Korotkova, M.; Jakobsson, P.-J. Microsomal Prostaglandin E Synthase-1 in Rheumatic Diseases. *Frontiers in Pharmacology* **2010,** 1, 146.

240. Westman, M.; Korotkova, M.; af Klint, E.; Stark, A.; Audoly, L. P.; Klareskog, L.; Ulfgren, A. K.; Jakobsson, P. J. Expression of microsomal prostaglandin E synthase 1 in rheumatoid arthritis synovium. *Arthritis Rheum* **2004,** 50, 1774-80.

241. Wang, M.; Song, W. L.; Cheng, Y.; Fitzgerald, G. A. Microsomal prostaglandin E synthase-1 inhibition in cardiovascular inflammatory disease. *J Intern Med* **2008,** 263, 500-5.

242. Radmark, O.; Samuelsson, B. Microsomal prostaglandin E synthase-1 and 5-lipoxygenase: potential drug targets in cancer. *J Intern Med* **2010,** 268, 5-14.

243. Murakami, M.; Kudo, I. Prostaglandin E synthase: a novel drug target for inflammation and cancer. *Curr Pharm Des* **2006,** 12, 943-54.

244. Hanaka, H.; Pawelzik, S. C.; Johnsen, J. I.; Rakonjac, M.; Terawaki, K.; Rasmuson, A.; Sveinbjornsson, B.; Schumacher, M. C.; Hamberg, M.; Samuelsson, B.; Jakobsson, P. J.; Kogner, P.; Radmark, O. Microsomal prostaglandin E synthase 1 determines tumor growth in vivo of prostate and lung cancer cells. *Proc Natl Acad Sci U S A* **2009,** 106, 18757-62.

245. Nakanishi, M.; Gokhale, V.; Meuillet, E. J.; Rosenberg, D. W. mPGES-1 as a Target for Cancer Suppression: A comprehensive invited review "Phospholipase A(2) and lipid mediators". *Biochimie* **2010,** 92, 660-664.

246.     von Rahden, B. H.; Stein, H. J.; Hartl, S. A.; Theisen, J.; Stigler, B.; Siewert, J. R.; Sarbia, M. Expression of prostaglandin E synthase in Barrett's cancer. *Dis Esophagus* **2008,** 21, 304-8.

247.     Nardone, G.; Rocco, A.; Vaira, D.; Staibano, S.; Budillon, A.; Tatangelo, F.; Sciulli, M. G.; Perna, F.; Salvatore, G.; Di Benedetto, M.; De Rosa, G.; Patrignani, P. Expression of COX-2, mPGE-synthase1, MDR-1 (P-gp), and Bcl-xL: a molecular pathway of H pylori-related gastric carcinogenesis. *J Pathol* **2004,** 202, 305-12.

248.     Gudis, K.; Tatsuguchi, A.; Wada, K.; Hiratsuka, T.; Futagami, S.; Fukuda, Y.; Kiyama, T.; Tajiri, T.; Miyake, K.; Sakamoto, C. Clinical significance of prostaglandin E synthase expression in gastric cancer tissue. *Hum Pathol* **2007,** 38, 1826-35.

249.     Yoshimatsu, K.; Golijanin, D.; Paty, P. B.; Soslow, R. A.; Jakobsson, P. J.; DeLellis, R. A.; Subbaramaiah, K.; Dannenberg, A. J. Inducible microsomal prostaglandin E synthase is overexpressed in colorectal adenomas and cancer. *Clin Cancer Res* **2001,** 7, 3971-6.

250.     Takii, Y.; Abiru, S.; Fujioka, H.; Nakamura, M.; Komori, A.; Ito, M.; Taniguchi, K.; Daikoku, M.; Meda, Y.; Ohata, K.; Yano, K.; Shimoda, S.; Yatsuhashi, H.; Ishibashi, H.; Migita, K. Expression of microsomal prostaglandin E synthase-1 in human hepatocelluar carcinoma. *Liver Int* **2007,** 27, 989-96.

251.     Hasan, S.; Satake, M.; Dawson, D. W.; Funahashi, H.; Angst, E.; Go, V. L.; Reber, H. A.; Hines, O. J.; Eibl, G. Expression analysis of the prostaglandin E2 production pathway in human pancreatic cancers. *Pancreas* **2008,** 37, 121-7.

252.     Mattila, S.; Tuominen, H.; Koivukangas, J.; Stenback, F. The terminal prostaglandin synthases mPGES-1, mPGES-2, and cPGES are all overexpressed in human gliomas. *Neuropathology* **2009,** 29, 156-65.

253.     Baryawno, N.; Sveinbjornsson, B.; Eksborg, S.; Orrego, A.; Segerstrom, L.; Oqvist, C. O.; Holm, S.; Gustavsson, B.; Kagedal, B.; Kogner, P.; Johnsen, J. I. Tumor-growth-promoting cyclooxygenase-2 prostaglandin E2 pathway provides medulloblastoma therapeutic targets. *Neuro Oncol* **2008,** 10, 661-74.

254.     Mehrotra, S.; Morimiya, A.; Agarwal, B.; Konger, R.; Badve, S. Microsomal prostaglandin E2 synthase-1 in breast cancer: a potential target for therapy. *J Pathol* **2006,** 208, 356-63.

255.     Omi, Y.; Shibata, N.; Okamoto, T.; Obara, T.; Kobayashi, M. Immunohistochemical demonstration of membrane-bound prostaglandin E2 synthase-1 in papillary thyroid carcinoma. *Acta Histochem Cytochem* **2009,** 42, 105-9.

256.     Cohen, E. G.; Almahmeed, T.; Du, B.; Golijanin, D.; Boyle, J. O.; Soslow, R. A.; Subbaramaiah, K.; Dannenberg, A. J. Microsomal prostaglandin E synthase-1 is overexpressed in head and neck squamous cell carcinoma. *Clin Cancer Res* **2003,** 9, 3425-30.

257.    Yoshimatsu, K.; Altorki, N. K.; Golijanin, D.; Zhang, F.; Jakobsson, P. J.; Dannenberg, A. J.; Subbaramaiah, K. Inducible prostaglandin E synthase is overexpressed in non-small cell lung cancer. *Clin Cancer Res* **2001,** 7, 2669-74.

258.    Kawata, R.; Hyo, S.; Maeda, T.; Urade, Y.; Takenaka, H. Simultaneous expression of cyclooxygenase-2 and microsomal prostaglandin E synthase in squamous cell carcinoma of the larynx. *Acta Otolaryngol* **2006,** 126, 627-32.

259.    Herfs, M.; Herman, L.; Hubert, P.; Minner, F.; Arafa, M.; Roncarati, P.; Henrotin, Y.; Boniver, J.; Delvenne, P. High expression of PGE2 enzymatic pathways in cervical (pre)neoplastic lesions and functional consequences for antigen-presenting cells. *Cancer Immunol Immunother* **2009,** 58, 603-14.

260.    Rask, K.; Zhu, Y.; Wang, W.; Hedin, L.; Sundfeldt, K. Ovarian epithelial cancer: a role for PGE2-synthesis and signalling in malignant transformation and progression. *Mol Cancer* **2006,** 5, 62.

261.    Golijanin, D.; Tan, J. Y.; Kazior, A.; Cohen, E. G.; Russo, P.; Dalbagni, G.; Auborn, K. J.; Subbaramaiah, K.; Dannenberg, A. J. Cyclooxygenase-2 and microsomal prostaglandin E synthase-1 are overexpressed in squamous cell carcinoma of the penis. *Clin Cancer Res* **2004,** 10, 1024-31.

262.    Seo, T.; Tatsuguchi, A.; Shinji, S.; Yonezawa, M.; Mitsui, K.; Tanaka, S.; Fujimori, S.; Gudis, K.; Fukuda, Y.; Sakamoto, C. Microsomal prostaglandin E synthase protein levels correlate with prognosis in colorectal cancer patients. *Virchows Archiv* **2009,** 454, 667-676.

263.    Kamata, H.; Hosono, K.; Suzuki, T.; Ogawa, Y.; Kubo, H.; Katoh, H.; Ito, Y.; Uematsu, S.; Akira, S.; Watanabe, M.; Majima, M. mPGES-1-expressing bone marrow-derived cells enhance tumor growth and angiogenesis in mice. *Biomed Pharmacother* **2010,** 64, 409-16.

264.    Koeberle, A.; Werz, O. Inhibitors of the microsomal prostaglandin E(2) synthase-1 as alternative to non steroidal anti-inflammatory drugs (NSAIDs)--a critical review. *Curr Med Chem* **2009,** 16, 4274-96.

265.    Chang, H. H.; Meuillet, E. J. Identification and development of mPGES-1 inhibitors: where we are at? *Future Med Chem* **2011,** 3, 1909-34.

266.    Pawelzik, S.-C.; Uda, N. R.; Spahiu, L.; Jegerschöld, C.; Stenberg, P.; Hebert, H.; Morgenstern, R.; Jakobsson, P.-J. Identification of Key Residues Determining Species Differences in Inhibitor Binding of Microsomal Prostaglandin E Synthase-1. *The Journal of Biological Chemistry* **2010,** 285, 29254-29261.

267.    Timmers, L.; Pasterkamp, G.; de Kleijn, D. P. Microsomal prostaglandin E2 synthase: a safer target than cyclooxygenases? *Mol Interv* **2007,** 7, 195-9, 180.

268.    Hartl, F. U. Molecular chaperones in cellular protein folding. *Nature* **1996,** 381, 571-580.

269.    Hartl, F. U.; Bracher, A.; Hayer-Hartl, M. Molecular chaperones in protein folding and proteostasis. *Nature* **2011,** 475, 324-332.

270.    Saibil, H. R. Chaperone machines in action. *Curr Opin Struct Biol* **2008,** 18, 35-42.

271.    Saibil, H. Chaperone machines for protein folding, unfolding and disaggregation. *Nat Rev Mol Cell Biol* **2013,** 14, 630-42.

272.    Taipale, M.; Jarosz, D. F.; Lindquist, S. HSP90 at the hub of protein homeostasis: emerging mechanistic insights. *Nat Rev Mol Cell Biol* **2010,** 11, 515-28.

273.    Kampinga, H. H.; Hageman, J.; Vos, M. J.; Kubota, H.; Tanguay, R. M.; Bruford, E. A.; Cheetham, M. E.; Chen, B.; Hightower, L. E. Guidelines for the nomenclature of the human heat shock proteins. *Cell Stress Chaperones* **2009,** 14, 105-11.

274.    Chang, H. C.; Lindquist, S. Conservation of Hsp90 macromolecular complexes in Saccharomyces cerevisiae. *J Biol Chem* **1994,** 269, 24983-8.

275.    Johnson, J. L. Evolution and function of diverse Hsp90 homologs and cochaperone proteins. *Biochimica et Biophysica Acta (BBA) - Molecular Cell Research* **2012,** 1823, 607-613.

276.    Pratt, W. B.; Toft, D. O. Regulation of signaling protein function and trafficking by the hsp90/hsp70-based chaperone machinery. *Exp Biol Med (Maywood)* **2003,** 228, 111-33.

277.    Whitesell, L.; Lindquist, S. L. HSP90 and the chaperoning of cancer. *Nat Rev Cancer* **2005,** 5, 761-72.

278.    Zhang, H.; Burrows, F. Targeting multiple signal transduction pathways through inhibition of Hsp90. *J Mol Med (Berl)* **2004,** 82, 488-99.

279.    Barrott, J. J.; Haystead, T. A. J. Hsp90, an unlikely ally in the war on cancer. *FEBS Journal* **2013,** 280, 1381-1396.

280.    Chiosis, G.; Vilenchik, M.; Kim, J.; Solit, D. Hsp90: the vulnerable chaperone. *Drug Discov Today* **2004,** 9, 881-8.

281.    Workman, P. Altered states: selectively drugging the Hsp90 cancer chaperone. *Trends Mol Med* **2004,** 10, 47-51.

282.    Sreedhar, A. S.; Kalmar, E.; Csermely, P.; Shen, Y. F. Hsp90 isoforms: functions, expression and clinical importance. *FEBS Lett* **2004,** 562, 11-5.

283.    Altieri, D. C.; Stein, G. S.; Lian, J. B.; Languino, L. R. TRAP-1, the mitochondrial Hsp90. *Biochimica et Biophysica Acta (BBA) - Molecular Cell Research* **2012,** 1823, 767-773.

284.	Marzec, M.; Eletto, D.; Argon, Y. GRP94: An HSP90-like protein specialized for protein folding and quality control in the endoplasmic reticulum. *Biochimica et Biophysica Acta (BBA) - Molecular Cell Research* **2012,** 1823, 774-787.

285.	Prodromou, C. The 'active life' of Hsp90 complexes. *Biochimica et Biophysica Acta (BBA) - Molecular Cell Research* **2012,** 1823, 614-623.

286.	Taipale, M.; Krykbaeva, I.; Koeva, M.; Kayatekin, C.; Westover, Kenneth D.; Karras, Georgios I.; Lindquist, S. Quantitative Analysis of Hsp90-Client Interactions Reveals Principles of Substrate Recognition. *Cell* **2012,** 150, 987-1001.

287.	Didier, P. http://www.picard.ch/downloads/Hsp90interactors.pdf (13 February 2015).

288.	Connell, P.; Ballinger, C. A.; Jiang, J.; Wu, Y.; Thompson, L. J.; Hohfeld, J.; Patterson, C. The co-chaperone CHIP regulates protein triage decisions mediated by heat-shock proteins. *Nat Cell Biol* **2001,** 3, 93-6.

289.	Theodoraki, M. A.; Caplan, A. J. Quality control and fate determination of Hsp90 client proteins. *Biochim Biophys Acta* **2012,** 1823, 683-8.

290.	McDonough, H.; Patterson, C. CHIP: a link between the chaperone and proteasome systems. *Cell Stress Chaperones* **2003,** 8, 303-8.

291.	Workman, P. Combinatorial attack on multistep oncogenesis by inhibiting the Hsp90 molecular chaperone. *Cancer Lett* **2004,** 206, 149-57.

292.	Bishop, S. C.; Burlison, J. A.; Blagg, B. S. Hsp90: a novel target for the disruption of multiple signaling cascades. *Curr Cancer Drug Targets* **2007,** 7, 369-88.

293.	Muchowski, P. J. Protein misfolding, amyloid formation, and neurodegeneration: a critical role for molecular chaperones? *Neuron* **2002,** 35, 9-12.

294.	Luo, G. R.; Le, W. D. Collective roles of molecular chaperones in protein degradation pathways associated with neurodegenerative diseases. *Curr Pharm Biotechnol* **2010,** 11, 180-7.

295.	Muchowski, P. J.; Wacker, J. L. Modulation of neurodegeneration by molecular chaperones. *Nat Rev Neurosci* **2005,** 6, 11-22.

296.	Chiosis, G.; Neckers, L. Tumor selectivity of Hsp90 inhibitors: the explanation remains elusive. *ACS Chem Biol* **2006,** 1, 279-84.

297.	Neckers, L. Heat shock protein 90: the cancer chaperone. *J Biosci* **2007,** 32, 517-30.

298.	Li, Y.; Zhang, T.; Schwartz, S. J.; Sun, D. New developments in Hsp90 inhibitors as anti-cancer therapeutics: mechanisms, clinical perspective and more potential. *Drug Resist Updat* **2009,** 12, 17-27.

299.    Powers, M. V.; Workman, P. Inhibitors of the heat shock response: biology and pharmacology. *FEBS Lett* **2007,** 581, 3758-69.

300.    Ferrarini, M.; Heltai, S.; Zocchi, M. R.; Rugarli, C. Unusual expression and localization of heat-shock proteins in human tumor cells. *Int J Cancer* **1992,** 51, 613-9.

301.    Bagatell, R.; Whitesell, L. Altered Hsp90 function in cancer: a unique therapeutic opportunity. *Mol Cancer Ther* **2004,** 3, 1021-30.

302.    Zuehlke, A.; Johnson, J. L. Hsp90 and co-chaperones twist the functions of diverse client proteins. *Biopolymers* **2010,** 93, 211-217.

303.    Li, J.; Soroka, J.; Buchner, J. The Hsp90 chaperone machinery: Conformational dynamics and regulation by co-chaperones. *Biochimica et Biophysica Acta (BBA) - Molecular Cell Research* **2012,** 1823, 624-635.

304.    Blagosklonny, M. V. Hsp-90-associated oncoproteins: multiple targets of geldanamycin and its analogs. *Leukemia* **2002,** 16, 455-62.

305.    Trepel, J.; Mollapour, M.; Giaccone, G.; Neckers, L. Targeting the dynamic HSP90 complex in cancer. *Nat Rev Cancer* **2010,** 10, 537-49.

306.    Hwang, M.; Moretti, L.; Lu, B. HSP90 inhibitors: multi-targeted antitumor effects and novel combinatorial therapeutic approaches in cancer therapy. *Curr Med Chem* **2009,** 16, 3081-92.

307.    Workman, P.; Burrows, F.; Neckers, L.; Rosen, N. Drugging the cancer chaperone HSP90: combinatorial therapeutic exploitation of oncogene addiction and tumor stress. *Ann N Y Acad Sci* **2007,** 1113, 202-16.

308.    da Silva, V. C.; Ramos, C. H. The network interaction of the human cytosolic 90 kDa heat shock protein Hsp90: A target for cancer therapeutics. *J Proteomics* **2012,** 75, 2790-802.

309.    Miyata, Y.; Nakamoto, H.; Neckers, L. The therapeutic target Hsp90 and cancer hallmarks. *Curr Pharm Des* **2013,** 19, 347-65.

310.    Ross, C. A.; Poirier, M. A. Protein aggregation and neurodegenerative disease. *Nat Med* **2004,** 10 Suppl, S10-7.

311.    Batulan, Z.; Taylor, D. M.; Aarons, R. J.; Minotti, S.; Doroudchi, M. M.; Nalbantoglu, J.; Durham, H. D. Induction of multiple heat shock proteins and neuroprotection in a primary culture model of familial amyotrophic lateral sclerosis. *Neurobiol Dis* **2006,** 24, 213-25.

312.    Zitvogel, L.; Kepp, O.; Kroemer, G. Decoding Cell Death Signals in Inflammation and Immunity. *Cell* **2010,** 140, 798-804.

313.    Broemer, M.; Krappmann, D.; Scheidereit, C. Requirement of Hsp90 activity for IkappaB kinase (IKK) biosynthesis and for constitutive and inducible IKK and NF-kappaB activation. *Oncogene* **2004,** 23, 5378-86.

314.    Qing, G.; Yan, P.; Xiao, G. Hsp90 inhibition results in autophagy-mediated proteasome-independent degradation of IkappaB kinase (IKK). *Cell Res* **2006,** 16, 895-901.

315.    Salminen, A.; Paimela, T.; Suuronen, T.; Kaarniranta, K. Innate immunity meets with cellular stress at the IKK complex: regulation of the IKK complex by HSP70 and HSP90. *Immunol Lett* **2008,** 117, 9-15.

316.    Pittet, J. F.; Lee, H.; Pespeni, M.; O'Mahony, A.; Roux, J.; Welch, W. J. Stress-induced inhibition of the NF-kappaB signaling pathway results from the insolubilization of the IkappaB kinase complex following its dissociation from heat shock protein 90. *J Immunol* **2005,** 174, 384-94.

317.    Bucci, M.; Roviezzo, F.; Cicala, C.; Sessa, W. C.; Cirino, G. Geldanamycin, an inhibitor of heat shock protein 90 (Hsp90) mediated signal transduction has anti-inflammatory effects and interacts with glucocorticoid receptor in vivo. *British Journal of Pharmacology* **2000,** 131, 13-16.

318.    Rice, J. W.; Veal, J. M.; Fadden, R. P.; Barabasz, A. F.; Partridge, J. M.; Barta, T. E.; Dubois, L. G.; Huang, K. H.; Mabbett, S. R.; Silinski, M. A.; Steed, P. M.; Hall, S. E. Small molecule inhibitors of Hsp90 potently affect inflammatory disease pathways and exhibit activity in models of rheumatoid arthritis. *Arthritis & Rheumatism* **2008,** 58, 3765-3775.

319.    Zhao, Y.; Huang, Z.-J.; Rahman, M.; Luo, Q.; Thorlacius, H. Radicicol, an Hsp90 inhibitor, inhibits intestinal inflammation and leakage in abdominal sepsis. *Journal of Surgical Research* **2013,** 182, 312-318.

320.    Shimp, S., III; Parson, C.; Regna, N.; Thomas, A.; Chafin, C.; Reilly, C.; Nichole Rylander, M. HSP90 inhibition by 17-DMAG reduces inflammation in J774 macrophages through suppression of Akt and nuclear factor-κB pathways. *Inflammation Research* **2012,** 61, 521-533.

321.    Madrigal-Matute, J.; Lopez-Franco, O.; Blanco-Colio, L. M.; Munoz-Garcia, B.; Ramos-Mozo, P.; Ortega, L.; Egido, J.; Martin-Ventura, J. L. Heat shock protein 90 inhibitors attenuate inflammatory responses in atherosclerosis. *Cardiovasc Res* **2010,** 86, 330-7.

322.    Poulaki, V.; Iliaki, E.; Mitsiades, N.; Mitsiades, C. S.; Paulus, Y. N.; Bula, D. V.; Gragoudas, E. S.; Miller, J. W. Inhibition of Hsp90 attenuates inflammation in endotoxin-induced uveitis. *The FASEB Journal* **2007,** 21, 2113-2123.

323.    De Paepe, B.; Creus, K. K.; Martin, J.-J.; Weis, J.; De Bleecker, J. L. A Dual Role for HSP90 and HSP70 in the Inflammatory Myopathies. *Annals of the New York Academy of Sciences* **2009,** 1173, 463-469.

324. Xavier, R. J.; Podolsky, D. K. Unravelling the pathogenesis of inflammatory bowel disease. *Nature* **2007,** 448, 427-34.

325. Tomasello, G.; Sciumè, C.; Rappa, F.; Rodolico, V.; Zerilli, M.; Martorana, A.; Cicero, G.; De Luca, R.; Damiani, P.; Accardo, F. M.; Romeo, M.; Farina, F.; Bonaventura, G.; Modica, G.; Zummo, G.; Conway de Macario, E.; Macario, A. J. L.; Cappello, F. Hsp10, Hsp70, and Hsp90 immunohistochemical levels change in ulcerative colitis after therapy. *European Journal of Histochemistry : EJH* **2011,** 55, e38.

326. Choi, S. R.; Lee, S. A.; Kim, Y. J.; Ok, C. Y.; Lee, H. J.; Hahm, K. B. Role of heat shock proteins in gastric inflammation and ulcer healing. *J Physiol Pharmacol* **2009,** 60 Suppl 7, 5-17.

327. Tsukimi, Y.; Okabe, S. Recent advances in gastrointestinal pathophysiology: role of heat shock proteins in mucosal defense and ulcer healing. *Biol Pharm Bull* **2001,** 24, 1-9.

328. Collins, C. B.; Aherne, C. M.; Yeckes, A.; Pound, K.; Eltzschig, H. K.; Jedlicka, P.; de Zoeten, E. F. Inhibition of N-terminal ATPase on HSP90 attenuates colitis through enhanced Treg function. *Mucosal Immunol* **2013,** 6, 960-71.

329. Ambade, A.; Catalano, D.; Lim, A.; Mandrekar, P. Inhibition of heat shock protein (molecular weight 90 kDa) attenuates proinflammatory cytokines and prevents lipopolysaccharide-induced liver injury in mice. *Hepatology* **2012,** 55, 1585-95.

330. Dello Russo, C.; Polak, P. E.; Mercado, P. R.; Spagnolo, A.; Sharp, A.; Murphy, P.; Kamal, A.; Burrows, F. J.; Fritz, L. C.; Feinstein, D. L. The heat-shock protein 90 inhibitor 17-allylamino-17-demethoxygeldanamycin suppresses glial inflammatory responses and ameliorates experimental autoimmune encephalomyelitis. *J Neurochem* **2006,** 99, 1351-62.

331. Bohonowych, J. E.; Hance, M. W.; Nolan, K. D.; Defee, M.; Parsons, C. H.; Isaacs, J. S. Extracellular Hsp90 mediates an NF-κB dependent inflammatory stromal program: Implications for the prostate tumor microenvironment. *The Prostate* **2014,** 74, 395-407.

332. Wandinger, S. K.; Richter, K.; Buchner, J. The Hsp90 Chaperone Machinery. *Journal of Biological Chemistry* **2008,** 283, 18473-18477.

333. Prodromou, C.; Roe, S. M.; O'Brien, R.; Ladbury, J. E.; Piper, P. W.; Pearl, L. H. Identification and structural characterization of the ATP/ADP-binding site in the Hsp90 molecular chaperone. *Cell* **1997,** 90, 65-75.

334. Hawle, P.; Siepmann, M.; Harst, A.; Siderius, M.; Reusch, H. P.; Obermann, W. M. The middle domain of Hsp90 acts as a discriminator between different types of client proteins. *Mol Cell Biol* **2006,** 26, 8385-95.

335. Soti, C.; Racz, A.; Csermely, P. A Nucleotide-dependent molecular switch controls ATP binding at the C-terminal domain of Hsp90. N-terminal nucleotide binding unmasks a C-terminal binding pocket. *J Biol Chem* **2002,** 277, 7066-75.

336. Garnier, C.; Lafitte, D.; Tsvetkov, P. O.; Barbier, P.; Leclerc-Devin, J.; Millot, J. M.; Briand, C.; Makarov, A. A.; Catelli, M. G.; Peyrot, V. Binding of ATP to heat shock protein 90: evidence for an ATP-binding site in the C-terminal domain. *J Biol Chem* **2002,** 277, 12208-14.

337. Soti, C.; Vermes, A.; Haystead, T. A.; Csermely, P. Comparative analysis of the ATP-binding sites of Hsp90 by nucleotide affinity cleavage: a distinct nucleotide specificity of the C-terminal ATP-binding site. *Eur J Biochem* **2003,** 270, 2421-8.

338. Chadli, A.; Bruinsma, E. S.; Stensgard, B.; Toft, D. Analysis of Hsp90 cochaperone interactions reveals a novel mechanism for TPR protein recognition. *Biochemistry* **2008,** 47, 2850-7.

339. Yamada, S.; Ono, T.; Mizuno, A.; Nemoto, T. K. A hydrophobic segment within the C-terminal domain is essential for both client-binding and dimer formation of the HSP90-family molecular chaperone. *Eur J Biochem* **2003,** 270, 146-54.

340. Shiau, A. K.; Harris, S. F.; Southworth, D. R.; Agard, D. A. Structural Analysis of E. coli hsp90 reveals dramatic nucleotide-dependent conformational rearrangements. *Cell* **2006,** 127, 329-40.

341. Ali, M. M.; Roe, S. M.; Vaughan, C. K.; Meyer, P.; Panaretou, B.; Piper, P. W.; Prodromou, C.; Pearl, L. H. Crystal structure of an Hsp90-nucleotide-p23/Sba1 closed chaperone complex. *Nature* **2006,** 440, 1013-7.

342. Huai, Q.; Wang, H.; Liu, Y.; Kim, H. Y.; Toft, D.; Ke, H. Structures of the N-terminal and middle domains of E. coli Hsp90 and conformation changes upon ADP binding. *Structure* **2005,** 13, 579-90.

343. Li, J.; Richter, K.; Buchner, J. Mixed Hsp90–cochaperone complexes are important for the progression of the reaction cycle. *Nat Struct Mol Biol* **2011,** 18, 61-66.

344. Rohl, A.; Rohrberg, J.; Buchner, J. The chaperone Hsp90: changing partners for demanding clients. *Trends Biochem Sci* **2013,** 38, 253-62.

345. Neckers, L.; Workman, P. Hsp90 Molecular Chaperone Inhibitors: Are We There Yet? *Clinical Cancer Research* **2012,** 18, 64-76.

346. Bhat, R.; Tummalapalli, S. R.; Rotella, D. P. Progress in the discovery and development of heat shock protein 90 (Hsp90) inhibitors. *J Med Chem* **2014,** 57, 8718-28.

347. Jhaveri, K.; Taldone, T.; Modi, S.; Chiosis, G. Advances in the clinical development of heat shock protein 90 (Hsp90) inhibitors in cancers. *Biochimica et Biophysica Acta (BBA) - Molecular Cell Research* **2012,** 1823, 742-755.

348. Soga, S.; Akinaga, S.; Shiotsu, Y. Hsp90 inhibitors as anti-cancer agents, from basic discoveries to clinical development. *Curr Pharm Des* **2013,** 19, 366-76.

349. McConnell, J. R.; McAlpine, S. R. Heat shock proteins 27, 40, and 70 as combinational and dual therapeutic cancer targets. *Bioorganic & medicinal chemistry letters* **2013,** 23, 1923-1928.

350. Modi, S.; Saura, C.; Henderson, C.; Lin, N. U.; Mahtani, R.; Goddard, J.; Rodenas, E.; Hudis, C.; O'Shaughnessy, J.; Baselga, J. A multicenter trial evaluating retaspimycin HCL (IPI-504) plus trastuzumab in patients with advanced or metastatic HER2-positive breast cancer. *Breast Cancer Research and Treatment* **2013,** 139, 107-113.

351. Gandhi, N.; Wild, A. T.; Chettiar, S. T.; Aziz, K.; Kato, Y.; Gajula, R. P.; Williams, R. D.; Cades, J. A.; Annadanam, A.; Song, D.; Zhang, Y.; Hales, R. K.; Herman, J. M.; Armour, E.; DeWeese, T. L.; Schaeffer, E. M.; Tran, P. T. Novel Hsp90 inhibitor NVP-AUY922 radiosensitizes prostate cancer cells. *Cancer Biology & Therapy* **2013,** 14, 347-356.

352. Goldman, J. W.; Raju, R. N.; Gordon, G. A.; El-Hariry, I.; Teofilivici, F.; Vukovic, V. M.; Bradley, R.; Karol, M. D.; Chen, Y.; Guo, W.; Inoue, T.; Rosen, L. S. A first in human, safety, pharmacokinetics, and clinical activity phase I study of once weekly administration of the Hsp90 inhibitor ganetespib (STA-9090) in patients with solid malignancies. *BMC Cancer* **2013,** 13, 152.

353. Oki, Y.; Copeland, A.; Romaguera, J.; Fayad, L.; Fanale, M.; Faria Sde, C.; Medeiros, L. J.; Ivy, P.; Younes, A. Clinical experience with the heat shock protein-90 inhibitor, tanespimycin, in patients with relapsed lymphoma. *Leuk Lymphoma* **2012,** 53, 990-2.

354. Heath, E. I.; Hillman, D. W.; Vaishampayan, U.; Sheng, S.; Sarkar, F.; Harper, F.; Gaskins, M.; Pitot, H. C.; Tan, W.; Ivy, S. P.; Pili, R.; Carducci, M. A.; Liu, G. A Phase II Trial of 17-Allylamino-17-Demethoxygeldanamycin (17-AAG) in Patients with Hormone-Refractory Metastatic Prostate Cancer. *Clinical cancer research : an official journal of the American Association for Cancer Research* **2008,** 14, 7940-7946.

355. Richardson, P. G.; Badros, A. Z.; Jagannath, S.; Tarantolo, S.; Wolf, J. L.; Albitar, M.; Berman, D.; Messina, M.; Anderson, K. C. Tanespimycin with bortezomib: activity in relapsed/refractory patients with multiple myeloma. *Br J Haematol* **2010,** 150, 428-37.

356. Samarasinghe, B.; Wales, C. T. K.; Taylor, F. R.; Jacobs, A. T. Heat shock factor 1 confers resistance to Hsp90 inhibitors through p62/SQSTM1 expression and promotion of autophagic flux. *Biochemical Pharmacology* **2014,** 87, 445-455.

357. Bagatell, R.; Paine-Murrieta, G. D.; Taylor, C. W.; Pulcini, E. J.; Akinaga, S.; Benjamin, I. J.; Whitesell, L. Induction of a Heat Shock Factor 1-dependent Stress Response Alters the Cytotoxic Activity of Hsp90-binding Agents. *Clinical Cancer Research* **2000,** 6, 3312-3318.

358.    Wang, Y.; McAlpine, S. R. N-terminal and C-terminal modulation of Hsp90 produce dissimilar phenotypes. *Chem Commun (Camb)* **2015,** 51, 1410-3.

359.    Conde, R.; Belak, Z. R.; Nair, M.; O'Carroll, R. F.; Ovsenek, N. Modulation of Hsf1 activity by novobiocin and geldanamycin. *Biochem Cell Biol* **2009,** 87, 845-51.

360.    Ghosh, S.; Shinogle, H. E.; Garg, G.; Vielhauer, G. A.; Holzbeierlein, J. M.; Dobrowsky, R. T.; Blagg, B. S. Hsp90 C-Terminal Inhibitors Exhibit Antimigratory Activity by Disrupting the Hsp90alpha/Aha1 Complex in PC3-MM2 Cells. *ACS Chem Biol* **2014**.

361.    Donnelly, A.; Blagg, B. S. Novobiocin and additional inhibitors of the Hsp90 C-terminal nucleotide-binding pocket. *Curr Med Chem* **2008,** 15, 2702-17.

362.    Marcu, M. G.; Chadli, A.; Bouhouche, I.; Catelli, M.; Neckers, L. M. The heat shock protein 90 antagonist novobiocin interacts with a previously unrecognized ATP-binding domain in the carboxyl terminus of the chaperone. *J Biol Chem* **2000,** 275, 37181-6.

363.    Marcu, M. G.; Schulte, T. W.; Neckers, L. Novobiocin and related coumarins and depletion of heat shock protein 90-dependent signaling proteins. *J Natl Cancer Inst* **2000,** 92, 242-8.

364.    Yun, B. G.; Huang, W.; Leach, N.; Hartson, S. D.; Matts, R. L. Novobiocin induces a distinct conformation of Hsp90 and alters Hsp90-cochaperone-client interactions. *Biochemistry* **2004,** 43, 8217-29.

365.    Matts, R. L.; Manjarrez, J. R. Assays for identification of Hsp90 inhibitors and biochemical methods for discriminating their mechanism of action. *Curr Top Med Chem* **2009,** 9, 1462-78.

366.    Allan, R. K.; Mok, D.; Ward, B. K.; Ratajczak, T. Modulation of chaperone function and cochaperone interaction by novobiocin in the C-terminal domain of Hsp90: evidence that coumarin antibiotics disrupt Hsp90 dimerization. *J Biol Chem* **2006,** 281, 7161-71.

367.    Burlison, J. A.; Neckers, L.; Smith, A. B.; Maxwell, A.; Blagg, B. S. Novobiocin: redesigning a DNA gyrase inhibitor for selective inhibition of hsp90. *J Am Chem Soc* **2006,** 128, 15529-36.

368.    Zhao, H.; Donnelly, A. C.; Kusuma, B. R.; Brandt, G. E.; Brown, D.; Rajewski, R. A.; Vielhauer, G.; Holzbeierlein, J.; Cohen, M. S.; Blagg, B. S. Engineering an antibiotic to fight cancer: optimization of the novobiocin scaffold to produce anti-proliferative agents. *J Med Chem* **2011,** 54, 3839-53.

369.    Zhao, H.; Garg, G.; Zhao, J.; Moroni, E.; Girgis, A.; Franco, L. S.; Singh, S.; Colombo, G.; Blagg, B. S. Design, synthesis and biological evaluation of biphenylamide derivatives as Hsp90 C-terminal inhibitors. *Eur J Med Chem* **2015,** 89, 442-66.

370. Zhao, H.; Moroni, E.; Yan, B.; Colombo, G.; Blagg, B. S. J. 3D-QSAR-Assisted Design, Synthesis, and Evaluation of Novobiocin Analogues. *ACS Medicinal Chemistry Letters* **2013,** 4, 57-62.

371. Palermo, C. M.; Westlake, C. A.; Gasiewicz, T. A. Epigallocatechin gallate inhibits aryl hydrocarbon receptor gene transcription through an indirect mechanism involving binding to a 90 kDa heat shock protein. *Biochemistry* **2005,** 44, 5041-52.

372. Yin, Z.; Henry, E. C.; Gasiewicz, T. A. (-)-Epigallocatechin-3-gallate is a novel Hsp90 inhibitor. *Biochemistry* **2009,** 48, 336-45.

373. Itoh, H.; Ogura, M.; Komatsuda, A.; Wakui, H.; Miura, A. B.; Tashima, Y. A novel chaperone-activity-reducing mechanism of the 90-kDa molecular chaperone HSP90. *Biochem J* **1999,** 343 Pt 3, 697-703.

374. Byrd, C. A.; Bornmann, W.; Erdjument-Bromage, H.; Tempst, P.; Pavletich, N.; Rosen, N.; Nathan, C. F.; Ding, A. Heat shock protein 90 mediates macrophage activation by Taxol and bacterial lipopolysaccharide. *Proceedings of the National Academy of Sciences of the United States of America* **1999,** 96, 5645-5650.

375. Vasko, R. C.; Rodriguez, R. A.; Cunningham, C. N.; Ardi, V. C.; Agard, D. A.; McAlpine, S. R. Mechanistic Studies of Sansalvamide A-Amide: An Allosteric Modulator of Hsp90. *ACS Medicinal Chemistry Letters* **2010,** 1, 4-8.

376. Ardi, V. C.; Alexander, L. D.; Johnson, V. A.; McAlpine, S. R. Macrocycles that inhibit the binding between heat shock protein 90 and TPR-containing proteins. *ACS Chem Biol* **2011,** 6, 1357-66.

377. Sellers, R. P.; Alexander, L. D.; Johnson, V. A.; Lin, C. C.; Savage, J.; Corral, R.; Moss, J.; Slugocki, T. S.; Singh, E. K.; Davis, M. R.; Ravula, S.; Spicer, J. E.; Oelrich, J. L.; Thornquist, A.; Pan, C. M.; McAlpine, S. R. Design and synthesis of Hsp90 inhibitors: exploring the SAR of Sansalvamide A derivatives. *Bioorg Med Chem* **2010,** 18, 6822-56.

378. Duerfeldt, A. S.; Peterson, L. B.; Maynard, J. C.; Ng, C. L.; Eletto, D.; Ostrovsky, O.; Shinogle, H. E.; Moore, D. S.; Argon, Y.; Nicchitta, C. V.; Blagg, B. S. Development of a Grp94 inhibitor. *J Am Chem Soc* **2012,** 134, 9796-804.

379. Ernst, J. T.; Neubert, T.; Liu, M.; Sperry, S.; Zuccola, H.; Turnbull, A.; Fleck, B.; Kargo, W.; Woody, L.; Chiang, P.; Tran, D.; Chen, W.; Snyder, P.; Alcacio, T.; Nezami, A.; Reynolds, J.; Alvi, K.; Goulet, L.; Stamos, D. Identification of novel HSP90alpha/beta isoform selective inhibitors using structure-based drug design. demonstration of potential utility in treating CNS disorders such as Huntington's disease. *J Med Chem* **2014,** 57, 3382-400.

380. Ernst, J. T.; Liu, M.; Zuccola, H.; Neubert, T.; Beaumont, K.; Turnbull, A.; Kallel, A.; Vought, B.; Stamos, D. Correlation between chemotype-dependent binding conformations of HSP90alpha/beta and isoform selectivity-Implications for the structure-based design of HSP90alpha/beta selective inhibitors for treating neurodegenerative diseases. *Bioorg Med Chem Lett* **2014,** 24, 204-8.

381.    Zhang, T.; Hamza, A.; Cao, X.; Wang, B.; Yu, S.; Zhan, C. G.; Sun, D. A novel Hsp90 inhibitor to disrupt Hsp90/Cdc37 complex against pancreatic cancer cells. *Mol Cancer Ther* **2008,** 7, 162-70.

382.    Zhang, T.; Li, Y.; Yu, Y.; Zou, P.; Jiang, Y.; Sun, D. Characterization of celastrol to inhibit hsp90 and cdc37 interaction. *J Biol Chem* **2009,** 284, 35381-9.

383.    Li, Y.; Karagoz, G. E.; Seo, Y. H.; Zhang, T.; Jiang, Y.; Yu, Y.; Duarte, A. M.; Schwartz, S. J.; Boelens, R.; Carroll, K.; Rudiger, S. G.; Sun, D. Sulforaphane inhibits pancreatic cancer through disrupting Hsp90-p50(Cdc37) complex and direct interactions with amino acids residues of Hsp90. *J Nutr Biochem* **2012,** 23, 1617-26.

384.    Khandelwal, A.; Hall, J.; Blagg, B. S. J. Synthesis and Structure activity relationships of EGCG Analogues, A Recently Identified Hsp90 Inhibitor. *The Journal of organic chemistry* **2013,** 78, 7859-7884.

385.    Kusuma, B. R.; Khandelwal, A.; Gu, W.; Brown, D.; Liu, W.; Vielhauer, G.; Holzbeierlein, J.; Blagg, B. S. Synthesis and biological evaluation of coumarin replacements of novobiocin as Hsp90 inhibitors. *Bioorg Med Chem* **2014,** 22, 1441-9.

386.    Zhao, H.; Reddy Kusuma, B.; Blagg, B. S. J. Synthesis and Evaluation of Noviose Replacements on Novobiocin That Manifest Antiproliferative Activity. *ACS Medicinal Chemistry Letters* **2010,** 1, 311-315.

387.    Zhao, H.; Yan, B.; Peterson, L. B.; Blagg, B. S. 3-Arylcoumarin derivatives manifest anti-proliferative activity through Hsp90 inhibition. *ACS Med Chem Lett* **2012,** 3, 327-331.

388.    Zhao, H.; Moroni, E.; Colombo, G.; Blagg, B. S. J. Identification of a New Scaffold for Hsp90 C-Terminal Inhibition. *ACS Medicinal Chemistry Letters* **2014,** 5, 84-88.

389.    Garg, G.; Zhao, H.; Blagg, B. S. J. Design, Synthesis, and Biological Evaluation of Ring-Constrained Novobiocin Analogues as Hsp90 C-Terminal Inhibitors. *ACS Medicinal Chemistry Letters* **2014,** 6, 204-209.

390.    Koay, Y. C.; McConnell, J. R.; Wang, Y.; Kim, S. J.; Buckton, L. K.; Mansour, F.; McAlpine, S. R. Chemically Accessible Hsp90 Inhibitor That Does Not Induce a Heat Shock Response. *ACS Medicinal Chemistry Letters* **2014,** 5, 771-776.

391.    Ramsey, D. M.; McConnell, J. R.; Alexander, L. D.; Tanaka, K. W.; Vera, C. M.; McAlpine, S. R. An Hsp90 modulator that exhibits a unique mechanistic profile. *Bioorg Med Chem Lett* **2012,** 22, 3287-90.

392.    Kappe, C. O. Biologically active dihydropyrimidones of the Biginelli-type--a literature survey. *Eur J Med Chem* **2000,** 35, 1043-52.

393.    Legraverend, M.; Grierson, D. S. The purines: potent and versatile small molecule inhibitors and modulators of key biological targets. *Bioorg Med Chem* **2006,** 14, 3987-4006.

394.    Hocek, M.; Pohl, R. Regioselectivity in Cross-Coupling Reactions of 2,6,8-Trichloro-9-(tetrahydropyran-2-yl)purine: Synthesis of 2,6,8-Trisubstituted Purine Bases. *Synthesis* **2004,** 2004, 2869-2876.

395.    Čapek, P.; Vrábel, M.; Hasník, Z.; Pohl, R.; Hocek, M. Aqueous-Phase Suzuki-Miyaura Cross-Coupling Reactions of Free Halopurine Bases. *Synthesis* **2006,** 2006, 3515-3526.

396.    Lu, W.; Sengupta, S.; Petersen, J. L.; Akhmedov, N. G.; Shi, X. Mitsunobu Coupling of Nucleobases and Alcohols: An Efficient, Practical Synthesis for Novel Nonsugar Carbon Nucleosides. *The Journal of Organic Chemistry* **2007,** 72, 5012-5015.

397.    Zhong, M.; Nowak, I.; Robins, M. J. Regiospecific and Highly Stereoselective Coupling of 6-(Substituted-imidazol-1-yl)purines with 2-Deoxy-3,5-di-O-(p-toluoyl)-α-d-erythro-pentofuranosyl Chloride. Sodium-Salt Glycosylation in Binary Solvent Mixtures: Improved Synthesis of Cladribine1. *The Journal of Organic Chemistry* **2006,** 71, 7773-7779.

398.    Legraverend, M. Recent advances in the synthesis of purine derivatives and their precursors. *Tetrahedron* **2008,** 64, 8585-8603.

399.    Brik, A.; Wu, C. Y.; Best, M. D.; Wong, C. H. Tetrabutylammonium fluoride-assisted rapid N9-alkylation on purine ring: application to combinatorial reactions in microtiter plates for the discovery of potent sulfotransferase inhibitors in situ. *Bioorg Med Chem* **2005,** 13, 4622-6.

400.    Jin, T.; Zhang, S.; Li, T. p-TOLUENESULFONIC ACID-CATALYZED EFFICIENT SYNTHESIS OF DIHYDROPYRIMIDINES: IMPROVED HIGH YIELDING PROTOCOL FOR THE BIGINELLI REACTION. *Synthetic Communications* **2002,** 32, 1847-1851.

401.    Hu, E. H.; Sidler, D. R.; Dolling, U.-H. Unprecedented Catalytic Three Component One-Pot Condensation Reaction: An Efficient Synthesis of 5-Alkoxycarbonyl- 4-aryl-3,4-dihydropyrimidin-2(1H)-ones. *The Journal of Organic Chemistry* **1998,** 63, 3454-3457.

402.    Bigi, F.; Carloni, S.; Frullanti, B.; Maggi, R.; Sartori, G. A revision of the Biginelli reaction under solid acid catalysis. Solvent-free synthesis of dihydropyrimidines over montmorillonite KSF. *Tetrahedron Letters* **1999,** 40, 3465-3468.

403.    Lu, J.; Ma, H. Iron(III)-Catalyzed Synthesis of Dihydropyrimidinones. Improved Conditions for the Biginelli Reaction. *Synlett* **2000,** 2000, 63-64.

404.    Lu, J.; Bai, Y.; Wang, Z.; Yang, B.; Ma, H. One-pot synthesis of 3,4-dihydropyrimidin-2(1H)-ones using lanthanum chloride as a catalyst. *Tetrahedron Letters* **2000,** 41, 9075-9078.

405.    Paraskar, A. S.; Dewkar, G. K.; Sudalai, A. Cu(OTf)2: a reusable catalyst for high-yield synthesis of 3,4-dihydropyrimidin-2(1H)-ones. *Tetrahedron Letters* **2003,** 44, 3305-3308.

406.    Russowsky, D.; Lopes, F. A.; Silva, V. S. S. d.; Canto, K. F. S.; D'Oca, M. G. M.; Godoi, M. N. Multicomponent Biginelli's synthesis of 3,4-dihydropyrimidin-2(1H)-ones promoted by SnCl2.2H2O. *Journal of the Brazilian Chemical Society* **2004,** 15, 165-169.

407.    Ranu, B. C.; Hajra, A.; Jana, U. Indium(III) chloride-catalyzed one-pot synthesis of dihydropyrimidinones by a three-component coupling of 1,3-dicarbonyl compounds, aldehydes, and urea: an improved procedure for the Biginelli reaction. *J Org Chem* **2000,** 65, 6270-2.

408.    Ma, Y.; Qian, C.; Wang, L.; Yang, M. Lanthanide triflate catalyzed Biginelli reaction. one-pot synthesis of dihydropyrimidinones under solvent-free conditions. *J Org Chem* **2000,** 65, 3864-8.

409.    Zhu, Y.; Pan, Y.; Huang, S. Trimethylsilyl Chloride: A Facile and Efficient Reagent for One-Pot Synthesis of 3,4-Dihydropyrimidin-2(1H)-ones. *Synthetic Communications* **2004,** 34, 3167-3174.

410.    Ahmed, B.; Khan, R. A.; Habibullah; Keshari, M. An improved synthesis of Biginelli-type compounds via phase-transfer catalysis. *Tetrahedron Letters* **2009,** 50, 2889-2892.

411.    Peng, J.; Deng, Y. Ionic liquids catalyzed Biginelli reaction under solvent-free conditions. *Tetrahedron Letters* **2001,** 42, 5917-5919.

412.    Dong, F.; Jun, L.; Xinli, Z.; Zhiwen, Y.; Zuliang, L. One-pot green procedure for Biginelli reaction catalyzed by novel task-specific room-temperature ionic liquids. *Journal of Molecular Catalysis A: Chemical* **2007,** 274, 208-211.

413.    De, S. K.; Gibbs, R. A. Ruthenium(III) Chloride-Catalyzed One-Pot Synthesis of 3,4-Dihydro-pyrimidin-2-(1H)-ones under Solvent-Free Conditions. *Synthesis* **2005,** 2005, 1748-1750.

414.    Dondoni, A.; Massi, A. Parallel synthesis of dihydropyrimidinones using Yb(III)-resin and polymer-supported scavengers under solvent-free conditions. A green chemistry approach to the Biginelli reaction. *Tetrahedron Letters* **2001,** 42, 7975-7978.

415.    Kappe, C. O. Highly versatile solid phase synthesis of biofunctional 4-aryl-3,4-dihydropyrimidines using resin-bound isothiourea building blocks and multidirectional resin cleavage. *Bioorganic & Medicinal Chemistry Letters* **2000,** 10, 49-51.

416.    Heravi, M. M.; Asadi, S.; Lashkariani, B. M. Recent progress in asymmetric Biginelli reaction. *Mol Divers* **2013,** 17, 389-407.

417. Stadler, A.; Kappe, C. O. Automated library generation using sequential microwave-assisted chemistry. Application toward the Biginelli multicomponent condensation. *J Comb Chem* **2001,** 3, 624-30.

418. Pisani, L.; Prokopcová, H.; Kremsner, J. M.; Kappe, C. O. 5-Aroyl-3,4-dihydropyrimidin-2-one Library Generation via Automated Sequential and Parallel Microwave-assisted Synthesis Techniques. *Journal of Combinatorial Chemistry* **2007,** 9, 415-421.

419. Stadler, A.; Kappe, C. O. Microwave-mediated Biginelli reactions revisited. On the nature of rate and yield enhancements. *Journal of the Chemical Society, Perkin Transactions 2* **2000**, 1363-1368.

420. Kappe, C. O.; Stadler, A. Building dihydropyrimidine libraries via microwave-assisted Biginelli multicomponent reactions. *Methods Enzymol* **2003,** 369, 197-223.

421. Dallinger, D.; Kappe, C. O. Automated generation of a dihydropyrimidine compound library using microwave-assisted processing. *Nat. Protocols* **2007,** 2, 1713-1721.

422. Ryabukhin, S. V.; Plaskon, A. S.; Ostapchuk, E. N.; Volochnyuk, D. M.; Tolmachev, A. A. N-Substituted Ureas and Thioureas in Biginelli Reaction Promoted by Chlorotrimethylsilane: Convenient Synthesis of N1-Alkyl-, N1-Aryl-, and N1,N3-Dialkyl-3,4-Dihydropyrimidin-2(1H)-(thi)ones. *Synthesis* **2007,** 2007, 417-427.

423. Hewings, D. S.; Wang, M.; Philpott, M.; Fedorov, O.; Uttarkar, S.; Filippakopoulos, P.; Picaud, S.; Vuppusetty, C.; Marsden, B.; Knapp, S.; Conway, S. J.; Heightman, T. D. 3,5-Dimethylisoxazoles Act As Acetyl-lysine-mimetic Bromodomain Ligands. *Journal of Medicinal Chemistry* **2011,** 54, 6761-6770.

424. McKeown, M. R.; Shaw, D. L.; Fu, H.; Liu, S.; Xu, X.; Marineau, J. J.; Huang, Y.; Zhang, X.; Buckley, D. L.; Kadam, A.; Zhang, Z.; Blacklow, S. C.; Qi, J.; Zhang, W.; Bradner, J. E. Biased multicomponent reactions to develop novel bromodomain inhibitors. *J Med Chem* **2014,** 57, 9019-27.

425. Fish, P. V.; Filippakopoulos, P.; Bish, G.; Brennan, P. E.; Bunnage, M. E.; Cook, A. S.; Federov, O.; Gerstenberger, B. S.; Jones, H.; Knapp, S.; Marsden, B.; Nocka, K.; Owen, D. R.; Philpott, M.; Picaud, S.; Primiano, M. J.; Ralph, M. J.; Sciammetta, N.; Trzupek, J. D. Identification of a Chemical Probe for Bromo and Extra C-Terminal Bromodomain Inhibition through Optimization of a Fragment-Derived Hit. *Journal of Medicinal Chemistry* **2012,** 55, 9831-9837.

426. Vidler, L. R.; Filippakopoulos, P.; Fedorov, O.; Picaud, S.; Martin, S.; Tomsett, M.; Woodward, H.; Brown, N.; Knapp, S.; Hoelder, S. Discovery of novel small-molecule inhibitors of BRD4 using structure-based virtual screening. *J Med Chem* **2013,** 56, 8073-88.

427. Fedorov, O.; Lingard, H.; Wells, C.; Monteiro, O. P.; Picaud, S.; Keates, T.; Yapp, C.; Philpott, M.; Martin, S. J.; Felletar, I.; Marsden, B. D.; Filippakopoulos, P.;

Müller, S.; Knapp, S.; Brennan, P. E. [1,2,4]Triazolo[4,3-a]phthalazines: Inhibitors of Diverse Bromodomains. *Journal of Medicinal Chemistry* **2013,** 57, 462-476.

428.    Martin, M. P.; Olesen, S. H.; Georg, G. I.; Schönbrunn, E. Cyclin-Dependent Kinase Inhibitor Dinaciclib Interacts with the Acetyl-Lysine Recognition Site of Bromodomains. *ACS Chemical Biology* **2013,** 8, 2360-2365.

429.    Rosemeyer, H. The chemodiversity of purine as a constituent of natural products. *Chem Biodivers* **2004,** 1, 361-401.

430.    U. S. Food and Drug Administration. http://www.fda.gov/ (13 February 2015).

431.    Gray, N. S.; Wodicka, L.; Thunnissen, A. M.; Norman, T. C.; Kwon, S.; Espinoza, F. H.; Morgan, D. O.; Barnes, G.; LeClerc, S.; Meijer, L.; Kim, S. H.; Lockhart, D. J.; Schultz, P. G. Exploiting chemical libraries, structure, and genomics in the search for kinase inhibitors. *Science* **1998,** 281, 533-8.

432.    Sherman, W.; Day, T.; Jacobson, M. P.; Friesner, R. A.; Farid, R. Novel Procedure for Modeling Ligand/Receptor Induced Fit Effects. *Journal of Medicinal Chemistry* **2005,** 49, 534-553.

433.    Sherman, W.; Beard, H. S.; Farid, R. Use of an induced fit receptor structure in virtual screening. *Chem Biol Drug Des* **2006,** 67, 83-4.

434.    Filippakopoulos, P.; Picaud, S.; Fedorov, O.; Keller, M.; Wrobel, M.; Morgenstern, O.; Bracher, F.; Knapp, S. Benzodiazepines and benzotriazepines as protein interaction inhibitors targeting bromodomains of the BET family. *Bioorg Med Chem* **2012,** 20, 1878-86.

435.    Kadoch, C.; Hargreaves, D. C.; Hodges, C.; Elias, L.; Ho, L.; Ranish, J.; Crabtree, G. R. Proteomic and bioinformatic analysis of mammalian SWI/SNF complexes identifies extensive roles in human malignancy. *Nat Genet* **2013,** 45, 592-601.

436.    Kang, J. U.; Koo, S. H.; Kwon, K. C.; Park, J. W.; Kim, J. M. Gain at chromosomal region 5p15.33, containing TERT, is the most frequent genetic event in early stages of non-small cell lung cancer. *Cancer Genet Cytogenet* **2008,** 182, 1-11.

437.    Scotto, L.; Narayan, G.; Nandula, S. V.; Subramaniyam, S.; Kaufmann, A. M.; Wright, J. D.; Pothuri, B.; Mansukhani, M.; Schneider, A.; Arias-Pulido, H.; Murty, V. V. Integrative genomics analysis of chromosome 5p gain in cervical cancer reveals target over-expressed genes, including Drosha. *Mol Cancer* **2008,** 7, 58.

438.    Cleary, S. P.; Jeck, W. R.; Zhao, X.; Chen, K.; Selitsky, S. R.; Savich, G. L.; Tan, T. X.; Wu, M. C.; Getz, G.; Lawrence, M. S.; Parker, J. S.; Li, J.; Powers, S.; Kim, H.; Fischer, S.; Guindi, M.; Ghanekar, A.; Chiang, D. Y. Identification of driver genes in hepatocellular carcinoma by exome sequencing. *Hepatology* **2013,** 58, 1693-702.

439.     Kandoth, C.; Schultz, N.; Cherniack, A. D.; Akbani, R.; Liu, Y.; Shen, H.; Robertson, A. G.; Pashtan, I.; Shen, R.; Benz, C. C.; Yau, C.; Laird, P. W.; Ding, L.; Zhang, W.; Mills, G. B.; Kucherlapati, R.; Mardis, E. R.; Levine, D. A. Integrated genomic characterization of endometrial carcinoma. *Nature* **2013,** 497, 67-73.

440.     Comprehensive genomic characterization of squamous cell lung cancers. *Nature* **2012,** 489, 519-25.

441.     Barbieri, C. E.; Baca, S. C.; Lawrence, M. S.; Demichelis, F.; Blattner, M.; Theurillat, J. P.; White, T. A.; Stojanov, P.; Van Allen, E.; Stransky, N.; Nickerson, E.; Chae, S. S.; Boysen, G.; Auclair, D.; Onofrio, R. C.; Park, K.; Kitabayashi, N.; MacDonald, T. Y.; Sheikh, K.; Vuong, T.; Guiducci, C.; Cibulskis, K.; Sivachenko, A.; Carter, S. L.; Saksena, G.; Voet, D.; Hussain, W. M.; Ramos, A. H.; Winckler, W.; Redman, M. C.; Ardlie, K.; Tewari, A. K.; Mosquera, J. M.; Rupp, N.; Wild, P. J.; Moch, H.; Morrissey, C.; Nelson, P. S.; Kantoff, P. W.; Gabriel, S. B.; Golub, T. R.; Meyerson, M.; Lander, E. S.; Getz, G.; Rubin, M. A.; Garraway, L. A. Exome sequencing identifies recurrent SPOP, FOXA1 and MED12 mutations in prostate cancer. *Nat Genet* **2012,** 44, 685-9.

442.     Ghosh, A. K.; Lagisetty, P.; Zajc, B. Direct Synthesis of 8-Fluoro Purine Nucleosides via Metalation−Fluorination. *The Journal of Organic Chemistry* **2007,** 72, 8222-8226.

443.     Roy, A.; Schneller, S. W. An Unusual Occurrence on Attempted Purine C-8 Electrophilic Fluorination of 5'-Noraristeromycin. *Organic Letters* **2005,** 7, 3889-3891.

444.     De, A.; Jasani, A.; Arora, R.; Gambhir, S. S. Evolution of BRET Biosensors from Live Cell to Tissue-Scale In vivo Imaging. *Front Endocrinol (Lausanne)* **2013,** 4, 131.

445.     Holm, P. J.; Bhakat, P.; Jegerschöld, C.; Gyobu, N.; Mitsuoka, K.; Fujiyoshi, Y.; Morgenstern, R.; Hebert, H. Structural Basis for Detoxification and Oxidative Stress Protection in Membranes. *Journal of Molecular Biology* **2006,** 360, 934-945.

446.     Jegerschold, C.; Pawelzik, S. C.; Purhonen, P.; Bhakat, P.; Gheorghe, K. R.; Gyobu, N.; Mitsuoka, K.; Morgenstern, R.; Jakobsson, P. J.; Hebert, H. Structural basis for induced formation of the inflammatory mediator prostaglandin E2. *Proc Natl Acad Sci U S A* **2008,** 105, 11110-5.

447.     Thoren, S.; Weinander, R.; Saha, S.; Jegerschold, C.; Pettersson, P. L.; Samuelsson, B.; Hebert, H.; Hamberg, M.; Morgenstern, R.; Jakobsson, P. J. Human microsomal prostaglandin E synthase-1: purification, functional characterization, and projection structure determination. *J Biol Chem* **2003,** 278, 22199-209.

448.     Li, D.; Howe, N.; Dukkipati, A.; Shah, S. T.; Bax, B. D.; Edge, C.; Bridges, A.; Hardwicke, P.; Singh, O. M.; Giblin, G.; Pautsch, A.; Pfau, R.; Schnapp, G.; Wang, M.; Olieric, V.; Caffrey, M. Crystallizing Membrane Proteins in the Lipidic Mesophase. Experience with Human Prostaglandin E2 Synthase 1 and an Evolving Strategy. *Cryst Growth Des* **2014,** 14, 2034-2047.

449.    Clark, J. H.; Macquarrie, D. J.; Sherwood, J. The combined role of catalysis and solvent effects on the Biginelli reaction: improving efficiency and sustainability. *Chemistry* **2013,** 19, 5174-82.

450.    Prokopcova, H.; Kappe, C. O. The Liebeskind-Srogl C-C cross-coupling reaction. *Angew Chem Int Ed Engl* **2009,** 48, 2276-86.

451.    Yu, Y.; Liebeskind, L. S. Copper-Mediated, Palladium-Catalyzed Coupling of Thiol Esters with Aliphatic Organoboron Reagents. *The Journal of Organic Chemistry* **2004,** 69, 3554-3557.

452.    Yang, H.; Li, H.; Wittenberg, R.; Egi, M.; Huang, W.; Liebeskind, L. S. Ambient temperature synthesis of high enantiopurity N-protected peptidyl ketones by peptidyl thiol ester-boronic acid cross-coupling. *J Am Chem Soc* **2007,** 129, 1132-40.

453.    Liebeskind, L. S.; Srogl, J. Heteroaromatic Thioether−Boronic Acid Cross-Coupling under Neutral Reaction Conditions. *Organic Letters* **2002,** 4, 979-981.

454.    Kusturin, C. L.; Liebeskind, L. S.; Neumann, W. L. A New Catalytic Cross-Coupling Approach for the Synthesis of Protected Aryl and Heteroaryl Amidines. *Organic Letters* **2002,** 4, 983-985.

455.    Savarin, C.; Srogl, J.; Liebeskind, L. S. Substituted Alkyne Synthesis under Nonbasic Conditions: Copper Carboxylate-Mediated, Palladium-Catalyzed Thioalkyne−Boronic Acid Cross-Coupling. *Organic Letters* **2000,** 3, 91-93.

456.    Kusturin, C.; Liebeskind, L. S.; Rahman, H.; Sample, K.; Schweitzer, B.; Srogl, J.; Neumann, W. L. Switchable Catalysis: Modular Synthesis of Functionalized Pyrimidinones via Selective Sulfide and Halide Cross-Coupling Chemistry. *Organic Letters* **2003,** 5, 4349-4352.

457.    Innitzer, A. Copper(I) Thiophene-2-carboxylate (CuTC). *Synlett* **2005,** 2005, 2405-2406.

458.    Lengar, A.; Kappe, C. O. Tunable Carbon−Carbon and Carbon−Sulfur Cross-Coupling of Boronic Acids with 3,4-Dihydropyrimidine-2-thiones. *Organic Letters* **2004,** 6, 771-774.

459.    He, S.; Lai, L. Molecular Docking and Competitive Binding Study Discovered Different Binding Modes of Microsomal Prostaglandin E Synthase-1 Inhibitors. *Journal of Chemical Information and Modeling* **2011,** 51, 3254-3261.

460.    Sorger, P. K. Heat shock factor and the heat shock response. *Cell* **1991,** 65, 363-366.

461.    Dai, C.; Whitesell, L.; Rogers, A. B.; Lindquist, S. Heat Shock Factor 1 Is a Powerful Multifaceted Modifier of Carcinogenesis. *Cell* **2007,** 130, 1005-1018.

462.    Fulda, S.; Gorman, A. M.; Hori, O.; Samali, A. Cellular stress responses: cell survival and cell death. *Int J Cell Biol* **2010,** 2010, 214074.

463. Shi, Y.; Mosser, D. D.; Morimoto, R. I. Molecular chaperones as HSF1-specific transcriptional repressors. *Genes Dev* **1998,** 12, 654-66.

464. Zou, J.; Guo, Y.; Guettouche, T.; Smith, D. F.; Voellmy, R. Repression of heat shock transcription factor HSF1 activation by HSP90 (HSP90 complex) that forms a stress-sensitive complex with HSF1. *Cell* **1998,** 94, 471-80.

465. Voellmy, R.; Boellmann, F. Chaperone regulation of the heat shock protein response. *Adv Exp Med Biol* **2007,** 594, 89-99.

466. Zuo, J.; Rungger, D.; Voellmy, R. Multiple layers of regulation of human heat shock transcription factor 1. *Molecular and Cellular Biology* **1995,** 15, 4319-4330.

467. Xia, W.; Voellmy, R. Hyperphosphorylation of heat shock transcription factor 1 is correlated with transcriptional competence and slow dissociation of active factor trimers. *J Biol Chem* **1997,** 272, 4094-102.

468. Holzbeierlein, J. M.; Windsperger, A.; Vielhauer, G. Hsp90: a drug target? *Curr Oncol Rep* **2010,** 12, 95-101.

469. Biamonte, M. A.; Van de Water, R.; Arndt, J. W.; Scannevin, R. H.; Perret, D.; Lee, W. C. Heat shock protein 90: inhibitors in clinical trials. *J Med Chem* **2010,** 53, 3-17.

470. Shelton, S. N.; Shawgo, M. E.; Matthews, S. B.; Lu, Y.; Donnelly, A. C.; Szabla, K.; Tanol, M.; Vielhauer, G. A.; Rajewski, R. A.; Matts, R. L.; Blagg, B. S.; Robertson, J. D. KU135, a novel novobiocin-derived C-terminal inhibitor of the 90-kDa heat shock protein, exerts potent antiproliferative effects in human leukemic cells. *Mol Pharmacol* **2009,** 76, 1314-22.

471. Li, Y.; Zhang, T.; Jiang, Y.; Lee, H. F.; Schwartz, S. J.; Sun, D. (-)-Epigallocatechin-3-gallate inhibits Hsp90 function by impairing Hsp90 association with cochaperones in pancreatic cancer cell line Mia Paca-2. *Mol Pharm* **2009,** 6, 1152-9.

472. Taldone, T.; Sun, W.; Chiosis, G. Discovery and development of heat shock protein 90 inhibitors. *Bioorganic & medicinal chemistry* **2009,** 17, 2225-2235.

473. Moroni, E.; Zhao, H.; Blagg, B. S.; Colombo, G. Exploiting conformational dynamics in drug discovery: design of C-terminal inhibitors of Hsp90 with improved activities. *J Chem Inf Model* **2014,** 54, 195-208.

474. Cooper, M. A. Label-free screening of bio-molecular interactions. *Anal Bioanal Chem* **2003,** 377, 834-42.

475. Vassallo, A.; Vaccaro, M. C.; De Tommasi, N.; Dal Piaz, F.; Leone, A. Identification of the plant compound geraniin as a novel Hsp90 inhibitor. *PLoS One* **2013,** 8, e74266.

476.    Liu, K. S.; Liu, H.; Qi, J. H.; Liu, Q. Y.; Liu, Z.; Xia, M.; Xing, G. W.; Wang, S. X.; Wang, Y. F. SNX-2112, an Hsp90 inhibitor, induces apoptosis and autophagy via degradation of Hsp90 client proteins in human melanoma A-375 cells. *Cancer Lett* **2012,** 318, 180-8.

477.    Nicoletti, I.; Migliorati, G.; Pagliacci, M. C.; Grignani, F.; Riccardi, C. A rapid and simple method for measuring thymocyte apoptosis by propidium iodide staining and flow cytometry. *J Immunol Methods* **1991,** 139, 271-9.

478.    Dal Piaz, F.; Vassallo, A.; Temraz, A.; Cotugno, R.; Belisario, M. A.; Bifulco, G.; Chini, M. G.; Pisano, C.; De Tommasi, N.; Braca, A. A chemical-biological study reveals C9-type iridoids as novel heat shock protein 90 (Hsp90) inhibitors. *J Med Chem* **2013,** 56, 1583-95.

479.    Lee, C. C.; Lin, T. W.; Ko, T. P.; Wang, A. H. The hexameric structures of human heat shock protein 90. *PLoS One* **2011,** 6, e19961.

480.    Irvine, J. D.; Takahashi, L.; Lockhart, K.; Cheong, J.; Tolan, J. W.; Selick, H. E.; Grove, J. R. MDCK (Madin-Darby canine kidney) cells: A tool for membrane permeability screening. *J Pharm Sci* **1999,** 88, 28-33.

481.    Stenberg, P.; Norinder, U.; Luthman, K.; Artursson, P. Experimental and Computational Screening Models for the Prediction of Intestinal Drug Absorption. *Journal of Medicinal Chemistry* **2001,** 44, 1927-1937.

482.    Wagner, S.; Bader, M. L.; Drew, D.; de Gier, J. W. Rationalizing membrane protein overexpression. *Trends Biotechnol* **2006,** 24, 364-71.

483.    Grisshammer, R. Understanding recombinant expression of membrane proteins. *Curr Opin Biotechnol* **2006,** 17, 337-40.

484.    Mancia, F.; Love, J. High throughput platforms for structural genomics of integral membrane proteins. *Curr Opin Struct Biol* **2011,** 21, 517-22.

485.    Gordon, E.; Horsefield, R.; Swarts, H. G.; de Pont, J. J.; Neutze, R.; Snijder, A. Effective high-throughput overproduction of membrane proteins in Escherichia coli. *Protein Expr Purif* **2008,** 62, 1-8.

486.    Freigassner, M.; Pichler, H.; Glieder, A. Tuning microbial hosts for membrane protein production. *Microb Cell Fact* **2009,** 8, 69.

487.    von Heijne, G. Recent advances in the understanding of membrane protein assembly and structure. *Q Rev Biophys* **1999,** 32, 285-307.

488.    Bannwarth, M.; Schulz, G. E. The expression of outer membrane proteins for crystallization. *Biochim Biophys Acta* **2003,** 1610, 37-45.

489.    Drew, D.; Froderberg, L.; Baars, L.; de Gier, J. W. Assembly and overexpression of membrane proteins in Escherichia coli. *Biochim Biophys Acta* **2003,** 1610, 3-10.

490.	Baneyx, F.; Mujacic, M. Recombinant protein folding and misfolding in Escherichia coli. *Nat Biotechnol* **2004,** 22, 1399-408.

491.	Hattab, G.; Suisse, A. Y. T.; Ilioaia, O.; Casiraghi, M.; Dezi, M.; Warnet, X. L.; Warschawski, D. E.; Moncoq, K.; Zoonens, M.; Miroux, B. Membrane Protein Production in Escherichia coli: Overview and Protocols. In *Membrane Proteins Production for Structural Analysis*, Mus-Veteau, I., Ed. Springer New York: 2014; pp 87-106.

492.	Bill, R. M.; Henderson, P. J. F.; Iwata, S.; Kunji, E. R. S.; Michel, H.; Neutze, R.; Newstead, S.; Poolman, B.; Tate, C. G.; Vogel, H. Overcoming barriers to membrane protein structure determination. *Nat Biotech* **2011,** 29, 335-340.

493.	Duquesne, K.; Sturgis, J. N. Membrane protein solubilization. *Methods Mol Biol* **2010,** 601, 205-17.

494.	Lin, S. H.; Guidotti, G. Purification of membrane proteins. *Methods Enzymol* **2009,** 463, 619-29.

495.	William Studier, F.; Rosenberg, A. H.; Dunn, J. J.; Dubendorff, J. W. [6] Use of T7 RNA polymerase to direct expression of cloned genes. In *Methods in Enzymology*, David, V. G., Ed. Academic Press: 1990; Vol. Volume 185, pp 60-89.

496.	Chamberlin, M.; McGrath, J.; Waskell, L. New RNA Polymerase from Escherichia coli infected with Bacteriophage T7. *Nature* **1970,** 228, 227-231.

497.	Iost, I.; Guillerez, J.; Dreyfus, M. Bacteriophage T7 RNA polymerase travels far ahead of ribosomes in vivo. *Journal of Bacteriology* **1992,** 174, 619-622.

498.	Makino, T.; Skretas, G.; Georgiou, G. Strain engineering for improved expression of recombinant proteins in bacteria. *Microbial Cell Factories* **2011,** 10, 32-32.

499.	Zhang, X.; Studier, F. W. Mechanism of inhibition of bacteriophage T7 RNA polymerase by T7 lysozyme. *J Mol Biol* **1997,** 269, 10-27.

500.	Wanner, B. L.; Kodaira, R.; Neidhardt, F. C. Physiological regulation of a decontrolled lac operon. *Journal of Bacteriology* **1977,** 130, 212-222.

501.	Studier, F. W. Use of bacteriophage T7 lysozyme to improve an inducible T7 expression system. *Journal of Molecular Biology* **1991,** 219, 37-44.

502.	Bruni, R.; Kloss, B. High-Throughput Cloning and Expression of Integral Membrane Proteins in Escherichia coli. In *Current Protocols in Protein Science*, John Wiley & Sons, Inc.: 2001.

503.	Wagner, S.; Baars, L.; Ytterberg, A. J.; Klussmeier, A.; Wagner, C. S.; Nord, O.; Nygren, P. A.; van Wijk, K. J.; de Gier, J. W. Consequences of membrane protein overexpression in Escherichia coli. *Mol Cell Proteomics* **2007,** 6, 1527-50.

504. Driessen, A. J.; Manting, E. H.; van der Does, C. The structural basis of protein targeting and translocation in bacteria. *Nat Struct Biol* **2001,** 8, 492-8.

505. Miroux, B.; Walker, J. E. Over-production of proteins in Escherichia coli: mutant hosts that allow synthesis of some membrane proteins and globular proteins at high levels. *J Mol Biol* **1996,** 260, 289-98.

506. Wagner, S.; Klepsch, M. M.; Schlegel, S.; Appel, A.; Draheim, R.; Tarry, M.; Högbom, M.; van Wijk, K. J.; Slotboom, D. J.; Persson, J. O.; de Gier, J.-W. Tuning Escherichia coli for membrane protein overexpression. *Proceedings of the National Academy of Sciences* **2008,** 105, 14371-14376.

507. Stano, N. M.; Patel, S. S. T7 lysozyme represses T7 RNA polymerase transcription by destabilizing the open complex during initiation. *J Biol Chem* **2004,** 279, 16136-43.

508. Giacalone, M. J.; Gentile, A. M.; Lovitt, B. T.; Berkley, N. L.; Gunderson, C. W.; Surber, M. W. Toxic protein expression in Escherichia coli using a rhamnose-based tightly regulated and tunable promoter system. *Biotechniques* **2006,** 40, 355-64.

509. Low, C.; Jegerschold, C.; Kovermann, M.; Moberg, P.; Nordlund, P. Optimisation of over-expression in E. coli and biophysical characterisation of human membrane protein synaptogyrin 1. *PLoS One* **2012,** 7, e38244.

510. Schlegel, S.; Rujas, E.; Ytterberg, A. J.; Zubarev, R. A.; Luirink, J.; de Gier, J. W. Optimizing heterologous protein production in the periplasm of E. coli by regulating gene expression levels. *Microb Cell Fact* **2013,** 12, 24.

511. Schlegel, S.; Lofblom, J.; Lee, C.; Hjelm, A.; Klepsch, M.; Strous, M.; Drew, D.; Slotboom, D. J.; de Gier, J. W. Optimizing membrane protein overexpression in the Escherichia coli strain Lemo21(DE3). *J Mol Biol* **2012,** 423, 648-59.

512. Wittig, I.; Karas, M.; Schagger, H. High resolution clear native electrophoresis for in-gel functional assays and fluorescence studies of membrane protein complexes. *Mol Cell Proteomics* **2007,** 6, 1215-25.

513. Nannenga, B. L.; Iadanza, M. G.; Vollmar, B. S.; Gonen, T. Overview of Electron Crystallography of Membrane Proteins: Crystallization and Screening Strategies Using Negative Stain Electron Microscopy. In *Current Protocols in Protein Science*, John Wiley & Sons, Inc.: 2001.

514. Hocek, M.; Holý, A.; Votruba, I.; Dvořáková, H. Synthesis and Cytostatic Activity of Substituted 6-Phenylpurine Bases and Nucleosides: Application of the Suzuki−Miyaura Cross-Coupling Reactions of 6-Chloropurine Derivatives with Phenylboronic Acids. *Journal of Medicinal Chemistry* **2000,** 43, 1817-1825.

515. Shailaja, M.; Manjula, A.; Rao, B. V.; Parvathi, N. Simple Protocol for the Synthesis of 3,4-Dihydropyrimidin-2(1H)-ones Using SnCl2 · 2H2O–LiCl as an Inexpensive Catalyst System. *Synthetic Communications* **2004,** 34, 1559-1564.

516.    Singh, K.; Arora, D.; Poremsky, E.; Lowery, J.; Moreland, R. S. N1-Alkylated 3,4-dihydropyrimidine-2(1H)-ones: Convenient one-pot selective synthesis and evaluation of their calcium channel blocking activity. *Eur J Med Chem* **2009,** 44, 1997-2001.

517.    Konkala, K.; Sabbavarapu, N. M.; Katla, R.; Durga, N. Y. V.; Kumar Reddy T, V.; Bethala L.A, P. D.; Rachapudi B.N, P. Revisit to the Biginelli reaction: a novel and recyclable bioglycerol-based sulfonic acid functionalized carbon catalyst for one-pot synthesis of substituted 3,4-dihydropyrimidin-2-(1H)-ones. *Tetrahedron Letters* **2012,** 53, 1968-1973.

## List of Abbreviations

| | |
|---|---|
| 17-AAG | 17-(Allylamino)-17-demethoxygeldanamycin |
| 17-DMAG | 17-Dimethylaminoethylamino-17-demethoxygeldanamycin |
| AA | Arachidonic Acid |
| ADMET | Absorption, Distribution, Metabolism, Elimination, Toxicology |
| ADP | Adenosine Diphosphate |
| ATP | Adenosine Triphosphate |
| Akt | Protein Kinase B |
| ASH1L | Absent, small, or homeotic-like protein |
| ATAD2 | ATPase Family, AAA domain-containing protein 2 |
| BET | Bromodomain and Extra C-Terminal domain |
| BAZ1B | Bromodomain Adjacent to Zinc finger domain 1B |
| BAZ2B | Bromodomain Adjacent to Zinc finger domain, 2B |
| BRD | Bromodomain |
| BRD2 | Bromodomain-containing protein 2 |
| BRD3 | Bromodomain-containing protein 3 |
| BRD4 | Bromodomain-containing protein 4 |
| BRD4(1) | BRD4 first bromodomain |
| BRD9 | Bromodomain-containing protein 9 |

| | |
|---|---|
| BRDT | Bromodomain Testis-specific protein |
| BRET | Bioluminescence Resonance Energy Transfer |
| BRPF1 | Bromodomain and PHD Finger containing, 1 |
| CDK | Cyclin-Dependent Kinase |
| COX | Cyclooxygenase |
| COXib | COX-2 selective inhibitor |
| CuTC | Cu(I)-thiophene-2-carboxylate |
| cPGES | cytosolic Prostaglandin $E_2$ Synthase |
| CREB | cAMP Response Element Binding protein |
| CREBBP | CREB Binding Protein |
| DEAD | Diethyl azodicarboxylate |
| DHPM | 3,4-dihydropyrimidin-2(1H)-one |
| DMSO | Dimethyl Sulfoxide |
| EGCG | (-)-Epigallocatechin-3-gallate |
| FLAP | 5-Lipoxygenase Activating Protein |
| GCN5 | General Control Nonderepressible-5 |
| GDA | Geldanamycin |
| GPCR | G-Protein Coupled Receptors |
| Grp94 | 94 kDa gluclose-regulated protein |
| GSH | Glutathione |
| GTP | Guanosine triphosphate |
| HAT | Histone Acetyl-Transferases |
| HDAC | Histone Deacetylases |
| HIV | Human Immunodeficiency Virus |
| hrCNE | High Resolution Clear Native Electrophoresis |

| | |
|---|---|
| HSF1 | Heat Shock Factor 1 |
| Hsp | Heat Shock Protein |
| HSR | Heat Shock Response |
| HTS | High-throughput screening |
| $IC_{50}$ | Half Maximal Inhibitory Concentration |
| IKK | IκB Kinase |
| IL | Interleukin |
| IMAC | Immobilized-metal affinity chromatography |
| IPTG | Isopropyl β-D-1-thiogalactopyranoside |
| ITC | Isothermal Titration Calorimetry |
| Kac | Acetylated Lysine |
| $K_D$ | Dissociation Constant |
| LB | Luria-Bertani Broth |
| LO | Lipoxygenase |
| LogP | Logarithm of the Partition coefficient between water and 1-octanol |
| LPS | Lipopolysaccharide |
| LT | Leukotriene |
| LTC4S | Leukotriene C4 Synthase |
| LVJ | 2-[[2,6-bis(chloranyl)-3-[(2,2dimethylpropanoylamino)-methyl]phenyl]amino]-1-methyl-6-(2-methyl-2-oxidanyl-propoxy)-N-[2,2,2-tris-(fluoranyl)ethyl]-benzimidazole-5-carboxamide |

| | |
|---|---|
| MAPEG | Membrane-Associated Proteins in Eicosanoid and Glutathione metabolism |
| MGST | Microsomal Glutathione S-Transferase |
| MLL | Mixed Lineage Leukemia protein |
| mPGES-1 | Microsomal Prostaglandin $E_2$ Synthase-1 |
| mPGES-2 | Microsomal Prostaglandin $E_2$ Synthase-2 |
| MS | Mass Spectrometry |
| MW | Microwaves |
| NF-κB | Nuclear Factor kappa B |
| NI-NTA | Nickel-nitrilotriacetic acid |
| NMC | NUT Midline Carcinoma |
| NMR | Nuclear Magnetic Resonance |
| NSAID | Non-Steroideal Antiinflammatory Drug |
| NUT | Nuclear protein in testis |
| PB1 | Protein Polybromo-1 |
| PCAF | P300/CBP-Associated Factor |
| PG | Prostaglandin |
| PLA$_2$ | Phospholipase $A_2$ |
| P-TEFb | Positive transcription elongation factor B |
| PTM | Post Translational Modification |
| RDC | Radicicol |
| RP-HPLC | Reverse Phase- High Performance Liquid Chromatogrphy |
| SAR | Structure Activity Relationship |
| SEM | Standard error of the mean |
| SET | Suppressor of variegation, Enhancer of zeste and Trithorax |

| | |
|---|---|
| SDS PAGE | Sodium Dodecyl Sulphate - PolyAcrylamide Gel Electrophoresis |
| SMARCA | SWI/SNF related, Matrix associated, Actin dependent Regulator of Chromatin, subfamily A |
| SPR | Surface Plasmon Resonance |
| STAT3 | Signal Transducer and Activator of Transcription 3 |
| SWI/SNF | SWItch/Sucrose Nonfermenting |
| T7Lys | T7 Lysozyme |
| T7RNAP | Bacteriophage T7 RNA polymerase |
| TAF1 | Transcription initiation factor TFIID subunit 1 |
| TB | Terrific Broth |
| TBAF | Tetrabutylammonium Fluoride |
| THF | Tetrahydrofuran |
| THP | Tetrahydropyran-2-yl |
| TMSCl | Chlorotrimethylsilane |
| TNFα | Tumor Necrosis Factor alpha |
| Trap1 | Hsp75/tumor necrosis factor receptor associated protein 1 |
| TRIM/TIF1 | Tripartite Motif/Transcriptional Intermediary Factor 1 |
| UTP | Uridine triphosphate |
| TXA$_2$ | Tromboxane |
| VEGF | Vascular Endothelial cell Growth Factor |

*Acknowledgements*

First and foremost I would like to thank my supervisor, Professor Ines Bruno, for her support and encouragements. I sincerely appreciated her scientific guidance and the opportunity she gave me to be part of the organic chemistry group.

I am very grateful to all the people who collaborated to the projects of my PhD: Professors Giuseppe Bifulco, Oliver Werz and Antonietta Leone, Dr. Panagis Filippakopoulos and Fabrizio Dal Piaz. Your scientific support had a great impact and was of key importance in all the projects. My gratitude is also for Prof. Hans Hebert and Dr. Caroline Jegerschöld, who welcomed me in the Electron Microscopy group at Karolinska Institutet with great kindness and professionalism. Many thanks to Ramki, Ram and Qie who helped me during my working experience at KI.

A special thank goes to Dr. Stefania Terracciano, who introduced me to the world of organic synthesis and welcomed me with great enthusiasm and friendliness. Your help and suggestions were essential during these three years; thank you especially for being a friend rather than a colleague.

My gratitude is also for Dr. Antonio Foglia who is a friend since many years, was a student who helped me with my projects and is now also a colleague, who joined the incredible world of PhD programs. Thank you for being a fantastic lab mate, for your encouragements, your help and your notable sense of humor.

All the other people of the Organic Chemistry lab supported me a lot and all of them deserve my acknowledgements: Maria Giovanna, Gianluigi, Alessandra and Simone. Many thanks also to the students who worked with me during this

period: Raffaella, Clementina, Stefania, Verdiana, Nicoletta, Maria, Emanuela, Michela, Francesco and Maria Luisa.

I am very grateful to the members of the Bioorganic Chemistry lab: Professor Agostino Casapullo, Dr. Chiara Monti, Luigi Margarucci and Chiara Cassiano, who all gave me precious advices during these years.

An exceptional thank is for Dr. Angela Capolupo, Michele Vasaturo and Enza Cantone, who have been close colleagues and friends, sharing with me pleasures and fears all along my journey: I wish them to enjoy the best of their PhD and to take great memories, as I did.

A huge acknowledgement goes to my "Swedish family": Nikenza, Aida and Riccardo, who have been amazing companions of adventures and discussion, sharing with me this unforgettable experience abroad. I am also grateful to Alessandra and Tomek for having been extraordinary corridor mates in Vårberg. I spent very good times with both of you: the awareness of your presence just outside my door was for me a reason of peace and happiness throughout my stay.

Thanks to Marco for taking life lightly and for never taking anything and anyone seriously, myself included. My level of stress would have been much higher without our "wise conversations".

Finally, my thanks go to my parents who encourage and support me every day, and to my brother Giuseppe who is making my life funnier and easier day by day. I will never find suitable words to thank you.


*Maria Strocchia*